A functional dissection of the relationships between BRAF, DNMT3B and the CpG island methylator phenotype in colorectal cancer

Douglas James MacKenzie
BSc (Hons) MBChB (Hons) MRCS

Submitted in fulfilment of the requirements
for the degree of Doctor of Philosophy

School of Medicine
College of Medical, Veterinary and Life Sciences
University of Glasgow
April 2017

Abstract

Approximately 10-20% of human colorectal cancers harbour an activating *BRAF*^{V600E} mutation, which acts as a founder mutation for an alternative, serrated pathway of colorectal carcinogenesis. Conversely, *BRAF*^{V600E} mutations are detectable in hyperplastic colonic polyps: lesions traditionally considered not to harbour malignant potential. Furthermore, both *in vitro* and *in vivo*, activated oncogenic BRAF^{V600E} induces a stable proliferation arrest: oncogene induced senescence, which is a fundamental intrinsic tumour-suppressor mechanism. Thus, for neoplastic transformation to occur, it is clear that additional genetic and epigenetic events are required. *BRAF*^{V600E}-mutant colorectal cancers are frequently associated with a CpG island methylator phenotype (CIMP), which is proposed to promote neoplastic transformation by bypass of intrinsic tumour-suppressor mechanisms, such as silencing of *CDKN2A/INK4A*. Consistent with this, neoplastic transformation in the serrated pathway is characterised by the progressive development of a CIMP phenotype. An emerging body of evidence supports a model in which the *BRAF*^{V600E} mutation directly induces CIMP through the *de novo* methyltransferase, DNMT3B. Separately, elevated DNMT3B expression has previously been linked to the development of CIMP in both murine and human colorectal cancer. The published data however do not universally support this model, and significant questions over its validity remain. In the present work, the relationships between *BRAF*^{V600E} mutation, DNMT3B expression and the CpG island methylator phenotype were examined by multiple approaches. A panel of DNMT3B antibodies were first characterised and validated. Significantly, the antibody previously used to link DNMT3B and CIMP in human colon cancer was demonstrated not to react with human DNMT3B. The ability of *BRAF*^{V600E} to induce CIMP was next tested by whole genome bisulfite sequencing in a primary cell culture model. Surprisingly, activated BRAF^{V600E} repressed expression of DNMT3B and failed to induce a CIMP phenotype. Consistent with this, human colorectal cancer cell lines expressing activated BRAF^{V600E} typically expressed a low level of DNMT3B, and inactivation of DNMT3B in a *BRAF*^{V600E}-mutant, CIMP-positive cell line did not reverse gene silencing characteristic of CIMP. An *in vitro* model system was next designed to test functional interactions between BRAF^{V600E} and DNMT3B. Ectopic expression of DNMT3B antagonised BRAF^{V600E}-induced proliferation arrest: a hallmark of senescence. Moreover, ectopic DNMT3B expression was demonstrated to accelerate *Braf*^{V600E}-induced intestinal carcinogenesis in a mouse model, and conversely, *Dnmt3b* knockout impaired *Braf*^{V600E}-induced murine intestinal carcinogenesis. Analysis of human colorectal cancer

TCGA data was next undertaken, and confirmed that expression of DNMT3B is frequently elevated in human colorectal cancer and that this is often linked to amplification of the *DNMT3B* gene. However, more detailed analysis of human TCGA data revealed that $BRAF^{V600E}$ mutation is neither necessary nor sufficient to induce CIMP, and that both $BRAF^{V600E}$ mutations and CIMP are both linked to low expression of DNMT3B. Thus, while both $BRAF^{V600E}$ and DNMT3B both harbour oncogenic potential, they do not appear to cooperate to induce CIMP, and do not appear to cooperate frequently in human colorectal cancer by any mechanism.

Table of Contents

List of Tables

List of Figures

List of Abbreviations

5mC	5’-methylcytosine
5hmC	5’-hydroxymethylcytosine
BrdU	5-bromo-2’-deoxyuridine
BSA	bovine serum albumin
CCS	colon cancer molecular subtypes
CDK	cyclin dependent kinase
cDNA	complementary deoxyribonucleic acid
CGI	CpG island
ChIP-seq	chromatin immunoprecipitation sequencing
CIMP	CpG island methylator phenotype
CIN	chromosomal instability
CMS	consensus molecular subtype
CRISPR	clustered regularly interspersed short palindromic repeats
DAB	3,3’-diaminobenzidine
DDR	deoxyribonucleic acid damage response
DAC	decitabine
DMEM	Dubelco’s modified Eagle medium
DMR	differentially methylated region
DNA	deoxyribonucleic acid
DNMT1	deoxyribonucleic acid methyltransferase 1
DNMT2	deoxyribonucleic acid methyltransferase 2
DNMT3A	deoxyribonucleic acid methyltransferase 3A
DNMT3B	deoxyribonucleic acid methyltransferase 3B
DNMT3C	deoxyribonucleic acid methyltransferase 3C
DNMT3L	deoxyribonucleic acid methyltransferase 3L
dsDNA	double stranded deoxyribonucleic acid
DTT	dithiothreitol
ECL	enhanced chemiluminescence
ECM	extracellular matrix
EDU	5-ethynyl-2’-deoxyuridine
EDTA	ethylenediaminetetraacetic acid
ES	embryonic stem cell
FACS	fluorescence-activated cell sorter
FBS	fetal bovine serum
FDR	false discovery rate
FPKM	fragments per kilobase million
GO	gene-ontology
GSEA	gene-set enrichment analysis
γH2AX	phosphorylated histone H2AX
H&E	haematoxylin and eosin
HDAC	histone deacetylase
HESCs	human embryonic steml cells
HGD	high grade dysplasia
HNPCC	hereditary non-polyposis colorectal cancer
HP	hyperplastic polyp
ICF	immunodeficiency centromeric instability syndrome
JCV	John-Cunningham virus
LGD	low grade dysplasia
LINE-1	long interspersed nuclear element-1

LOH	loss of heterozygosity
MAPK	mitogen activated protein kinase
MBD	methyl-binding domain
MCA	methylated CpG island amplification
MEF	mouse embryonic fibroblast
MMR	mismatch repair
mRNA	messenger ribonucleic acid
miRNA	micro ribonucleic acid
mSA	murine serrated adenoma
mSH	murine serrated hyperplasia
MSI	microsatellite instability
MSI-L	microsatellite instability-low
MSI-H	microsatellite instability-high
MSP	methylation-sensitive PCR
MSS	microsatellite stable
NCBI	National Center for Biotechnology Information
OIS	oncogene induced senescence
ORF	open reading frame
PAGE	polyacrylamide gel electrophoresis
PCA	principal component analysis
PBS	phosphate-buffered saline
PBT	phosphate-buffered saline and Tween
PCR	polymerase chain reaction
PcG	polycomb group complex
PD	population doubling
PRC	polycomb repressive complex
PTEN	phosphate and tensin homologue
PVDF	polyvinylidene fluoride
PWWP	proline-tryptophan-tryptophan-proline motif
RIN	ribonucleic acid integrity number
RNA	ribonucleic acid
RNA-seq	ribonucleic acid sequencing
ROS	reactive oxygen species
RS	replicative senescence
SASP	senescence associated secretory phenotype
SCNA	somatic copy number alteration
SDS	sodium dodecyl sulphate
SEM	standard error of the mean
siRNA	short interfering ribonucleic acid
sgRNA	single guide ribonucleic acid
shRNA	short hairpin ribonucleic acid
SSA/P	sessile serrated adenoma/polyp
STD-dev	standard deviation
TAE	Tris-Acetate-EDTA buffer
TCGA	The Cancer Genome Atlas
TSA	traditional serrated adenoma
UCSC	University of California, Santa Cruz
UV	ultraviolet
WGBS	whole-genome bisulfite sequencing
WB	Western blot
WT	wild-type

Acknowledgements

This thesis is dedicated to Rachael, Ruairidh and Olivia, without whose patience and support, none of this would have been possible, and to my parents and grandparents for the support, encouragement and opportunities they afforded me during my formative years.

I was exceptionally fortunate to have the opportunity to work in Professor Peter Adams' laboratory at the Beatson Institute for Cancer Research. I would like to thank all members of the lab (past and present) for their support and friendship during my transition from the bedside to the bench. I am deeply grateful for the outstanding supervision and support provided by Professor Adams during my time in the laboratory and during the composition of this thesis. A special debt of gratitude is owed to Claire Reid, Mark Drotar, Dr Karen Blyth, and Dr Taranjit Singh Rai, whose outstanding tuition in the fundamental techniques of laboratory science helped me get the whole project on track, and to Neil Robertson for his assistance with computational biology aspects of the project.

Author's Declaration

I am the sole author of this thesis, and all work presented is entirely my own unless stated otherwise. No part of this work has been submitted for consideration as part of any other degree or award.

1 Introduction

1.1 The serrated pathway of colorectal carcinogenesis

1.1.1 Introduction

The majority of sporadic colorectal cancers arise from adenomatous polyps through the well-characterised adenoma-carcinoma sequence, driven by the inactivation of *APC* [1]. These lesions are typically characterised by activating *KRAS* mutations, loss of *TP53*, chromosomal instability (CIN), and microsatellite stability [2]. There is now recognition of an alternative sporadic pathway to colorectal cancer with different precursor lesions: the so-called "sessile serrated lesions". Whilst a description of serrated lesions was first published in the same year as the adenoma-carcinoma sequence [3] it is only comparatively recently that an understanding of their role in colorectal carcinogenesis and the molecular pathways that underlie their transformation has been established. An emerging body of evidence suggests that serrated pathway colorectal neoplasms represent a distinct clinicopathological subtype, which has implications both for the management of pre-malignant serrated pathway lesions and established carcinoma. Whilst pre-malignant sessile serrated lesions can be appropriately managed by polypectomy with subsequent colonoscopic surveillance, and invasive carcinoma confined to the colorectum by surgical resection of the affected colonic segment, it remains the case that a significant cohort of patients present at the time of diagnosis with metastatic disease, or develop recurrence after prior surgical treatment with curative intent. To date, the treatment of metastatic colorectal carcinoma has involved little in the way of targeted therapies, and all current chemotherapeutic treatments are considered palliative. There is therefore a clear need for better understanding of the molecular events driving the serrated pathway of colorectal carcinogenesis.

1.1.2 Classification of serrated lesions

The classification of serrated lesions is complex and there is a lack of concordance even amongst expert gastrointestinal pathologists in the reporting of colonic serrated lesions [4]. This has significant clinical importance in the context of colorectal cancer screening programmes given the variable risk of progression to invasive carcinoma of these lesions. Below, the classification of serrated lesions is reviewed.

The most common serrated neoplasm encountered in clinical practice is the "hyperplastic polyp". Hyperplastic polyps account for 25-30% of colonic polyps, with an estimated prevalence in adults of 10-15% [5-8]. Hyperplastic polyps are generally <5mm in diameter, and whilst the majority (88%) are located in the rectosigmoid, are found throughout the colon [9]. Hyperplastic polyps frequently possess mutations in *KRAS* (6-16.5%) or *BRAF* (62-69.6%) [10,11]. Despite a high frequency of oncogenic mutations, hyperplastic polyps are traditionally regarded as having no malignant potential. In this regard, they might be considered similar to melanocytic nevi, which also exhibit a high frequency of *BRAF* or *NRAS* mutations [12]. Recent North American guidance however does propose interval colonoscopy at ten years in asymptomatic patients with any number of hyperplastic polyps and at five years in patients with ≥ 4 hyperplastic polyps proximal to the sigmoid colon and ≥1 hyperplastic polyps of ≥ 10mm in diameter because of a perceived increased risk of colorectal cancer development [13].

"Sessile serrated adenomas" (SSA/P) also termed "sessile serrated lesions" (SSL) can be difficult to differentiate from the microvesicular subtype of hyperplastic polyp [14]. They are reported to be detected in between 1.7-9% of patients undergoing colonoscopy. Similar to hyperplastic polyps, they have a high rate of *BRAF* mutation (60.9-92.7%), and are more common in women. In contrast to hyperplastic polyps, approximately 75% of SSA/P are located in the proximal colon and tend to be larger than hyperplastic polyps (>64% are greater than 5mm). Unlike hyperplastic polyps, SSA/P are widely believed to possess malignant potential. [15-19]. Approximately 13.2% of SSA/P exhibit dysplasia, which confers a high risk of malignant transformation [16], and it is proposed that adenocarcinoma develops rapidly in this pathway [19-21].

"Traditional serrated adenomas" (TSA) are uncommon lesions, with a prevalence of around 0.6-0.7% [15,22]. In contrast to SSA/P, TSA are predominantly located in the left colon, and exhibit a tubulovillous rather than sessile morphology [23]. Mutations in *KRAS* are detected in 29% of TSA and associated with high-grade dysplasia and intramucosal carcinoma. Whilst *BRAF* mutations are detected in 55% of TSA, they have been associated with low-grade dysplasia [24].

Serrated carcinomas are most commonly found in the right colon (52%) and rectum (33%) and are more common in women [25]. Tumours arising from serrated pre-cursors often lose their serrated morphology, and only a third of carcinomas arising through this pathway exhibit serrated morphology [14].

1.1.3 The serrated pathway in the wider colorectal cancer context

Several classification systems for colorectal cancer have been proposed. Jass proposed a system of classification for colorectal cancers which combined morphological and molecular features of colorectal cancers, proposing five distinct groups of colon cancer [2]. These are summarised in Table 1-1. Importantly, this classification system highlighted the molecular heterogeneity of colorectal cancers, and related these to morphological features, including serration, lending weight to the concept that serrated cancers might arise via a different pathway.

Table 1-1 Jass classification system for colorectal cancer

Summary of Jass classification system for colorectal cancer. SP = serrated polyp; Ad = adenoma CIN = chromosomal instability; MSI-H = microsatellite instability-high; MSI-L= microsatellite instability-low; MSS = microsatellite stable; CIMP-H = CpG island methylator phenotype-high; CIMP-L = CpG island methylator phenotype-low; CIMP-N = CpG island methylator phenotype-negative. Adapted from Jass [2]

Subgroup	MSI	CIN	CIMP	*APC*	*BRAF*	*KRAS*	Precursor	Incidence
1	MSI-H	-	CIMP-H	+/-	+	-	SP	12%
2	MSS/ MSI-L	-	CIMP-H	+/-	+	+	SP	8%
3	MSS/ MSI-L	+	CIMP-L	+	-	+	Ad/SP	20%
4	MSS	+	CIMP-N	+	-	+	Ad	57%
5	MSI-H	-	CIMP-N	+	-	+	Ad	3%

More recent molecular-based classification systems lend further support to the existence of a molecularly distinct serrated pathway to carcinogenesis. Two recent papers have attempted to classify colon cancers by molecular subtypes. The first of these defined three colon cancer molecular subtypes (CCS 1-3) using an unsupervised consensus-based clustering technique. Using gene-expression data from sessile-serrated adenomas and principal-component analysis, CCS3 tumours were demonstrated to most likely arise from serrated precursors. Significantly, CCS3 tumours were enriched for histologically poorly-differentiated tumours, exhibited significantly reduced disease-free survival (>50% developed recurrence within two years) and resistance to cetuximab [26]. More recently, four consensus-molecular subtypes of colorectal cancer have been defined [27]. These are summarised in Table 1-2. Using this classification system, serrated pathway tumours might

largely be considered to be CMS1 (MSI-immune) as these tumours are *BRAF*-mutant, MSI-H and CIMP-H: each a feature associated with serrated colorectal carcinogenesis. This is however an over-simplification as CMS3 (Metabolic) tumours are *KRAS*-mutant and CIMP-L (also features of some serrated precursors). Furthermore, whilst 70% of *BRAF* mutant tumours are CMS1, 2% were CMS2, 5% CMS3 and 17% CMS4.

Table 1-2 Consensus molecular subtypes of colorectal cancer

The consensus molecular subtypes of colon cancer are summarised together with their reported incidence and associated clinical and molecular features. Adapted from Guinney et al. [27]

Consensus Molecular Subtype	Incidence	Clinical and Molecular Features
1 (“MSI immune”)	14%	MSI, CIMP-H, hypermutation, *BRAF* mutation, immune cell infiltration, low incidence of SCNA, female preponderance, proximal colonic location
2 (“Canonical”)	37%	CIMP-N, MSS, high frequency of SCNA, epithelial-type, Wnt & Myc activation, male preponderance, distal colonic location
3 (“Metabolic”)	13%	Mixed MSI status, CIMP-L, *KRAS* mutation, low frequency of SCNA, metabolic dysregulation
4 (“Mesenchymal”)	23%	CIMP-N, high frequency of SCNA, stromal infiltration, TGFβ activation, angiogenesis

1.2 Mechanisms of serrated pathway colorectal neoplasia

An understanding of the molecular events underlying neoplastic transformation in the serrated pathway is principally informed by *in vitro* studies and modelling of the disease in the murine intestine, together with correlative *in situ* data from human cancers. The principle molecular event associated with the serrated pathway of colorectal neoplasia is thought to be the development of an activating mutation in the RAS-RAF-MEK-ERK signalling pathway (Figure 1-1) with subsequent activation of oncogene-induced senescence-like tumour suppressive mechanisms, which are suppressed during tumour progression. Wnt pathway activation, a CpG island methylator phenotype (CIMP) and microsatellite instability are also associated with this pathway to colorectal cancer, and these are reviewed below.

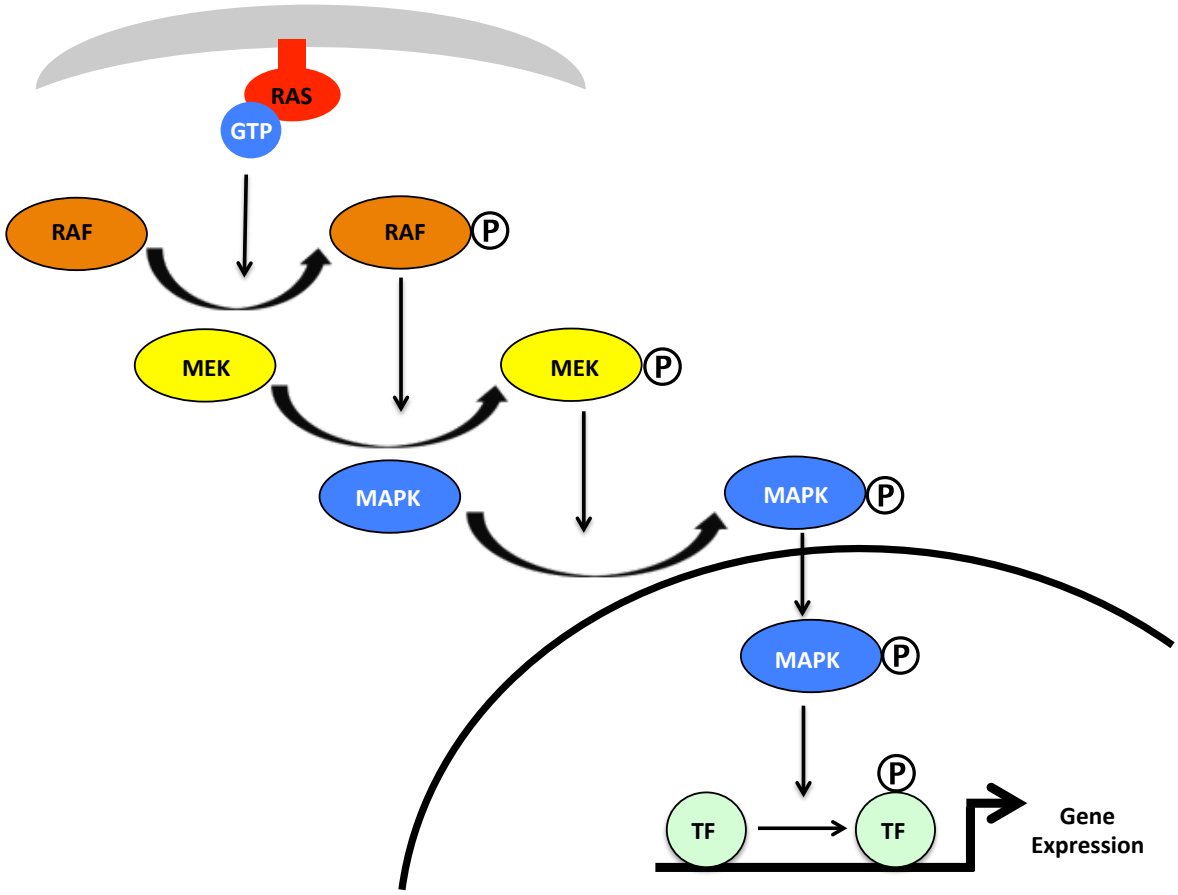

Figure 1-1 RAS-RAF-MEK-ERK (MAPK) signalling cascade[1]

Diagrammatic overview of the RAS-RAF-MEK-ERK (MAPK) signalling cascade. GTP-binding results in a conformational change in RAS, with subsequent activation. RAS activation leads to activation of the downstream serine/threonine kinase, RAF. Activated RAF phosphorylates MEK with subsequent activation. Similarly, phosphorylated-MEK (pMEK) phosphorylates MAPK (aka ERK). Phosphorylated MAPK (pMAPK) translocates to the nucleus where it results in phosphorylation and activation of transcription factors, with resultant activation of MAPK signalling pathway target genes.

[1] Figure and text adapted from Pecorino, L. *Molecular Biology of Cancer: Mechanisms, Targets and Therapeutics* 4e; Oxford; Oxford University Press; 2016; pp84-86

1.2.1 *BRAF* and evidence for an oncogene-induced senescence pathway in serrated pathway carcinogenesis

BRAF is a member of the RAF family of kinases and is mutated in around 7% of human carcinomas (including melanoma, thyroid, ovarian, colorectal and non-small cell lung cancer) with the highest incidence being in malignant melanoma. The most common *BRAF* mutation in human cancers is the T → A substitution at nucleotide 1796. This results in conversion of valine 600 to glutamate [28]. The mutation was originally defined as $BRAF^{V599E}$, though following revised sequencing data (NCBI accession number NM_004333.2), a missing codon was demonstrated in the original sequence, with resultant C-terminal shift of one position of all amino acids following position 32. The mutation was therefore renamed $BRAF^{V600E}$ [29-31]. V600E is an activating mutation, which results in significantly enhanced kinase activity, and induces transformation in NIH3T3 cells and promotes transformation of immortalised human diploid fibroblasts [28,30,32]. Furthermore, mutant-$BRAF^{V600E}$ induces a transformed phenotype in MEFs [33]. Conversely, mutational activation of the RAS-RAF-MEK-ERK pathway in untransformed primary cells has been demonstrated to induce an oncogene-induced senescence phenotype. RAF has been demonstrated to induce oncogene-induced senescence in primary human fibroblasts, though in contrast to RAS-induced senescence, cells typically arrest in G2/M rather than G1, and do not exhibit upregulation of p53/p21 [30,34,35]. In further contrast to RAS-induced senescence, whilst RAF-induced senescence is associated with upregulation of $p16^{INK4A}$ expression, it has been demonstrated that expression of the latter is not required for the maintenance of RAF-induced senescence [30,36]. Furthermore, *BRAF* mutations are detected in pre-malignant lesions, such as melanocytic naevi and sessile serrated lesions in the colon [10,12,30,37,38].

Activating *BRAF* mutations are detectable in 10-20% of human colorectal adenocarcinomas [39-43]. *BRAF* mutations are mutually exclusive with *KRAS* mutations [39,44]. *BRAF* mutations develop early in the progression of serrated pathway neoplasia, and are detectable in pre-malignant lesions [45]. Until recently, the ability of mutant-$BRAF^{V600E}$ to drive intestinal tumourigenesis had not been demonstrated mechanistically, and the induction of senescence by mutant-$BRAF^{V600E}$ and the presence of $BRAF^{V600E}$ mutations in pre-malignant lesions is suggestive of a model where additional molecular events are necessary for tumourigenesis. The ability of $BRAF^{V600E}$ to act as a founder mutation in serrated pathway intestinal tumours has been demonstrated *in vivo* in murine models [46,47].

The first murine study to examine the effects of oncogenic *Braf*^{V600E} in the intestine used the *AhCreEr*^{T} model system crossed to the conditional ^{LSL}*Braf*^{V600E} allele. In this model, recombination occurs in both the small intestine and colon, although recombination also occurs in non-intestinal tissues (including bladder, liver and stomach). *Braf*^{V600E} mutation in the intestine was found to result in an initial period of hyperproliferation, characterised by hyperplastic crypts. This initial proliferative burst was followed by crypt senescence, with upregulation of p16^{INK4A} and senescence-associated-β-galactosidase as well as phospho-H2AX (γH2AX). Proliferation (assayed by immunohistochemistry for phosphorylated-H3 and BrdU) was almost completely undetectable in senescent crypts. Other senescence markers, including p53, p21^{WAP} and p19^{ARF} were not detected in senescent crypts. Crypt senescence was not sustained, and mice developed tumours which were proliferative, and exhibited repression of p16^{INK4A}. The phenotype was drastically accelerated when the *AhCreEr*^{T};^{LSL}*Braf*^{V600E} mice were crossed to *Cdkn2a*$^{\Delta Ex2,3/\Delta Ex2,3}$ mice, in which crypt senescence was not observed, supporting a crucial role for p16^{INK4A} in tumour suppression. Silencing of *Cdkn2a/Ink4a* associated with tumour progression was demonstrated to be associated with CpG methylation of exon 1 [47].

The ability of activated oncogenic BRAF^{V600E} to induce serrated pathway tumours in mice was confirmed in a subsequent model in which the conditional ^{LSL}*Braf*^{V637E} allele (the resultant missense mutant protein is the murine equivalent of the BRAF^{V600E} mutant in humans) was crossed to the *villin-Cre* allele, with resultant *Cre* recombination in the small intestine and colon from before birth. Like in the *AhCreEr*^{T};^{LSL}*Braf*^{V600E} model, activated *Braf*^{V637E} was associated with crypt hyperplasia and villous serration, though crypt senescence in early stage hyperplasias was not demonstrated. The lesions exhibited similarities to human hyperplastic polyps, and were termed murine serrated hyperplasia (mSH). As the *villin-Cre* system circumvents the extraintestinal phenotypic manifestations associated with *AhCreEr*^{T}, the full continuum of serrated carcinogenesis was demonstrated in this model, with the development of dysplastic lesions (termed mSA-LGD and mSA-HGD) and eventual progression to invasive carcinoma in some mice. Morphologically, *Braf*^{V637E}-induced mSA-LGD and mSA-HGD lesions had characteristics of traditional serrated adenoma rather than sessile serrated adenoma, though histological comparison was complicated by the majority of tumours being in the small intestine, compared to the corresponding lesions in humans, where disease occurs in the colon. Upregulation of p16^{INK4A} was not demonstrated in "healthy" *Braf*-mutant mucosa when compared to *Braf*-WT mucosa, but significant upregulation of p16^{INK4A} was demonstrated in mSA-LGD and mSA-HGD lesions, with this being most pronounced in mSA-HGD lesions. Unlike in the

AhCreER^{T};^{LSL}*Braf*^{V600E} model, p16^{INK4A} upregulation was not associated with proliferation arrest. Furthermore, whilst crossing to a *p16*^{Ink4a} allele led to a significant increase in invasive carcinoma, it did not significantly increase the number of mSAs. Furthermore, CpG methylation of the *Cdkn2a/Ink4a* promoter was demonstrated in a subset of *Braf*^{V637E}-induced mSA-HGD and carcinomas. Whilst this supports the model of a tumour-suppressive role for p16^{INK4A} in serrated neoplasia, it would suggest that it has a less critical role in dysplasia. In further contrast to *AhCreEr*^{T};^{LSL}*Braf*^{V600E} model, *VilCre*;^{LSL}*Braf*^{V637E} mice exhibited activation of the p53/p21 pathway during tumour progression. Activated p53 was not demonstrated in mSH and was infrequently detected in mSA-LGD. Activated p53 was detected in 97% of mSA-HGD however. The role of a p53-mediated tumour suppressor program was further demonstrated by crossing *VilCre*;^{LSL}*Braf*^{V637E} to *p53*$^{LSL\text{-}R172H}$ mice. The resultant *VilCre*;^{LSL}*Braf*^{V637E};*p53*$^{LSL\text{-}R172H}$ mice developed mSA with the same frequency as *Tp53* WT mice, though developed invasive carcinoma with much higher frequency than *Tp53* WT mice, suggesting that the p53-pathway has a tumour-suppressive role, but does not prevent dysplasia [46].

Whilst both murine models differ in certain critically important aspects, together they are broadly supportive of an oncogene-induced senescence-like tumour suppressive barrier in serrated pathway carcinogenesis, and this is supported by various *in situ* data. Alterations in p16^{INK4A} expression have been demonstrated in human serrated pathway carcinogenesis. Expression and promoter hypermethylation of *CDKN2A/INK4A* have been characterised in *BRAF*-mutant serrated pathway lesions. In normal colonic mucosa, p16^{INK4A} was undetectable. By contrast, p16^{INK4A} expression was demonstrated in 100% of hyperplastic polyps and 86% of sessile serrated adenomas, but was absent in invasive carcinoma. These sequential expression changes in p16^{INK4A} were demonstrated to correlate with promoter hypermethylation: hypermethylation of the *CDKN2A/INK4A* promoter was not demonstrated in normal tissue, but was present in 100% of carcinomas. Furthermore, high p16^{INK4A} expression was associated with absent Ki67 positivity, suggesting that p16^{INK4A} mediates proliferation arrest [48]. Subsequent studies have independently reported dysregulated p16^{INK4A} expression in serrated carcinogenesis. In a study of traditional serrated adenomas, p16^{INK4A} staining was present in 74% of non-dysplastic, but only 45% of dysplastic, *BRAF*-mutant TSA [49]. A further immunohistochemical study examined 137 sessile serrated adenomas specimens exhibiting either dysplasia or carcinoma with adjacent non-dysplastic SSA. *BRAF* was mutated in 92.7% of the specimens examined. Loss of p16^{INK4A} expression was demonstrated in 9% of non-dysplastic SSA and 43% of dysplastic/carcinoma components, and was pronounced at the interface between HGD and

carcinoma, supporting a tumour-suppressive function, though in this study, $p16^{INK4A}$ loss was not correlated with its promoter methylation [19].

These latter two studies also examined p53 expression in *BRAF*-mutant TSA and SSA. Interestingly, this was broadly concordant with the pattern of p53 expression reported in *VilCre;Braf*^{V637E} driven murine serrated neoplasia [46]. In *BRAF*-mutant TSA, p53 staining was positive in 7% of non-dysplastic TSA, compared to 45% of dysplastic *BRAF*-mutant TSA [49]. Furthermore, p53 was detected in 14% of dysplastic SSA but was absent in non-dysplastic SSA. Furthermore, p53 positivity was significantly associated with MSS, consistent with previous reports [19,50].

Loss of function mutations in key regulators of oncogene-induced senescence (both the $p16^{INK4A}$-Rb and ATM-ATR-DDR pathways) have also been demonstrated in individuals with hyperplastic polyposis syndrome, a rare condition in which individuals develop multiple SSA lesions. 90% of the individuals in this study harboured a *BRAF*^{V600E} mutation [51].

1.2.2 *KRAS* and evidence for an oncogene-induced senescence pathway in serrated pathway carcinogenesis

Mutationally active *RAS* genes were first reported in human cancer cell lines in 1982 [52-54]. Subsequently, elevated expression of human RAS family members were recognised in colorectal cancer, and adenomas [55]. Three human RAS genes were subsequently identified: *HRAS*, *NRAS* and *KRAS* [56]. Mutational activation of the RAS pathway is now recognised as a common event in a multitude of cancers. *KRAS* is the most commonly mutated of the three RAS family members in human cancer, with the highest incidence in pancreatic, cholangiocarcinoma and colorectal cancers [57]. *HRAS*^{V12} was demonstrated to be transformative in fibroblasts, though only in the context of immortalisation by carcinogens or oncogenes: so-called oncogenic cooperation [58-60]. The ability of RAS proteins to transform primary epithelial cells *in vitro* in the context of a cooperating oncogene was subsequently confirmed [61,62]. By contrast, activated RAS alone has been demonstrated to trigger oncogene-induced senescence: with proliferation arrest in G1, associated with upregulation of p53 and $p16^{INK4A}$ and expression of SA-β-galactosidase. This was first demonstrated in the context of activated $HRAS^{V12}$ [63]. Furthermore, *RAS* mutations are detectable in premalignant lesions such as melanocytic naevi and sessile serrated lesions in the colon [10,38,64-68].

A number of murine studies have examined the ability of *Kras* mutations to drive intestinal tumourigenesis, though until recently, none had specifically related this to oncogene-induced senescence or the serrated pathway. Janssen et al. [69] reported intestinal tumours in *VilCreER^{T2};Kras^{V12G}* mice, and these were predominantly located in the small intestine (93%). By contrast, Sansom et al. [70] demonstrated that whilst *Kras^{V12G}* mutation accelerated intestinal tumourigenesis in the context of *Apc* loss, alone it was insufficient to induce intestinal tumourigenesis. Similarly, KRAS^{G12D} expression in the murine intestine was shown to be insufficient to result in tumourigenesis, but did induce a crypt hyperplasia phenotype in the colon, characterised by crypt lengthening and prominent goblet cells [71]. A similar colonic hyperproliferative phenotype with prominent goblet cells, was demonstrated in a subsequent study in *VilCre;^{LSL}Kras^{G12D}* mice, in which *Kras* mutation alone was once again demonstrated to be insufficient to induce tumours [72].

A recent study specifically addressed the ability of oncogenic KRAS to induce serrated pathway carcinogenesis. *VilCre;Kras^{G12D}* mice developed a pan-colonic serrated phenotype, termed murine serrated hyperplasia (mSH). *VilCre;Kras^{G12D}* mice did not develop colonic tumours, and exhibited features consistent with oncogene-induced senescence. Increased senescence-associated-β-galactosidase positivity, Dec1 and p16^{INK4A} expression were demonstrated, though p53 and p19^{ARF} were not detected. Additionally, in *VilCre;Kras^{G12D}* mice, upregulation of p16^{INK4A} and OIS were detectable 21 days post-induction, and this was associated with absent BrdU positivity. Consistent with the observed OIS phenotype, a critical tumour-suppressive role of p16^{INK4A} in *Kras*-driven serrated neoplasia was demonstrated by generating *VilCreER^{T2};Kras^{G12D};Ink4a/Arf$^{-/-}$* mice. These developed lesions resembling human TSA in the proximal colon. These exhibited absent senescence-associated-β-galactosidase positivity, and were proliferative. A significant proportion of these lesions progressed to invasive carcinoma. Conversely, intestine-specific *Tp53* deletion did not accelerate the colonic phenotype in *VilCreER^{T2};Kras^{G12D}* mice or promote colonic tumourigenesis [66].

KRAS mutations develop early in the serrated pathway, and are detectable in hyperplastic polyps [38,68]. In a small cohort of *KRAS*-mutant serrated lesions, p16^{INK4A} was demonstrated to be upregulated in serrated neoplasms [73]. In common with *BRAF*-mutant serrated lesions, p16^{INK4A} positivity has also been noted in *KRAS*-mutant TSA, but a loss of p16^{INK4A} positivity is much less tightly associated with dysplasia and invasion in *KRAS*-mutant TSA than *BRAF*-mutant TSA. Ki67 positivity is significantly higher in advanced TSA than TSA, but no formal analysis of the relationship between this and p16^{INK4A} was

made. By contrast, whilst non-dysplastic TSA were negative for p53, 70% of advanced TSA exhibited p53 positivity [49]. In serrated tubulovillous adenoma, which has been proposed as a precursor to *KRAS*-mutant MSS colorectal cancer, there is a non-significant trend to higher $p16^{INK4A}$ expression in HGD compared to LGD. By contrast, progression from LGD to HGD in this subgroup of tumours is associated with a significant increase in p53 positivity [74]. The *in situ* evidence therefore is broadly supportive of a *KRAS*-mediated, oncogene-induced senescence-like barrier in serrated neoplasia, though the human data are somewhat contradictory to the murine *Kras*–driven serrated neoplasia data, which support the primacy of $p16^{INK4A}$- over p53-mediated tumour suppression in this pathway to carcinogenesis [66].

1.2.3 Wnt pathway activation

The Wnt signalling pathway is a highly conserved signalling pathway of considerable importance in human colorectal adenocarcinoma. A summary of the Wnt signalling pathway is given in in Figure 1-2. Evidence of Wnt pathway activation has been demonstrated in murine models of *Braf*-induced serrated colorectal neoplasia. In $AhCreEr^{T};^{LSL}Braf^{V600E}$ mice, Wnt pathway activation was demonstrated in intestinal crypts during the initial hyperproliferative phase, but conversely, was suppressed in senescent crypts. In this model, Wnt pathway activation was associated with MAPK-dependent, AKT-independent phosphorylation of serine 9 of GSK3β [47]. Wnt pathway activation was also demonstrated in $VilCre;^{LSL}Braf^{V637E}$ mice, though in this model system, was only demonstrable in mSA-HGD and carcinoma and in a single mSA-LGD, but not in mSH or histologically normal intestine from $Braf^{V637E}$ mice. Furthermore, mutations in Wnt pathway genes were demonstrated in a significant number of murine $Braf^{V637E}$ carcinomas, though the most commonly mutated genes (*Apc*, *Ctnn1b* and *Lrp1b*) have not been linked mechanistically with the serrated pathway in human colon cancer [46]. In a further murine model of *Braf*-induced serrated neoplasia, activated oncogenic BRAF was demonstrated to lead to stem cell depletion in the intestine with conversion of ISC into TA cells. Whilst mutant-BRAF activation was associated with upregulation of DNA damage markers, other features of oncogene-induced senescence were not observed in this model. This BRAF-driven stem cell depletion was however rescued (both *in vitro* and *in vivo*) by activated Wnt signalling. This model presents a somewhat different role for Wnt signalling in serrated neoplasia: namely a requirement for dual activation of both Wnt signalling and MAPK signalling to maintain ISC and hence tumour viability in BRAF-driven tumours and prevent clonal elimination [75]. By contrast, in *Kras*-induced murine serrated pathway

neoplasia, evidence for activated Wnt signalling has not been demonstrated. Wnt signalling is not detectable in *Kras*-induced murine serrated cancers, which do not exhibit *Apc* mutations, and demonstrate membranous β-catenin staining [66].

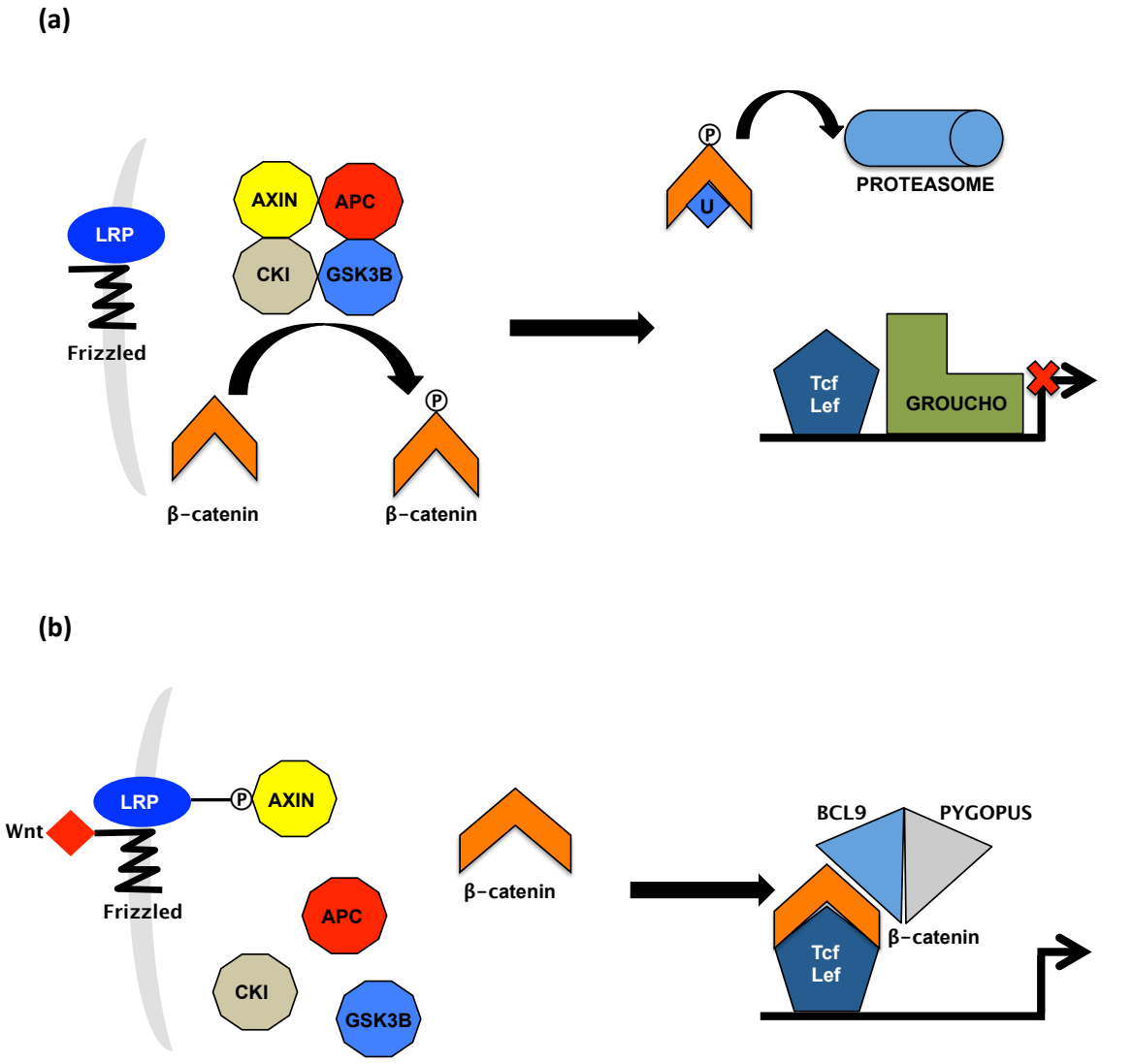

Figure 1-2 The Wnt signalling pathway[2]

Diagrammatic overview of the Wnt signalling pathway. **(a)** In the absence of the Wnt ligand, a degradation complex exists, comprising Axin, APC, GSK3β and CKI. The two latter proteins are serine/threonine kinases, and phosphorylate β-catenin. Phosphorylated β-catenin is further modified by ubiquitination, which results in its targeting for degradation in the proteasomes. Consequently, β-catenin is not present in the nucleus to bind to the Tcf/Lef transcription factor. In the absence of β-catenin, Tcf associates with the transcription-repressor Groucho, with resultant transcription repression of Wnt target genes. **(b)** The Wnt ligand binds to the transmembrane Wnt receptor Frizzled and its co-receptor LRP. Binding of the Wnt ligand to Frizzled/LRP results in a conformational change, resulting in GSK3β- and CKI-mediated phosphorylation of LRP. Phosphorylated LRP recruits Axin, with resultant disruption of the Axin-APC-GSK3β−CKI degradation complex. In the absence of the Axin-APC-GSK3β−CKI degradation complex, β-catenin remains unmodified, and is not targeted for proteasomal degradation. β-catenin migrates to the nucleus, where it binds to the Tcf/Lef transcription factors to induce expression of Wnt target genes. Activation of Wnt target genes also requires the nuclear proteins Bcl9 and Pygopus.

[2] Figure and text adapted from Pecorino, L. *Molecular Biology of Cancer: Mechanisms, Targets and Therapeutics* 4e; Oxford; Oxford University Press; 2016; pp183-184

The contribution of Wnt signalling to human serrated pathway cancer is less clearly defined. Whilst Wnt pathway activation is present in 93% of colorectal cancers, *APC* and *BRAF* mutations are anticorrelated, but not mutually exclusive. Moreover, *APC* mutations are infrequent in serrated adenomas, and it was initially hypothesised that serrated pathway carcinogenesis did not involve Wnt signalling [2,40,76-79]. This early view was however refuted when subsequent studies demonstrated aberrant, nuclear localisation of β-catenin in serrated lesions. Nuclear β-catenin has been reported in both TSA and SSA/P. The majority of these studies report absent nuclear β-catenin staining in hyperplastic polyps, and positive nuclear β-catenin in SSA/P and TSA, though there is wide variation in the reported incidence of nuclear β-catenin localisation in these lesions [80-82]. Furthermore, nuclear β-catenin labelling is demonstrable more frequently in dysplastic compared to non-dysplastic serrated lesions, implying a role for Wnt signalling in disease progression [19,83]. Indeed, in one study, nuclear β-catenin staining was demonstrated exclusively in SSA/P with dysplasia or carcinoma [84]. Nuclear β-catenin localisation in SSA/P has also been associated with *BRAF* mutation [81]. Nuclear β-catenin localisation in serrated lesions is typically not associated with mutations in *CTNNB1*, and *BRAF*-mutant cancers infrequently possess an *APC* mutation, implying that Wnt pathway activation in serrated pathway lesions arises in a mechanism distinct from that of cancers arising through the adenoma-carcinoma sequence [81,85]. Whilst the aforementioned studies are supportive of a role of Wnt signalling in serrated neoplasia, the literature on Wnt signalling in the serrated pathway remains conflicted, and a recent study demonstrated a very low incidence of β-catenin nuclear positivity in sporadic MSI-H colon cancers (which are proposed to arise through the serrated pathway) [86].

The strong association of serrated pathway lesions with a CpG island methylator phenotype (CIMP) has led to exploration of epigenetic regulatory mechanisms of Wnt signalling in this pathway. Promoter hypermethylation of secreted frizzled related proteins (SFRPs) has been demonstrated to activate Wnt signalling in colorectal cancer, and is detectable in a significant proportion of colorectal cancers. Moreover *SFRP* methylation was demonstrated in aberrant crypt foci, which typically lack *APC* mutations, suggesting that this is an early event in colorectal carcinogenesis, though this study did not specifically address serrated pathway tumours [87]. More recent studies have examined promoter DNA methylation of Wnt regulators in the specific context of serrated neoplasia. Hypermethylation of *APC* promoter 1A has been reported in serrated polyps and associated with Wnt pathway activation, though interestingly *APC* promoter methylation has previously shown to be inversely correlated with *BRAF* mutation [76,88]. Promoter

methylation of the Wnt antagonists *DKK1* and *SFRP1* has been examined in a large cohort study of over 1000 colorectal cancers. Promoter methylation of *DKK1* was strongly correlated with MSI and $BRAF^{V600E}$ mutation (common features of serrated cancers) whereas *SFRP1* promoter methylation demonstrated an anti-correlation with MSI [89]. Promoter methylation of *WNT5A* is associated with silencing of its expression and Wnt pathway activation, and has also been reported in colorectal cancer [90]. *WNT5A* promoter methylation exhibits strong correlation with $BRAF^{V600E}$ mutation and MSI (both features of serrated pathway cancers) [91]. A further study examined promoter methylation of a number of Wnt regulators at various stages of the serrated neoplasia pathway, and compared these to traditional adenomas. This study also compared β-catenin staining in these lesions. Notably, whilst nuclear β-catenin positivity was demonstrated in serrated lesions, it was less marked than in traditional adenomas, though increased nuclear β-catenin expression was associated with dysplasia and intramucosal carcinoma in serrated lesions. Promoter methylation of *AXIN2*, *MCC* and *SFRP4* were detected more frequently in serrated lesions than traditional adenomas, and increasing methylation was associated with progression through dysplasia to intramucosal carcinoma. Both *AXIN2* and *MCC* methylation correlated significantly with nuclear β-catenin positivity [92]. This is consistent with earlier reports, demonstrating significantly higher levels of promoter methylation of *MCC* and *SFRP4* in serrated lesions compared to traditional adenomas [93,94]. *AXIN2* demonstrated incremental increases in promoter methylation from SSA/P to intramucosal carcinoma, though intriguingly was significantly anticorrelated with *BRAF* mutation despite having previously been associated with MSI [92,95].

In addition to epigenetic regulators of Wnt signalling, mutations in Wnt pathway genes have been reported in serrated colorectal cancers, and exhibit increasing frequency in serrated pathway cancers when compared to SSA/P and TSA [40,96]. A number of recent studies have linked Wnt pathway activation in serrated neoplasia to *RNF43* mutations. A high frequency of *RNF43* mutations has been reported in colorectal cancer, and these exhibit mutual exclusivity with *APC* mutations [97]. RNF43 is an E3 ubiquitin ligase which is a Wnt antagonist which negatively regulates frizzled receptor expression by ubiquitination [98]. Wild type RNF43 is an inhibitor of both canonical and non-canonical Wnt signalling. By contrast, mutant RNF43 loses its cell surface localisation and accumulates in the endoplasmic reticulum, leading to a failure of internalisation of Frizzled and thus promotes canonical Wnt signalling but inhibits non-canonical Wnt signalling, promoting tumourigenesis [99]. RNF43 has also been demonstrated to bind to TCF4 and sequester it to the nuclear membrane, with associated reduction in mRNA expression of its

targets (including AXIN2, TWIST, LGR5 and MMP7). Furthermore, functional studies of RNF43 mutants revealed that these prevent binding to TCF4, and impair its Wnt inhibitory function [100]. An association between *RNF43* mutations and serrated pathway colon cancer was first described in the context of the rare hereditary serrated polyposis syndrome [51]. A subsequent study demonstrated *RNF43* mutations in sporadic serrated lesions, with a reported frequency of 6% in SSA/P and 24% in TSA. By contrast, *RNF43* mutations were not detected in hyperplastic polyps or traditional adenomas [101]. In a further independent study, similar rates of *RNF43* mutations were described in sporadic serrated lesions: 10% in SSA/P, 28% in TSA and 29% in *BRAF*-mutant serrated carcinoma. Furthermore, once again an absence of *RNF43* mutations was confirmed in tubulovillous adenomas [102]. Furthermore, a significant association between *RNF43* mutations and both *BRAF* mutation and *MLH1* methylation has been reported [103].

1.2.4 Microsatellite instability

During DNA replication, the DNA mismatch repair system is responsible for the recognition and correction of base-pair mismatch. Microsatellites are short (1-6bp) repeating DNA sequences distributed across the genome, and are consequently prone to replication errors. Microsatellite instability (MSI) represents a phenotype of genetic hypermutability and is driven by deficient mismatch repair activity. MSI is present in approximately 15% of colorectal cancers [104]. Several diagnostic panels have been described to diagnose MSI in colon cancer. Boland published a panel of five MSI loci in 1998: BAT25, BAT26, D5S346, D2S13 and D17S250. Tumours were classified as either MSI-high (≥2 markers), MSI-low (1 MSI marker) or MSS (no instability) [105]. A further, modified panel of five markers (BAT25, BAT26, NR21, NR24 and NR27) was subsequently described, and included in the revised Bethesda guidelines [106]. This so-called “pentaplex” panel was demonstrated to exhibit similar specificity and sensitivity for MSI detection except for MSI-L [107].

Much of the original work on MSI focussed on Lynch syndrome (HNPCC or hereditary, non-polyposis colorectal cancer), a familial colon cancer syndrome caused by germline mutations in MMR proteins (MLH1, MSH2, MSH6 and PMS2) [108-110] though two of the three original descriptions published in 1993 were made in non-hereditary cancer specimens [111,112]. As only approximately 2% of colon cancers are attributable to HNPCC [110] it became apparent that the majority of MSI occurred sporadically. Sporadic MSI has been demonstrated to be associated with bialleic promoter-methylation (with

resultant loss of expression) of *MLH1* and this was subsequently proposed to explain the close association with CIMP (CpG island methylator phenotype) [113-115]. Another defining characteristic of sporadic MSI is a high frequency of $BRAF^{V600E}$ mutations [39,116-118]. MSI-H tumours exhibit a low frequency of *KRAS* mutations and a low incidence of *APC* mutations, whereas MSI-L tumours exhibit a higher frequency of *KRAS* mutations [119]. Thus, MSI is correlated with various molecular features of serrated neoplasia. MSI was in fact reported relatively early to be associated with serrated colorectal neoplasms (predating much of the mechanistic data which explains the association of MSI and serrated pathway lesions). Serrated polyps were noted to be detected more commonly in the resected specimens of patients with MSI cancers than MSS cancers [120]. Tuppurainen et al. [121] examined MSI in both serrated and non-serrated colorectal carcinomas, and demonstrated more frequent MSI in serrated (45.2%) compared to non-serrated (8.2%) cancers. Furthermore, MSI was noted to increase in frequency from hyperplastic polyps (29%) to serrated adenomas (53%) [122]. Similarly, Hawkins et al. reported MSI in both hyperplastic polyps and serrated adenomas [120]. A number of other studies have examined the presence of MSI in serrated precursor lesions, but failed to confirm these findings. Hiyama et al. reported a low frequency of MSI in both serrated adenoma (5%) and serrated adenocarcinoma (10%) [123]. A similarly low incidence of MSI in serrated adenoma was reported by Sawyer et al. who reported an incidence of MSI of 5% in a cohort of serrated adenomas that included dysplastic lesions [124]. A larger and more contemporary series is supportive of a late development of MSI in the serrated pathway. Whilst MSI was demonstrated in 81% of serrated adenocarcinoma, MSI was not detected in hyperplastic polyps or serrated adenomas [125]. Furthermore, in a large cohort of serrated adenomas, loss of MLH1 was not seen in non-dysplastic SSA/P, but was detected in 75% of SSA/P with dysplasia or carcinoma [19].

The murine data largely mirror the *in situ* data with regards to the timing and molecular associations of MSI in serrated pathway neoplasia. $Braf^{V637E}$-driven murine serrated hyperplastic lesions have been demonstrated to be MSS or MSI-L, whereas dysplastic serrated neoplastic lesions and carcinomas induced by murine $Braf^{V637E}$ were commonly MSI-H [46]. By contrast, KRAS-driven murine serrated cancers were predominantly MSI-L or MSS, with only one tumour exhibiting MSI-H [66].

1.2.5 RAC1b overexpression

An additional molecular feature of serrated lesions exhibiting *BRAF* mutation, (but to a much lesser extent in those exhibiting *KRAS* mutation) is overexpression of the *RAC1* splice variant RAC1b, which is present in approximately 81.8% of *BRAF*-mutant colon cancers (compared to 12.5% in *KRAS*-mutant tumours) [126]. Similarly, in papillary thyroid cancer, a strong association between $BRAF^{V600E}$ mutation and RAC1b over-expression has been reported [127]. RAC1b has been demonstrated to promote cell cycle progression through activation of NF-κB [128,129]. Depletion of RAC1b in over-expressing cell lines is associated with impaired proliferation and increased apoptosis [126]. RAC1b overexpression has been associated with poor prognosis in colon cancer [130]. The reported over-expression of RAC1b in *BRAF*-mutant tumours has a potential mechanistic link with the oncogene-induced senescence phenotype reported to contribute to this pathway of colorectal carcinogenesis. Overexpression of RAC1b in NCM460 colonocytes transformed with $BRAF^{V600E}$ was demonstrated to antagonise BRAF-mediated proliferation arrest [131]. Furthermore, RAC1b overexpression has been linked mechanistically to Wnt pathway activation [132-134].

1.3 DNA methylation

1.3.1 Introduction

Cytosine DNA methylation, by addition of a methyl group at the 5' carbon position of the pyrimidine ring of cytosine, is a covalent modification of the DNA molecule, and it has been proposed since the 1970s that this modification constitutes an epigenetic mark that is heritable and influences gene regulation and cellular differentiation [135]. DNA methylation was originally described as a repressive mark. Early *in vitro* experiments demonstrated that methylated DNA is transcriptionally inactive in *Xenopus* and mammalian systems, confirming a causative link between DNA methylation and gene silencing [136,137].

DNA methylation is not uniform throughout the genome, and exhibits a bimodal distribution. DNA methylation in mammals occurs predominantly at CpG dinucleotides, though non-CpG methylation does occur, particularly in the context of embryonic development, where it is enriched at gene bodies [138,139]. The mammalian genome contains short CpG-rich regions, defined as CpG islands (CGIs). CpG islands have a DNA sequence of at least 500bp, a GC content of greater than 55% and an observed/expected

ratio of CpG dinucleotide content greater than 0.65. Whilst CpG islands comprise less than 1% of genomic DNA, 72% of annotated gene promoters are associated with a CGI [140]. In somatic tissues, CGIs located at the TSS are predominantly unmethylated in contrast to CGIs located elsewhere in the genome [141]. There are exceptions to this however: for example, promoter CGI methylation is associated with X chromosome inactivation in females and genomic imprinting [142-144]. Unmethylated CGIs at the TSS are associated with active transcription, and are relatively resistant to DNA methylation. This resistance to DNA methylation is associated with engaged RNA-polymerase II [145]. Active promoter CGIs also demonstrate enrichment of transcription factor binding motifs, including Sp1, Nrf-1, E2F and ETS [146]. Furthermore, the chromatin at promoters with unmethylated CGIs exhibits a characteristic configuration of nucleosome-depleted regions (NDRs) at the TSS, which are marked by H3K4me3 and H2A.Z [147,148]. The localisation of H3K4me3 at unmethylated promoter CGIs has been shown to be directly linked to the relative protection of CGIs from DNA methylation, as the interaction of DNMT3L with H3 is inhibited by methylation of lysine 4 of H3 [149]. Unmethylated promoter CGIs are also bound by Cfp1. Depletion of the former results in reduced levels of H3K4me3 as it is a component of the Setd1 H3K4me3 methyltransferase complex [150,151].

By contrast, DNA methylation at promoter CpGs is considered a stable lock on transcription. DNA methylation results in the recruitment of methyl-binding domain proteins (MBD) in a sequence-independent fashion [152]. MBD binding to methylated DNA results in the recruitment of chromatin modifiers [153]. The chromatin landscape of methylated CpGs contrasts with that of unmethylated CpGs, and the former is associated with nucleosome occupancy, repressive histone modifications (deacetylated H3 and H3K9 methylation) and transcription repression [154,155]. Both in cancer and embryonic development, promoter CGI methylation exhibits a preference for genes marked by H3K27me3 [156,157]. A direct interaction between H3K27me3 and DNA methylation has been proposed: namely that EZH2 (the catalyst for H3K27me3) directly recruits DNA methyltransferases [158].

DNA methylation is not restricted to promoter CpGs, and the functions of DNA methylation at other genomic elements is increasingly understood. At gene bodies, methylation has traditionally been considered to silence the so-called repetitive elements (e.g. LINE-1, *Alu* elements etc.) [159]. Closer examination of DNA methylation at gene bodies has also revealed differences in DNA methylation between introns and exons.

Exons exhibit markedly higher methylation than introns, with an abrupt change at the intron/exon boundary. It has been proposed that this is supportive of a role for DNA methylation in splicing [160,161]. In contrast to promoter CGIs, gene body methylation has also been associated with increased gene expression [139,162]. Reestablishment of gene body methylation following treatment with 5-aza-2'-deoxycytidine has been demonstrated to be mediated by DNMT3B [163]. Furthermore, the targeting of DNMT3B to the gene bodies of transcribed genes has been confirmed by chromatin immunoprecipitation, and it has been demonstrated that this is mediated by H3K36me3 [164]. Recently, the central role of DNMT3B in gene body methylation has been confirmed. *Dnmt3b* knockout in mouse embryonic stem cells results in depletion of DNA methylation at a genome-wide level, with reductions in 5-methylcytosine at introns and exons. Furthermore DNMT3B binding has been demonstrated to correlate strongly with H3K36me3 abundance. Intragenic DNA methylation has been demonstrated to prevent aberrant transcription by preventing incorrect targeting of RNA polymerase II [165].

Transcriptional enhancers are situated at a variable distance from promoters, are key regulators of expression and exhibit variable levels of DNA methylation [166]. Schmidl et al. [167] identified methylation-sensitive enhancers involved in lineage-determination in T cells, and a correlation between enhancer methylation and gene expression during haematopoiesis has been noted [168]. Aran et al. [169] characterised transcriptional enhancer methylation in both normal and cancer cells, noting upregulation of expression of genes associated with a hypomethylated enhancer, and downregulation of those with a hypermethylated enhancer. Furthermore, alterations in gene expression were more tightly related to enhancer than promoter methylation status. Whole genome analysis of HCT116 DKO1 cells (which are null for both *DNMT1* and *DNMT3B*) has demonstrated a paucity of reactivated promoters in comparison to WT HCT116 cells, but a large number of active enhancers located in gene bodies, which are highly methylated and frequently associated with the H3K4me1 mark in parental HCT116 cells. In DKO1 cells, expression of several hundred genes silenced in parental HCT116 was associated with hypomethylated intronic enhancers [170]. In sum, while the role of DNA methylation at enhancers might be more nuanced than at CpG islands, a substantial body of data indicates that enhancers are activated by hypomethylation.

1.3.2 The DNA methyltransferases

In humans, three catalytically-active DNA methyltransferases enzymes have been characterised (DNMT1, DNMT3A and DNMT3B) in addition to a fourth, catalytically inactive enzyme, DNMT3L. A fifth protein, initially named DNMT2 is no longer considered a DNA methyltransferase. A novel DNA methyltransferase, DNMT3C, has also been described recently [171]. An overview of the DNA methyltransferase proteins and their respective isoforms is given in Figure 1-3.

1.3.3 DNMT1

DNMT1 was the first of the mammalian DNA methyltransferases to be described [172]. Mammalian DNMT1 preferentially methylates hemimethylated DNA [173]. DNMT1 binds to proliferating cell nuclear antigen (PCNA) [174] and is localised to the replication fork during S phase and acts primarily as a maintenance methyltransferase [175]. DNMT1 forms a complex with PCNA and UHRF1 (also called Np95) which mediates its recruitment to hemimethylated DNA during DNA replication [176]. DNMT1 has however, been demonstrated to able to maintain DNA methylation even when uncoupled from the DNA replication machinery [177]. Homozygous germline mutation of *DNMT1* is embryonically lethal [178]. Consistent with this, knockout of *DNMT1* in human embryonic stem cells results in global hypomethylation and cell death [179]. By contrast, *Dnmt1*$^{-/-}$ mouse embryonic stem cells are viable [180]. Furthermore, in both murine and human fibroblasts, *DNMT1* knockout is associated with proliferation arrest and p53-dependent apoptosis [181,182]. DNMT1 depletion in mice results in chromosomal instability and has been demonstrated to induce tumours [183,184]. Paradoxically, suppression of DNMT1, both by genetic knockdown and treatment with 5-aza-2'-deoxycytidine has been shown to reduce tumour formation in a mouse model of colon cancer [185,186]. The role of DNMT1 in aberrant promoter methylation will be discussed in a later section.

1.3.4 DNMT2

The human *DNMT2* gene is located at chromosome 10p13, and encodes a protein of 384 amino acids[3]. *DNMT2*, a homologue of the yeast *pmt1p* gene, exhibits many structural features of the other DNA methyltransferases, and was initially thought to represent a separate DNA methyltransferase [187]. Subsequently however, the yeast homologue of DNMT2, pmt1, was found not to exhibit demonstrable methyltransferase activity *in vitro*.

[3] https://www.ncbi.nlm.nih.gov/gene/1787

Furthermore, *Dnmt2* knockout in mouse embryonic stem cells did not affect viability, and was required neither for *de novo* nor maintenance methylation [188]. Whole genome bisulfite sequencing has revealed that DNA methylation is absent in organisms whose only candidate DNMT is DNMT2, and triple knockout (*Dnmt1*, *Dnmt3a* and *Dnmt3b*) mouse embryonic stem cells which retain *Dnmt2* exhibit an unmethylated genome [189]. Goll et al. [190] demonstrated that DNMT2 exhibits cytoplasmic rather than nuclear distribution (in sharp contrast to the other DNA methyltransferases) and that it is an RNA methyltransferase, which methylates $tRNA^{Asp}$. Consistent with this revised understanding of its function, the gene has subsequently been renamed *TRDMT1*.

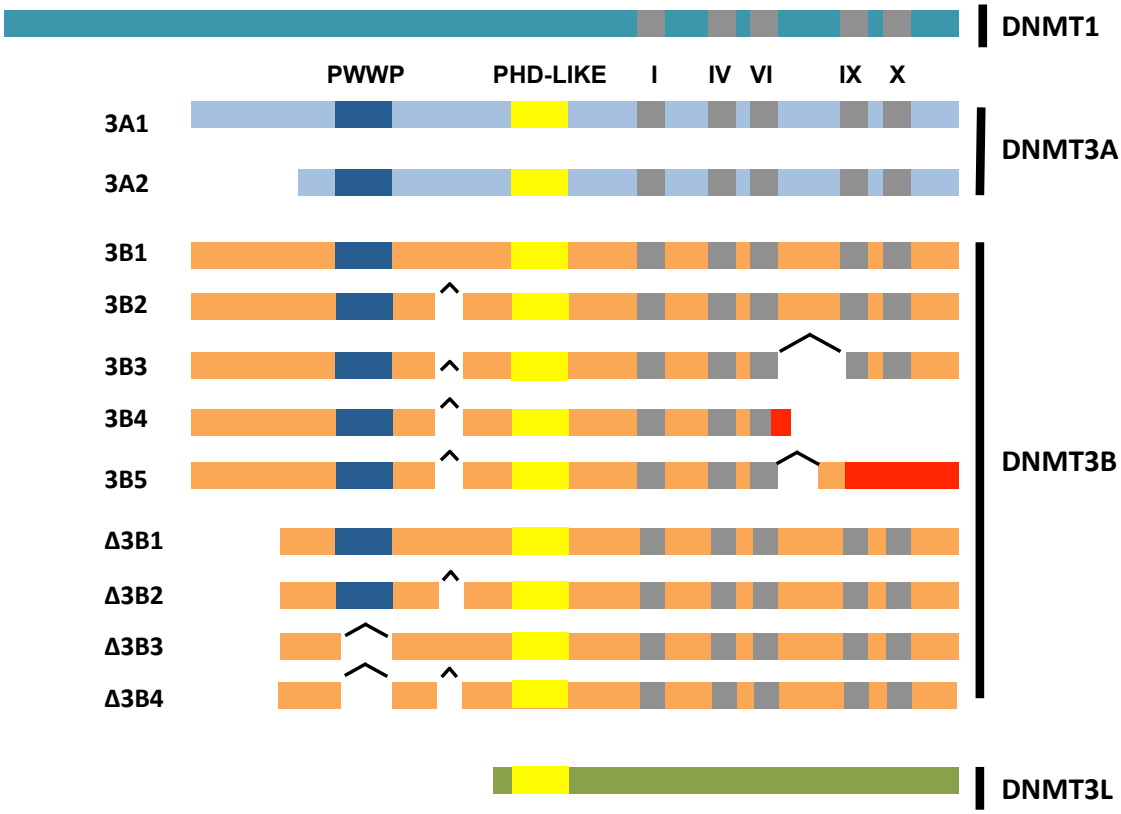

Figure 1-3 The DNA methyltransferase proteins

Schematic diagram of the DNA methyltransferase family of proteins, demonstrating the conserved PWWP and PHD-like domains, and the carboxy-terminal methyltransferase catalytic domain. Splice isoforms are represented, together with their respective alternate splicing sites/truncations. Adapted from Choi et al. [191].

1.3.5 DNMT3A

1.3.5.1 Introduction

The existence of separate *de novo* DNA methyltransferases was postulated following the observation that *Dnmt1*-null embryonic stem cells maintained *de novo* methylation activity [192]. Subsequently, the DNMT3 family, comprising *DNMT3A* and *DNMT3B*, was identified and both members were demonstrated to exhibit cytosine-5 methyltransferase activity [193]. *In vivo* activity of both enzymes was also subsequently confirmed [194]. The human *DNMT3A* gene is located at position 2p23 and encodes a protein of 908 amino acids. Human DNMT3A exhibits 98% structural homology with murine DNMT3A. DNMT3A is a *de novo* methyltransferase which exhibits equal affinity for both hemimethylated and unmethylated DNA [193]. DNMT3A is detectable in most somatic tissues [195,196]. *Dnmt3a*-knockout mice are viable, but die in early infancy [197]. A number of splice variants of *DNMT3A* in both mouse and human have been described. *Dnmt3a1* is expressed in somatic tissues. By comparison, *Dnmt3a2* is abundant in mouse embryonic stem cells, but expressed at very low levels in somatic tissues, and it has been proposed that this reflects a specific role for this splice variant in the establishment of methylation during development [198]. In humans, a truncated isoform, DNMT3A2, is expressed from an alternative promoter in intron 6 of *DNMT3A*. DNMT3A2 is catalytically active, but does not possess the N-terminal 233 amino acids of the full-length protein. In contrast to full-length DNMT3A, DNMT3A2 localises to euchromatin. Furthermore, DNMT3A2 is highly expressed in embryonic stem cells, but by contrast is absent in most somatic tissues (with the exceptions of testis, ovary, spleen and thymus) [199].

DNMT3A knockout using the CRISPR/Cas9 system in human embryonic stem cells does not affect viability, and *DNMT3A*$^{-/-}$ HESCs retain pluripotency and differentiation ability. *DNMT3A* knockout is associated with a mild reduction in global methylation, though this is less pronounced than in combined *DNMT3A* and *DNMT3B* knockout (the latter will be discussed below in the context of *DNMT3B*). Analysis of endodermal cells derived from the *DNMT3A*$^{-/-}$ line reveals that these exhibit hypomethylated DMRs relative to wild-type endodermal cells, with enrichment for promoters and gene bodies: implying that DNMT3A is required for the *de novo* methylation of these features [179].

1.3.5.2 DNMT3A in cancer

Elevated expression of DNMT3A has been reported in cancer cell lines and primary human tumour tissue [195,196]. The oncogenic function of DNMT3A has been explored in several models. Antisense mediated knockdown of DNMT3A in a melanoma cell line does not affect proliferation, migration, invasion or colony-formation *in vitro*. However in the *in vivo* context, DNMT3A depletion is associated with reduced melanoma growth and metastasis [200]. Similarly, in gastric cancer, high DNMT3A expression is detected in tumour compared to paired normal tissue; furthermore high DNMT3A expression is associated with poor outcome [201]. Knockdown of DNMT3A in gastric cancer cell lines is associated with reduced proliferation, and conversely ectopic expression accelerates growth. The growth acceleration associated with DNMT3A overexpression is mediated by depletion of $p18^{INK4C}$, consequent upon hypermethylation of its promoter. Furthermore, in human gastric cancer tissue, DNMT3A expression is significantly associated with downregulation of $p18^{INK4C}$ [202].

Elevated DNMT3A expression has been reported in both murine and human colon cancer [203,204]. Conditional knockout of *Dnmt3a* in the $Apc^{min/+}$ model is associated with a 40% reduction in colonic tumour formation. *Fabp-Cre* results in mosaic recombination in the intestine. Interestingly genotyping of colonic tumours and microadenomas arising in *Fabp-Cre;*$Dnmt3a^{2lox/2lox}$*;*$Apc^{min/+}$ revealed only the active (2lox) *Dnmt3a* allele whereas the inactive (1lox) *Dnmt3a* was not detected, suggesting DNMT3A is required for tumour initiation. DNA methylation analysis of Cre^{+} and Cre^{-} colonic mucosa was undertaken. Whilst overall a very small reduction in global methylation was noted in Cre^{+} animals, there was no difference in LINE-1 methylation, a surrogate of global methylation. By contrast, Cre^{+} animals exhibited promoter demethylation, and increased expression of tumour suppressors, including CDKN1C and TFF2 [204].

There are conflicting data published on the effects of over-expression of DNMT3A on colorectal tumourigenesis. Linhart et al. [205] overexpressed DNMT3A in the $Apc^{min/+}$ model using a tetracycline-inducible *Dnmt3a* transgene, and reported no increase in tumour number. By contrast, a subsequent study revisited intestine-specific overexpression of DNMT3A using the $A33^{Dnmt3a}$ transgene. A small proportion of aged $A33^{Dnmt3a}$ mice developed sporadic intestinal adenomas, though there was a significant latency (>18 months). Tumours from these mice exhibited upregulation of Wnt targets and promoter hypermethylation of the Wnt antagonists *Sfrp1* and *Sfrp5*. The authors also crossed

A33^{Dnmt3a} to the *Apc*$^{min/+}$ strain. *A33*^{Dnmt3a}*;Apc*$^{min/+}$ developed significantly more (three-fold increase) macroscopic tumours compared to *Apc*$^{min/+}$ mice. Polyps from both *A33*^{Dnmt3a}*;Apc*$^{min/+}$ and *Apc*$^{min/+}$ exhibited activated Wnt signalling as evidenced by nuclear β-catenin, though in *A33*^{Dnmt3a}*;Apc*$^{min/+}$ mice, approximately a third of tumours did not exhibit *Apc* LOH. Expression analysis of *A33*^{Dnmt3a}*;Apc*$^{min/+}$ mice tissues demonstrated upregulation of Wnt targets including AXIN2 and repression of the Wnt antagonist SFRP5, and this was associated with hypermethylation of its promoter. Furthermore, the authors demonstrated a correlation between DNMT3A overexpression and SFRP5 repression in human colorectal cancer samples [206].

Together these data are supportive of an oncogenic function of DNMT3A. This role however appears to be context-dependent. In contrast to the oncogenic function described in the colon, DNMT3A has been demonstrated to exhibit a tumour suppressive role in the *Ad-Cre;Kras*^{G12D} model of lung adenocarcinogenesis. *Dnmt3a* deletion in this model does not increase tumour number, but significantly increases tumour size. Furthermore, homozygous deletion of *Dnmt3a* in this model significantly shortens survival. This oncogenic effect of *Dnmt3a* deletion is associated with altered expression of genes involved in angiogenesis, cell adhesion and motility. *Dnmt3a* deletion was also associated with a loss of methylation at gene bodies [207]. In a follow-up study, the authors used whole-genome bisulfite sequencing to comprehensively assess the methylation changes consequent upon *Dnmt3a* deletion in *Ad-Cre;Kras*^{G12D} tumours. In contrast to *Ad-Cre;Kras*^{G12D} tumours with wild-type *Dnmt3a*, which exhibited hypomethylation of lamin-associated domains, *Dnmt3a* knockout induced global hypomethylation with loss of methylation at partially-methylated domains. *Dnmt3a*-null tumours exhibited a significant reduction in gene body and intergenic methylation. By contrast, *Dnmt3a* knockout was not associated with significant changes in promoter CpG methylation. Analysis of expression data from the same model demonstrated that hypomethylation of 5' UTRs was associated with gene upregulation, whereas downregulated genes demonstrated hypomethylation in exons [208].

Similarly, in leukaemia, DNMT3A has been associated with a tumour-suppressive role. *DNMT3A* mutations are detected in approximately 22.1% of patients with acute myeloid leukaemia, most commonly at amino acid R882. Furthermore, *DNMT3A* mutations are associated with reduced survival [209]. The R882H mutation results in significantly reduced DNA methyltransferase activity and an inability to form homotetramers. Furthermore, the mutant protein exerts a dominant negative effect on the wild-type protein.

AML samples with the R882H mutation exhibit focal DNA hypomethylation throughout the genome [210]. *DNMT3A* knockout in haematopoietic stem cells (HSPCs) results in significant methylation changes at DNA methylation canyons. Canyons marked by H3K4me3 demonstrate expansion, whilst those marked by H3K27me3 contract. Significantly, canyon-associated genes are significantly enriched for genes differentially expressed in human AML with and without *DNMT3A* mutations [211]. Furthermore, conditional knockout of *DNMT3A* in HSPCs impairs differentiation and is associated with both hypo- and hypermethylation events: the latter notably but somewhat paradoxically at CpG islands. Interestingly, hypomethylation in *DNMT3A*-null HSPCs was associated with activation of HSP multipotency genes [212]. A more recent study has suggested that hypomethylation driven by $DNMT3A^{R882}$ is an initiating event in leukaemogenesis, whereas CpG hypermethylation is not associated with gene-silencing, and occurs as a response to, rather than drives cellular proliferation [213].

1.3.6 DNMT3B

1.3.6.1 Introduction

The human *DNMT3B* gene is at position 20q11.21 and encodes a protein consisting of 853 amino acid residues. Human DNMT3B exhibits 94% sequence homology with murine DNMT3B. Whilst DNMT3A and DNMT3B exhibit high sequence homology in their catalytic domains, they exhibit low sequence homology in the N-terminal variable domains [196].

In mice, germline deletion of *Dnmt3b* is embryonically lethal, and combined *Dnmt3a* and *Dnmt3b* deletion prevents *de novo* methylation of proviral DNA by ES cells. Furthermore, DNMT3B methylates pericentric satellite regions, and may thus have a role in the maintenance of chromosomal stability [197]. Both DNMT3A and DNMT3B localise to pericentric heterochromatin in embryonic stem cells. Furthermore, this localisation is preserved in *Dnmt1*-null ES, implying that this localisation occurs independently of DNA methylation [214]. Targeting of DNMT3B to the pericentric chromatin has been demonstrated to be dependent on the N-terminal PWWP domain [215]. DNMT3B interacts with CENP-C, a constitutive centromere protein. Disruption of either DNMT3B or CENP-C results in chromosomal segregation defects, and hypomethylation of pericentric repeats [216]. In humans, mutations in the *DNMT3B* gene are responsible for a rare autosomal recessive syndrome, termed ICF syndrome, which results in immunodeficiency, centromeric instability, and facial anomalies [197,217]. Whole genome bisulfite

sequencing of an ICF patient has demonstrated genome-wide global hypomethylation, with the most significant changes being observed at inactive heterochromatic regions, satellite repeats and transposons. Whilst the methylome in ICF is globally attenuated, there is relative sparing of transcriptionally active loci. Unexpectedly, hypermethylated DMRs were also identified in the ICF patient, particularly at loci marked by H3K4. It was hypothesised that this might be due to an impaired interaction between the mutant protein and DNMT3L [218].

Loss of function experiments in embryonic stem cells and cancer cell lines have helped to clarify the functions of DNMT3B. Deletion of *DNMT3B* using the CRISPR/Cas9 genome editing system in human embryonic stem cells has demonstrated that *DNMT3B*$^{-/-}$ HESCs retain pluripotency and do not exhibit impaired differentiation. Overall, *DNMT3B*$^{-/-}$ cells exhibit only a very modest decrease in global methylation. Interestingly, DNMT3B depletion had a more marked effect on non-CpG methylation than DNMT3A depletion. By contrast, in double knockout cells (*DNMT3A*$^{-/-}$;*DNMT3B*$^{-/-}$) whilst there was a gradual loss of CpG methylation, non-CpG methylation was rapidly depleted. Approximately 96% of DMRs between wild-type and knockout lines lost methylation only in the double-knockout line, implying considerable functional redundancy between DNMT3A and DNMT3B. Those DMRs that did not exhibit functional redundancy were enriched for CpG islands [179]. Further insight into the function of DNMT3B has been gained from antisense-mediated knockdown in the human embryonic carcinoma line NCCIT. DNMT3B siRNA knockdown was unexpectedly associated with a larger number of hypermethylated than hypomethylated DMRs. There was a significant enrichment for DNMT3B knockdown hypermethylation DMRs at gene bodies, 3' UTRs and intergenic sequences. Loci gaining methylation upon DNMT3B knockdown overlapped with those losing methylation on knockdown of DNMT1 implying a role of the latter in establishing this hypermethylation. Consistent with the HESC data reviewed above, DNMT3B knockdown was associated with hypomethylation of non-CpG sites. Conversely, DNMT3L knockdown was associated with hypermethylation of non-CpG sites; implying that DNMT3L regulates non-CpG methylation by DNMT3B [219]. DNMT3B has been further implicated in gene-body methylation in transcribed genes. Selective binding of DNMT3B to the gene-bodies of transcribed genes has been demonstrated by ChIP, and this targeting is dependent on the H3K36me3 mark and requires an intact PWWP domain [164].

A number of splice isoforms of *DNMT3B* have been described, some of which lack or possess a truncated C-terminal catalytic domain. Some of these exhibit tissue-specific

expression patterns, and interestingly, DNMT3B3 which lacks the C-terminal catalytic domain is the one of the most widely expressed isoforms in adult somatic tissues [195]. Moreover, the most highly expressed DNMT3B isoforms in human cancer cell lines are DNMT3B2 and DNMT3B3 rather than DNMT3B1 [220]. Initially the function of *DNMT3B* splice isoforms was unclear, though studies (predominantly in a cancer context) have shed some light on their roles in the regulation and dysregulation of DNA methylation. Wang et al. [221] described the ΔDNMT3B family (ΔDNMT3B1-7) transcribed from an alternative promoter in intron 4, which are expressed at higher levels in tumour compared to normal tissues. Consistent with this relative overexpression in tumour tissue, ΔDNMT3B4 was strongly correlated with promoter hypermethylation of the tumour-suppressor *RASSF1A*. A further study has characterised over 20 aberrant DNMT3B isoforms in cancer cell lines from multiple tumour types, confirming these as a common feature of a variety of solid and haematological tumours [222]. Furthermore, these were confirmed to be predominantly nuclear rather than cytoplasmic in their distribution. Interestingly, functional studies with ectopic expression of one such isoform, DNMT3B7, in 293T cells have demonstrated that this results in an altered transcriptome, and targeted methylation analysis demonstrated that this was associated with altered methylation at the promoters of certain genes whose promoters exhibit methylation changes in cancer (*CDH1*, *MAGEA3*, *SH2D1A*, *PLP2*) [222]. More recent work has clarified the contribution of *DNMT3B* isoforms to *de novo* DNA methylation. A novel isoform, DNMT3B3Δ5, originally isolated from an embryonic carcinoma cell line, which is structurally related to DNMT3B3, is upregulated in pluripotent cells, and downregulated upon differentiation. Whilst expressed in fetal and adult brain, it is expressed at low levels in adult somatic tissues and furthermore is aberrantly expressed in certain cancers. Ectopic expression of DNMT3B3Δ5 in HCT-116 results in loss of DNA methylation at centromeric and pericentromeric repetitive elements, and is associated with increased clonogenic growth [223].

A further study has characterised the effects of the *DNMT3B* splice variants DNMT3B3 and DNMT3B4 on DNA methylation. Both DNMT3B3 and DNMT3B4 were demonstrated to bind to and thus modulate the catalytic function of DNMT3A and DNMT3B. Whilst itself lacking an intact catalytic domain, DNMT3B3 can modestly stimulate *de novo* methylation activity, however in the presence of DNMT3L, counteracts the stimulation effect of the latter, implying a degree of context dependency. It has been suggested that this might reflect a regulatory function of the DNMT3B3 isoform in the development context. DNMT3B4 by contrast, impairs the *de novo* methylating activity of

the DNMT3 family by binding to them and reducing their DNA-binding affinity [224]. An elegant study has further analysed the function of DNMT3B isoforms by reintroduction of particular isoforms to the HCT-116 derived cell lines 3BKO and DKO8, which have a homozygous deletion of *DNMT3B* (DKO8 also have a hypomorphic *DNMT1* allele). Subsequent methylation analysis revealed that re-expression of *DNMT3B* isoforms results in restoration of methylation at specific CpG sites, (most of which were methylated in parental HCT-116 cells) with the most significant gains being at gene bodies, which were enriched for H3K36me3 (associated with active transcription). Interestingly, the catalytically-inactive DNMT3B3 isoform was also demonstrated to result in restoration of methylation: supporting the previously reviewed evidence that it can result in increased DNA methylating activity whilst itself catalytically-inactive. Furthermore, in the *DNMT3A* and *DNMT3B* null cell line 3ABDKO, only DNMT3B1 was able to restore methylation, implying that the observed effects of other *DNMT3B* isoforms may be mediated through recruitment of DNMT3A in a fashion similar to DNMT3L [225].

1.3.6.2 DNMT3B in cancer

In contrast to *DNMT3A*, mutations in *DNMT3B* have not been described in human cancer. DNMT3B is highly expressed in embryonic stem cells, but at very low levels in differentiated adult tissues (with the exception of adult testis) [193]. By contrast, DNMT3B is over-expressed in multiple tumour types [195]. The over-expression of DNMT3B in multiple tumour types has prompted many authors to explore an oncogenic function. DNMT3B knockdown has been demonstrated to have an anti-proliferative effect and induce apoptosis in cancer cell lines, but not untransformed cell lines [226]. Furthermore, in both transformed human bronchial epithelial cells and MEFs, DNMT3B was demonstrated to be required for soft agar colony growth, and antisense-mediated knockdown resulted in re-expression of tumour suppressor genes [227].

A number of murine studies support an oncogenic function of DNMT3B in colon cancer. A transgenic mouse model with *Cre*-lox mediated conditional *Dnmt3b* deletion, was developed and crossed to the $Apc^{Min/+}$ model [228]. *Dnmt3b*-null mice exhibited fewer macroscopic colon tumours than wild-type *Dnmt3b* controls, but *Dnmt3b* deletion did not affect the number of microadenomas in this model. The authors concluded that *Dnmt3b* knockout impaired the progression of microadenomas to macroscopic adenomas. In the converse experiment, transgenic mouse models with tetracycline-inducible *Dnmt3a* and *Dnmt3b* transgenes were developed and crossed to the well-characterised $Apc^{Min/+}$ model

[229]. Whilst DNMT3A overexpression had no effect on tumour number, DNMT3B overexpression was associated with a doubling in the number of colon tumours in *Apc*$^{Min/+}$ mice, and increased the average size of microadenomas. Furthermore, these effects on tumourigenesis were not seen in mice overexpressing DNMT3B3, a catalytically-inactive isoform of *Dnmt3b*, implying that the effect was methylation-dependent. DNMT3B overexpression resulted in loss of imprinting and re-expression of IGF2 due to hypermethylation of the *H19-DMR*, in addition to silencing of the tumour-suppressors SFRP2, SFRP4 and SFRP5. Whilst this paper did not explicitly address whether DNMT3B induces a CIMP-Phenotype, it did demonstrate that DNMT3B induces locus-specific promoter CpG island methylation, and associate this with a potential oncogenic function. Paradoxically, in contrast to these studies, silencing of *DNMT3B* due to its promoter hypermethylation has also been reported in both colon cancer cell lines and primary human colon cancers, and linked to an oncogenic function [230].

DNMT3B has also been demonstrated to have an oncogenic function in malignant melanoma. DNMT3B is overexpressed in human melanoma and DNMT3B knockdown impairs proliferation in human melanoma cell lines. Overexpression of DNMT3B is also associated with reduced survival in human melanoma. Furthermore, in an *in vivo* melanoma model, conditional *Dnmt3b* knockout abrogates melanoma formation, and improves survival. *Dnmt3b* knockout results in hypomethylation of miR-196b, with consequent loss of RICTOR, which prevents activation of mTORC2 [231]. Interestingly, in this latter study, there was no association between DNMT3B expression and *CDKN2A/INK4A* promoter methylation in melanoma, despite an earlier report to the contrary [232].

In contrast to an apparent oncogenic function of DNMT3B in melanoma and epithelial cancers, DNMT3B has been proposed to have a tumour suppressor function in the context of lymphoma. In a murine model of MYC-induced T cell lymphoma, *Dnmt3b* knockout has been demonstrated to accelerate lymphoma progression, and this was associated with hypomethylation and re-expression of GM128 (MENT), whose expression was similarly correlated with DNMT3B expression in human lymphoma [233]. Furthermore, the oncogenic function of DNMT3A in murine MYC-induced T cell lymphoma has been demonstrated to be mediated in part by suppression of DNMT3B [234]. Similarly, in the Eμ-Myc model of B-cell lymphoma, *Dnmt3b* has been demonstrated to be a haploinsufficient tumour suppressor gene [235]. However, in human diffuse large B-cell lymphoma, DNMT3B overexpression is an independent predictor of poor disease-free and

overall survival, which does not fit with a tumour-suppressive role [236]. There are also data suggesting a tumour-suppressive role of DNMT3B in leukaemia. In two murine models of leukaemia (*Myc-Bcl2* and *MLL-AF9),* ectopic DNMT3B expression has been demonstrated to impair leukaemogenesis [237]. Furthermore, DNMT3B expression is reduced in leukaemic stem cells compared to haematopoietic stem cells and deletion of *Dnmt3b* in murine *MLL-AF9* accelerates leukaemogenesis [238]. Similarly, in a murine model of CLL driven by deletion of *Dnmt3a*, synchronous *Dnmt3b* deletion accelerates tumourigenesis [239]. There is however, an apparent paradox, as high DNMT3B expression correlates with poor prognosis in acute myeloid leukaemia in humans [237,240,241].

1.3.7 DNMT3L

The human *DNMT3L* gene is located at 21q22.3 and encodes a 387 amino acid protein which exhibits structural similarities with DNMT3A and DNMT3B [242]. DNMT3L however lacks key catalytic domains on its C terminus, and does not exhibit DNA methyltransferase activity [243]. DNMT3L is virtually undetectable in adult tissues with the exception of testis, ovary and thymus [242]. Repression of DNMT3L in adult tissues is associated with promoter CpG hypermethylation [244]. DNMT3L is however highly expressed in embryonic stem cells and has been demonstrated to have an essential role in maternal imprinting [243,245].

Whilst itself lacking DNA methyltransferase activity, DNMT3L is an important co-factor in the DNA methylation machinery, and has been demonstrated, by coimmunoprecipitation, to physically interact with DNMT3A and DNMT3B [245]. DNMT3L stimulates the activity of both DNMT3A and DNMT3B [246,247]. DNMT3L enhances the binding of S-adenosyl-L-methionine to DNMT3A2 resulting in a significantly increased catalytic activity [248]. In mouse embryonic stem cells, DNMT3L competes with DNMT3A and DNMT3B to form a complex with PRC2, promoting methylation at gene bodies, whilst impairing DNA methylation at bivalent promoters, allowing continued expression of developmental genes [249]. Targeted DNMT3L knockdown in an embryonic carcinoma cell line (NCCIT) results in hypermethylation of non-CpG sites supporting a role for DNMT3L in restricting non-CpG methylation by DNMT3A and DNMT3B [219]. DNMT3L is not over-expressed in tumours arising from somatic tissues, but is overexpressed in testicular germ cell tumours, in which DNMT3L knockdown inhibits growth and promotes apoptosis [250].

1.3.8 DNMT3C

The most recently-described member of the DNA methyltransferase family is *Dnmt3c*. *Dnmt3c* maps 9kb downstream of *Dnmt3b* and had previously been considered a pseudogene. Like the other members of the DNMT3 family, DNMT3C possesses six catalytic methyltransferase motifs at its C-terminus, and an ADD domain at its N-terminus, which binds unmethylated H3K4. Unlike the other members of the DNMT3 family, it does not posess the PWWP domain, which recognises H3K36me3 and targets these proteins to gene bodies. It has been demonstrated to be a catalytically-active member of the DNMT3 family and is responsible for methylation of evolutionarily-young retrotransposons in the male germline. Functional disruption in a murine model results in hypogonadism and male infertility. Whilst present in members of the orders *Rodentia* and *Muroidea*, *Dnmt3c* is absent in primates [171].

1.4 DNA methylation in normal intestinal homeostasis and ageing

As in embryonic development, DNA methylation has been demonstrated to be a crucial regulator of differentiation in self-renewing somatic tissues [251]. The mammalian intestine is a highly proliferative tissue with replacement of the epithelium every 3-5 days. In the murine intestine, small intestinal crypts produce approximately 25 cells/hour [252] and in the colon, around 16 cells/hour [253]. Inducible deletion of *Dnmt1* in the murine intestine leads to crypt expansion and decreased differentiation (with increased expression of LGR5 and OLMF4) as a result of impaired repression of intestinal stem cell genes [254]. This is in contrast to other self-renewing somatic tissues, in which loss of DNMT1 leads to failure of tissue self-renewal [251,255,256]. Furthermore, deletion of *DNMT1* in human embryonic stem cells results in loss of viability [179].

Moreover, there is an apparent paradox in the intestine, as deletion of *Dnmt1* in ‘perinatal’ intestinal epithelium leads to global hypomethylation, loss of progenitors and failure of self-renewal [257,258]. It has subsequently been noted that DNMT3B is upregulated after *Dnmt1* deletion in the adult mouse intestine, in contrast to ‘perinatal’ mouse intestine, where upregulation of DNMT3B is not seen in *Dnmt1*-null animals. Combined deletion of *Dnmt1* and *Dnmt3b* in the murine intestine is lethal, causing hypomethylation, DNA damage and cell death [257-259]. Whole genome bisulfite sequencing has been used to map changes in DNA methylation dynamics in perinatal and adult murine colonic epithelium. In both ‘perinatal’ and adult colon, global methylation levels are significantly lower in differentiated stem cells than in intestinal stem cells. Interestingly, there are more

DMRs during intestinal maturation than during differentiation. During maturation, there are gains of methylation at CGIs and loss of methylation at non-CGIs. Conditional knockout of *Dnmt1* in adult intestinal stem cells leads to disruption of normal crypt homeostasis in both small intestine and colon [258]. The relative lack of DMRs detected during adult intestinal stem cell differentiation in this study is consistent with a previous report [260]. In this latter study, intestinal stem cell differentiation in the small intestine was associated with reduced expression of DNMT1, DNMT3A and DNMT3B, but globally, only a very modest decrease was seen in DNA methylation upon differentiation.

Consistent with a role for DNA methylation in normal tissue homeostasis, DNA methylation changes in the intestine have been reported in association with ageing in healthy individuals, though the biological significance of these is unclear [113,261,262]. Renewed interest in the "epigenetic drift" associated with ageing as a putative risk factor for neoplastic transformation, has prompted more comprehensive analysis of the DNA methylation changes that accompany ageing in the mammalian intestine. Analysis of promoter CpG-island methylation at 3627 autosomal genes in murine intestine revealed significant DNA methylation changes associated with ageing, with 21% of genes exhibiting age-associated hypermethylation and 13% exhibiting hypomethylation. Of note, there was an apparent enrichment for polycomb targets in the hypermethylated genes. This study furthermore sought to compare age-associated methylation changes in human and murine intestine. This comparison was relatively limited by a lack of sequence conservation at promoter CpGs between mice and humans, but did reveal some commonality. In human colon, the degree of age-associated hypermethylation was markedly less pronounced with only 10% of autosomal genes demonstrating age-associated hypermethylation, and 1% hypomethylation. Furthermore only 42% of conserved genes hypermethylated in aged human-colon were hypermethylated in murine intestine, and only 3% of conserved hypomethylated genes in aged human colon were hypomethylated in aged murine intestine [263]. A subsequent, much more limited study, has confirmed ageing-associated DNA hypomethylation in the intestine and colon of C57Bl/6J mice [264]. Reflecting the generalizability of ageing-associated DNA methylation, genome-wide DNA methylation has been demonstrated to be a robust biomarker of chronological age [265]. A panel of so-called "clock CpGs" has been proposed as a predictor of biological age across a diverse range of human tissues. Of relevance to the main subject matter of this thesis, this study reported that colon cancers with a $BRAF^{V600E}$ mutation exhibit "age acceleration", though these data were subsequently retracted by the authors [266].

The significance of ageing-associated DNA methylation changes remains uncertain. Whilst it is recognised that DNA methylation patterns are tissue-specific, it is notable that there is a tendency for ageing-associated DNA changes to occur at developmental genes, bivalent chromatin domains, and polycomb target genes: mirroring the patterns seen in cancer [267-269]. Furthermore, DNA methylation changes in the ageing colon have been analysed in the context of accepted risk factors for colorectal carcinoma. Aspirin and HRT use (which are generally accepted as reducing colorectal cancer risk) suppressed age-associated DNA hypermethylation, whereas the converse was true for smoking and obesity. Moreover, the methylation changes observed were more pronounced at those CpG sites which exhibited differential methylation in ageing and cancer as compared to those exhibiting differential methylation in ageing alone [270]. LINE-1 hypomethylation in the normal colonic mucosa of patients with colon cancer has also been proposed as a biomarker of both synchronous and metachronous neoplasm risk [271].

1.5 DNA methylation in senescence

Further interesting parallels are found in the senescence literature. Mammalian cells *in vitro* undergo a finite number of divisions before entering a stable proliferation arrest termed cellular senescence [272]. It is now recognised that senescent cells accumulate in both normal ageing mammalian tissues and tissues exhibiting ageing-associated pathology [273-277]. Furthermore, the accumulation of senescent cells in aged tissues has been proposed to contribute to neoplastic transformation [278]. It is therefore of considerable interest that senescent cells develop significant changes in DNA methylation, which mirror those seen in ageing and cancer.

Senescent cells have been demonstrated to exhibit DNA hypomethylation and this has been associated with decreased expression of DNMT1, and increased expression of DNMT3B [279,280]. With the development of more sophisticated methods of DNA methylation analysis, a number of studies have expanded on these observations. Analysis of DNA methylation changes in mesenchymal stromal cells undergoing senescence using Human Methylation27 bead chip arrays identified specific CpG-sites that exhibited significant methylation changes in senescence, with enrichment for homeobox genes and genes involved in cellular differentiation [267]. A more recent study mapped the DNA methylome of replicative senescence at a genome-wide level. The authors performed single-nucleotide bisulfite sequencing in proliferating and replicatively senescent fibroblasts. They demonstrated that gains and losses of methylation in replicative

senescence exhibit many similarities to those seen in the cancer epigenome, with global hypomethylation, especially in association with lamin-associated domains, but small increases in methylation at CpG islands. Furthermore, this study also reported that the methylation changes associated with replicative senescence were associated with both repression and relocalisation of DNMT1 and increased expression of DNMT3B. Interestingly, CpG islands exhibiting hypermethylation in replicative senescence included several "cell cycle genes", repression of which is required for proliferation arrest, including histones, *CCNA2*, *CENPA*, *MCM2* and *TOPA2*, implying that DNA methylation may play a role in establishing the stable proliferation arrest associated with replicative senescence [281]. A subsequent study has however cast doubt on this hypothesis, demonstrating that the DNA methylation changes that accompany cellular senescence may occur stochastically rather than contributing mechanistically as effectors of cellular senescence [282]. Mirroring the situation in ageing and cancer, senescence-associated DNA methylation changes are enriched in developmental genes such as homeobox genes, and senescence-associated hypomethylation is enriched at H3K9me3, H3K27me3 and polycomb group 2 target genes [283].

Perhaps more intriguingly, CpG islands that have been associated with a CpG island methylator phenotype in colorectal cancer (namely *RUNX3*, *CACNA1G*, *SFRP2* and *SOCS1*) also showed hypermethylation in replicative senescence. Significantly, the authors also demonstrated that when senescence bypass was initiated, that these abnormal methylation patterns were retained [281], an observation supported by a separate study published in the same year [283]. This has potentially significant implications for tumour development, as senescent cells that escape stable proliferation arrest may possess an abnormal methylome.

1.6 DNA methylation in cancer

Whilst cancer has traditionally been considered to arise as a result of genetic mutations, there has been increasing recognition that many cancers possess a dysregulated epigenome, and aberrations of DNA methylation are a significant feature of the cancer epigenome. Analysis of the temporal relationship of the DNA methylation changes accompanying carcinogenesis has revealed that different elements of the methylome become dysregulated at varying stages during the process of carcinogenesis. For example, in the context of colon cancer, whole genome analysis of paired normal colonic tissue, adenomas and carcinoma has revealed that hypomethylation accompanies the transformation from normal tissue to

adenoma, whilst the majority of hypermethylation events occur during the transition from adenoma to carcinoma [284]. Below the methylation changes associated with the cancer genome are discussed, together with their putative contributions to carcinogenesis.

Hypomethylation is a common feature of the cancer epigenome [285,286]. Although initially characterised as a global hypomethylation, more recent studies employing more sophisticated methodology have mapped the distribution of cancer-associated hypomethylation at genomic features in more detail. Whole genome bisulfite sequencing of primary human colorectal cancer tissue and paired adjacent normal tissue has revealed that cancer-associated hypomethylation is concentrated at late-replicating lamin-associated domains, which are gene poor and contain repetitive sequences [287].

Initially the significance of global hypomethylation in cancer remained undefined, but mounting evidence supports the ability of global hypomethylation to promote tumourigenesis. Dietary methyl deficiency in rats results in the development of liver tumours, and this is associated with hypomethylation of *Hras* and *Kras* oncogenes [288]. Moreover, in murine dichloroacetic acid and trichloroacetic acid-induced liver carcinogenesis, hypomethylation of the promoters of the proto-oncogenes *c-Jun* and *c-Myc* has been demonstrated and is associated with upregulation of their mRNA and protein products [289]. Mice with a hypomorphic *Dnmt1* allele, which exhibit global hypomethylation, develop T-cell lymphoma between 4-8 months of age, and this is associated with increased chromosomal instability [184]. In a further study in this murine thymic lymphoma model, hypomethylation has been demonstrated to lead to activation of endogenous retroviral elements, which is associated with activation of oncogenic NOTCH1 [290]. Furthermore, *Dnmt1*-null mouse embryonic stem cells (which exhibit global hypomethylation) have been demonstrated to possess a "mutator phenotype" [291]. Hypomethylation may also promote tumourigenesis by triggering loss of imprinting [292].

By contrast, the cancer epigenome is also characterised by hypermethylation of promoters, which are unmethylated in normal tissues, and this feature is amongst the most comprehensively characterised features of the cancer epigenome. The earliest report of promoter hypermethylation in cancer was in the calcitonin gene in small cell lung cancer [293]. Subsequently, aberrant promoter methylation of the oestrogen-receptor gene was demonstrated in breast cancer cells cultured *in vitro,* linking promoter DNA methylation to carcinogenesis [294]. A key paper characterised the silencing of the tumour-suppressor *CDKN2A/INK4A* by promoter CpG hypermethylation in both cancer cell lines and primary

human cancer samples, demonstrating this to be an alternative method of transcriptional silencing of tumour suppressors in cancer [295]. Subsequently the oncogenic function of promoter methylation has been extensively investigated. For example, promoter CpG methylation has been demonstrated to result in Wnt pathway activation in the context of colon cancer [87]. Similarly, promoter methylation of $p14^{ARF}$ and *PTEN* has been functionally linked to silencing of *TP53* in breast cancer [296].

Whilst the accepted dogma proposes a direct link between promoter CpG methylation and transcription repression, more recent evidence suggests that transcription repression may not be initiated by DNA methylation *per se*. Resilencing of $p16^{INK4A}$ (associated with H3K9 methylation) has been demonstrated in the absence of DNA methyltransferase activity [297]. Furthermore, reactivation of genes silenced by promoter methylation has been demonstrated following HDAC inhibition, without demonstrable DNA methylation changes at promoters [298,299]. Interestingly, reactivation of genes marked by promoter methylation following HDACi was transient when compared to treatment with 5-aza-2'-deoxycytidine, suggesting that rather than acting as a "stable lock" on transcription, promoter DNA methylation acts as an epigenetic memory marker to maintain long-term gene-silencing [298].

More recent work has characterised abnormal methylation at CpG shores in the cancer context. CpG shores immediately flank CpG islands and can lie up to 2kb distant to CpG islands. In normal tissue, up to 76% of tissue-specific DMRs are at CpG shores. Interestingly, in the context of colon cancer, a majority of cancer-associated DMRs are at CpG shores rather than promoters, and a significant enrichment is noted for cancer-associated DMRs at loci that are considered tissue-specific DMRs [300]. Similarly in the context of reprogramming, DMRs associated with reprogramming are highly significantly enriched at CpG shores, and there is a significant overlap of reprogramming-associated hypomethylated DMRs with cancer-associated hypermethylated DMRs. Significantly, these overlapping DMRs are highly enriched for bivalent chromatin marks [301]. The ability of CpG shore methylation to silence oncogenes has been confirmed in breast cancer. In breast cancer cell lines, *CAV1* expression is related to differential methylation at CpG shores but not its promoter CpG island, which is hypomethylated in all cell lines examined. Treatment of breast cancer cell lines with 5-aza-2'-deoxycytidine results in increased expression of *CAV1*, and this is associated with significant reduction in methylation at both the 5' and 3' CpG shore, but not with altered methylation of its promoter CpG island [302].

A further model postulates that CpG island hypermethylation in cancer may be a 'passenger event'. It has been demonstrated that many of the genes that undergo hypermethylation in cancer are transcriptionally-repressed in the corresponding normal tissues. Furthermore, many of the genes methylated in cancer are PRC targets in embryonic stem cells, expression of which determines lineage. It has been speculated that this might impair differentiation, and maintain cancer cells in 'stem-like state'. This model proposes that promoter hypermethylation is a secondary 'epigenetic reprogramming event', rather than the primary driver of gene silencing *per se* [303].

1.7 The CpG island methylator phenotype (CIMP)

1.7.1 Introduction

The most extensively characterised feature of the DNA methylome of colorectal cancer is the CpG island methylator phenotype (CIMP). The concept of CIMP was first proposed 18 years ago [113]. In this original description, DNA methylation was examined at 30 CGIs methylated in colorectal cancer (termed *MINT1-33*) in addition to *CDKN2A*, *THBS1*, and *MLH1* by methylated CpG amplification (MCA) in a panel of 50 primary human colorectal carcinomas and 15 adenoma samples. Significantly, two specific patterns of DNA methylation in colorectal tumours were demonstrated, termed type A and type C methylation. Type A loci were frequently methylated in all tumours, but also to a lesser extent in normal colonic tissue. The degree of methylation in normal colonic tissue correlated with age and it was proposed that methylation of type A loci was age-specific. Seven of the clones examined were methylated only in tumours and not in normal tissue. These were termed type C loci (cancer specific). The authors noted that a whilst all tumours examined exhibited high levels of methylation of type A loci, tumours could be divided into to subgroups based on the methylation of type C loci: a subset exhibiting high levels of methylation of type C loci (greater than 3, mean 5.1) and a second subset exhibiting low levels of type C methylation (mean of 0.3 locus per tumour). The term CIMP (CpG island methylator phenotype) was proposed to describe this subset of tumours exhibiting high levels of methylation of type C loci. Notably, tumours identified as CIMP-P exhibited high levels of methylation of the tumour suppressor *CDKN2A/INK4A*, suggesting a possible oncogenic function of CIMP, and a significant proportion exhibited methylation of *MLH1*, providing a mechanistic link to explain a previously noted relationship between CGI methylation and microsatellite instability in human colorectal carcinoma [304].

The concept of CIMP was initially not universally accepted, and several authors have questioned whether CIMP exists at all. It was proposed that somatic hypermethylation events in colorectal cancer were stochastic and age-dependent [305]. A further study examined hypermethylation of the promoter regions of five genes (*DAPK*, *MGMT*, *MLH1*, $p16^{INK4A}$, and $p14^{ARF}$) in 106 colorectal cancers by methylation-specific PCR. In this study, DNA methylation in colorectal cancers demonstrated continuous decreasing distribution rather than the binary CIMP/non-CIMP distribution noted in the original description of CIMP [113] leading to the affirmation that CIMP was a "statistical artefact" [306].

Jean-Pierre Issa, whose lab first proposed CIMP, has suggested that much of the controversy surrounding CIMP is explicable on the basis of the classification system used to define it, and the use of highly sensitive, but non-quantitative assays to assess methylation [307]. In particular, the use of MSP based assays has been criticised due to their inability to discriminate between very high and very low levels of methylation. This is significant, as low levels of promoter methylation at CIMP loci, including *MLH1*, *CDKN2A*, and *MGMT* have been demonstrated to have no effect on protein expression [308].

1.7.2 CIMP classifications in human colorectal adenocarcinoma

Since the original description of CIMP a considerable focus has been placed on optimising the classification systems used to define it. Samowitz et al. [309] examined CIMP by methylation-specific PCR in a cohort of 864 tumours from North American patients, using a five marker panel adapted from the "classic panel" consisting of *MLH1*, *MINT1*, *MINT2*, *MINT31* and *CDKN2A*. Using this classification system, 29.8% of patients were classified as CIMP high. The study confirmed a significant association with $BRAF^{V600E}$ mutation (independent of MSI status), proximal tumour location, and increasing age. MSS, CIMP high tumours were significantly associated with *KRAS* mutation, whereas MSI CIMP high tumours were significantly associated with wild-type *KRAS*. A new five marker panel for CIMP (*CACNA1G*, *CDKN2A*, *CRABP1*, *MLH1* and *NEUROG1*) was examined by Ogino et al. in a panel of 460 colorectal cancers [310]. *MGMT* was also evaluated in this study in light of earlier inclusion in CIMP panels [305,306]. Notably, *MGMT* was found to have a low specificity and sensitivity for CIMP, and was excluded from the final panel by the authors. Once again, a clear bimodal distribution of CIMP-P and non-CIMP tumours was demonstrated, and a significant association demonstrated between CIMP and $BRAF^{V600E}$

mutation, female sex, MSI and wild-type *KRAS*. In the same year, a stepwise screen of 195 CGI methylation markers using the quantitative MethylLight assay in a cohort of 295 primary human colorectal tumours was published [311]. Unsupervised cluster analysis confirmed the bimodal distribution of tumours into CIMP-P and CIMP-N categories as previously described [113]. A new five-marker panel, consisting of *CACNA1G*, *IGF2*, *NEUROG1*, *RUNX3* and *SOCS1*, was proposed, which exhibited superior positive predictive value for CIMP-P than the "classic panel". Significantly, both studies confirmed the association between CIMP-P and microsatellite instability in addition to noting a tight association with $BRAF^{V600E}$ mutant tumours, and an anticorrelation with *KRAS* mutation.

Whilst a bimodal distinction between CIMP-P and CIMP-N tumours is fundamental to the original classification system, subsequent studies have raised the interesting possibility of subclasses of CIMP in colorectal cancer. It has been demonstrated that colorectal cancers can be subclassified as CIMP-high (≥4/5 methylated promoters), CIMP-low (1-3/5 methylated promoters) and CIMP-0 (0/5 methylated promoters) [312]. In contrast to CIMP-high (CIMP-H) tumours, CIMP-low (CIMP-L) tumours exhibited a strong male preponderance and incidence of *KRAS* mutation. Subsequent studies have supported this sub-classification of CIMP using different marker panels [313-316]. Interestingly, CIMP-L tumours exhibit hypermethylation of a subset of the genes that are hypermethylated in CIMP-H tumours rather than a separate group, implying some commonality in the mechanism [313]. The more commonly used CIMP panels are summarised in Table 1-3**.**

Table 1-3 Comparison of commonly employed CIMP panels

A number of different panels have been proposed to describe CIMP in human colorectal carcinoma. Notably the panel employed influences the proportion of tumours defined as CIMP positive, and clinicopathological associations.

Author/Year	Assay	Gene panel	CIMP Definition	CIMP Incidence	Clinicopathological associations
Toyota et al. (1999) [113]	MCA	*MINT1, MINT2, MINT12, MINT17, MINT25, MINT27, MINT31*	≥3/7	58%	*p16* methylation Proximal location *MLH1* methylation MSI Proximal tumour location
Hawkins et al. (2002) [317]	MSP & BPCR	*MINT1, MINT2, MINT12, MINT31, CDKN2A*	≥2/5	18.9%	Proximal location Female sex Older age WT *TP53* *KRAS* mutations MSI
Samowitz et al. (2005) [309]	MSP	*MINT1, MINT2, MINT31, CDKN2A, MLH1*	≥2/5	29.8%	$BRAF^{V600E}$ mutation *KRAS* mutation Older age Increased stage
Ogino et al. (2006) [310]	MethyLight	*CACNA1G, CDKN2A, CRABP1, MLH1, NEUROG1*	≥4/5	17%	Female sex MSI *BRAF* mutation WT *KRAS*
Ogino et al. (2006) [318]	MethyLight	*CACNA1G, CDKN2A, CRABP1, MLH1, NEUROG1*	**CIMP-H** ≥4/5 **CIMP-L** 1-3/5 **CIMP-0** 0/5	15.5% (CIMP-H) 33.2% (CIMP-L) 51.3% (CIMP-0)	Female sex *BRAF* mutation Male sex *KRAS* mutation
Weisenberger et al. (2006) [311]	MethylLight	*CACNA1G, IGF2, NEUROG1, RUNX3, SOCS1*	≥3/5	18%	Female sex Proximal location MSI *BRAF* mutation
Ogino et al. (2007) [319]	MethyLight	*CACNA1G, CDKN2A, CRABP1, IGF2, MLH1, NEUROG1, RUNX3, SOCS1*	**CIMP-H** ≥6/8 **CIMP-L** 1-5/8	15% (CIMP-H) 38% (CIMP-L)	Female sex MSI-H *BRAF* mutation Male sex MSS/MSI-L *KRAS* mutation

1.7.3 CIMP and the wider colorectal cancer epigenome

By definition, CIMP clusters tumours on the basis of promoter methylation. Whilst promoter methylation has historically been the most extensively characterised DNA methylation change in cancer, there is emerging evidence that aberrant DNA methylation is a feature at other genomic elements, and the extent to which CIMP represents a dysregulated DNA methylome is unclear. Genome-wide analysis of DNA methylation profiles of normal colon, CIMP and non-CIMP colorectal cancers has revealed that CIMP cancers exhibit global hypermethylation when compared to non-CIMP cancers. Whilst this hypermethylation is not limited to promoter CGIs, there is enrichment for CpG methylation, with 80% of CIMP-specific hypermethylation being at CpG islands. Interestingly, a significant proportion of CIMP-specific hypermethylated DMRs flank sites that are hypermethylated in all tumours. Furthermore, this spreading of hypermethylation associated with CIMP is predominantly unidirectional [320].

Some studies have characterised the relationship between CIMP status and DNA methylation at other genomic features. Hypomethylation of repetitive elements, such as LINE-1 is a well-documented feature of colorectal cancer, is associated with poor survival, and may contribute to tumourigenesis by the activation of proto-oncogenes [321,322]. LINE-1 hypomethylation has been demonstrated to correlate inversely with CIMP status by a number of authors, suggesting that genome-wide hypomethylation and promoter CIMP are distinct epiphenomena in colorectal cancer [323,324].

Exome sequencing of 16 colorectal tumours and corresponding normal colonic tissue has recently demonstrated that CIMP-H colon cancers frequently possess mutations in chromatin regulators. Mutations in 74 chromatin-regulating genes were identified, and significant enrichment for these mutations was noted in CIMP-H tumours. Enrichment for these mutations in CIMP-H tumours was also demonstrated in the larger TCGA colorectal cancer cohort. The most commonly mutated chromatin modifiers in this study were *CHD7* and *CHD8*. A significant association was noted between *CHD7* and *CHD8* mutations and CIMP-H tumours compared to CIMP-N tumours. *CHD7* and *CHD8* mutations were also significantly associated with MSI. Significantly, genes methylated in CIMP-P colorectal cancers were identified as CHD7 targets [325]. Another chromatin regulator, the histone deacetylase SIRT1, has also been implicated in CIMP. SIRT1 expression was examined in a cohort of 485 colorectal cancers, and a significant association noted with CIMP-H and

MSI [326]. Notably, SIRT1 expression did not correlate with global DNA methylation as assessed by LINE-1 methylation, suggesting a specificity to CGI methylation.

1.7.4 The aetiology of CIMP in human colorectal adenocarcinoma

One of the most interesting, and unresolved questions in the field is the mechanism responsible for the induction of CIMP in colorectal carcinoma. A significant number of putative associations and mechanisms have been described. In the original paper describing CIMP, the authors speculated on potential drivers of the phenomenon: predicting a failure of normal homeostatic protection against *de novo* methylation either due to DNA-methyltransferase mutation or loss of a trans-activating factor [113]. Below, the potential drivers of CIMP are discussed.

1.7.4.1 DNA methyltransferases

The role of the DNA methyltransferase enzymes as potential modulators of the CIMP phenotype has been explored by a number of authors. The literature is at best conflicted, and at times, contradictory. Early functional studies in the *in vitro* context demonstrated that ectopic expression of DNMT1 in primary human fibroblasts induced *de novo* methylation of CpG islands [327]. Subsequently, it was demonstrated that knockdown of DNMT1 alone was insufficient to repress promoter hypermethylation of *CDKN2A/INK4A* and *TIMP3*, and did not lead to re-expression [328]. It was subsequently proposed that DNMT1 and DNMT3B cooperate to maintain promoter methylation in cancer cells. It has been demonstrated in HCT116 that targeted knockout of *DNMT1* or *DNMT3B* alone is insufficient to induce demethylation of the *CDKN2A/INK4A* promoter. Combined knockout of *DNMT1* and *DNMT3B* however was associated with demethylation of the *CDKN2A/INK4A* promoter and expression of the WT allele [329]. This model is challenged however by a subsequent *in vitro* study in which re-expression of $p16^{INK4A}$ was demonstrated upon siRNA knockdown of DNMT1. Furthermore, DNMT1 but not DNMT3A or DNMT3B knockdown, enhanced the reactivation of tumour-suppressors (e.g. $p16^{INK4A}$) following treatment with 5-aza-2'-deoxycytidine, implying DNMT1 alone is required to maintain aberrant CpG island hypermethylation in cancer cells [330].

The primacy of DNMT1 in establishing aberrant CpG island hypermethylation in cancer cells has however further been challenged [331]. In this study DNMT1 RNAi was employed in HCT116 cells, demonstrating maintenance of promoter CpG island hypermethylation and gene-silencing (e.g. *CDKN2A/INK4A*) upon knockdown of DNMT1.

In an attempt to resolve this contradiction, a further study used a quantitative assay to assess *de novo* methylating activity at the CpG islands of *TIMP3*, *O^6-MGMT* and *MLH1* in HCT116, and provided further support for the dominance of DNMT1 in establishing aberrant CpG island hypermethylation in cancer cells [332].

As previously discussed, suppression of DNMT1 has been shown to reduce tumour formation in the *$Apc^{Min/+}$* model, though the role of CpG island methylation was not formally examined in these studies. In a subsequent study, *$Apc^{Min/+}$;Dnmt1* hypomorphs were generated, and once again demonstrated to exhibit a significant reduction in intestinal polyp number and size compared to wild-type *Dnmt1* controls. Furthermore, this reduction was shown to be directly proportional to the level of DNMT1 expression in the different *Dnmt1* hypomorphs examined. Importantly, in this context, *Dnmt1* hypomorphs exhibited lower levels of CpG island methylation both in normal intestinal mucosal tissue and polyps than wild-type *Dnmt1* controls. Once again, this reduction in CpG methylation was shown to be directly proportional to the level of DNMT1 expression in the different *Dnmt1* hypomorphs examined, with no detectable CpG methylation > 1 PMR threshold in the intestinal mucosa of *$Apc^{Min/+}$;$Dnmt1^{N/R}$* mice [333].

The role of DNMT3B in establishing CIMP has been explored *in vitro*. DNMT3B expression was examined in a panel of colon cancer cell lines, with no relationship demonstrated between DNMT3B overexpression and CIMP status. DNMT3B knockdown by RNAi in HCT116, (which expresses high levels of DNMT3B) led to reduced cell viability and upregulation of apoptosis markers. The authors examined whether this antiproliferative effect of DNMT3B knockdown might be due to altered DNA methylation, using Infinium 450K arrays. Overall there was no significant change in global DNA methylation in DNMT3B shRNA HCT116 cells compared to controls, and specifically no difference was noted in DNA methylation at CIMP loci [334].

Steine et al. [335] comprehensively addressed the methylation changes induced by DNMT3B in the murine intestine. In this study, DNA methylation was examined by RRBS in *$Apc^{Min/+}$* mice with tetracycline-inducible DNMT3B overexpression. The authors confirmed a distinct subpopulation of promoter regions exhibiting hypermethylation in DNMT3B overexpressing tissue, and compared these to aberrant promoter methylation in human colon cancer [336]. A highly significant overlap was seen for genes methylated by DNMT3B in the mouse and those methylated in human colon cancer (84% of genes methylated in human colon cancer were also methylated in DNMT3B overexpressing

mice). Moreover, DNMT3B appeared to be specifically inducing a "cancer-specific" methylation pattern, as 92% of genes unmethylated in colon cancer were also unmethylated in DNMT3B overexpressing mice. Whilst CIMP *per se* was not comprehensively assessed in this paper, closer examination of the supplementary data reveals a distinct CIMP phenotype in the DNMT3B overexpressing mice: with hypermethylation of a number of loci previously proposed as CIMP markers (*Cacna1g*, *Cdkn2a*, *Crabp1*, *Igf2*, *Neurog1*, *Socs1* and *Timp3*). Notably however, *Mlh1* did not exhibit hypermethylation in DNMT3B overexpressing mouse colon.

An early study examined the relationship between DNA methyltransferase enzyme expression and CIMP in a small cohort of 25 human colorectal cancers and paired normal colonic tissue, demonstrating no correlation between DNMT1, DNMT3A or DNMT3B expression and CIMP [337]. Two subsequent studies have however implicated aberrant DNMT3B expression and CIMP in primary human colorectal tumour samples. In a further study, CIMP was examined by pyrosequencing in a cohort of 765 colorectal carcinomas together with DNMT3B immunohistochemistry in the same cohort. A significant association between DNMT3B expression and CIMP was noted, though the relationship between DNMT3B and methylation varied markedly from locus to locus [338]. Subsequently, DNA methylation was examined at five CIMP loci (in addition to *SFRP2* and *IGF2*) in normal colonic mucosa, pre-neoplastic lesions and established carcinoma and correlated with DNMT3B expression assessed by immunohistochemistry. Sequential increases in DNA methylation during neoplastic transformation were associated with upregulation of DNMT3B. DNMT3B expression correlated positively with methylation of some markers of CIMP (*NEUROG1*, *CACNA1G* and *CDKN2A*) but there was no significant correlation between DNMT3B expression and *SOCS1*, *RUNX3* or *MLH1* methylation [339]. DNMT3B overexpression has also been correlated with CIMP in breast cancer [340].

1.7.4.2 IDH/TET

Isocitrate dehydrogenase (IDH), a component of the Kreb cycle, catalyses the decarboxylation of isocitrate to α-ketoglutarate. *IDH1* (R132) mutations have been shown to induce CIMP in glioblastoma [341]. Subsequently, *IDH* mutations have been identified in a number of other cancers, including acute myelogenous leukaemia, follicular and anaplastic thyroid carcinoma, and certain cartilaginous tumours [342-344]. Cancer-

associated *IDH1* mutations produce a so-called "onco-metabolite", 2-hydroxyglutarate, which impairs the function of TET2 [345,346].

The IDH-TET-CIMP pathway has been explored as a putative driver of CIMP in colorectal cancer. *IDH1* mutations have been examined in a cohort of 180 colorectal cancers, identifying *IDH1* mutations in 1% of tumours. This study did not clarify the histological subtype or cytogenetic profile of *IDH1*-mutant tumours [347]. *IDH1* mutations have also been demonstrated in a small number of inflammatory bowel disease-associated cancers. R132C mutations were identified in IBD-cancers with low-grade tubulo-glandular histology. No *IDH1* mutations were detected in the sporadic colorectal adenocarcinomas examined in this study [348]. *IDH1* and *IDH2* mutations have also been analysed in a cohort of 152 colorectal cancers with deficient mismatch repair [349]. As noted previously, sporadic dMMR colorectal cancers exhibited a close association with CIMP. No mutations in *IDH1* or *IDH2* were noted in this cohort of tumours. *IDH* mutations have been also been examined in 224 human colorectal cancers in the publically available Cancer Genome Atlas data. It was noted that these were uncommon: *IDH1* mutations were found in 0.5% of cases, and *IDH2* mutations in 1% of cases [350].

Whilst little evidence has been found for *IDH* mutations in colorectal cancer, epigenetic dysregulation of *TET1* has been associated with CIMP. The expression of the TETs has been examined in human colon cancer cell lines, primary human tumour samples and in the publically-available Cancer Genome Atlas data, and correlated with CIMP status [350]. In colon cancer cell lines, TET1 expression was inversely related to CIMP status, and re-expression was noted upon treatment with decitabine, suggesting promoter CpG methylation as a possible mechanism of *TET1* silencing in colon cancer. Furthermore, TET1 expression was significantly lower in CIMP-P tumours compared to CIMP-N cancers, though in corresponding normal tissues, there was no difference in TET1 expression between CIMP-P and CIMP-N cases. There was a significant association between $BRAF^{V600E}$ mutation and *TET1* methylation in CIMP-P tumours. *TET1* methylation was also demonstrated in preneoplastic lesions, implying it may be an early event in colorectal tumourigenesis. Consistent with this observation, a number of other studies have reported altered expression of TETs in colorectal cancer. Downregulation of TET1, TET2 and TET3 in primary human colorectal cancer samples relative to normal colonic tissue has been demonstrated, though in this particular study, no formal analysis was made of a relationship with CIMP status [351]. Low levels of 5hmC and TET1 expression in colorectal cancers compared to normal colonic tissue have also been reported

[352]. In this latter study, ectopic expression of TET1 inhibited colorectal cancer cell proliferation *in vitro* and in cell-line derived xenografts. TET1 reactivation was associated with promoter demethylation and re-expression of Wnt pathway inhibitors, including *DKK3* and *DKK4*. In this study, no formal assessment of CIMP status was made, though the generalizability to CIMP is questionable: nuclear β-catenin (a surrogate for Wnt pathway activation) has previously been shown to be inversely correlated with CIMP-H in colorectal cancer, though CIMP-L cancers exhibited similar levels of nuclear β-catenin to CIMP-N cancers [324,353].

Interestingly, it has recently been demonstrated that promoters marked by 5-hydroxymethylcytosine in normal colon are inherently resistant to DNA methylation in tumours, and that global 5-hydroxymethylcytosine levels are reduced in colorectal tumours compared to normal colonic tissue. In the same study however, no difference in TET expression was noted between tumour and normal tissue, implying that aberrant levels of 5hmC in colorectal cancers is not a result of TET silencing [354].

1.7.4.3 BRAF

A consistently robust association with $BRAF^{V600E}$ mutation and CIMP has been noted [113,311,355-357]. Certain CIMP markers (*MLH1-5'* region, *MLH1-3'* region, $p16^{INK4A}$, *MINT1*, *MINT2*, *MINT31*) have also been reported to be methylated more frequently in $BRAF^{V600E}$-mutant tumours compared to other tumour subtypes [358]. A strong association between *BRAF* mutation and CIMP has also been reported in sessile serrated adenomas [37]. Increasing methylation of CIMP markers has also been demonstrated during the progression of the $BRAF^{V600E}$-driven serrated adenoma pathway [359]. Whilst *BRAF* mutation is an early event in this pathway, CIMP develops more gradually with disease progression. In a more recent study in which the CIMP status of 106 *BRAF*-mutant precancerous colorectal lesions from 94 patients was examined, only 53.8% of lesions were CIMP positive [360]. One interpretation of these studies is that CIMP is selected for in parallel with, rather than arising directly as a result of, $BRAF^{V600E}$ mutation.

Conflicting evidence has however been published on the ability of $BRAF^{V600E}$ to induce CIMP. Promoter methylation of *MLH1* has been demonstrated in NCM460 transformed with activated $BRAF^{V600E}$ [361]. In a subsequent study however, stable expression of $BRAF^{V600E}$ in the CIMP-N colon cancer cell line, COLO 320DM, was found to be insufficient to induce a CIMP phenotype [362]. *In vivo* evidence for $BRAF^{V600E}$ mutation as

a direct driver of a CIMP-like phenotype was recently provided in a novel murine model of *Braf*^{V600E}-mutant colon cancer, in which transgenic expression of mutant BRAF^{V600E} in the murine intestine was demonstrated to result in tumour formation. Tumour development was associated with repression of *p16*^{INK4A} by promoter hypermethylation which was associated with upregulation of DNMT3B at the mRNA and protein level [47].

BRAF^{V600E} mutation has been demonstrated to cause widespread changes in the DNA methylation profile of melanoma cells. RNA interference (shRNA) was used to stably knockdown *BRAF*^{V600E} in melanoma cells, and combined with MCA/CpG array to assay the effects on DNA methylation. Widespread changes in DNA methylation were demonstrated upon *BRAF*^{V600E} knockdown, including both hyper- and hypomethylation events. Significantly, *BRAF*^{V600E} knockdown caused a significant reduction in the expression of both DNMT1 and EZH2 [363]. Whilst this study did not assess CIMP *per se,* it adds weight to the evidence for the *BRAF*^{V600E} oncogene as a mechanistic driver of altered DNA methylation in a cancer context.

A recently-described model has proposed a mechanism by which *BRAF*^{V600E} directly induces CIMP [364]. The authors performed an RNAi screen in the *BRAF*^{V600E}-mutant colon cancer cell line RKO to identify mediators of *MLH1* transcriptional silencing, identifying the transcriptional co-repressor MAFG, which was subsequently demonstrated by ChIP, to bind to the *MLH1* promoter. MAFG was demonstrated to co-localise at the *MLH1* promoter with DNMT3B, BACH1 and CHD8, and furthermore, targeted knockdown of MAFG decreased binding of these cofactors at the *MLH1* promoter. Stable expression of BRAF^{V600E} in primary foreskin fibroblasts increased MAFG protein expression, but did not alter MAFG mRNA levels. Significantly, MAFG was demonstrated to be a phosphorylation target of ERK1, and targeted disruption of BRAF/MEK/ERK signalling led to loss of binding of MAFG, BACH1, CHD8 and DNMT3B to the *MLH1* promoter. The authors have subsequently demonstrated the generalizability of this mechanism to other solid tumours [365]. The model proposed by which BRAF^{V600E} might directly induce CIMP is summarised below. (Figure 1-4)

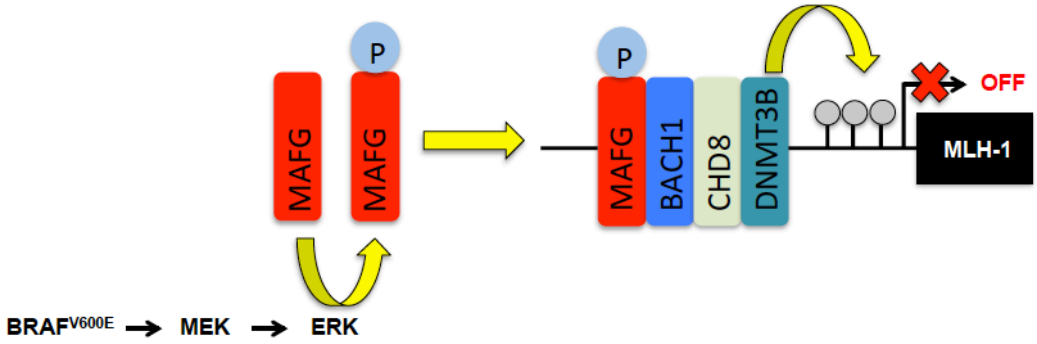

Figure 1-4 Proposed model by which BRAF^{V600E} induces CIMP in colorectal cancer

MAFG is a phosphorylation target of ERK1. Stable expression of BRAF^{V600E} in primary foreskin fibroblasts results in ERK-induced MAFG phosphorylation, with a resultant increase in MAFG protein expression. Phosphorylated MAFG forms a complex with DNMT3B, BACH1 and CHD8, and co-localises at the *MLH1* promoter, resulting in gene silencing. Modified from Fang et al. [364].

1.7.4.4 KRAS

Mutant KRAS has been demonstrated to induce a methylator phenotype *in vitro* [366]. Initial reports on the association between *KRAS* mutation and CIMP in colorectal cancer were however conflicting. Shortly after the original description of CIMP was published, the same group reported frequent *KRAS* mutations in CIMP-P cancers [367]. A number of subsequent studies confirmed this association [317,368]. Some studies however have suggested the converse: proposing a correlation between wild-type *KRAS* and CIMP-P [310,311]. The principle reason for this apparent dichotomy is in the method used to classify CIMP. In studies in which CIMP tumours are sub-classified into CIMP-H and CIMP-L, an association has been noted between *KRAS* mutation and CIMP-L tumours [312,315,316,358]. Interestingly, in a murine model of *Kras*-driven serrated colon tumourigenesis, tumours were found to be CIMP negative [66].

A mechanism by which mutant KRAS can induce a CIMP phenotype has recently been proposed [369]. The authors performed an RNAi screen in the $KRAS^{G13D}$-mutant DLD-1 colon cancer cell line to identify mediators of INK4-ARF silencing, identifying the zinc finger DNA-binding protein ZNF304. Knockdown of ZNF304 was noted to reverse transcriptional silencing of $p14^{ARF}$, $p15^{INK4B}$ and $p16^{INK4A}$. Binding of ZNF304 to the promoters of $p14^{ARF}$, $p15^{INK4B}$ and $p16^{INK4A}$ was confirmed by ChIP, together with the co-repressors KAP1, SETDB1 and DNMT1. Furthermore, shRNA-mediated knockdown of *KRAS* in DLD-1 cells was associated with reactivation of $p14^{ARF}$, $p15^{INK4B}$ and $p16^{INK4A}$, and reduced binding of ZNF304 complex at all three promoter sites. Mutant KRAS was demonstrated to upregulate ZNF304 through PRKD1 and USP28, with the former responsible for phosphorylation of USP28, which protects ZNF304 from proteolytic degradation. The model proposed is summarised below. (Figure 1-5)

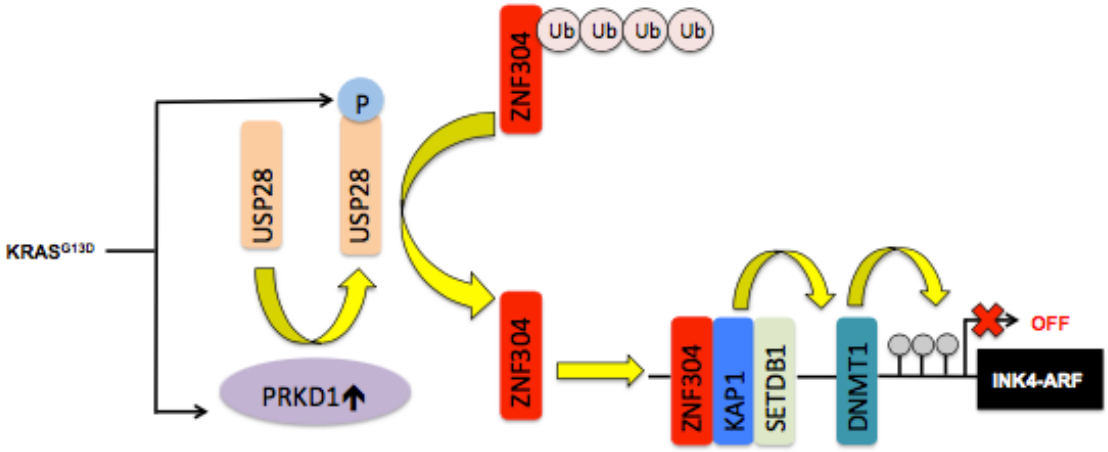

Figure 1-5 Proposed model by which KRAS^{G13D} induces CIMP in colorectal cancer

Mutant KRAS^{G13D} upregulates ZNF304 expression, through PRKD1 and USP28, with the former responsible for phosphorylation of USP28, which protects ZNF304 from proteolytic degradation. ZNF304 forms a complex with KAP1, SETDB1 and DNMT1, which localises to the *p16^{INK4A}* promoter, and prevents expression. Modified from Serra et al. [369].

1.7.4.5 "Hypermutator Phenotype"

A subset of colorectal cancers exhibit a "hypermutator phenotype". The Cancer Genome Atlas analysis has recently demonstrated a strong correlation between a "hypermutator phenotype", CIMP-H and $BRAF^{V600E}$ mutation [314]. A subsequent analysis of a much larger cohort of colorectal cancers (n=4151 patients) has led to the classification of colorectal cancers into four consensus molecular subtypes (CMS1-4). Notably this classification system has confirmed an association between CIMP-H and a "hypermutator phenotype". CMS1 ("MSI immune") tumours exhibit MSI, *BRAF* mutations, a "hypermutator phenotype" and are CIMP-H [27]. It is not however clear whether or not hypermutation is a driver of, or consequent upon CIMP.

1.7.4.6 CIMP: a marker of cell lineage?

Much of the interest in CIMP relates to the dogma that hypermethylation of promoter CGIs has an oncogenic function through the silencing of tumour suppressors. Whilst an attractive model, the significance of hypermethylation of CGIs in cancer is debated, and it remains unclear whether DNA methylation facilitates or reinforces stable transcription repression rather than directly causing it [370,371]. It has previously been suggested that cancer-associated methylation is a marker of cell lineage, rather than a driver of tumour progression, and arises in an "instructive manner" [372,373]. This has significant implications for the concept of CIMP, which has traditionally been associated with, and interpreted in, the context of an oncogenic phenomenon. In breast cancer, tumour methylation patterns reflect cell lineage [372]. The same group subsequently examined the generalizability of this model in a larger cohort of cancers from seven different tissue types. The authors demonstrated that genes that are hypermethylated in cancer are depleted of repetitive elements at their promoters and are repressed in the corresponding normal tissues [374]. This leads to the question of whether CIMP may in fact simply reflect the developmental origin of a particular subset of colon cancers, and might explain the tendency for CIMP-H and CIMP-L tumours to cluster with particular consensus-molecular subtypes of colon cancer [27].

1.7.4.7 Chronic inflammation

Chronic inflammatory stress is increasingly recognised as a driver of neoplasia [375]. Chronic inflammatory stress increases cellular reactive oxygen species (ROS), which both directly affect cellular processes, and promote inflammatory cell recruitment [376]. *In*

vitro, oxidative stress has been demonstrated to result in the recruitment of a complex including DNMT1, DNMT3B and PRC4 to damaged chromatin, with redeployment from GC-poor regions to GC-rich regions, including promoter CpG islands. In the same study, in a murine colitis model, recruitment of DNMT1 to chromatin was not demonstrated. Consistent with the *in vitro* data however, increased binding of PRC components (SIRT1 and EZH2) to chromatin was demonstrated. Moreover, enrichment of EZH2 and DNMT1 at the promoter CpG islands of a number of loci methylated in human cancer was demonstrated. Notably, this model provides one possible explanation for the apparently paradoxical findings of genome wide hypomethylation and promoter CGI hypermethylation in cancer [377].

Ulcerative colitis is a chronic inflammatory condition of the colonic mucosa, which significantly increases the life-time risk of colorectal cancer. Upregulation of DNMT1 has been demonstrated in inflammatory-bowel disease associated cancers relative to sporadic colorectal cancers. Furthermore, *in vitro* treatment of colorectal cancer cell lines with interleukin-6 increases expression of both DNMT1 and DNMT3B, which is associated with gains of methylation at promoter CpG islands [378]. Similarly, in human intestinal epithelial cells cultured *in vitro*, IFN-γ has been demonstrated to increase levels of 5'-methylcytodine, which was associated with upregulation of DNMT3B mRNA. Increased expression of both S-adenosylmethionine-synthetase and S-adenosylmethionine-hydrolase was also demonstrated in this cell culture model. This latter finding was confirmed *in vivo* in DSS-induced colitis in mice, in which DSS treatment increases expression of both S-adenosylmethionine-synthetase and S-adenosylmethionine-hydrolase [379].

Genome-wide analysis of DNA methylation changes in aged, inflamed and tumour tissue from GPX1/2-KO mice (a murine model of inflammatory bowel disease driven carcinogenesis) has demonstrated inflammation-driven gains of methylation with enrichment for polycomb targets associated with frequent loss of H3K27me3 at these loci. Only very limited overlap was demonstrated between the gains of methylation seen in inflamed compared to aged intestinal tissues, suggesting that inflammation-induced methylation changes do not simply represent an accelerated ageing phenotype. By contrast, significant overlap was seen between the gains in methylation in tumours and inflamed tissue: with approximately 60% of tumour-specific DNA methylation changes being present in inflamed tissues, compared to 2% of aged tissues [380].

An early study demonstrated hypermethylation of the *CDKN2A/INK4A* promoter in association with the development of dysplasia in ulcerative colitis [381]. A subsequent study reported higher levels of promoter CpG island hypermethylation in the dysplastic epithelium of ulcerative colitis (UC) patients compared to non-dysplastic epithelium in patients with ulcerative colitis, and "normal colon". Furthermore, there is evidence for a "field effect", with the "normal" colon from UC patients with high-grade dysplasia and cancer, exhibiting high levels of promoter CpG island hypermethylation. Intriguingly and in contrast to the murine data reviewed above, this apparent accelerated promoter CGI hypermethylation was shown to affect the so-called "type A" (age-associated) loci rather than "type C" (CIMP loci) [382]. Consistent with this, two studies have reported a significantly lower incidence of CIMP in colitis-associated cancer than sporadic tumours. Global DNA methylation however (estimated by assay of LINE-1 methylation) is significantly higher in colitis-associated cancer than sporadic colorectal cancer [383,384]. There is therefore somewhat of a discord between the mechanistic research linking chronic inflammation to promoter CpG island hypermethylation, and the reported DNA methylome of inflammation-associated human colorectal cancer, though it is feasible that other inflammation-independent factors involved in colitis-associated cancer may select against a CIMP phenotype.

1.7.4.8 The microbiome

John Cunningham virus (JCV) is a 5.22kb dsDNA polyomavirus which is related to SV40T and in common with the former, encodes T antigen (T-Ag), which is transformative in mammalian cells [385]. JCV DNA is detectable in the colonic mucosa of 81.2% of normal individuals and JCV T-Ag sequences have been demonstrated in human colorectal carcinomas [385,386]. A number of studies have explored correlation between JCV and CIMP positivity in colorectal cancer. Analysis of JCV T-Ag expression by both IHC and PCR in a cohort of 100 sporadic colorectal carcinomas demonstrated a significant association between JCV T-Ag expression and promoter CpG methylation at genes now accepted as CIMP markers ($p16^{INK4A}$, *MLH1*, *RUNX3*). Furthermore, the relationship between JCV and CIMP was stronger in those samples positive for JCV both by T-Ag IHC and detection of JCV DNA by PCR compared to those expressing JCV DNA alone [387]. An association between JCV T-Ag expression and CIMP positivity has also been reported in colorectal adenomas [388]. In a more recent study in a much larger cohort of colorectal cancer patients (n=766) JCV T-Ag expression was significantly associated on univariate analysis with *TP53* mutation, CIN and LINE-1 hypomethylation, but inversely related to

CIMP positivity. On multivariate analysis however, there was no significant relationship between CIMP status and JCV T-Ag expression [389]. A lack of significant association between CIMP status and JCV T-Ag expression has also been reported in a further subsequent study [390].

An association between CIMP and *Fusobacterium* species has also been described. *Fusobacterium* species are Gram-negative anaerobic commensals in the human oral cavity and gastrointestinal tract, which have recently been linked to colorectal carcinogenesis. *Fusobacterium* spp. DNA has been found to be enriched in primary human colorectal tumours, and in colorectal cancer metastases [391,392]. *Fusobacterium* spp. have previously been associated with a number of pathologies of the gastrointestinal tract, including inflammatory bowel disease (a well-established risk factor for colorectal cancer) and acute appendicitis, and is recognised to be a pro-inflammatory organism [393,394]. A number of studies have examined the relationship of *Fusobacterium* and CIMP in human colorectal cancer. A significant relationship between *Fusobacterium spp.* and CIMP positivity has been noted in a cohort of 149 colorectal cancers [395]. The relationship between CIMP status and *Fusobacterium nucleatum* has also been examined in pre-neoplastic lesions, where a significant association was noted with CIMP-H [396]. A larger subsequent study examined the relationship between *Fusobacterium nucleatum* (as opposed to *Pan-Fusobacterium*) and a number of molecular features (including *BRAF* mutation, CIMP status and MSI status) in a large cohort of colorectal cancers. Whilst a significant relationship was noted between *Fusobacterium nucleatum*, CIMP-H and *BRAF* mutation on univariate analysis, on multivariate analysis, the relationship was not significant [397]. A number of subtle differences between the study designs may explain these apparently conflicting results. Tahara et al.[395] examined *pan-Fusobacterium* whereas Mima et al. [397] examined specifically *Fusobacterium nucleatum*. Furthermore, Tahara et al. [395] compared CIMP-P (including CIMP-H and CIMP-L) to CIMP-N, whereas Mima et al. [397] grouped tumours into two cohorts: CIMP-H and CIMP-L/CIMP-N.

1.7.4.9 CIMP in the wider cancer context

Whilst originally described in colorectal cancer, CIMP has now been reported in a number of other tumour types [341,398-405]. A common feature of several of these studies is a significant degree of variation in the thresholds used to define CIMP positivity and a reliance on CIMP panels described in the colorectal cancer literature. The advent of large cohort studies such as the Cancer Genome Atlas project, which have generated large quantities of methylation data across a number of different cancer types, have realised the possibility of examining CIMP as a universal feature of human cancer.

A recent integrative analysis of TCGA data on SCNAs, somatic mutations and DNA methylation data from twelve cancer subtypes has revealed some commonalities in tumour hypermethylation patterns. A candidate gene analysis of a panel of genes commonly hypermethylated in cancer was performed in this cohort. The most frequently hypermethylated genes were *MGMT*, *GSTP1*, *MLH1* and *CDKN2A* [406]. A separate analysis of DNA methylomes from ten tumour types has revealed commonalities in hypermethylation events across tumour types. Across tumour types, hypermethylation events were noted to be enriched in developmental and morphogenesis pathways, and PRC2 target genes. Whilst overall, hypermethylation events were relatively depleted in cell cycle and DNA repair pathways, certain cell cycle genes including *APC*, *CDKN2A* and *CDKN2B* exhibited frequent hypermethylation across tumour types [407].

The existence of similarities in hypermethylation events across cancer types and the identification of CIMP-phenotypes in extra-colonic tumours have prompted analysis of CIMP as a "pan-cancer phenomenon". Sánchez-Vega et al. [408] examined methylation data from 5,253 tumours across 15 cancer types from the cancer genome atlas and identified a panel of 89 DMR probes that reliably differentiate CIMP-positive from CIMP-negative tumours across 12 of the 15 tumour types examined. A similar analysis of methylation data from The Cancer Genome Atlas data for five solid organ tumours (bladder, breast, colon, lung and stomach) has identified a different "cross-cancer CIMP signature" of 89 CGIs within 51 genes that identifies CIMP positive tumours irrespective of the tissue of origin (Table 1-4).

Despite the apparent commonalities in methylation signatures, there were no somatic mutations that correlated with CIMP across all cancer types, though a previously described relationship between *BRAF* mutation and CIMP in colon cancer was confirmed [409].

Table 1-4 The "cross cancer CIMP signature"

89 CGIs within this panel of 51 genes define a "cross-cancer CIMP signature". Adapted from Moarri et al. [409]

"Cross-cancer CIMP signature"	*LOC339524, GSTM1, CD1D, LMX1A, CACNA1E, NR5A2, WNT3A, GNG4, EMX1, CTNNA2, LRRTM1, DLX1, EVX2, HOXD13, GBX2, SYN2, HAND2, NBLA00301, EBF1, HIST1H2BB, HIST1H3C, HLA-DRB1, C6orf186, IKZF1, CDKN2A, HMX3, KNDC1, KLHL35, HOTAIR, SLC6A15, ALX1, RFX4, CLDN10, ADCY4, RIPK3, NID2, OTX2, OTX20S1, GSC, KIF26A, GREM1, SEC14L5, HS3ST3B1, IGF2BP1, HOOK2, NFIX, ZNF577, ZNF649, CPXM1, CDH22, CHRNA4*

1.8 Summary, hypothesis and thesis aims

Approximately 10-20% of human colorectal cancers are associated with activated *BRAF*^{V600E} mutation, typically in absence of *APC* mutation and often associated with a CpG island methylator phenotype. To protect from cancer, normal intestinal epithelial cells are thought to respond to oncogenic *BRAF*^{V600E} by activation of intrinsic p53- and p16-dependent tumour-suppressor mechanisms, such as cellular senescence. Conversely, CIMP is thought to contribute to bypass of these tumour-suppressor mechanisms, e.g. via epigenetic silencing of tumour-suppressor genes, such as *CDKN2A/INK4A*. An emerging body of evidence proposes that DNMT3B is responsible for *BRAF*^{V600E}-induced CIMP in human colorectal carcinoma, though the literature is conflicted and at times contradictory. In this thesis, the putative BRAF^{V600E}-DNMT3B-CIMP pathway will be examined by multiple approaches.

1.8.1 Hypothesis

Activated oncogenic BRAF^{V600E} induces the CpG island methylator phenotype in human colorectal adenocarcinoma through the *de novo* methyltransferase DNMT3B.

1.8.2 Specific Aims

The specific aims of this thesis are:

- To characterise the DNA methylation changes induced by activated oncogenic BRAF^{V600E}
- To examine oncogenic cooperation between BRAF^{V600E} and DNMT3B in both *in vitro* and *in vivo* model systems of BRAF^{V600E}-mediated neoplasia
- To analyse relationships between BRAF^{V600E}, DNMT3B and CIMP in human colorectal adenocarcinoma.

2 Materials and Methods

2.1 Materials

2.1.1 Reagents

Reagents used in this thesis are summarised in Table 2-1.

Table 2-1 Summary of reagents

Reagent	Details	Manufacturer	Catalogue Number
Agarose	Molecular biology grade	Sigma Aldrich	A9539
Ampicillin	Plasmid selection antibiotic	Sigma Aldrich	10835242001
Blasticidin	Nucleoside antibiotic	Thermo Fisher	A1113903
BrdU	5-Bromo-2'-deoxyuridine	Sigma Aldrich	B5002
β-napthoflavone	Murine transgene induction agent	Sigma Aldrich	N3633
Doxycyline hyclate	>98% (HPLC)	Sigma Aldrich	D9891
DNA ladder	O'Gene Ruler^{TM} DNA ladder mix 100-10,000 bp; 0.1µg/mL in 10mM Tris-HCl (pH 7.6) 0.15% orange G, 0.03% xylene cyanol FF, 60% glycerol, 60mM EDTA10mM	Fermentas	SM1173
DNA loading dye	6 x orange loading dye 10mM Tris-HCl (pH 7.6) 0.15% orange G, 0.03% xylene cyanol FF, 60% glycerol, 60mM EDTA	Fermentas	RO631
DMEM	Dubelco's Modified Eagle Medium	Life Technologies	21969-035
ECL Western Blotting Substrate	ECL-horseradish peroxidase	Thermo Fisher	32106
Ethanol		VWR Chemicals	20821.365
Ethidium bromide	10mg/mL in H_2O	Sigma Aldrich	E1510
Fetal bovine serum	Cell culture medium	Life Technologies	10270
Formalin	10% neutral buffered formalin	Sigma Aldrich	HT501128
L-Glutamine	L-Glutamine 200mM	Life Technologies	
Lipofectamine 2000	Transfection reagent	Life Technologies	11668-027
Methanol		VWR Chemicals	20846.326
Penicillin-Streptomycin	10,000 units/mL penicillin 10,000 µg/mL streptomycin	Thermo Fisher	15140-122
Phosphate buffered saline (PBS)	170mM NaCl 3.3mM KCl 1.8mM Na_2HPO_4 10.6mM H_2PO_4	BICR Central Services	N/A
Phosphate buffered saline with Tween (PBST)	1 x PBS + 0.5% v/v Tween20	BICR Central Services	N/A
Polybrene	10mg/mL sterile Ultra Pure water	Millipore	TR-1003-g
Puromycin	Aminonucleoside antibiotic	Thermo Fisher	A1113803

Reagent	Details	Manufacturer	Catalogue Number
RPMI	RPMI Medium 1640	Life Technologies	31870-025
Sample buffer + dithiothreitol (DTT)	62.5mM Tris HCl pH 6.8 2% w/v SDS 10% v/v glycerol 0.1M DTT 0.01% w/v bromophenol blue	Prepared in house	N/A
Sucrose	Murine placebo induction agent	Sigma	S7903
SDS	10% sodium dodecyl sulphate	BICR Central Services	N/A
Tamoxifen	Murine transgene induction agent	Sigma	T5648
Transfer buffer	50mM Tris, 40mM glycine, 0.04% SDS, 20% methanol	BICR Central Services	N/A
Tris-acetate-EDTA (TAE buffer)	40mM Tris, 0.1% glacial acetic acid, 1mM EDTA	BICR Central Services	N/A
Tris-buffered saline	10mM Tris-HCl, pH 7.4 150mM NaCl	BICR Central Services	N/A
Tris-EDTA (TE buffer)	10mM Tris-HCl, pH 8.0 1mM EDTA	BICR Central Services	N/A
Trypsin	2.5% phenol red free	Gibco	15090-046
Xylene	C_8H_{10}	Thermo Fisher	X5-1
2-β-mercaptoethanol	99% molecular biology grade	Sigma Aldrich	M752

2.1.2 Antibodies

Antibodies used in this thesis are summarised in Table 2-2.

Table 2-2 Summary of antibodies

Antigen	Species	Manufacturer	Catalogue	Assay	Dilution
Alexa-fluor488 goat	Mouse	Life Technologies	C10425	FACS	1:40
α-goat-HRP	Donkey	Santa Cruz	SC2020	WB	1:5000
α-mouse-HRP	Horse	Cell Signalling	7076	WB	1:5000
α-rabbit-HRP	Goat	Cell Signalling	7074	WB	1:5000
β-actin	Mouse	Sigma	A1978	WB	1:200,000
β-catenin	Mouse	BD Biosciences	610154	IHC	1:1200
BRAF	Mouse	Santa Cruz	SC5284	WB	1:200
BrdU	Mouse	BD Biosciences	M0744	FACS	1:40
Cyclin A	Rabbit	Santa Cruz	SC751	WB	1:500
Cyclin D1	Rabbit	Dako	M3642	IHC	1:50
DNMT3B	Rabbit	Abcam	AB79822	WB	1:1000
DNMT3B	Mouse	Imgenex	IMG184A	WB (murine) IHC (murine)	1:1000 1:300
DNMT3B	Rabbit	NEB	M0232	WB	1:1000
DNMT3B	Rabbit	Novus Biologicals	100-266	WB	1:1000
DNMT3B	Goat	Santa Cruz	SC10236	WB	1:500
EZH2	Rabbit	Cell Signalling	5246	WB	1:1000
GAPDH	Rabbit	Cell Signalling	14C10	WB	1:2000
Ki67	Rabbit	Thermo Fisher	RM9106	IHC	1:200
MLH-1	Mouse	Cell Signalling	3515	WB	1:1000
γH2AX	Rabbit	Cell Signalling	9718	IHC	1:50
IL1α	Goat	R&D Systems	AF400	IHC	1:100
$p16^{INK4A}$	Rabbit	BD Biosciences	BD51-1352GR	WB	1:1000
$p21^{WAF}$	Rat	CNiO Institute	T3413	IHC	1:4
$p27^{KIP}$	Rabbit	Cell Signalling	2552s	WB	1:1000
ppRb (Ser807/811)	Rabbit	Cell Signalling	9308s	WB	1:1000
Sox9	Rabbit	Millipore	AB5535	IHC	1:700
Total Rb	Mouse	Cell Signalling	9309s	WB	1:1000

2.1.3 Enzymes and kits

Enzymes and kits used in this thesis are summarised in Table 2-3.

Table 2-3 Enzymes and kits

Kit	Purpose	Manufacturer	Catalogue
DNA blood mini kit	DNA extraction from adherent cells	Qiagen	51104
GoTaq® Flexi DNA polymerase	PCR	Promega	M8305
QIAquick gel extraction kit	Gel extraction of plasmid DNA	Qiagen	28704
Qiashredder Columns	RNA extraction	Qiagen	79654
Qubit RNA HS assay kit	RNA quantification	Thermo Fisher Scientific	Q32852
Qubit DNA HS assay kit	DNA quantification	Thermo Fisher Scientific	Q32851
Qubit protein assay kit	Protein quantification	Thermo Fisher Scientific	Q33211
Rapid DNA ligation kit	DNA ligation for molecular cloning	Sigma Aldrich	11635379001
RNeasy Mini Kit	RNA extraction	Qiagen	74104

2.1.4 Plasmids

Plasmids used in this thesis are summarised in Table 2-4. Specific details related to plasmid utilisation are detailed in the text of the relevant chapters.

Table 2-4 Summary of plasmids

Plasmid	Source
HIV-CS-CG-puromycin	Gift of Peeper Laboratory
HIV-CS-CG-BRAF^{V600E}-puromycin	Gift of Peeper Laboratory
HIV-CS-CG-blasticidin	Gift of Peeper Laboratory
HIV-CS-CG-BRAF^{V600E}-blasticidin	Gift of Peeper Laboratory
lentiCRISPRv2-puromycin	Addgene
pLKO.1-puromycin	GE LifeSciences/Dharmacon
plKO.1-shDNMT3B685-puromycin	GE LifeSciences/Dharmacon
plKO.1-shDNMT3B686-puromycin	GE LifeSciences/Dharmacon
plKO.1-shDNMT3B687-puromycin	GE LifeSciences/Dharmacon
plKO.1-shDNMT3B688-puromycin	GE LifeSciences/Dharmacon
psPAX2	Addgene
plpVSVG	Invitrogen
pcDNA3/Myc-DNMT3B1	Addgene
pcDNA3/Myc-DNMT3B3	Addgene

2.1.5 Cell lines

The cell lines used in this study together with their respective growth media requirements are summarised in Table 2-5. Cell line verification was performed by Mr William Clark in the sequencing facility at the Beatson Institute for Cancer Research, Glasgow.

Table 2-5 Summary of cell lines

Cell Line	Description	Base Culture Media	Source
3BKO	HCT116-derived DNMT3B knockout line	McCoy's 5A medium 10% FBS	Gift of Meehan Laboratory
DLD1	Human colorectal adenocarcinoma	DMEM 10% FBS	ATCC CCL-221
HEK293T/17	Highly-transfectable human kidney cells	DMEM 10% FBS	ATCC CRL-11268
HCT116	Human colorectal adenocarcinoma	DMEM 10% FBS	ATCC CCL-247
HT29	Human colorectal adenocarcinoma	DMEM 10% FBS	ATCC HTB-38
IMR90	Human fetal lung fibroblasts	DMEM 10% FBS	ATCC CCL-186
LS411N	Human colorectal adenocarcinoma	RPMI 1640 10% FBS	ATCC CRL-2159
RKO	Human colorectal adenocarcinoma	DMEM 10% FBS	ATCC CRL-2577
SW1417	Human colorectal adenocarcinoma	Leibovitz L15 10% FBS	ATCC CCL-238
SW480	Human colorectal adenocarcinoma	Leibovitz L15 10% FBS	ATCC CCL-228

2.2 Methods

2.2.1 Cell culture

2.2.1.1 Maintenance of cell lines

Human colorectal cancer cell lines (3BKO, DLD1, HCT116, HT29, LS411N, RKO, SW1417 and SW480) were grown in their respective base culture media (as detailed above) supplemented with 2mM L-glutamine, 10 units/mL Penicillin G and 10µg/ml streptomycin. Cells were cultured in 10cm plates in a humidified atmosphere with 5% CO_2 at 37°C. Human fetal lung fibroblasts (IMR-90) were grown in DMEM supplemented with 10% FBS, 2mM L-glutamine, 10 units/mL Penicillin G and 10µg/ml streptomycin. Cells were cultured in 10cm plates in a humidified atmosphere with 3% O_2 and 5% CO_2.

Passaging of cells was performed at 70-80% confluency. Culture media were aspirated, and the cells lavaged twice with sterile phosphate-buffered saline to remove remaining traces of culture media. Trypsinisation was then performed with 1mL of 1% trypsin in phosphate-buffered EDTA solution for 3 minutes at 37°C. With cell detachment confirmed

by visual inspection with a microscope, the trypsin solution was neutralised by the addition of fresh culture media (supplemented with FBS) to the plate. Cells were then resuspended in culture media, passaged to fresh plates, and returned to the incubator.

2.2.2 Lentivirus

2.2.2.1 Transfection of HEK-293T lentiviral packaging cells

$12x10^6$ HEK-293T cells were seeded in 25mL of culture medium to TC175 flasks 20 hours prior to transfection. Cells were approximately 70% confluent for transfection. Immediately prior to transfection, 13mL of culture medium was aspirated from flasks, and the cells returned to the incubator. Lipofectamine 2000 was selected as a transfection agent for all lentivirus production. 120µL of transfection agent were added dropwise to 1.5mL of sterile DMEM in a 15mL centrifuge tube, gently agitated and incubated for five minutes at room temperature. Concurrently, packaging plasmids (5µg plpVSVG and 8µg psPAX2) were combined with 20µg of vector genome in 1.5mL of sterile DMEM in a separate 15mL centrifuge tube. Thereafter the DNA and transfection reagent solutions were combined, gently agitated and incubated for 20 minutes at room temperature. The transfection solution was then added to the prepared HEK-293T flasks to yield a total final transfection volume of 15mL. Following transfection, HEK-293T cells were returned to the incubator for six hours, following which the transfection solution was aspirated, and a fresh 15mL of culture medium added to the flask. For all transfections, a separate lentiviral green fluorescent protein (pLenti6-CMV-GFP-puromycin) control transfection was performed in parallel to confirm transfection efficiency. Transfection efficiency was assessed by visual inspection.

2.2.2.2 Collection and concentration of lentivirus

After a period of twenty hours following transfection, GFP controls were examined to confirm transfection efficiency. Lentiviral supernatant was then aspirated from transfected HEK-293T cells, reserved and stored at 4°C. A further 15mL of culture medium was added to the HEK-293T cells and returned to the incubator for a further twenty hours. The second lentiviral supernatant fraction was then combined with the first, centrifuged at 3000RPM in a table-top centrifuge, and filtered through a 0.45µM low-protein binding PVDF filter prior to concentration. Filtered viral supernatants were transferred to sterile 38.5mL polypropylene centrifuge tubes (Beckman 326823) and weights equalised by the addition of sterile PBS. Ultracentrifugation was performed at 47,000 x *g* in an SW-28 Beckman-

Coulter ultracentrifuge for two hours at 10°C. Following centrifugation, the supernatant was discarded by gentle inversion, and the viral pellet resuspended in 100µL of sterile PBS overnight at 4°C, prior to being aliquoted and stored at -80°C.

2.2.2.3 Lentiviral transduction for adherent cells

The multiplicity of infection (MOI) for lentiviral preparations was calculated empirically by seeding cell lines to a 6-well plate twenty-four hours prior to transduction. Culture medium was then aspirated from each well, replaced with 1mL of fresh culture medium supplemented with polybrene at a final concentration of 8µg/mL, and the cells returned to the incubator for four hours prior to transduction. Concentrated lentivirus was then added to each well at 0, 1, 2, 4, 8 and 16µL/mL, and returned to the incubator for sixteen hours. Following transduction, the infection medium was removed from each well, and replenished with 2mL of fresh culture medium supplemented with the appropriate drug-selection as determined by the construct design. The minimum volume of lentiviral construct required to yield 100% cell survival following drug-selection was then employed for all subsequent experiments. All experiments involving lentivirus were performed in their entirety under drug selection.

2.2.3 Cell cycle analysis by flow cytometry

Cell cycle analysis by fluorescence-activated cell sorting (FACS) was performed by combined 5-bromo-2'-deoxyuridine (BrdU) and propidium iodide (PI) staining. Cells were incubated with BrdU at a final concentration of 25µM for 4-24 hours, after which the culture medium was aspirated, the cells washed in PBS and trypsinised before being resuspended in culture medium. Following resuspension, cells were pelleted, washed in PBS and pelleted. Cell pellets were resuspended in 200µL of PBS at 4°C, and fixation achieved by the addition of 2mL of ice-cold ethanol prior to gentle vortexing, and storage at 4°C for a minimum of 12 hours prior to further analysis.

Following fixation, cells were pelleted and resuspended in 1mL of PBS before the addition of 1mL of 4N HCl. Cells were then incubated for 15 minutes at room temperature, pelleted and the supernatant aspirated. Cells were then resuspended in 1mL of PBS, pelleted and resuspended in 1mL of PBT. The cells were then pelleted, before being resuspended in 200µL of anti-BrdU antibody diluted 1:40 in PBT. Cells were incubated with primary antibody for one hour at room temperature, following which they were pelleted, washed with 1mL PBT and then pelleted before being resuspended in 200µL of Alexa-Fluor® 488

goat anti-mouse antibody, diluted 1:40 in PBT. Cells were incubated in the dark with secondary antibody at room temperature for one hour, following which they were pelleted, and resuspended in 1mL of PBS containing propidium iodide at a final concentration of 10μg/mL and RNase A at a final concentration of 250μg/mL. FACS analysis was performed using the FACSCalibur analyser, and subsequent analysis performed using FlowJo software.

2.2.4 Protein

2.2.4.1 Preparation of protein lysates

Protein lysates were prepared in 1x sample buffer (62.5mM Tris-HCl pH 6.8, 2% SDS, 10% glycerol, 0.1M DTT, 0.01% bromophenol blue). Media was aspirated from tissue culture plates, and the cells washed in 10mL of sterile PBS. The PBS was then aspirated, and the cells scraped into boiled 1x sample buffer using a plastic scraper and transferred to an Eppendorf tube. The contents were vortexed vigorously, aspirated through an 18-gauge needle, and boiled for five minutes at 100°C. Lysates were then centrifuged for 5 minutes in a bench-top microcentrifuge at 12,000 x *g*, and flash-frozen in a dry-ice ethanol bath. Protein lysates were stored at -80°C.

2.2.4.2 Quantification of protein lysates

The protein concentration of lysates in 1 x sample buffer was determined using the Qubit® protein assay kit. Pre-diluted BSA standards provided with the kit were used to calibrate the fluorometer prior to use, with the addition of 1μL of 1x sample buffer to each of the three protein standards. Quantification was undertaken in triplicate for all samples, and a mean protein concentration calculated.

2.2.4.3 SDS-PAGE electrophoresis

Electrophoresis of proteins was undertaken using pre-cast SDS-PAGE gradient gels. Protein lysates were boiled, and 25μg of total protein loaded per well. Sample volumes were equalised using 1x sample buffer. Electrophoresis was undertaken using the Bio Rad Mini-PROTEAN® Tetra cell system. Loaded gels were assembled in a Mini-PROTEAN® Tetra cell, which was filled with 1x SDS-PAGE running buffer (25mM Tris, 192mM glycine, 0.1% SDS, pH 8.3), and protein separation achieved by application of a constant current of 200 V. The total electrophoresis time was varied depending on the molecular weight of the peptide of interest.

2.2.4.4 Western blotting

Following electrophoresis, proteins were immobilised to polyvinylidene fluoride (PVDF). Prior to transfer, membranes were soaked in methanol for 30s with gentle agitation, rinsed with dH_2O, and placed in cold 1x blotting buffer (25mM Tris pH 8.3, 192mM glycine, 0.01% SDS, 20% methanol). A transfer cassette was assembled, incorporating the gradient gel and PVDF membrane, and placed in a Mini Trans-Blot® tank containing 1x blotting buffer. Protein transfer was achieved by application of a constant current of 100V, 350mA for 1 hour.

2.2.4.5 Immunohistochemistry

Immunohistochemistry was performed by the histology service at the Beatson Institute for Cancer Research, Glasgow. Following embedding in paraffin, 4μm sections were cut using a microtome. Sections were first dewaxed by immersion in xylene for ten minutes, followed by rehydration through serially graded ethanol solutions. Tissues were then washed in deionised water for 5 minutes prior to antigen retrieval. Antigen retrieval was achieved by immersion of sections in boiled 1x pH 6.0 sodium citrate antigen retrieval buffer for 25 minutes, and sections then allowed to cool for 30 minutes, prior to a single wash in Tris-buffered Tween. Endogenous peroxidases were then quenched by immersion in a solution of 2% (v/v) hydrogen peroxide in methanol for 15 minutes. Following quenching of endogenous peroxidases, samples were washed with Tris-buffered Tween. Samples were then blocked by immersion in Tris-buffered Tween 1% BSA for 30 minutes. Following blocking, sections were incubated at room temperature for 30 minutes with primary antibody prior to 2 washes in Tris-buffered Tween. Samples were then incubated with an appropriate HRP-linked secondary antibody for a further 30 minutes at room temperature prior to a further 2 washes in Tris-buffered Tween. Samples were then developed with 3,3'-diaminobenzidine tetrahydrochloride for 10 minutes, washed in deionised water for 1 minute, and counterstained for 7 minutes with Haematoxylin Z. Sections were then "blued" by submersion for 1 minute in Scott's water, washed for a further 1 minute in deionised water then dehydrated through serially graded alcohols prior to mounting and coverslip application.

2.2.5 DNA

2.2.5.1 DNA extraction from adherent cells

Genomic DNA was isolated using the QiaAmp DNA blood mini kit (Qiagen) according to the manufacturer's instructions. The QiaAmp DNA blood mini kit allows silica-membrane based DNA purification. In summary, cells pellets were resuspended in 200µL of PBS, and treated with proteinase K. After addition of lysis buffer (buffer AL), samples were vortexed and incubated at 56°C for 10 minutes. DNA was then precipitated by the addition of 200µL of 100% ethanol. Following centrifugation, additional washing (buffer AW1 and buffer AW2) and centrifugation steps were performed. DNA was then eluted from the column using 200µL of buffer AE, and stored at 4°C prior to subsequent analysis. DNA quantification was performed using the Qubit DNA HS assay kit (Thermo Fisher Scientific).

2.2.5.2 Diagnostic restriction digest

For plasmid verification etc. diagnostic restriction digests were performed. Enzymes and appropriate buffers were selected based on plasmid design. 500ng of purified plasmid DNA was incubated with 1 unit of the appropriate restriction enzyme together with the supplied buffer and distilled water at 37°C for 1 hour prior to subsequent analysis by agarose gel electrophoresis.

2.2.5.3 Agarose gel electrophoresis

Electrophoresis of DNA was performed on agarose gels of pre-determined percentages dependent on the fragment size of interest. Typically 0.7 – 1.2% (w/v) gels were used. Electrophoresis-grade agarose was dissolved in TAE (Tris-Acetate-EDTA) buffer, and heated. Agarose-TAE solution was allowed to cool before the addition of ethidium bromide at a final concentration of 0.5µg/ml, and transferred to an electrophoresis tank. Appropriate volumes of 10X DNA loading dye were added to DNA samples to achieve a 1X final concentration, and samples loaded to individual wells with the addition of a DNA ladder to the first well. Separation was achieved by the application of a constant current of 100V. Following electrophoresis, DNA samples were visualised by UV transillumination.

2.2.5.4 PCR

PCR was performed using the Promega GoTaq Flexi DNA Polymerase kit (Promega, Madison, Wisconsin, USA) according to the manufacturer's instructions. Specific details of PCR primer design are outlined in the relevant sections of chapter 3. For PCR reactions, 500ng of template DNA was combined with forward and reverse primers (final concentration 1μM), GoTaq® buffer (final concentration 1x), $MgCl_2$ (final concentration 1mM), PCR nucleotide mix (final concentration 0.2mM each dNTP), GoTaq® DNA polymerase (1.2 units) in nuclease-free water in sterile microcentrifuge tubes incubated on ice to a final reaction volume of 50 μL. Thermal cycling was performed using a BioRad DNA Engine Peltier thermal cycler using the settings specified in Table 2-6.

Table 2-6 PCR settings

Step	Temperature	Time	Number of Cycles
Initial denaturation	95°C	2 minutes	1
Denaturation	95°C	30 seconds	35
Annealing	60°C	30 seconds	
Extension	72°C	1 minute	
Final extension	72°C	5 minutes	1
Soak	4°C	Indefinite	NA

2.2.5.5 Molecular Cloning

Specific details of DNMT3B CRISPR and ectopic DNMT3B expression plasmid design and cloning strategy are discussed in chapter 3 of this thesis. Subcloning of CRISPR sgRNAs and DNMT3B cDNAs into lentiCRISPRv2-puromycin and pLenti6-puromycin respectively was achieved by preparative digest of the individual vector plasmids with preselected restriction enzymes (according to the cloning strategy) overnight at 37°C with their respective buffer and distilled water. Digested plasmid DNA was then resolved by agarose gel electrophoresis, and the digested vector excised under UV guidance. The digested plasmid was purified using the QIAquick gel extraction kit, and eluted in 30μL of elution buffer. Ligation of inserts into digested vector plasmids was performed using the Rapid DNA Ligation Kit (Roche) according to the manufacturer's instructions. Vector and insert DNAs were mixed and diluted in 1x DNA dilution buffer to a final volume of 10μL. Thereafter 10μL of T4 DNA ligation buffer was added to the reaction together with 1μL of T4 DNA ligase. After gentle mixing, ligations were incubated at room temperature for 5 minutes, and then used to transform chemically-competent bacteria.

2.2.5.6 Transformation of chemically-competent bacteria

Plasmid DNA was transformed into OneShot® Stbl3 chemically-competent *Escherichia coli* (Life Technologies) according to the manufacturer's instructions. Bacteria were thawed on ice prior to the addition of 1μL of plasmid DNA and mixed by gentle agitation. Vials were incubated for 30 minutes on ice prior to heat-shocking at 42°C for 45 seconds. Thereafter, vials were placed on ice for 2 minutes, before the addition of 250μL of L-Broth. Vials were then capped and incubated in a rotational incubator at 37°C for 1 hour at 225 RPM. 25μL from any particular transformation was then spread onto L-Broth agar plates impregnated with the appropriate drug selection marker, followed by incubation overnight at 37°C. Individual colonies were picked, and submitted to the Beatson Institute for Cancer Research sequencing facility for "Mini-Prep". Plasmid identify was then variously confirmed by diagnostic restriction digest or targeted sequencing.

2.2.5.7 Whole genome bisulfite sequencing

Whole genome bisulfite sequencing was performed by the Beijing Genomics Institute (BGI, Shenzhen, China). Following DNA quantification and assessment by agarose electrophoresis, genomic DNA was sent for bisulfite sequencing. Briefly, DNA was fragmented by sonication to a mean size of approximately 100-300bp, followed by "end-blunting": the addition of dA to the 3'-end and adapter ligation (the latter allows assessment of the efficiency of bisulfite conversion). Bisulfite-conversion was then performed using the Zymo EZ DNA methylation-Gold kit, which converts unmethylated cytosines to uracils. Bisulfite-treated DNA was then subjected to a PCR assay, whereby uracils are converted to thymidines. The PCR amplicons were then subject to 90bp paired-end sequencing using an Illumina HiSeq-4000 machine.

2.2.5.8 Processing and analysis of whole genome bisulfite sequencing data

Initial alignment and analysis of bisulfite-sequencing data was performed by Mr Neil Robertson, a computational biologist in Professor Peter Adams' lab at the Beatson Institute for Cancer Research, Glasgow. Whole genome bisulfite sequencing alignment data are summarised in Table 2-7 below. The analysis pipeline has been described previously, and is summarised below [281]. The quality of sequenced reads was first tested using FastQC (version 0.10.0). Thereafter, adapters and low-quality sequence tails were excluded using trim-galore (version 0.3.0). Alignment of sequence reads to UCSC (hg19) genome was performed using Bismark (version 0.10.1) based on the Bowtie2 aligner (version 2.1.0)

[410]. The methylation status of each aligned sequence tag was then inferred by comparison to the unconverted reference genome. Potential duplicate reads (defined as those reads for which both ends of a given fragment align to the same genomic position on the same strand) were then removed to control for PCR bias using Bismark (version 0.10.1). Furthermore, the exclusion of reads with >3 methylated cytosines in a non-CpG context controlled for incomplete bisulfite-conversion.

Methylated cytosines were then identified by aggregation of processed reads on a per CpG basis, followed by the collapsing of CpG dyads into a single score for the cytosine on the forward strand. Differentially-methylated CpGs were then identified using a two-tailed Fisher's exact test. Only those CpGs with ≥10 reads within each condition tested were considered for statistical analysis. False-positives were controlled at a rate of 5% by means of FDR-correction of p-values using the Benjimini-Hochberg FDR function.

Global percentage methylation was determined by division of the total number of methylated counts by the total number of methylated and unmethylated counts in the entire data set, followed by multiplication by 100 for each biological condition.

Differentially-methylated regions (DMRs) were identified using 500bp sliding-windows. At each window, DMR significance was determined using Fisher's exact test, together with a χ^2 test of heterogeneity between biological replicates for each condition tested. Multi-sample correction was performed using the Benjimini-Hochberg FDR function, and DMRs defined as those windows with an FDR-corrected p-value <0.05 and non-significant heterogeneity between biological replicates (χ^2 test p >0.05). Percentage methylation at any particular DMR was then calculated by division of the total number of methylated cytosines by the total number of methylated and unmethylated cytosines, multiplied by 100.

Genomic feature overlaps were calculated on a per-base pair basis between two data sets, and the genomic average expected overlap calculated using a permutation test. For composite methylation profiling, the midpoints of a series of regions of interest were taken and used as a base. The area around the midpoint of each feature was then split into 100bp windows spanning 2.5kb upstream and downstream of this central position. The average methylation proportion was then calculated for each window for every genomic feature. A global mean was then taken for each window across all features to aggregate a composite of the mean methylation per window across all probed genomic features.

Smoothened methylation plots were generated using the BSmooth algorithm from the bsseq package. Methylation levels were kernel-smoothed, and plotted against a range of DMR and annotated features in bed format [411].

Table 2-7 Whole genome bisulfite (WGBS) sequencing alignment data

Alignment data for whole genome bisulfite sequencing (WGBS) performed in this thesis detailing the number of WGBS reads and CpG coverage per replicate.

Sample	Raw Sequence Reads	Coverage	Aligned Reads (% of raw sequence reads)	Filtered Reads	Final Reads
PD28 (Proliferating) Replicate 1	280793198	16.4x	230705384 (82.2%)	1444820	229260564
PD28 (Proliferating) Replicate 2	299999994	17.5x	237707257 (79.2%)	2129142	235578115
PD28 Proliferating Replicate 3	299999994	17.5x	233404112 (77.8%)	1908532	231495580
PD88 (Replicative senescence) Replicate 1	267705080	15.6x	228482997 (85.3%)	1791493	226691504
PD88 (Replicative senescence) Replicate 2	299999994	17.5x	208002740 (69.3%)	2136382	205866358
PD88 (Replicative senescence) Replicate 3	299999994	17.5x	213082930 (71.0%)	2144371	210938559
HIV-CS-CG-puromycin ("vector") Replicate 1	268923920	12.4x	222896869 (82.9%)	1880745	219058143
HIV-CS-CG-puromycin ("vector") Replicate 2	257233279	12.3x	214388237 (83.3%)	3716489	210671748
HIV-CS-CG-$BRAF^{V600E}$-puromycin ("BRAF") Replicate 1	270308969	12.5x	213657482 (79.0%)	3332368	210325114
HIV-CS-CG-$BRAF^{V600E}$-puromycin ("BRAF") Replicate 2	268940674	12.3x	209259871 (77.8%)	1880745	207379126

2.2.6 RNA

2.2.6.1 RNA extraction from adherent cells

RNA was extracted from adherent cells using the RNeasy Mini Kit according to the manufacturer's protocol. In summary, cell pellets were lysed on ice into buffer RLT supplemented with β-mercaptoethanol. Cell lysates were then homogenised by centrifugation in QiaShredder columns. RNA isolation was then performed using RNeasy mini kit columns, with residual DNA removed by on-column treatment with DNaseI. Following wash steps, RNA was eluted into RNase-free distilled water, and stored at -80°C prior to subsequent analysis. Prior to sequencing, RNA quantification was performed using the Qubit RNA HS assay kit, and qualitative assessment performed using the Agilent RNA ScreenTape assay according to the manufacturer's instructions.

2.2.6.2 RNA-sequencing

RNA-sequencing was performed by Mr William Clark in the sequencing facility at the Beatson Institute for Cancer Research, Glasgow. RNA was prepared for sequencing using the TruSeq RNA sample preparation kit. RNA is first purified, fragmented and reverse transcribed to produce cDNA. Following the removal of any remaining RNA, single-stranded cDNA is converted to double-stranded cDNA. Blunt-end DNA fragments are then generated. The subsequent addition of an "A" base to blunt ends prepares them for ligation to the sequencing adapters, which possess a "T" base overhang at the 3' end, thus providing a complementary overhang for adapter ligation. Adapters possess sequencing primer hybridisation sites for single, paired-end and multiplex reads. PCR is then employed to selectively enrich for those DNA fragments in possession of an adapter molecule on both ends (12 cycles only to prevent skewed representation in the library) and then libraries validated using the Agilent DNA 1000 kit. Libraries were then sequenced using the Illumina GAIIX sequencer at the Beatson Institute for Cancer Research, Glasgow, with paired-end sequencing at a length of 36bp.

2.2.6.3 Processing and analysis of RNA-sequencing data

Initial alignment and analysis of RNA-sequencing data was performed by Mr Neil Robertson, a computational biologist in Professor Peter Adams' laboratory. Alignment data are summarised in the tables below (Table 2-8, Table 2-9). Paired-end 36bp reads were aligned to the human genome (hg19) using a splicing-aware aligner (TopHat2) [412]. Only unique reads were retained. Reference splice junctions were provided by a reference

transcriptome (Ensembl build 73) and novel splicing junctions defined by the detection of reads that spanned exons not in the reference annotation. True read abundance at each transcript isoform was assessed using HTSeq (Python) before determination of differential expression using DESEQ2, from which differential expression and splicing can be derived [413]. Significance was determined using an FDR corrected p-value of <0.05. Heatmaps were created in *R* using the *ggplots* package.

Table 2-8 RNA-sequencing alignment data (mapped reads)

Sample	Rep	L-input	Mapped Reads	Percentage Mapped	R-input	Mapped Reads	Percentage Mapped
Vector/Vector	1	37229172	33687092	90.5	37225533	33390240	89.7
Vector/Vector	2	38737372	35048504	90.5	38735310	34543858	89.2
Vector/Vector	3	30163343	26909263	89.2	30166640	26103594	86.5
DNMT3B Only	1	36661514	33251854	90.7	36660294	32726704	89.3
DNMT3B Only	2	39174576	35380661	90.3	39173048	34892547	89.1
DNMT3B Only	3	36178544	32629468	90.2	36175385	32315402	89.3
BRAF Only	1	39271629	35322633	89.9	39268910	34938527	89
BRAF Only	2	35072830	31633130	90.2	35070976	31281539	89.2
BRAF Only	3	31744881	28609166	90.1	31743248	28302228	89.2
BRAF/DNMT3B	1	32859073	29776592	90.6	32856761	29455321	89.6
BRAF/DNMT3B	2	33450768	30059459	89.9	33458280	29119061	87
BRAF/DNMT3B	3	39054674	35337104	90.5	39051964	34954629	89.5

Table 2-9 RNA-sequencing alignment data (multiple alignments/discordant alignments)

Sample	Rep	Pairs Aligned	Multiple Alignments	Multiple Alignments (%)	Discordant-Alignments	Discordant Alignment (%)	Concordant Rate (%)
Vector/Vector	1	28096538	2433151	8.7	1222075	4.3	81.8
Vector/Vector	2	27811183	2375467	8.5	1141686	4.1	79.7
Vector/Vector	3	33328904	2884942	8.7	1445333	4.3	81.6
DNMT3B Only	1	31819317	3185101	10	1609436	5.1	81.2
DNMT3B Only	2	32957346	3188938	9.7	1583627	4.8	81
DNMT3B Only	3	24765670	2376869	9.6	1245875	5	78
BRAF Only	1	31223251	3160825	10.1	1515496	4.9	81
BRAF Only	2	33261534	3402639	10.2	1670127	5	80.6
BRAF Only	3	30772907	3099406	10.1	1483176	4.8	81
BRAF/DNMT3B	1	33277059	2713880	8.2	1445246	4.3	81.1
BRAF/DNMT3B	2	29808783	2496360	8.4	1270514	4.3	81.4
BRAF/DNMT3B	3	26959783	2138070	7.9	1131557	4.2	81.4

2.2.7 *In vivo* work

2.2.7.1 Home Office project and personal licencing

All experiments were carried out in accordance with the requirements of the UK Home Office guidelines under the auspices of Personal Licence I6C161323, and Project Licence 70/8354.

2.2.7.2 Colony maintenance and routine husbandry

Routine husbandry of all colonies, including nutrition, hydration, setting up of matings, weaning and ear-notching for genotyping was undertaken by Biological Services technicians at the Beatson Institute for Cancer Research. Mice were fed a standard diet with water *ad libitum*.

2.2.7.3 Transgenic strains and alleles

The following transgenic alleles were used in this thesis. The full transgenic allele name and abbreviation used hereafter in this thesis are detailed in Table 2-10. Specific details of the allele designs are discussed in chapter 6.

Table 2-10 Summary of transgenic alleles

Allele	Abbreviation	Source
Tg(Cyp1a1-cre/ERT)1Dwi	*AhCreEr^{T}*	Sansom Laboratory
Tg(Vil-cre/ERT2)23Syr	*VilCreEr^{T2}*	Sansom Laboratory
Braf^{tm1Cpri}	*^{LSL}Braf^{V600E}*	Pritchard Laboratory
B6;129S4-Dnmt3b^{tm1Jae}/Mmnc	*Dnmt3b$^{fl/fl}$*	MMRRC[4]
B6.Cg-Gt(ROSA)26Sor$^{tm1(rtTA*M2)Jae}$/J	*R26-M2-rtTA*	Jackson Laboratory
B6.Cg-Col1a1$^{tm9(tet0-Dnmt3b_i1)Jae}$/J	*Col1a1-tetO-Dnmt3b1*	Jackson Laboratory
Apc^{tm1Tno}	*Apc$^{fl/+}$*	Sansom Laboratory

2.2.7.4 Genotyping

Routine genotyping was undertaken at weaning (6 weeks age). Ear notches were obtained from mice by technical staff in the Beatson Institute for Cancer Research animal facility. Automated PCR genotyping of mouse strains was undertaken by Transnetyx.

[4] MMRRC = Mutant Mouse Resource and Research Centers (www.mmrrc.org)

2.2.7.5 Tissue harvest

Mice were culled at clinical endpoint by exposure to carbon dioxide gas in a rising concentration in accordance with the requirements of the Animals (Scientific Procedures) Act 1986. Death was confirmed by confirmation of permanent cessation of the circulation and dislocation of the neck. The skin was shaved and prepared with ethanol. The abdomen was then opened through a midline laparotomy, and the abdominal viscera carefully inspected for evidence of tumour formation or metastatic disease. The stomach was divided at the gastro-oesophageal junction, and the small intestine dissected from its mesentery from gastro-duodenal junction to the ileo-caecal junction. The colon was separately dissected from its mesentery, and dissection continued to the pelvis where it was amputated at the anorectal junction. Both the small intestine and colon were flushed with PBS, before being opened longitudinally in their entirety with iris scissors. Following harvest of intestinal tissues, a full necropsy was undertaken to exclude other pathology.

2.2.7.6 Tissue fixation and processing

For tumour scoring and routine haematoxylin and eosin staining, tissues were fixed in Methacarn (60% Methanol, 30% chloroform, 10% glacial acetic acid) for 20 hours. Thereafter, the intestine and colon were wound into a “Swiss roll” in 10% neutral buffered formalin and processed for histology. For immunohistochemistry, the small intestine and colon were “pinned out” in a paraffin wax dish containing 10% neutral buffered formalin. After 24 hours, the intestine and colon were wound into a “Swiss roll” in 10% neutral buffered formalin, and processed for histological analysis by the histology service at the Beatson Institute for Cancer Research, Glasgow.

2.2.8 Statistical Analysis

Statistical analysis was performed using GraphPad Prism (GraphPad Software Inc. La Jolla, California, USA) Details of statistical tests used in individual experiments are detailed in the respective figure legends. Statistical analysis of RNA-sequencing and whole genome bisulfite sequencing data was performed separately by Mr Neil Robertson, a computational biologist in Professor Peter Adams laboratory at the Beatson Institute for Cancer Research, Glasgow, and is described in more detail in the description of these methods above.

3 Validation of DNMT3B antibodies and development of constructs for ectopic expression and knockdown

3.1 Rationale

Any experiment in which antibodies to a particular protein are required mandates the validation of the specificity of these to the particular protein target in question. A central aim of this thesis was to examine the contribution of DNMT3B to the establishment of CIMP in the context of an activated *BRAF* oncogene. An early priority was therefore the identification and validation of a panel of DNMT3B antibodies and other reagents for use in future experiments.

3.2 Aims

The specific aims of this chapter are:

1. To validate a panel of DNMT3B antibodies for future *in vitro* and *in vivo* experimental work

2. To develop lentiviral constructs to direct ectopic expression of DNMT3B in primary human cells for later *in vitro* functional experiments

3. To develop knockdown strategies for DNMT3B for later loss of function experiments in colon cancer cell lines

3.3 Results

3.3.1 Selection of DNMT3B antibodies and initial screening in HCT116 cells

Based on previous studies published in the literature, a panel of five commercially-available DNMT3B antibodies was selected for testing, and these are summarised in Table 3-1. All candidate antibodies selected were reported to detect human DNMT3B by their respective manufacturers. For verification purposes, the human colon cancer cell line HCT116 was selected. HCT116 is a well-characterised cell line, and is documented to express DNMT3B [329]. In order to test whether candidate DNMT3B antibodies were able to detect a polypeptide of the correct size by western blot, whole cell protein lysates were produced from HCT116, separated by SDS-PAGE electrophoresis, and immobilised to PVDF. Western blotting was then undertaken with each candidate DNMT3B antibody.

The predicted molecular weight of full length human DNMT3B is 95.75 kDa [222]. As outlined in the introduction to this thesis, multiple splice isoforms of *DNMT3B* have been described, which further complicates interpretation of the specificity of candidate antibodies. The molecular weights of several DNMT3B isoforms are summarised in Table 3-2 overleaf. Notably, all but one of the antibodies tested detected a band in the correct molecular weight range for DNMT3B (Figure 3-1). Significantly, the only antibody that did not detect a protein band in the correct molecular weight range for full length DNMT3B was the mouse monoclonal antibody, IMG184A (clone 52A1018) produced by Imgenex/Novus Biologicals. This antibody is perhaps one of the most extensively used in the literature, and of particular note to the subject matter of this thesis, it is the antibody that has previously been used in studies linking DNMT3B expression to the CpG island methylator phenotype (CIMP) in human colorectal cancer [414,415]. As splice isoforms of *DNMT3B* have been characterised in cancer cell lines, it is formally possible that the lower polypeptide band detected by this antibody in HCT116 represents a truncated DNMT3B isoform [222]. Given the central role of this antibody in the published evidence linking DNMT3B to CIMP, it was carried forward, together with the other candidate antibodies, for further validation by means of ectopic expression and knockdown of DNMT3B.

Table 3-1 Summary of DNMT3B antibodies evaluated in this thesis

Antibody	Manufacturer	Epitope	Species	Clonality
SC10236	Santa Cruz Biotechnology	Internal region of human DNMT3B	Goat	Polyclonal
IMG184A	Imgenex	Bacterial expressed full length recombinant mouse DNMT3B	Mouse	Monoclonal
NB100-266	Novus Biologicals	Amino acids 4-101 of human DNMT3B	Rabbit	Polyclonal
NEBM0232	New England Biosciences	Synthetic peptide corresponding to the carboxy terminus of human DNMT3B	Rabbit	Polyclonal
AB79822	Abcam	Synthetic peptide corresponding to residues in human DNMT3B	Rabbit	Monoclonal

Table 3-2 Predicted molecular weights of human DNMT3B isoforms[5]

Isoform	Length	Predicted Molecular Weight (kDa)
DNMT3B1	853	95.75
DNMT3B2	833	93.41
DNMT3B3	770	86.18
DNMT3B4	724	80.85
DNMT3B5	792	88.57
DNMT3B6	845	94.69
DNMT3B7	694	77.72
DNMT3B8	728	81.31

[5] Data adapted from http://www.uniprot.org/uniprot/Q9UBC3

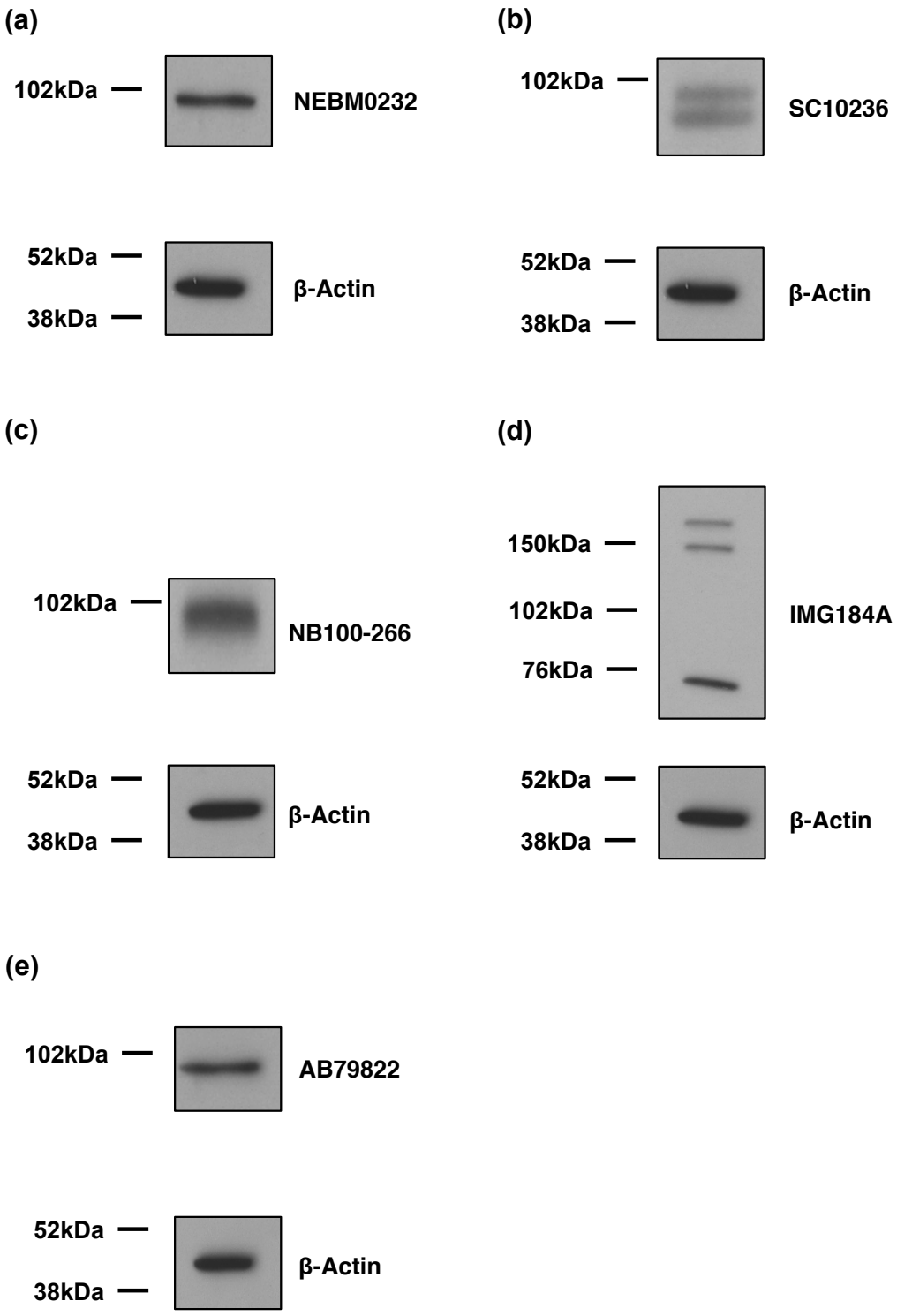

Figure 3-1 A panel of five putative DNMT3B antibodies was tested by Western blot in protein lysates produced from the colon cancer cell line HCT116

Western blots of whole cell lysates from the colon cancer cell line HCT116 were prepared, separated by SDS-PAGE, immobilised to PVDF and probed with the candidate DNMT3B antibodies (a) NEBM0232, (b) SC10236, (c) NB100-266, (d) IMG184A and (e) AB79822. With the exception of IMG184A (clone 52A1018) all antibodies tested detected a polypeptide band in the correct molecular weight range for human DNMT3B. No other polypeptide bands in the molecular weight range for DNMT3B were detected in the full-length blots (n=3 biological replicates).

3.3.2 Development of lentiviral constructs for ectopic expression of DNMT3B

For future functional *in vitro* experiments, and in order to provide a robust positive control for DNMT3B expression, expression plasmids for two isoforms of human DNMT3B (DNMT3B1 and DNMT3B3) were obtained from Addgene[6], and sequence verified by Mr William Clark in the sequencing facility at the Beatson Institute for Cancer Research, Glasgow. In these pcDNA3/Myc-DNMT3B1 and pcDNA3/Myc-DNMT3B3 plasmids, the cDNA for each DNMT3B isoform is cloned into the EcoRI and BamHI sites of a modified pcDNA3 vector, in which the multiple cloning site has been altered, with the inclusion of a Kozak consensus sequence, ATG start site and Myc epitope tag [416].

As future functional *in vitro* experiments and ectopic expression assays were to be performed in primary human fibroblasts in which simple transfection can be very difficult to achieve, the decision was made to subclone the DNMT3B1 and DNMT3B3 cDNAs into the lentiviral construct pLenti6-puromycin, in order to allow stable ectopic expression of DNMT3B. As a result of the way in which the cDNAs had been cloned into pcDNA3/Myc vector, it was necessary to adopt a PCR-based cloning strategy, with the addition of restriction sites to yield compatible cohesive ends to allow subcloning into the unique XbaI and EcoRI restriction sites in the pLenti6-puromycin construct. Primers were designed to include the Myc tag, with the addition of the restriction sites NheI and AvrII to the forward primer and MfeI to the reverse primer. A plasmid map of pLenti6-puromycin and a schema of the PCR primer design is shown overleaf (Figure 3-2). Following ligation of the PCR product into the digested pLenti6-puromycin backbone, and plasmid purification, successful incorporation of the product to the vector was confirmed by diagnostic restriction digest (data not shown).

[6] pcDNA3/Myc-DNMT3B1 and pcDNA3/Myc-DNMT3B3 were gifts from Arthur Riggs (Addgene plasmids # 35522; 37546)

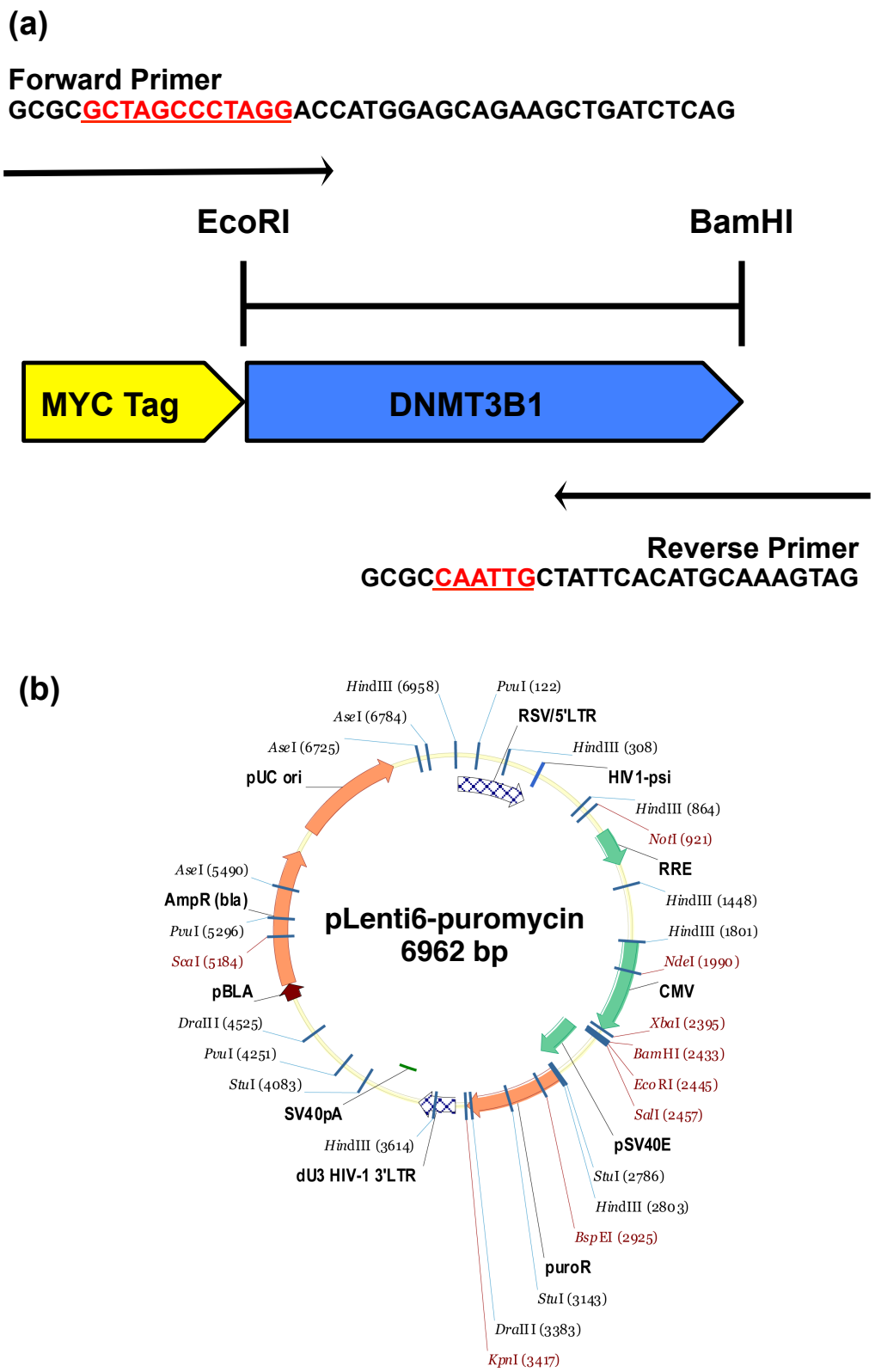

Figure 3-2 Cloning strategy for creation of lentivirus to direct ectopic expression of DNMT3B in subsequent experiments

(a) Diagrammatic representation of DNMT3B plasmid with cloning sites EcoRI and BamHI identified. PCR forward and reverse primer design is demonstrated (restriction sites highlighted in bold red underline) **(b)** Plasmid map of pLenti6-puromycin into which DNMT3B1 and DNMT3B3 were subcloned.

With successful incorporation of the DNMT3B1 and DNMT3B3 cDNAs into pLenti6-puromycin confirmed, lentivirus was produced as described previously (chapter 2; section 2.2.2) and used to transduce primary human fibroblasts (IMR-90). After 7 days, whole cell lysates were prepared from cells directed to express the empty vector or ectopic DNMT3B isoforms, separated by SDS-PAGE electrophoresis, and immobilised to PVDF. Western blotting was then undertaken with each candidate DNMT3B antibody in order to test their ability to detect ectopically expressed human DNMT3B. Three of the five antibodies tested (NEBM0232, SC10236, and NB100-266) clearly detected ectopically expressed human DNMT3B1 and DNMT3B3. IMG184A and AB79822 detected identical polypeptide bands in both the empty vector and ectopic expression lanes, suggesting that they do not detect ectopically expressed human DNMT3B (Figure 3-3).

As murine tissues were also to be analysed in later experiments, candidate DNMT3B antibodies were tested in protein lysates made from intestinal tissues from a genetically modified mouse model heterozygous for the tetracycline-inducible *Dnmt3b* allele (*Col1a1-tetO-Dnmt3b1)* and tetracycline-responsive transactivator (*R26-M2-rtTa*) [229,417]. Protein lysates were also made from a control mouse heterozygous for the *R6-M2-rtTa* allele, and wild type for the *Col1a1-tetO-Dnmt3b1* allele. Lysates from both mice were prepared following two weeks of treatment with doxycycline in the drinking water at a concentration of 0.5mg/mL. Only three of the candidate antibodies (IMG184A, NB100-266 and SC10236) were tested in the murine intestinal tissues, as these were specifically identified by their respective manufacturers as detecting murine DNMT3B. Intriguingly, IMG184A, which did not detect ectopically expressed human DNMT3B, detected a strong signal in murine intestinal lysate ectopically expressing DNMT3B. Notably, the antigenic target for this antibody is cited in the product literature as bacterial-expressed full-length mouse DNMT3B. This raised the possibility that this antibody detects murine DNMT3B but not human DNMT3B. This is particularly interesting given the significant structural homology reported between murine DNMT3B and human DNMT3B [196]. Both of the other candidate DNMT3B antibodies detected a polypeptide band of the correct molecular weight for DNMT3B in lysates expressing ectopic murine DNMT3B (Figure 3-4).

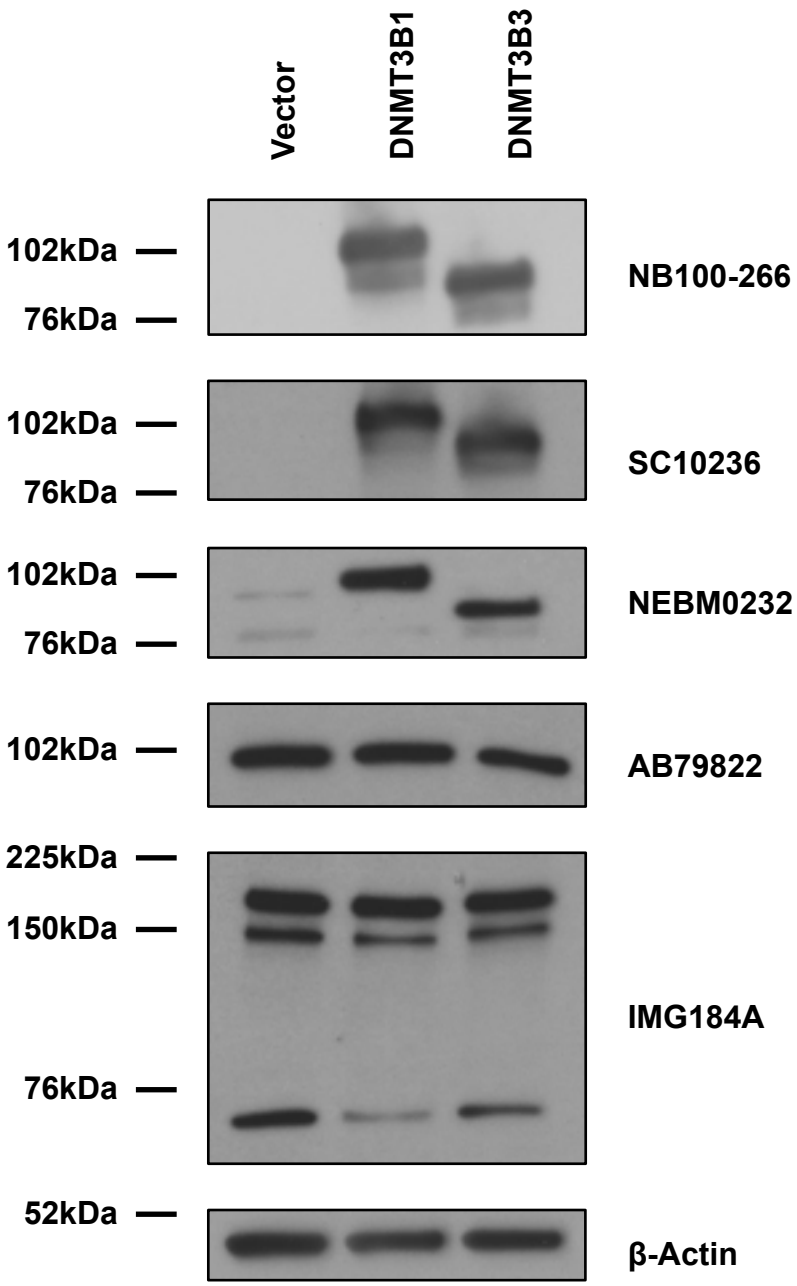

Figure 3-3 The ability of candidate DNMT3B antibodies to detect ectopically-expressed human DNMT3B by Western blot was assessed

Western blot of whole cell lysates from IMR-90 human fetal lung fibroblasts one week following transduction with pLenti6-puromycin ("vector"), pLenti6-DNMT3B1-puromycin ("DNMT3B1") or pLenti6-DNMT3B3-puromycin ("DNMT3B3"). Expression of DNMT3B is once again assessed using a panel of DNMT3B antibodies. Neither AB79822 nor IMG184A detect ectopically expressed human DNMT3B1 or DNMT3B3. By comparison, NB100-266, SC10236, and NEBM0232 all detect ectopically-expressed DNMT3B1 and DNMT3B3 (n=3 biological replicates).

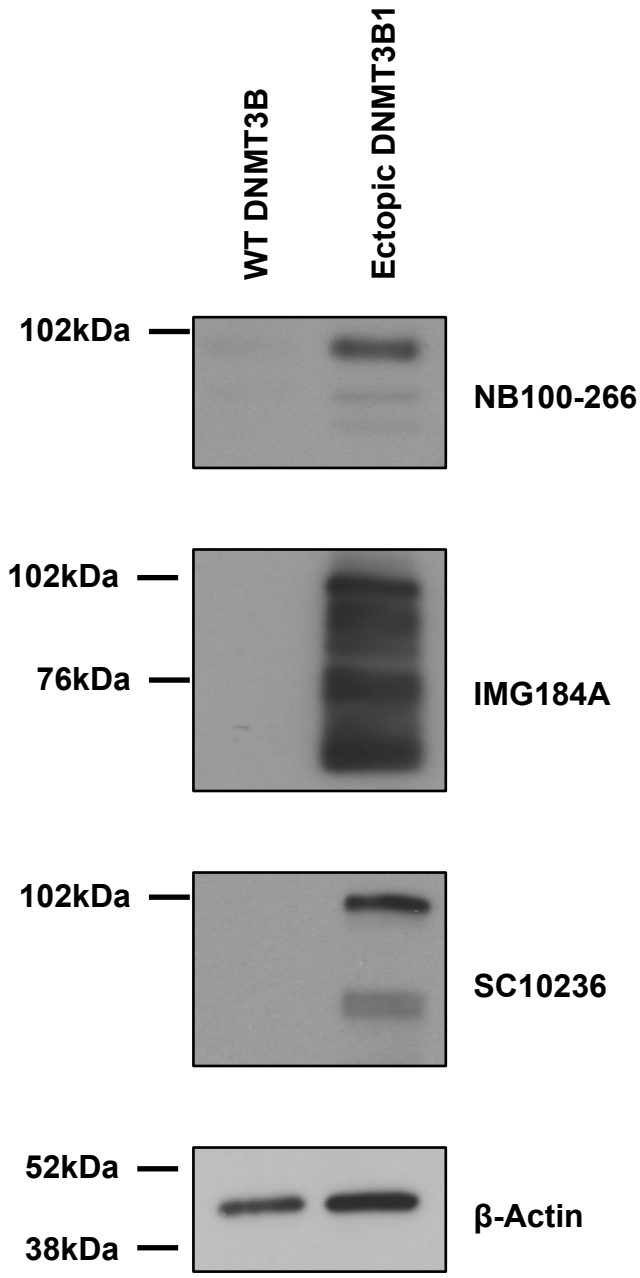

Figure 3-4 The ability of candidate DNMT3B antibodies to detect ectopically-expressed murine DNMT3B1 by Western blot was assessed

Western blot of whole cell lysates from murine intestine from mice heterozygous ("ectopic DNMT3B1") or wild-type ("WT DNMT3B") for the *Col1a1-tetO-Dnmt3b1* transgene. Both mice were heterozygous for the *R26-M2-rtTA* transgene. Transgene induction was achieved by addition of doxycycline hyclate to the drinking water for fourteen days prior to tissue harvest. All three candidate DNMT3B antibodies detect peptide targets in the correct molecular weight range for murine DNMT3B1 (n=1 biological replicate).

3.3.3 Testing a panel of DNMT3B shRNA constructs

For future loss-of-function experiments, and as an additional means of validating the specificity of DNMT3B antibodies, commercially-produced DNMT3B shRNAs (obtained from Dharmacon/GE Life Sciences) were tested. A pool of four shRNAs in the pLKO.1-puromycin vector were obtained (pLKO.1-shDNMT3B685-688-puromycin). The details of each of the shRNA clones tested are summarised in Table 3-3 below, and their alignment to human *DNMT3B* is represented diagrammatically in Figure 3-5. Lentiviral transduction was again performed in HCT116 cells with both the empty vector (pLKO.1-puromycin) and each of the four lentiviral shRNA-DNMT3B constructs. Cells were harvested 7 days following transduction for protein lysates, which were separated by SDS-PAGE electrophoresis, immobilised to PVDF and assessed by Western blotting for DNMT3B expression.

Table 3-3 shRNA DNMT3B constructs tested in this thesis[7]

Clone ID	Target Sequence	Intrinsic Score	Adjusted Score
TRCN0000035685 (shDNMT3B685)	GCCCGTGATAGCATCAAAGAA	5.625	4.500
TRCN0000035686 (shDNMT3B686)	CCATGCAACGATCTCTCAAAT	13.200	9.240
TRCN0000035687 (shDNMT3B687)	GCAGGCAGTAGGAAATTAGAA	5.625	3.938
TRCN0000035688 (shDNMT3B688)	CCTGTCATTGTTTGATGGCAT	2.640	1.848

In keeping with its inability to detect ectopically expressed human DNMT3B, IMG184A did not detect DNMT3B knockdown with any of the four shRNA constructs tested, reinforcing the argument that this antibody does not detect human DNMT3B by western blot. More perplexingly, each of the remaining three antibodies tested (SC10236, NB100-266 and NEBM0232) detected knockdown with different shRNA constructs, with no single shRNA construct demonstrating consistent knockdown with all antibodies. The most likely explanation for this is that each antibody detects different isoforms of DNMT3B, which are knocked down to different degrees by each individual shRNA construct (Figure 3-6).

[7] Target sequences, intrinsic and adjusted scores are obtained from Broad Institute Genetic Perturbation Platform (http://portals.broadinstitute.org/gpp/public/clone/)

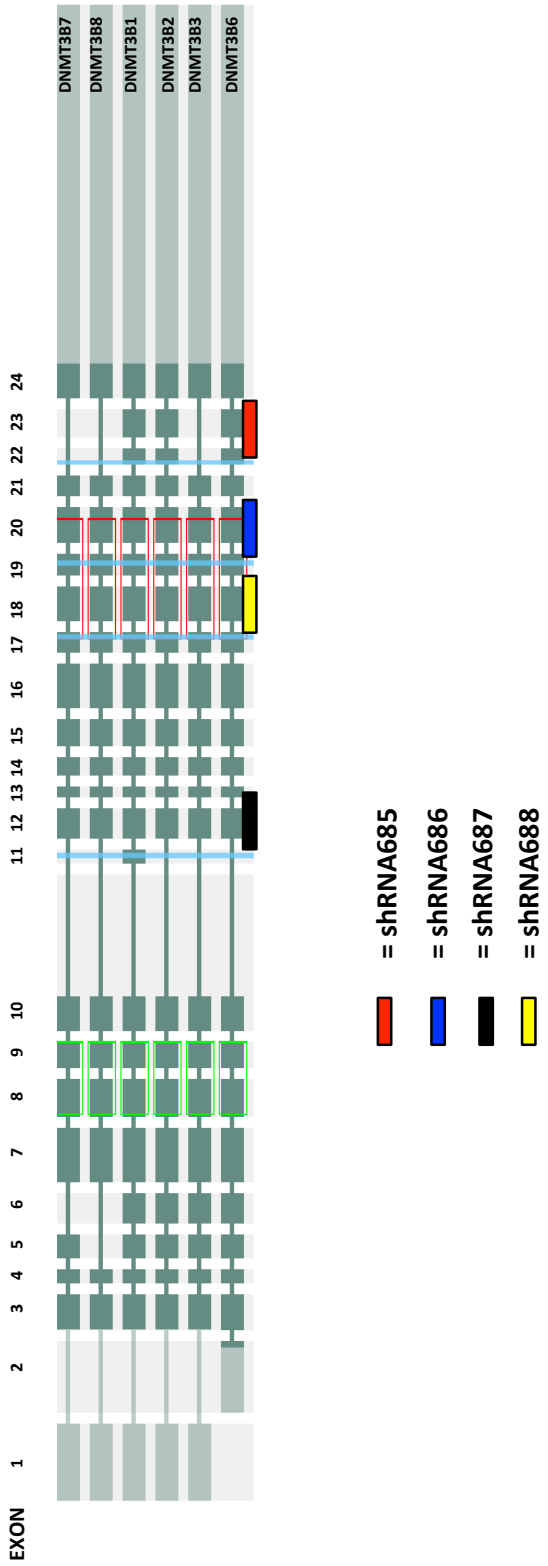

Figure 3-5 Alignment of shRNAs to human *DNMT3B*

Diagrammatic representation of the alignment of candidate DNMT3B shRNAs to the human *DNMT3B* gene. The shRNA sequences were aligned using the NIH basic local alignment tool (BLAST[8]), and diagrams created using *SpliceCenter*[9].

[8] https://blast.ncbi.nlm.nih.gov/Blast.cgi
[9] http://projects.insilico.us/SpliceCenter/siRNACheck.

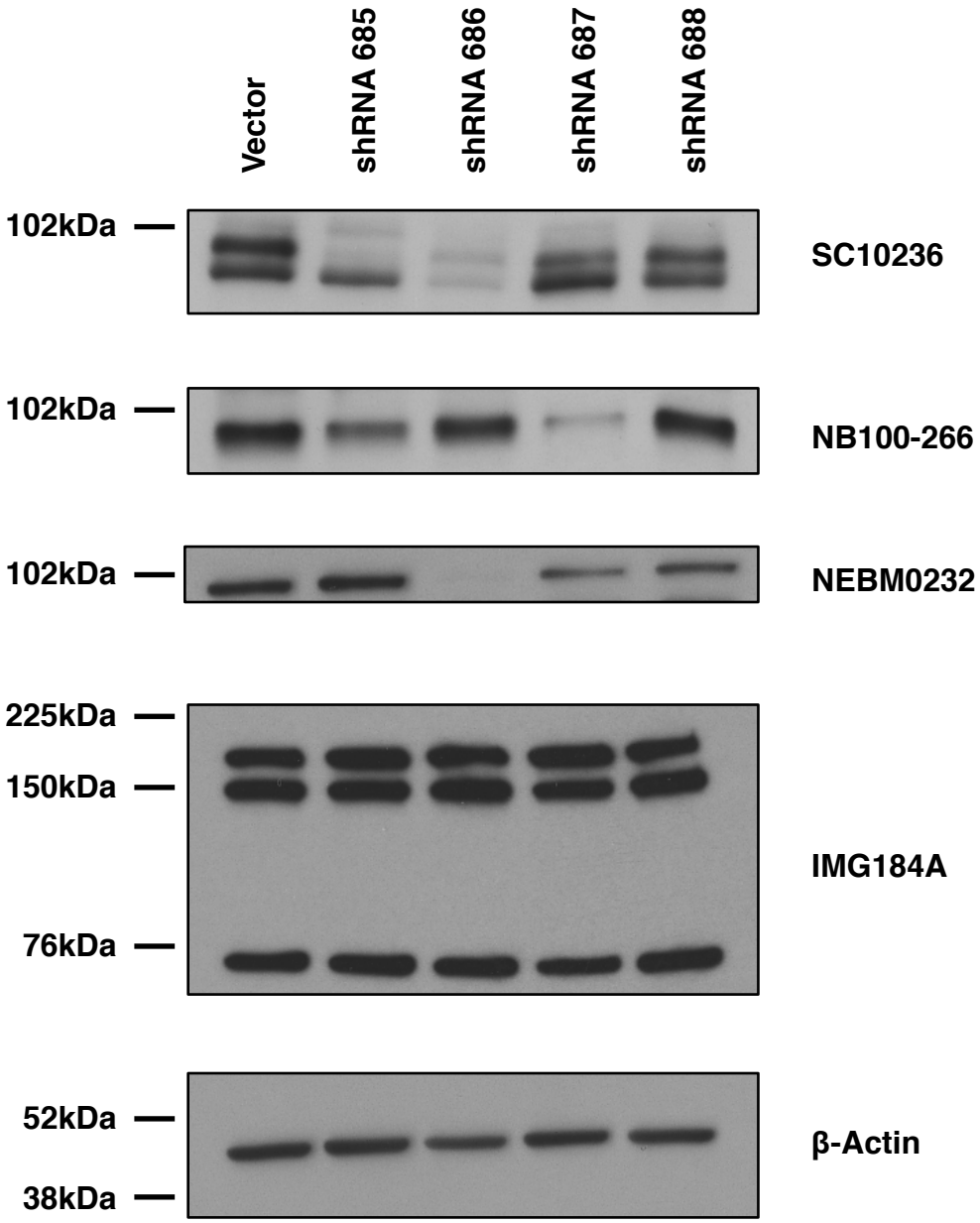

Figure 3-6 A panel of DNMT3B shRNAs were tested in HCT116 colon cancer cells

Western blot of whole cell lysates of HCT116 one week following transduction with vector (pLKO.1) or DNMT3B shRNA lentivirus (pLKO.1-shDNMT3B-685-688). Apparent knockdown of DNMT3B is seen with sh685 and sh686 using SC10236; whereas knockdown detected by NB100-266 is seen with sh687 by NB100-266 and sh686 by NEBM0232. By contrast, no apparent knockdown is noted with any shRNA when IMG184A is used to detect DNMT3B (n=1 biological replicate).

3.3.4 Development and testing of a panel of CRISPR sgRNAs to human *DNMT3B*

As inconsistent results were obtained with shRNA-mediated knockdown of DNMT3B, further methods of experimental DNMT3B depletion were sought. Advances in genome editing technology continue to be made, and one of the most significant in recent times is the development of the CRISPR/*Cas9* system [418,419]. Design of DNMT3B CRISPR sgRNAs was dual purpose: firstly to allow stable knockdown of DNMT3B for future loss of function experiments, and secondly as a further validation tool for DNMT3B antibody specificity.

A panel of four sgRNAs were selected and cloned into the lentiCRISPRv2-puromycin construct. In this lentiviral construct, the sgRNA and *hSpCas9* are delivered simultaneously by a single plasmid. Digestion of the plasmid with the restriction enzyme BsmBI removes a 2kb filler and allows subcloning of specific sgRNAs. A plasmid map is shown in Figure 3-7 [420]. The sgRNA sequences were designed using the Zhang lab CRISPR design tool[10], with the exception of sgRNA4, which was modified from a previously published sequence [421]. All sgRNA oligonucleotides were designed with compatible cohesive ends to allow subcloning into lentiCRISPRv2-puromycin following digestion with BsmBI (Table 3-4). The alignment of each sgRNA to human *DNMT3B* is represented diagrammatically in Figure 3-8.

Table 3-4 sgRNA sequences designed to CRISPR human *DNMT3B*

Restriction site overhangs for cloning into lentiCRISPRv2-puromycin are in bold

sgRNA	Forward Sequence	Reverse Sequence
1	**CACCG**AGACTCGATCCTCGTCAACG	**AAAC**CGTTGACGAGGATCGAGTCT**C**
2	**CACCG**AGAGTCGCGAGCTTGATCTT	**AAAC**AAGATCAAGCTCGCGACTCT**C**
3	**CACCG**ATGCTGTTGCCCGCCGTCTC	**AAAC**GAGACGGCGGGCAACAGCAT**C**
4	**CACCG**GAATTACTCACGCCCCAAGG	**AAAC**CCTTGGGGCGTGAGTAATTC**C**

The annealed forward and reverse oligonucleotides were ligated into lentiCRISPRv2-puromycin digested with BsmBI, and used to transform chemically competent bacteria. Following plasmid purification, sequence verification was undertaken by Mr William Clark at the sequencing facility at the Beatson Institute for Cancer Research to ensure incorporation of the desired sgRNA sequence to lentiCRISPRv2-puromycin (data not shown).

[10] http://crispr.mit.edu

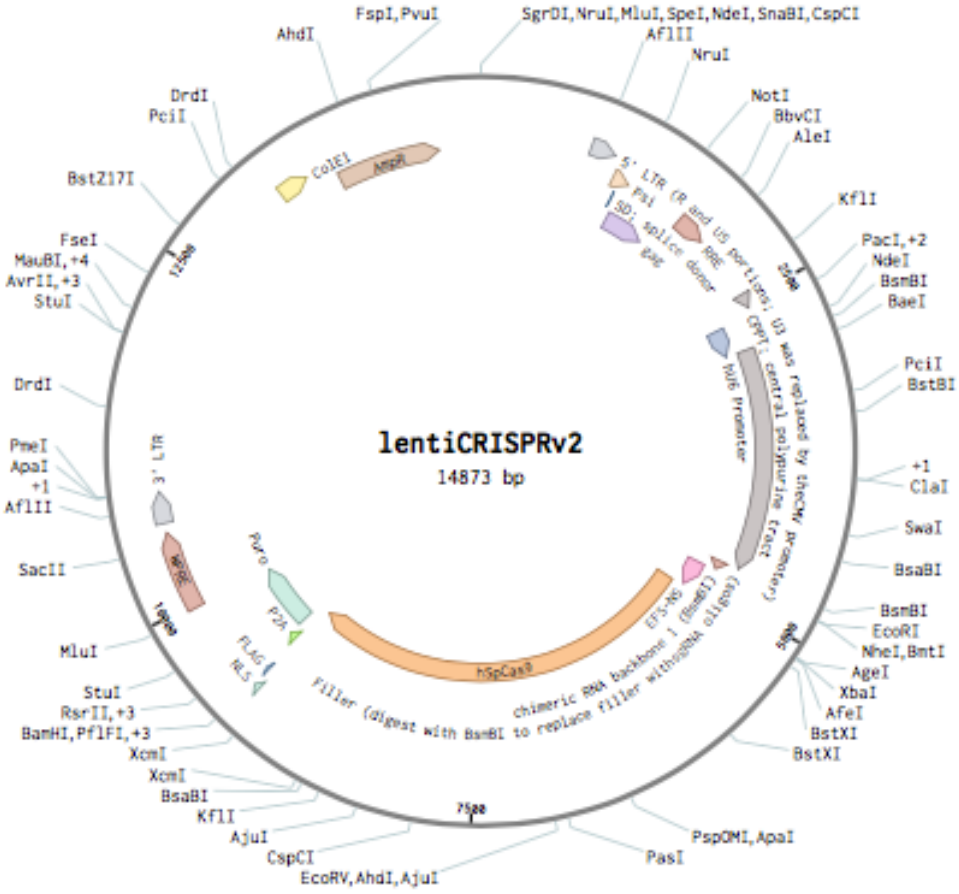

Figure 3-7 Plasmid map of lentiCRISPRv2

Plasmid map of the lentiCRISPRv2-puromycin vector designed by the Zhang lab, demonstrating the unique BsmBI restriction site that allows subcloning of CRISPR sgRNAs[11].

HCT116 cells were then transduced with either the lentiCRISPRv2-puromycin vector or lentiCRISPRv2-DNMT3B-sgRNA1-4-puromycin, drug-selected with puromycin, and after 7 days, harvested for protein lysates. Protein lysates were separated by SDS-PAGE, immobilised to PVDF and DNMT3B expression was tested by Western blot with candidate DNMT3B antibodies. Efficient knockdown of DNMT3B was seen with sgRNAs 1, 2 and 4, but not with sgRNA 3. This knockdown was demonstrable only with SC10236 and not with the other antibodies tested (Figure 3-9). This raised the possibility that the polypeptide bands detected by NB100-266, NEBM0232, and IMG184A did not represent DNMT3B. This raised an obvious conflict both with the ectopic expression, and shRNA knockdown data, which together were suggestive of sensitivity and specificity of NB100-266 and NEBM0232 (but not IMG184A) for human DNMT3B.

[11] Figure from www.genome-engineering.org.

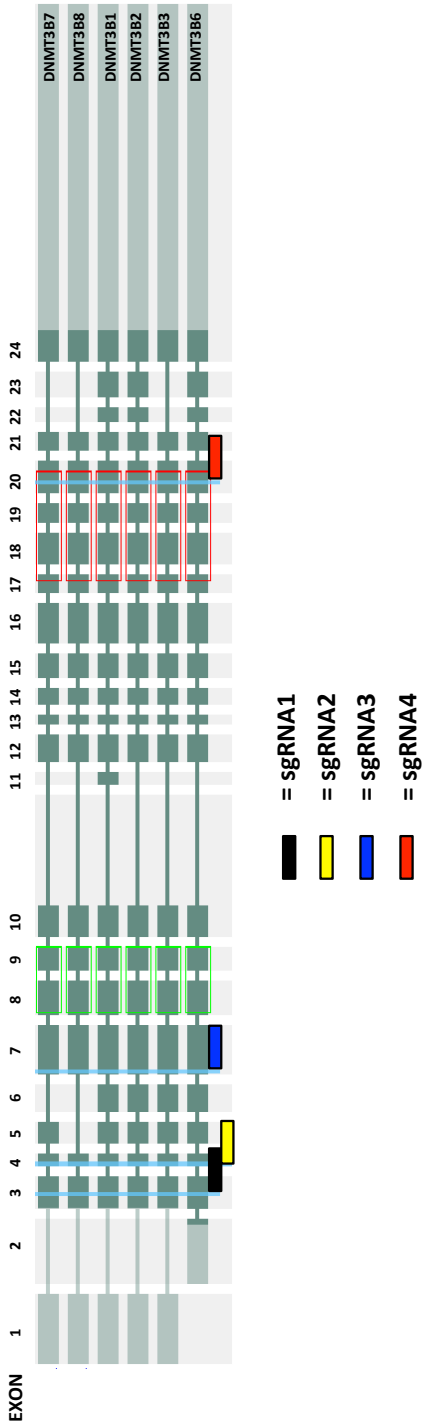

Figure 3-8 Alignment of DNMT3B CRISPR sgRNAs to human *DNMT3B*

Diagrammatic representation of the alignment of candidate DNMT3B CRISPR sgRNAs to the human *DNMT3B* gene. The sgRNA sequences were aligned using the NIH basic local alignment tool (BLAST[12]), and diagrams created using *SpliceCenter*[13].

[12] https://blast.ncbi.nlm.nih.gov/Blast.cgi
[13] http://projects.insilico.us/SpliceCenter/siRNACheck.

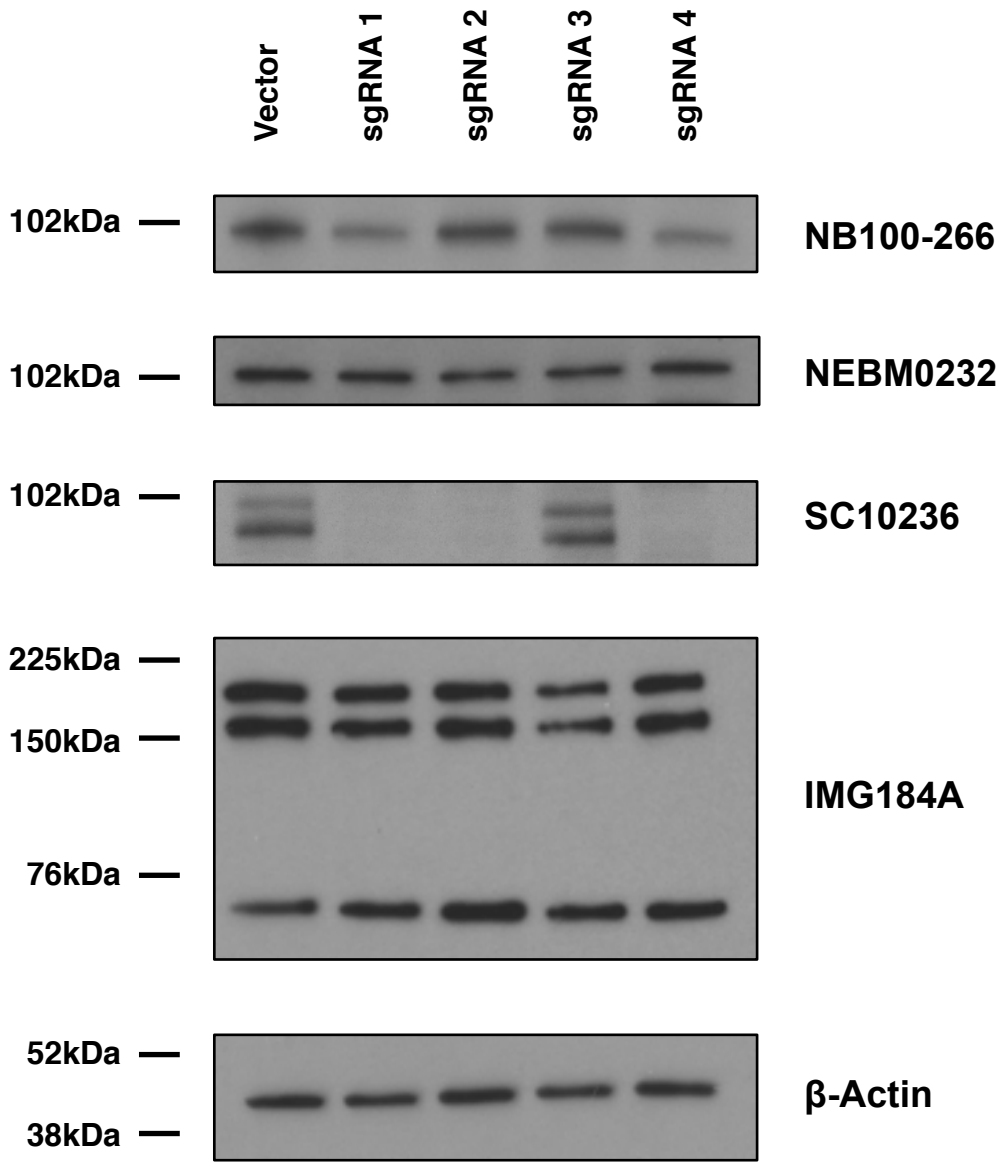

Figure 3-9 A panel of DNMT3B CRISPR sgRNAs in were tested in HCT116

Western blot of whole cell lysates from HCT116 7 days following transduction with lentiCRISPRv2-puromycin ("vector") or lentiCRISPRv2-DNMT3B-sgRNA1-4-puromycin ("sgRNA1-4") demonstrating specific knockdown of DNMT3B in HCT116 with sgRNAs 1,2 and 4. Knockdown is detected only with SC10236 and not NB100-266, NEBM0232 or IMG184A, implying that the polypeptide targets detected by these antibodies do not represent DNMT3B (n=1 biological replicate).

3.3.5 Testing a panel of DNMT3B antibodies in HCT116 WT and HCT116 3BKO cells

In order to address the apparently conflicting data generated by shRNA-mediated, and CRISPR-mediated knockdown respectively, and in an attempt to finally resolve the issue of DNMT3B antibody sensitivity and specificity, the HCT116-derived cell line "3BKO" which is null for *DNMT3B*, was obtained and authenticated using short tandem repeat DNA profiling analysis[14]. In 3BKO cells, the carboxy-terminal catalytic domain is replaced by hygromycin- or neomycin-resistance genes [329]. The targeting construct used to disrupt DNMT3B in this cell line is summarised in Figure 3-10 below. Protein lysates were prepared from cultured HCT116 parental and HCT116 3BKO populations, separated by SDS-PAGE, immobilised to PVDF and tested with the panel of DNMT3B antibodies (Figure 3-11).

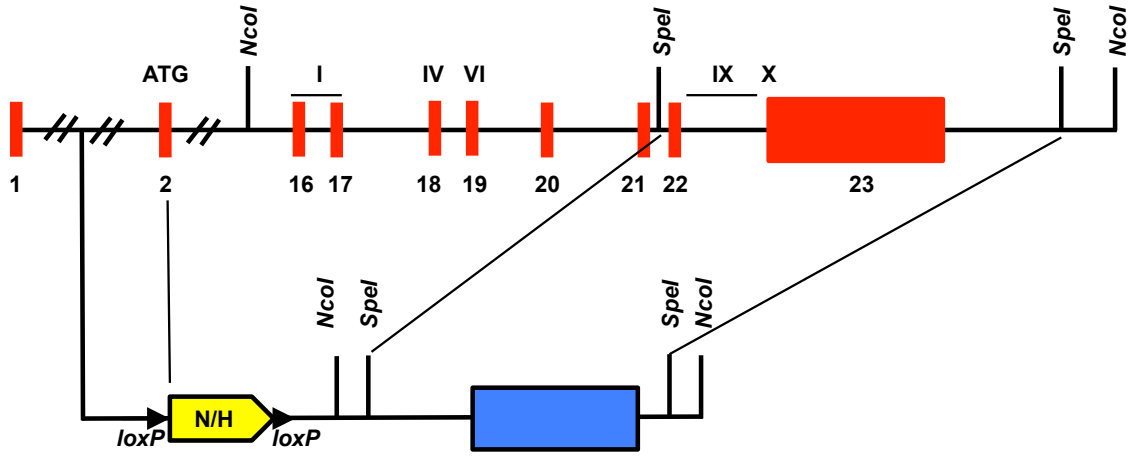

Figure 3-10 Diagram of DNMT3B targeting construct used to generate 3BKO cells

Diagram of the DNMT3B targeting construct used to generate 3BKO cells. Neomycin- or hygromycin-resistance genes (N/H) replace the catalytic domain. Numbered boxes represent exons. Roman numerals represent the conserved methyltransferase motifs targeted by this strategy. Adapted from Rhee et al.[422].

[14] 3BKO cells were a gift of Professor Richard Meehan

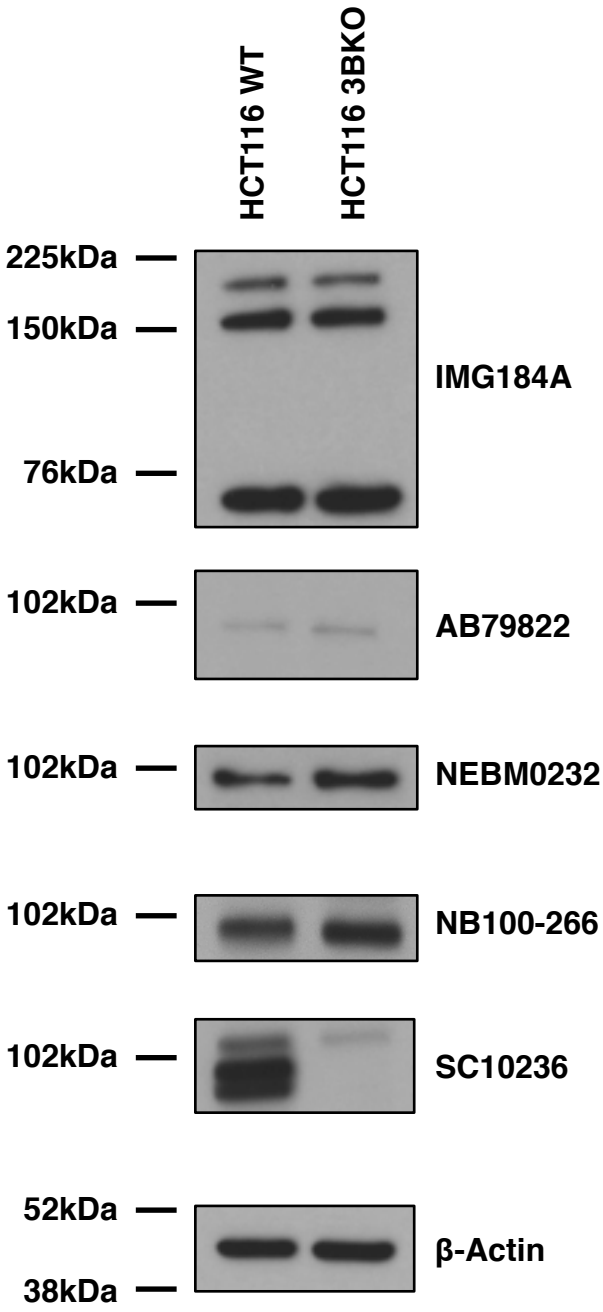

Figure 3-11 The specificity of DNMT3B antibodies was confirmed in HCT116 and HCT116 3BKO cells

A panel of DNMT3B antibodies was tested in HCT116 parental ("HCT116 WT") and HCT116 3BKO cells. Only SC10236 detects polypeptide bands in parental HCT116 cell lysate that are not detectable in 3BKO cells (n=1 biological replicate).

Consistent with all of the earlier data presented in this chapter, IMG184A detected identical polypeptide bands in both HCT116 parental and 3BKO cell lysates. Similarly, AB79822 which does not detect ectopically-expressed human DNMT3B, also detected identical polypeptide bands in both parental and 3BKO cell lysates. Only SC10236 detected polypeptide bands present in the WT HCT116 but not the 3BKO (Figure 3-11). Interestingly, two antibodies (NB100-266 and NEB M0232) which demonstrated an apparent knockdown with some of the DNMT3B shRNAs tested earlier in this chapter (Figure 3-6) detect identical polypeptide bands in both the WT and 3BKO HCT116.

3.4 Discussion

In this chapter, commercially-available DNMT3B antibodies have been validated by a number of methods. The most significant finding is that the putative DNMT3B antibody IMG184A (clone 52A1018) detects murine DNMT3B but not human DNMT3B, which casts significant doubts on the validity of the conclusions of two independent studies which have linked DNMT3B and CIMP in human colorectal adenocarcinoma using this antibody [423,424]. The majority of the antibodies tested detect ectopically expressed human DNMT3B (NB100-266, SC10236, NB100-266). Furthermore, all three antibodies reported to detect murine DNMT3B (SC10236, IMG184A and NB100-266) were confirmed to detect ectopically expressed murine DNMT3B1.

Interpretation of the data regarding the ability of the respective antibodies to detect endogenous DNMT3B are more challenging. The discrepancy between the shRNA knockdown, CRISPR knockdown and 3BKO data with regard to antibody specificity is clearly extremely difficult to reconcile. Given the design of the targeting construct used to generate 3BKO cells it would seem unlikely that the polypeptide targets detected by NEBM0232 and NB100-266 represent DNMT3B, as in these cells, exons 2-21 of DNMT3B are replaced by a neomycin or hygromycin resistance gene expressed from the endogenous DNMT3B promoter. Furthermore however, it seems inconceivable that shRNAs specifically designed to target DNMT3B would knockdown a polypeptide target other than DNMT3B that is detectable by two independently-designed DNMT3B antibodies. Given that the epitope for NEBM0232 corresponds to the carboxy terminus of DNMT3B, which exhibits structural homology with that of DNMT3A, the possibility that this antibody detects DNMT3A and not DNMT3B was considered. Cross-recognition of DNMT3A however would not explain the apparent knockdown demonstrated using NB100-266 in shRNA lysates, as the epitope for this antibody is in the N-terminal domain,

which does not exhibit the same degree of structural homology as the C-terminal catalytic domain [196]. Moreover, BLAST[15] analysis of the shRNA sequences was performed and was not suggestive of DNMT3A targeting by any of the shRNAs tested.

Most importantly, the antibody that can most robustly be concluded to detect human DNMT3B is SC10236. This antibody (which also detects murine DNMT3B) detects ectopically expressed DNMT3B, and exhibited consistent specificity for endogenous DNMT3B in shRNA and CRISPR knockdown and 3BKO cells. All subsequent human DNMT3B protein analysis presented in this thesis is performed using the SC10236 antibody unless explicitly stated otherwise. All subsequent murine DNMT3B protein analysis presented in this thesis is performed using IMG184A unless stated otherwise.

3.5 Summary

1. AB79822 detects neither human DNMT3B nor murine DNMT3B.

2. IMG184A detects murine DNMT3B but not human DNMT3B.

3. SC10236 detects both murine DNMT3B and human DNMT3B.

4. NB100-266 and NEBM0232 detect ectopically expressed human DNMT3B, but their reactivity with endogenous human DNMT3B cannot be unambiguously verified.

5. Lentiviral constructs to direct ectopic expression of human DNMT3B1 and DNMT3B3 in primary human cells have been developed and validated.

6. Both shRNA and CRISPR sgRNA constructs have been designed and validated for later loss-of-function experiments.

[15] https://blast.ncbi.nlm.nih.gov/Blast.cgi

4 Whole genome bisulfite sequencing of the DNA methylation changes induced by activated oncogenic $BRAF^{V600E}$

4.1 Rationale

As outlined in the introduction to this thesis, a consistent association has been noted between $BRAF^{V600E}$ mutation and a CpG island methylator phenotype in colorectal adenocarcinoma and precursor sessile serrated lesions [113,116,125,355,360,367,425]. The ability of the $BRAF^{V600E}$ oncogene to directly induce the CpG island methylator phenotype however remains controversial. Some features associated with CIMP (e.g. promoter CGI methylation of *CDKN2A/INK4A*) have been reported in both *in vitro* and *in vivo* model systems in association with $BRAF^{V600E}$ activation [47,426]. By comparison, stable expression of activated oncogenic BRAF in a CIMP-negative colon cancer cell line (COLO 320DM) has been demonstrated to be insufficient to induce a CpG island methylator phenotype: although this study used a relatively low-coverage methodology to assess CpG island methylation, which assesses only 1505 CpG sites (Illumina GoldenGate DNA methylation technology) [362]. Most recently, however a mechanism by which mutant-$BRAF^{V600E}$ might directly induce CIMP has been published [364,365]. The published evidence concerning the role of the $BRAF^{V600E}$ oncogene in inducing CIMP thus remains conflicted. Although activation of mutant-BRAF has been suggested to be an initiating event in human serrated colorectal cancer, there is a notable lack of an unbiased genome-wide study to examine the consequences of $BRAF^{V600E}$ activation on the DNA methylome of normal human cells [46,47].

An additional context in which to consider the methylation changes induced by an activated oncogenic $BRAF^{V600E}$ oncogene is that of the oncogene-induced senescence program, which is triggered by the activation of mutant-$BRAF^{V600E}$ in primary cells [30]. Genome wide DNA methylation analysis (by whole genome bisulfite sequencing) in primary cells that have undergone replicative senescence has revealed some striking parallels between the DNA methylation changes that accompany replicative senescence and those associated with cancer. One of the most interesting findings of the latter study was that replicatively-senescent primary cells develop focal gains in DNA methylation at CpG islands associated with the CpG island methylator phenotype (namely *RUNX3*, *CACNA1G*, *SFRP2*, *SOCS1* and *NEUROG1*), and that such changes persist when such cells are immortalised and bypass senescence. Furthermore, these methylation changes

were associated with upregulation of the *de novo* methyltransferase DNMT3B, which has also been linked mechanistically and correlatively to CIMP [47,281,364,427,428].

A model by which aberrant cancer-associated methylation patterns, such as CIMP, might have their origins in the oncogene-induced senescence program is attractive, and is of particular relevance to the serrated pathway of colon cancer, which is tightly associated with the *BRAF*^{V600E} mutation and thus CIMP, especially in light of the emerging *in vivo* and *in situ* evidence of a senescence-like tumour suppressor program in its pathogenesis reviewed in the introduction to this thesis.

In this chapter therefore, the DNA methylation changes induced by activated oncogenic BRAF^{V600E} will be characterised.

4.2 Aims

The specific aims of this chapter are:

1. To develop an *in vitro* model of BRAF^{V600E}-induced proliferation arrest.

2. To compare the DNA methylation changes induced by an activated *BRAF*^{V600E} oncogene to those previously described in replicative senescence.

3. To assess whether activated mutant-BRAF^{V600E} is sufficient to induce a CpG island methylator phenotype in primary cells.

4.3 Results

4.3.1 Establishing a cellular model of $BRAF^{V600E}$-induced proliferation arrest

An *in vitro* model system was required in which to examine the DNA methylation changes induced by activated oncogenic $BRAF^{V600E}$. $BRAF^{V600E}$-induced oncogene-induced senescence has perhaps been most comprehensively characterised in melanocytes [30,429]. By contrast, the published data on DNA methylation changes in replicative senescence were in a human fetal lung fibroblast model system. To allow direct comparison therefore, the decision was made to utilise a similar human fetal lung fibroblast model (IMR-90) for these experiments. This approach was further justified in light of the fact that in the initial paper characterising $BRAF^{V600E}$-induced senescence in melanocytes, physiological levels of $BRAF^{V600E}$ were demonstrated to induce senescence in human BJ fibroblasts; furthermore, previous studies have characterised RAF-induced senescence in fibroblasts [30,34].

In order to stably transduce primary human fetal lung fibroblasts to ectopically express activated oncogenic $BRAF^{V600E}$, the lentiviral constructs HIV-CS-CG-$BRAF^{V600E}$-puromycin and its corresponding empty vector, HIV-CS-CG-puromycin were obtained from Prof Daniel Peeper's laboratory. Plasmid identity was first verified by diagnostic restriction digest of both the $BRAF^{V600E}$ and empty vector plasmids. Single and double cut digests were performed with NheI, EcoRV and the two enzymes in combination. A single cut with NheI or EcoRV linearised the plasmids resolving a band of approximately 8.6kbp for the vector and 11kbp for the $BRAF^{V600E}$ plasmid. Double cut with NheI and EcoRV resolved two bands, corresponding to the insert and parental plasmid respectively (Figure 4-1).

IMR-90 at low passage number (PD<30) were transduced with HIV-CS-CG-$BRAF^{V600E}$-puromycin or the empty-vector plasmid. Twenty-four hours after transduction, cells were drug-selected with culture media supplemented with 1μg/mL puromycin. Whilst cells initially underwent a period of hyperproliferation, $BRAF^{V600E}$ transduced cells developed a mixed spindle-like and rounded morphology, did not require further passaging, and at seven days post-transduction appeared to have undergone proliferation arrest. Initial attempts to characterise this by means of immunocytochemistry for EDU or BrdU, or assay for senescence-associated β-galactosidase were unsuccessful, as multiple attempts to culture cells on glass coverslips were unsuccessful, due to cell detachment. The decision was made to assay the proliferation phenotype of these cells by Western blot for

established markers associated with cellular senescence. Whole cell lysates were prepared from tissue culture plates, separated by SDS-PAGE, immobilised to PVDF and assessed by Western blotting. As demonstrated in Figure 4-2, in comparison to proliferating ("vector") controls, $BRAF^{V600E}$-transduced fibroblasts demonstrated upregulation of the cell cycle inhibitors p16 and p27, and repression of cyclin A, and phosphorylated pRb (Ser807/811) relative to total pRb. In sum, $BRAF^{V600E}$ induces a proliferation arrest phenotype in IMR-90 at the 7 day timepoint. As prolonged maintenance of these cells in culture could not be achieved, this phenotype is referred to hereafter as BRAF-induced proliferation arrest, as it cannot unambiguously be characterised as senescence.

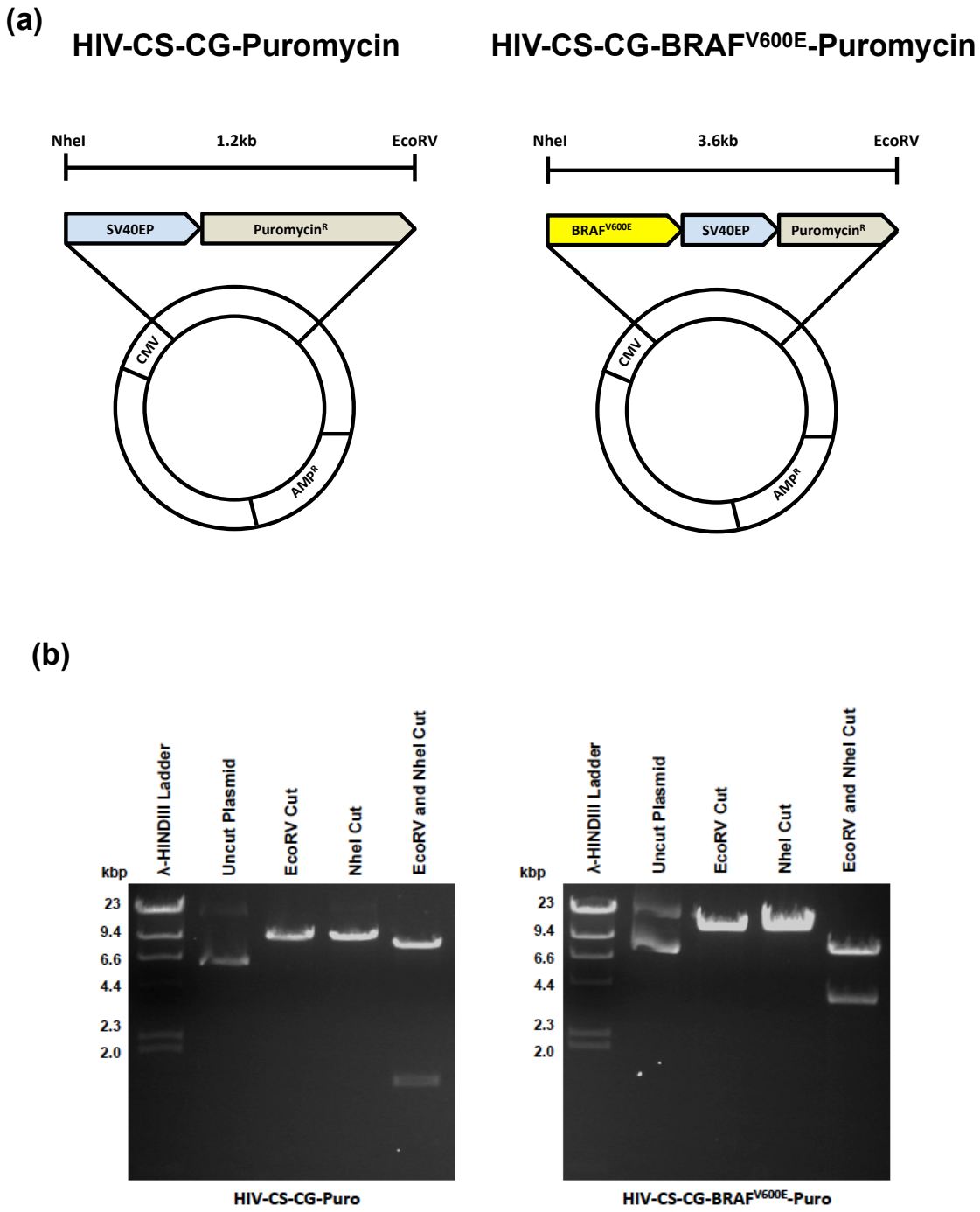

Figure 4-1 Schematic diagrams and diagnostic restriction digests of HIV-CS-CG-Puromycin and HIV-CS-CG-BRAF^{V600E}-Puromycin

(a) Schematic diagrams of lentiviral plasmids used for transduction of IMR-90 human fetal lung fibroblasts. **(b)** Diagnostic restriction digests were performed in order to verify plasmid identity prior to transduction. A single cut with NheI or EcoRV linearised the plasmids resolving a band of approximately 8.6kbp for the vector and 11kbp for the BRAF^{V600E} plasmid. Double cut with NheI and EcoRV resolved two bands, corresponding to the insert and parental plasmid respectively.

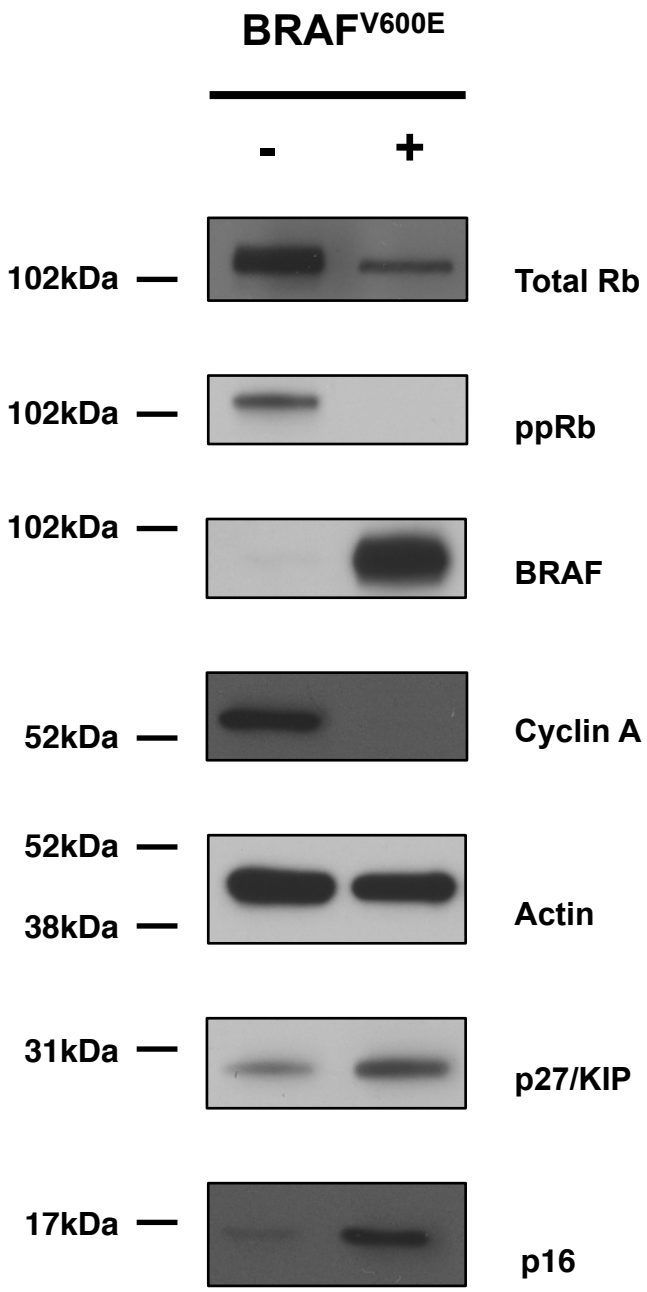

Figure 4-2 BRAF^{V600E} induces a proliferation arrest phenotype in human fetal lung fibroblasts (IMR-90)

Western blot of protein lysates from human fetal lung fibroblasts (IMR-90) transduced with lentivirus directing expression of BRAF^{V600E} or the corresponding empty vector. Cells were harvested for protein lysates seven days following transduction. Whole cell lysates were separated by SDS-PAGE, immobilised to PVDF and assessed by Western blotting. Analysis of protein expression of cell-cycle regulators reveals a proliferation arrest phenotype associated with acute BRAF^{V600E} activation, with repression of cyclin A, and upregulation of p16 associated with dephosphorylation of pRb. Upregulation of the cell cycle inhibitor p27 was also demonstrated (n=3 biological replicates).

4.3.2 Comparison of the DNA methylation changes in BRAF-induced proliferation arrest and replicative senescence

In order to characterise the DNA methylation changes induced by activated oncogenic $BRAF^{V600E}$, human fetal lung fibroblasts were once again transduced with HIV-CS-CG-$BRAF^{V600E}$-puromycin or the corresponding empty vector, drug-selected with puromycin, and harvested for DNA. Two independent biological replicates were performed for each condition. As detailed above, $BRAF^{V600E}$-transduced IMR-90 were deemed to have undergone proliferation arrest at 7 days post-transduction, and were harvested at this timepoint. In order to minimise artefact generated by passaging, proliferating, "vector" controls were harvested at 3 days post transduction, to ensure that both "vector" and "BRAF" populations had undergone approximately equivalent population doublings. Genomic DNA was extracted from "vector" and $BRAF^{V600E}$ transduced populations using the Qiagen QiaAmp DNA blood mini kit according to the manufacturer's protocol. Prior to whole genome bisulfite sequencing, DNA samples were quantified using the Qubit DNA assay, and measurement of OD at 260/280 was performed (data not shown). Furthermore, DNA samples were tested by agarose gel electrophoresis, to confirm isolation of genomic DNA (Figure 4-3).

Whole genome bisulfite sequencing was performed by BGI, Shenzhen. A summary of the protocol is given in chapter 2. Data alignment and subsequent analysis was performed by Mr Neil Robertson, a computational biologist in the Adams' lab at the Beatson Institute for Cancer Research, Glasgow. For direct comparison of the DNA methylation changes in this $BRAF^{V600E}$-induced proliferation arrest system with those previously reported in replicative senescence, whole-genome bisulfite sequencing data for replicative senescence and proliferating cells generated by Dr Hazel Cruickshanks, a previous post-doctoral researcher in the Adams' lab were employed [281].

Following initial alignment and processing of WGBS data, both independent replicates of "vector" control and $BRAF^{V600E}$ transformed populations were subject to principal component analysis. In comparison to replicative senescence, principal component analysis did not significantly separate the methylome of $BRAF^{V600E}$-expressing cells and "vector" controls by cohort: with the first, second and third components accounting for 35.3%, 32.6% and 31.9% of the cumulative variance respectively. By comparison, the replicative senescence cohorts displayed high levels of divergence between cohorts on the first principal component (56.6% of cumulative variance). In sum, this indicates that in the comparison of "vector" control and BRAF conditions, replicates were not substantially

different based on $BRAF^{V600E}$ status, in comparison to proliferating and replicative senescence replicates, which clustered much more distinctly by cellular phenotype (Figure 4-4).

In order to characterise the global DNA methylation changes associated with activated oncogenic $BRAF^{V600E}$, global CpG methylation was calculated at each CpG across both replicates for each condition. The same comparison was performed in replicatively senescent and proliferating controls. In the $BRAF^{V600E}$ population, 63.4% of CpGs were methylated in comparison to 63.14% of proliferating "vector controls": corresponding to a 0.26% increase in global methylation associated with an activated $BRAF^{V600E}$ oncogene. By comparison, in proliferating (PD28) IMR-90, 65.8% of CpGs were methylated, and in replicatively senescent (PD88) fibroblasts, 59.22% of CpGs were methylated, accounting for a 6.58% reduction in global methylation. Thus whilst activated mutant-$BRAF^{V600E}$ is associated with a global gain in methylation, the magnitude of this change is much more subtle than the reduction in CpG methylation associated with replicative senescence (Figure 4-5, Figure 4-6).

In order to facilitate further dissection of the methylation changes accompanying $BRAF^{V600E}$ activation, and investigate the variance between these, and those accompanying replicative senescence, the genome was next divided into base-pair "windows" in order to define differentially-methylated regions (DMRs). The low coverage (10 reads per CpG) provided by WGBS makes accurate "calling" of the methylation status of any single CpG difficult as low numbers of reads can introduce constant scaling factors. The use of "windowing" increases the number of reads for any given region, with a resultant increase in the accuracy of methylation "calls". Consistent with the observed modest increase in global CpG methylation associated with $BRAF^{V600E}$ in comparison to "vector" control cells, relative to the much larger contrast seen between replicatively senescent and proliferating populations, the number of DMRs associated with $BRAF^{V600E}$ activation was significantly lower than in replicative senescence: several thousand ($BRAF^{V600E}$) compared to several million (RS). Furthermore, variation in the size of candidate DMRs from 50bp to 1000bp did not significantly alter this vast difference in DMR number (Figure 4-7).

The distribution of observed DMRs was next compared, by plotting the base-pair overlap of DMRs by genomic feature (Figure 4-8). Whilst the latter provides an impression of the distribution of DMRs across genomic features, it can provide a skewed picture due to the significant differences in size between particular genomic features. Thus, in order to obtain

a clearer impression of the relative distribution of differentially methylated regions with respect to individual genomic features, the observed-to-expected ratio for DMRs at individual genomic features was calculated and plotted. Overlaps were computed on a per base pair basis between two datasets (A and B). For every region within A the number of base pairs that were occupied by a region within B was computed. A permutation test was carried out to determine the background genomic average expected overlap. 1000 sets of regions with properties (length distribution and chromosome distribution) equal to those of set B were generated. Randomly generated regions of B were prevented from being generated within unsequenced regions of the genome (as defined by UCSC mapping and sequencing track—gap). The overlap of A and B was repeated for each randomly generated set of B to determine the average expected random overlap. Next, p-values were estimated empirically from the observed overlaps of the randomly generated sets[16]. Interestingly, although the total number of DMRs associated with $BRAF^{V600E}$ were relatively few in number, observed-to-expected plots revealed some interesting trends. The most significant relative enrichment of hypermethylated DMRs was at CpG islands, and the fold-overlap was in fact much greater than that observed in replicative senescence. Furthermore, there was a further enrichment of hypermethylated DMRs at CpG shores, and once again the fold-overlap at this feature was much greater than observed in replicative senescence. Interestingly, the most significant enrichment of hypomethylated DMRs was at enhancers. Hypomethylation of enhancers has recently been described in association with cancer-specific gene expression [169]. Thus whilst the overall methylation changes associated with activated $BRAF^{V600E}$ were very subtle, those observed did exhibit some interesting parallels with what one might consider a cancer methylation phenotype (Figure 4-9).

[16] Overlap computation method from, Cruickshanks HA, McBryan T, Nelson DM, Van der Kraats ND, Shah PP, van Tuyn J, et al. Senescent cells harbour features of the cancer epigenome. Nat Cell Biol. 2013 Nov 24;15(12):1495–506

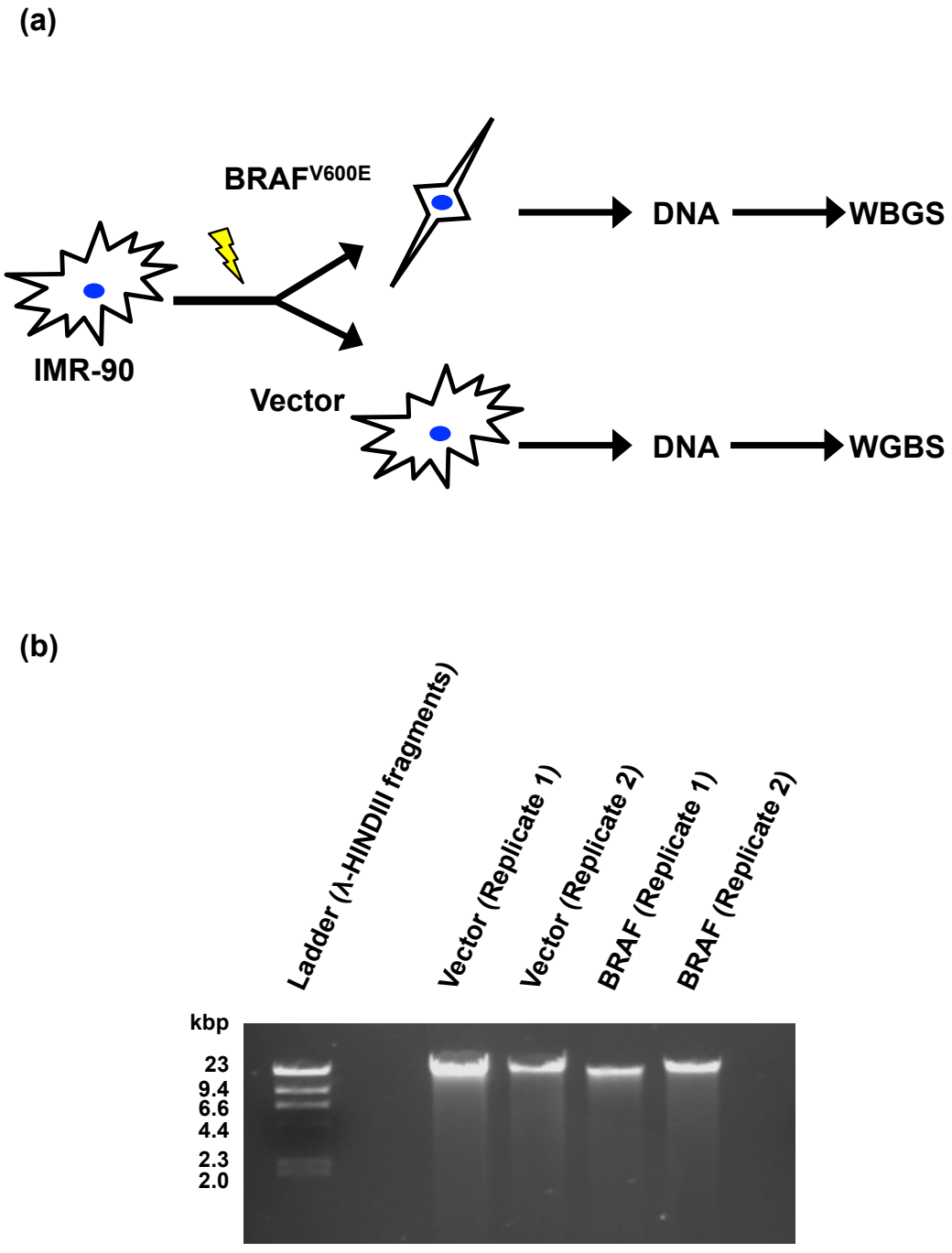

Figure 4-3 Genomic DNA was isolated from IMR-90 human fetal lung fibroblasts transformed with HIV-CS-CG-puromycin or HIV-CS-CG-BRAF^{V600E}-puromycin, and DNA methylation assessed by whole genome bisulfite sequencing.

(a) Schema of experimental design. Human fetal lung fibroblasts transduced with lentiviral-directed ectopic expression of BRAF^{V600E} or the corresponding empty vector. **(b)** Extraction of genomic DNA was confirmed by agarose gel electrophoresis prior to submission for whole genome bisulfite sequencing.

(a)

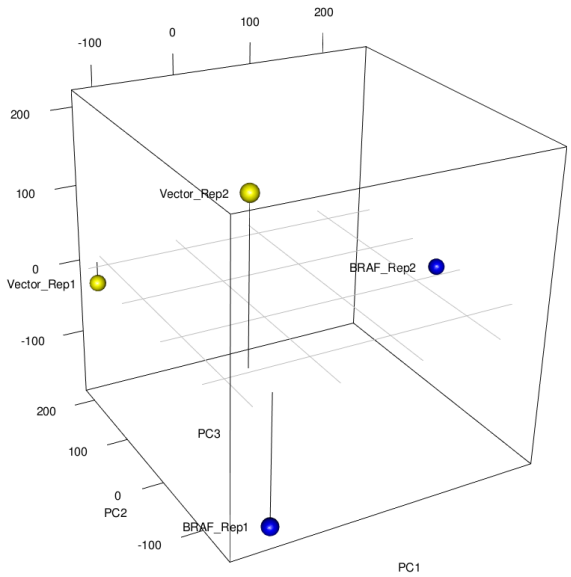

(b)

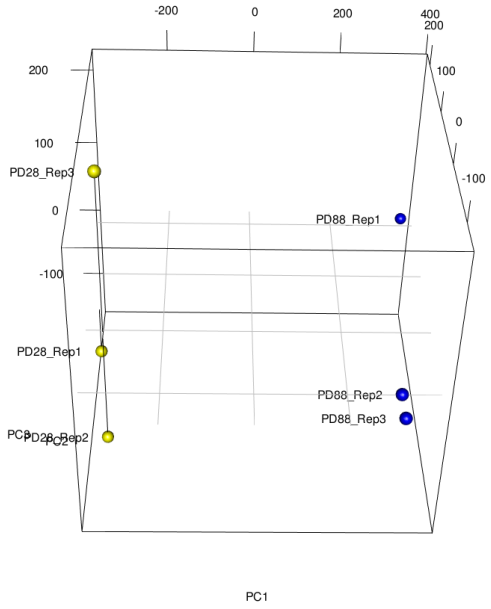

Figure 4-4 Principal-component analysis did not significantly separate the methylome of BRAF^{V600E}-expressing cells compared to that of proliferating controls.

Following initial alignment and processing of WGBS data, principal component analysis (PCA) was undertaken to compare the variance in methylation data between BRAF^{V600E} and proliferating (vector) controls, and proliferating (PD28) and replicatively senescent (PD88) cells. **(a)** PCA did not significantly separate the methylome of BRAF^{V600E}-expressing cells and "vector" controls by cohort: with the first, second and third components accounting for 35.3%, 32.6% and 31.9% of the cumulative variance respectively. **(b)** By comparison, the replicative senescence cohorts displayed high levels of divergence between cohorts on the first principal component (56.6% of cumulative variance). In sum, this indicates that in the comparison of "vector" control and BRAF conditions, replicates were not substantially different based on BRAF^{V600E} status, in comparison to proliferating and replicative senescence replicates, which clustered much more distinctly by cellular phenotype.

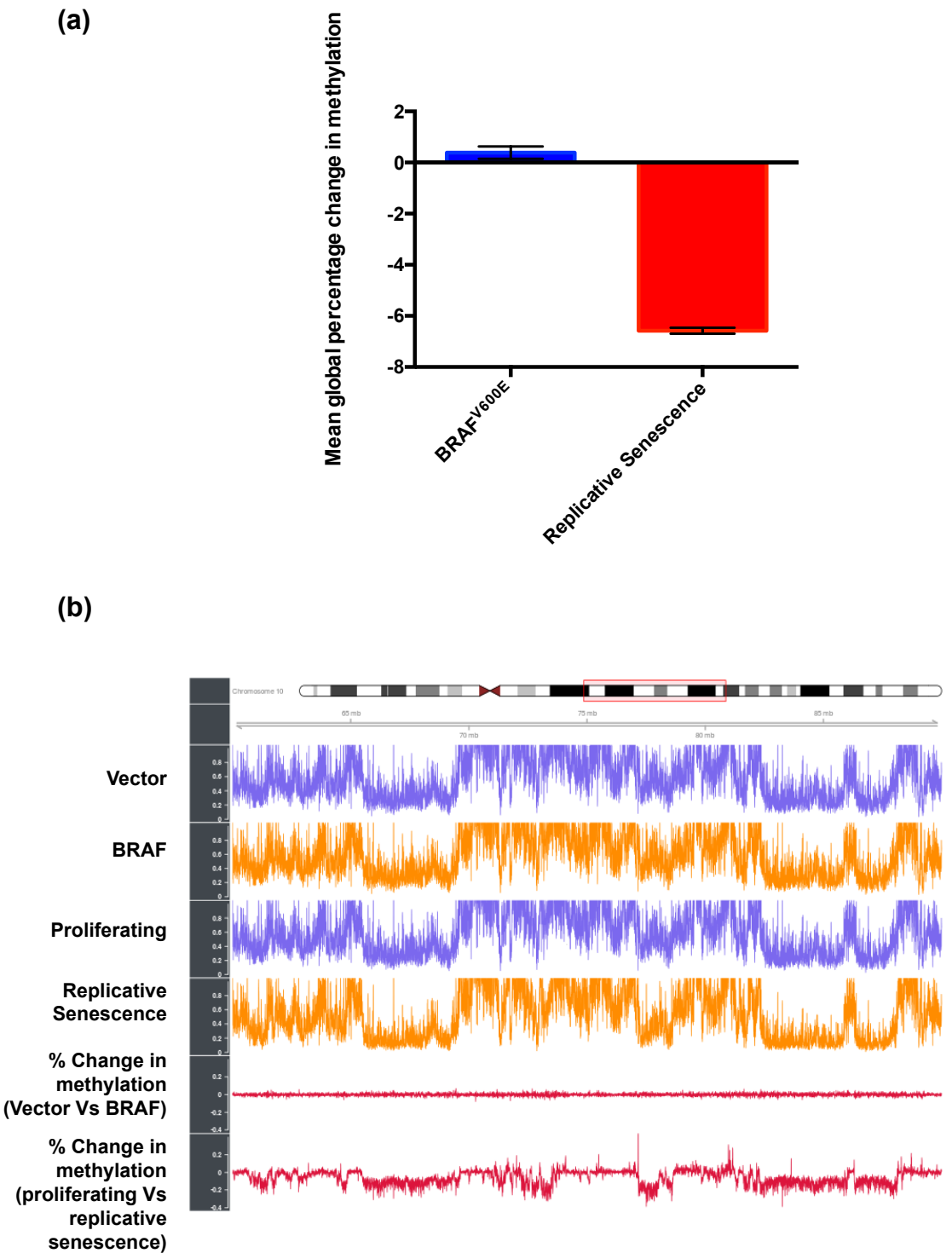

Figure 4-5 BRAF^{V600E} evokes a modest increase in global methylation, compared to the profound hypomethylation associated with replicative senescence

(a) Mean global percentage change in methylation was compared between BRAF-induced proliferation arrest and proliferating "vector" populations and replicatively-senescent fibroblasts and proliferating controls. A modest increase in global methylation of 0.26% is observed upon activation of BRAF^{V600E} compared to a reduction of 6.58% in global methylation in replicative senescence (n=2 biological replicates; error bars represent SEM; unpaired t-test p=0.006). **(b)** Graphical representation of a representative region of chromosome 10 demonstrating the lack of substantial methylation changes induced by BRAF^{V600E} compared to regions of marked hypomethylation associated with replicative senescence.

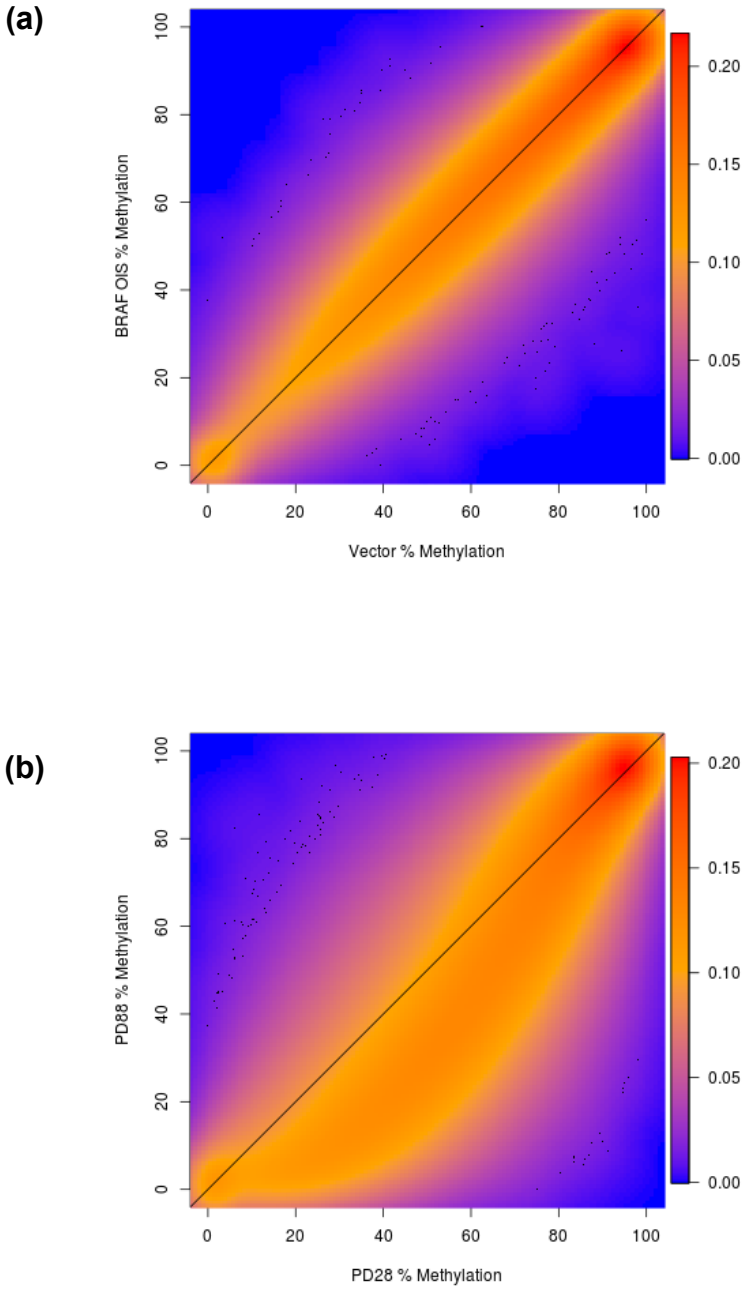

Figure 4-6 Smoothened scatterplots of CpG methylation changes in BRAF^{V600E}-induced proliferation arrest and replicative senescence

Smoothened scatter plots of percentage CpG methylation in 2kbp windows in **(a)** BRAF^{V600E}-induced proliferation arrest compared to proliferating "vector" controls and **(b)** replicatively senescent fibroblasts compared to proliferating controls. Colour intensity denotes the number of data points per pixel (red = highest density of points). **(a)** Activated BRAF^{V600E} induces very little demonstrable change in percentage CpG methylation relative to proliferating "vector" controls. **(b)** By comparison, in replicative senescence there is global loss of methylation (particularly mid-band methylation) relative to proliferating controls.

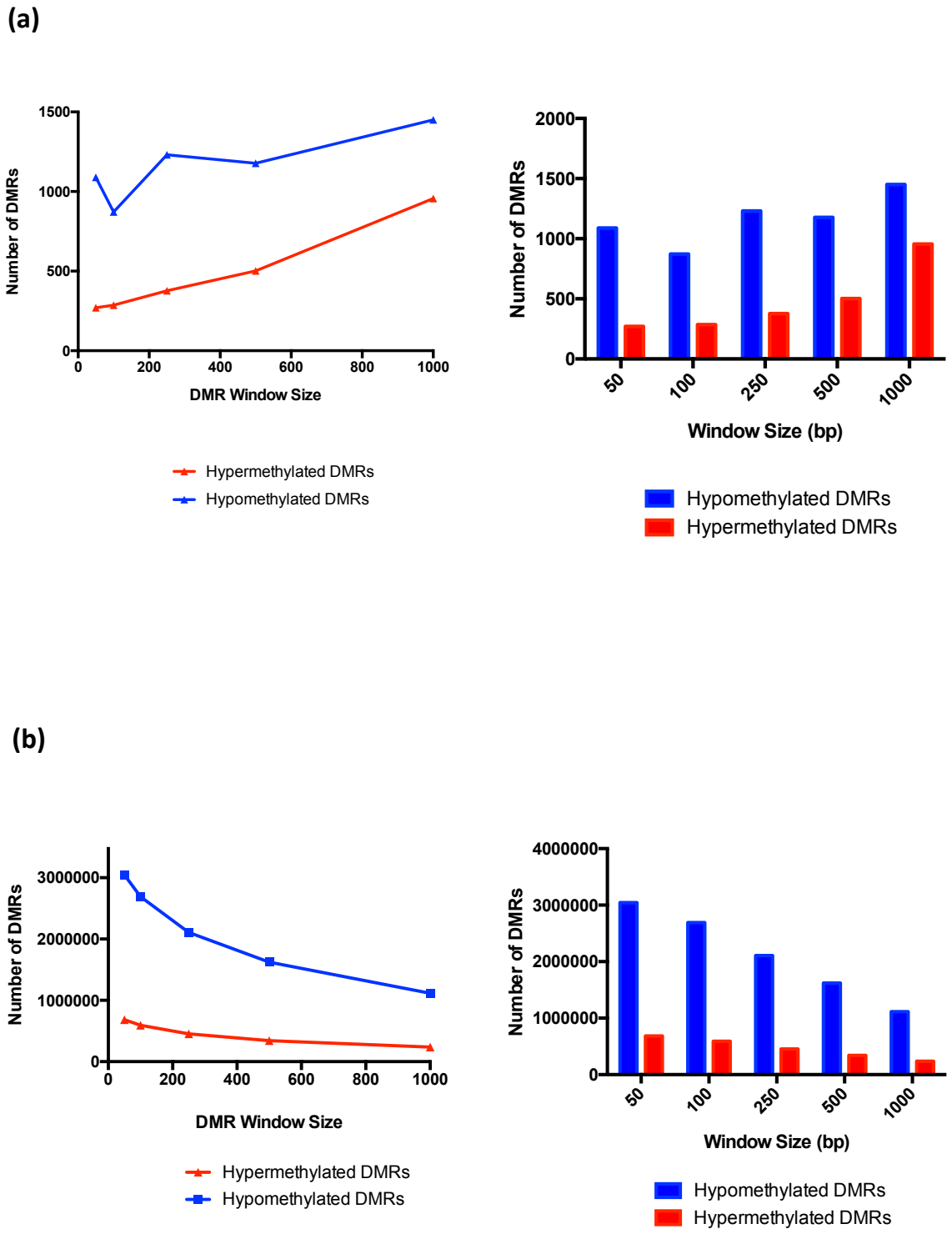

Figure 4-7 Comparison of number of differentially methylated regions (DMRs) by window size in BRAF^{V600E}-induced proliferation arrest and replicative senescence

Differentially methylated regions (DMRs) were called by dividing the genome into base-pair "windows". Consistent with the observed modest increase in global CpG methylation associated with BRAF^{V600E} in comparison to "vector" control cells, relative to the much larger contrast seen between replicatively senescent and proliferating populations, the number of DMRs associated with BRAF^{V600E} activation is significantly lower than in replicative senescence. **(a)** Line graph and bar-chart of DMR number by window size comparing vector and BRAF^{V600E} populations. Even adjusting the window size, relatively few DMRs (several thousand) are identified between vector- and BRAF^{V600E}-transduced IMR-90 **(b)** Line graph and bar-chart of DMR number by window size comparing proliferating and replicatively senescent populations. By comparison, several million DMRs are identified between proliferating cells and those that have undergone replicative senescence.

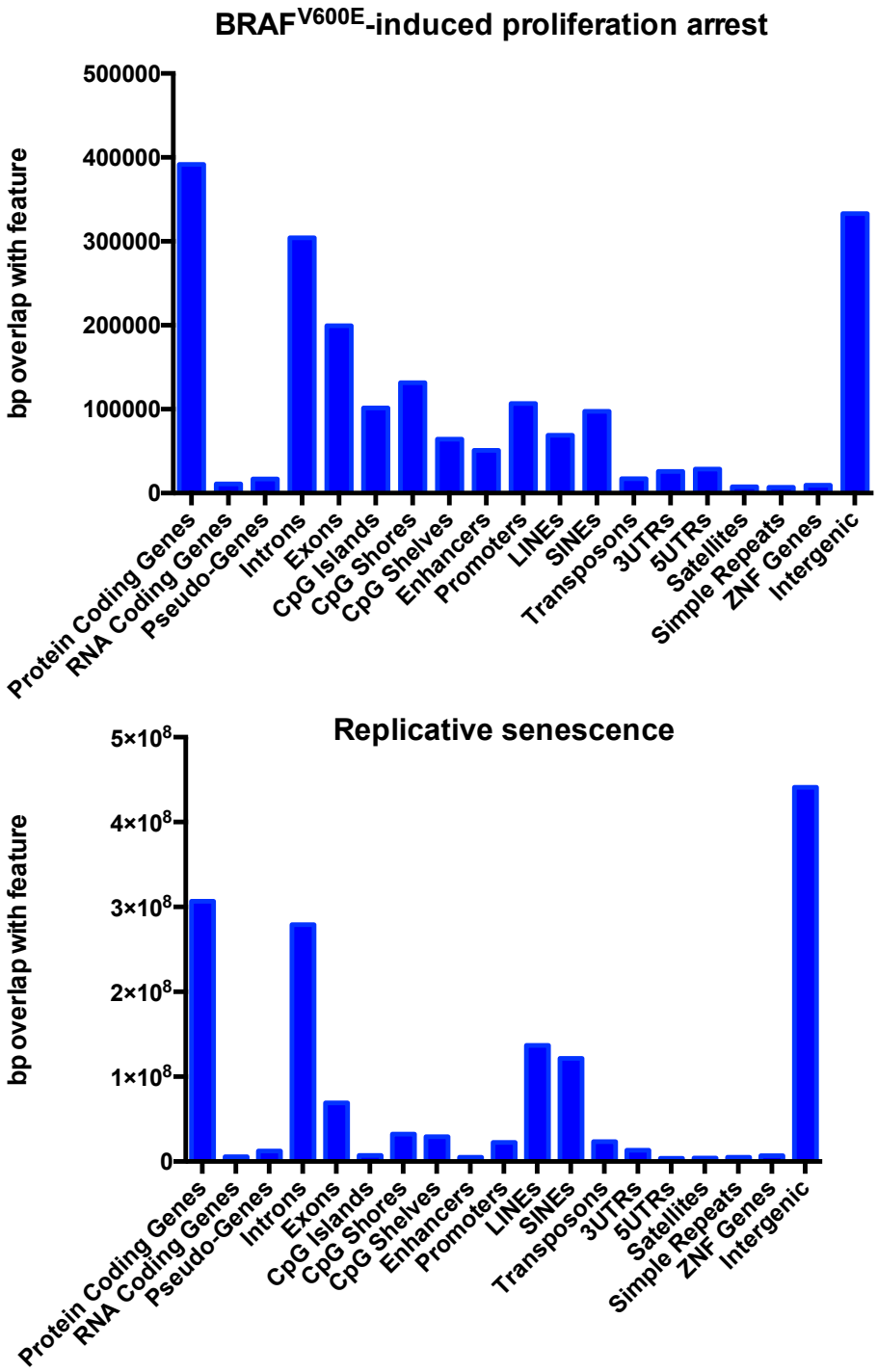

Figure 4-8 Overlap of DMRs at genomic features in BRAF^{V600E}-induced proliferation arrest and replicative senescence

Bar-charts of basepair overlap of DMRs at genomic features in **(a)** BRAF^{V600E}-induced proliferation arrest and **(b)** replicative senescence. Reflecting the significantly smaller number of DMRs associated with activated oncogenic BRAF^{V600E} in comparison to replicative senescence, a correspondingly smaller DMR base-pair overlap across all genomic features is demonstrable in association with activated BRAF^{V600E} compared with replicative senescence.

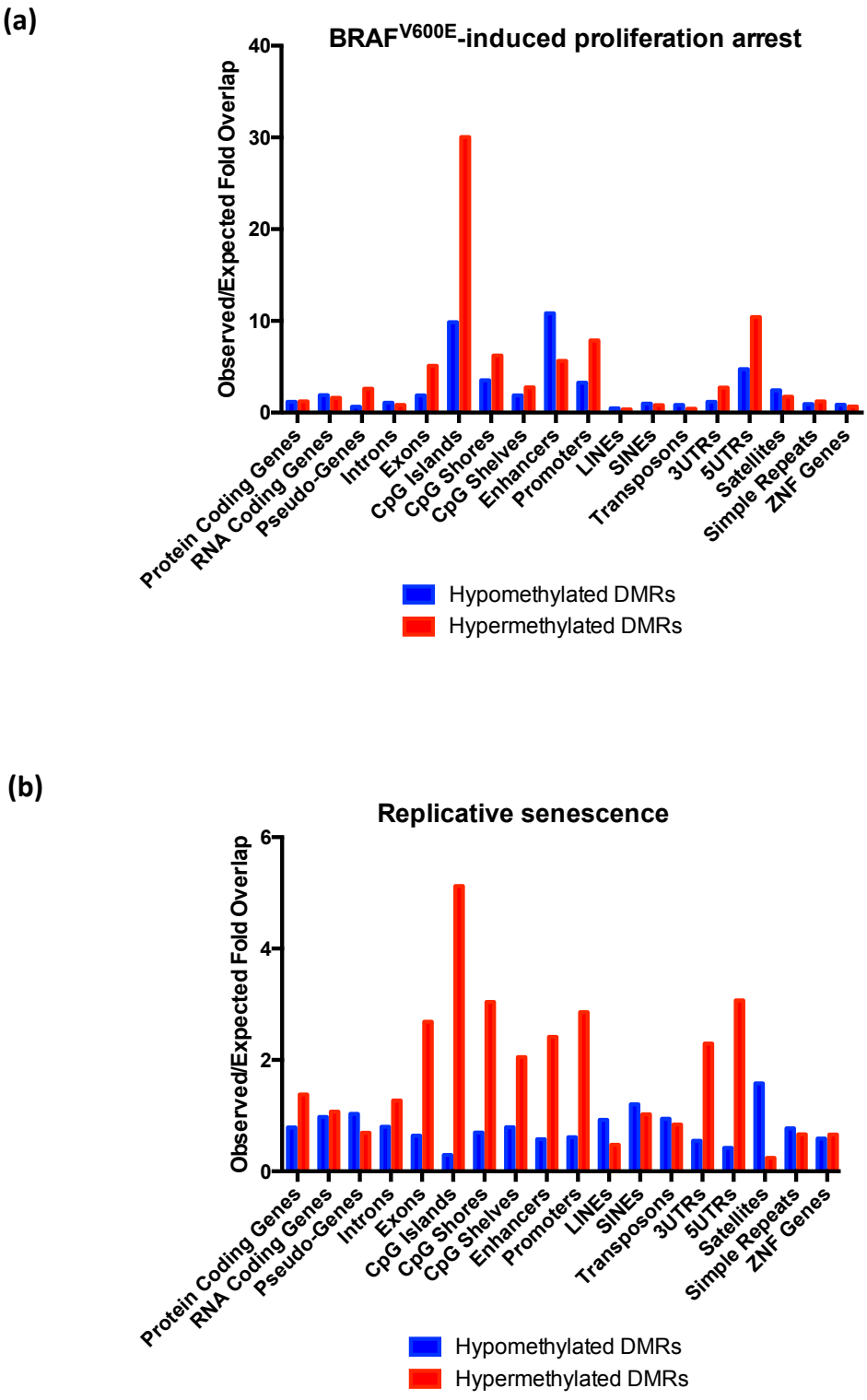

Figure 4-9 Comparison of observed to expected ratios of DMR overlap between BRAF^{V600E}-induced proliferation arrest and replicative senescence.

Bar-charts of observed to expected DMR overlap by genomic feature in **(a)** BRAF^{V600E}-induced proliferation arrest and **(b)** replicative senescence. Despite the numerical lack of DMRs associated with activated oncogenic BRAF^{V600E}, these observed-to-expected plots revealed some interesting trends. The most notable relative enrichment of hypermethylated DMRs is at CpG islands, where the fold-overlap is greater than that observed in replicative senescence. Furthermore, there is further enrichment of hypermethylated DMRs at CpG shores, where again the fold-overlap is much greater than observed in replicative senescence. There is also marked enrichment of hypomethylated DMRs at enhancers associated with activated BRAF^{V600E}.

4.3.3 Activated oncogenic BRAF downregulates expression of DNMT3B and does not induce a CpG island methylator phenotype

Overall, compared to replicative senescence, activated oncogenic $BRAF^{V600E}$ induces only a very modest change in global methylation relative to proliferating "vector" controls. Despite this, as outlined above, in contrast to replicative senescence, activated oncogenic $BRAF^{V600E}$ appears to cause a small overall gain in global methylation, with relative enrichment of hypermethylated DMRs at CpG islands when assessed in an "observed to expected" manner. As CpG island hypermethylation is a defining feature of the CpG island methylator phenotype (CIMP), it was of interest to assess whether the modest gains in CpG island methylation detected by analysis of the WGBS data corresponded to a CIMP phenotype.

As outlined in chapter 1, various marker panels have been proposed for the characterisation of CIMP positivity in colorectal adenocarcinoma. For this analysis, the CIMP panel described by Ogino et al. [310] was selected (*CACNA1G*, *CDKN2A*, *CRABP1*, *MLH1* and *NEUROG1*). In order to assess CpG island methylation at these loci, individual methylated base-calls in proliferating "vector" cells and $BRAF^{V600E}$-transformed cells at each "CIMP panel gene" were compared, and plotted as "smoothened methylation" plots. Notably, CpG island hypermethylation at CIMP genes was not observed in any of the five CIMP panel genes assessed when comparing $BRAF^{V600E}$-expressing cells to proliferating controls, and no overlap was observed between the previously identified DMRs and the CpG islands of the aforementioned CIMP genes when examined by intersecting the previously identified DMRs with their respective promoter CpG island sites (Figure 4-10). Interestingly, this is in contrast to replicative senescence, in which hypermethylation of CpG island CpGs in certain "CIMP marker" genes (*RUNX3*, *CACNA1G*, *SFRP2*, *SOCS1* and *NEUROG1*) has been described compared to proliferating controls [281].

In replicative senescence, in addition to the observed gains in methylation at CpG islands traditionally associated with CIMP, increased DNMT3B expression was noted in senescent fibroblasts compared to proliferating controls. As a CIMP phenotype was not evident in association with $BRAF^{V600E}$ activation in this model system, and in view of the published evidence linking $BRAF^{V600E}$, DNMT3B and CIMP, it was pertinent to examine the effects of acute $BRAF^{V600E}$ activation on DNMT3B expression. Whole cell lysates were prepared from proliferating "vector" and $BRAF^{V600E}$-transformed controls, separated by SDS-PAGE, immobilised to PVDF, and DNMT3B protein expression compared by Western blotting with a validated DNMT3B antibody. Significantly, and in keeping with the

observed lack of a CIMP-phenotype in this population, $BRAF^{V600E}$-transduced cells exhibited marked repression of DNMT3B protein expression compared to proliferating "vector" controls (Figure 4-11).

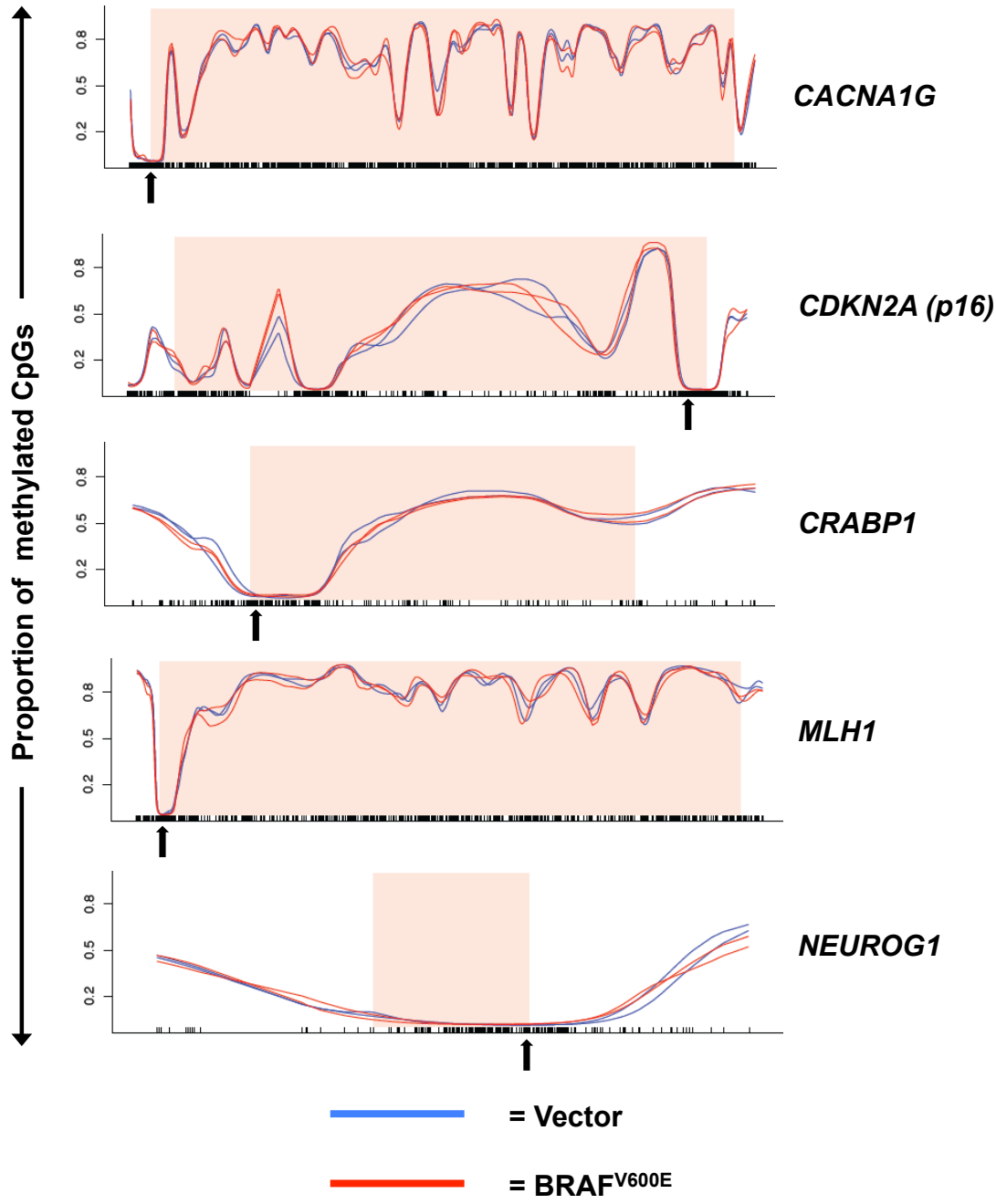

Figure 4-10 BRAF^{V600E} does not induce a CpG island methylator phenotype (CIMP)

Smoothened methylation plots of CIMP panel genes [310] in vector and BRAF^{V600E}-expressing cells. A CpG island methylator phenotype is not observed upon activation of BRAF^{V600E}. Red and blue lines indicate the smoothened average percentage methylation at corresponding CpGs. Individual CpGs are indicated by black "ticks" along the x-axis. The TSS is marked by a black arrow (↑). No significant change in CIMP gene promoter CpG island methylation is noted between BRAF^{V600E}-expressing cells and proliferating controls.

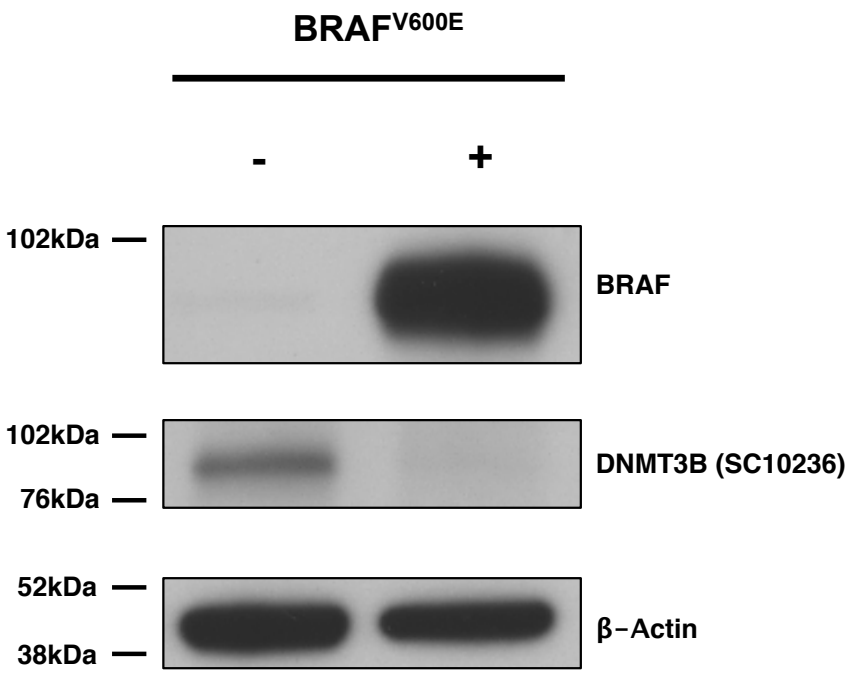

Figure 4-11 Acute BRAF^{V600E} activation in human fetal lung fibroblasts (IMR-90) downregulates protein expression of the *de novo* methyltransferase DNMT3B.

Western blot of whole cell protein lysates from human fetal lung fibroblasts (IMR-90) transduced with lentivirus directing expression of BRAF^{V600E} or the corresponding empty vector. Whole cell lysates were separated by SDS-PAGE, immobilised to PVDF and assessed by Western blotting for DNMT3B and BRAF. Consistent with the lack of a CIMP phenotype in human fetal lung fibroblasts transformed with activated oncogenic BRAF^{V600E}, striking downregulation of protein expression of DNMT3B is observed upon activation of BRAF^{V600E} (n=2 biological replicates).

4.4 Discussion

In this chapter, whole genome bisulfite sequencing has been used to assess, at base-pair resolution, the DNA methylation changes associated with activated oncogenic $BRAF^{V600E}$ in primary human cells. These data are interpretable, and have been presented in two different but potentially interrelated contexts: namely oncogene-induced senescence and the CpG island methylator phenotype. Both the former and the latter are features associated with the serrated pathway of colorectal adenocarcinoma [46,47,116,430,431].

Significantly, in comparison to replicative senescence, $BRAF^{V600E}$-induced proliferation arrest is associated with a much less dramatic change in global DNA methylation, and is associated with a very modest overall increase in CpG methylation. Despite the significant difference in the order of magnitude of observed DMRs associated with activated $BRAF^{V600E}$ when compared to replicative senescence (several million in replicative senescence compared to several thousand with activated $BRAF^{V600E}$), a relative enrichment for CpG island CpGs is noted in the observed hypermethylated DMRs associated with $BRAF^{V600E}$. Despite this, and in contrast to the previously published data in replicative senescence, specific analysis of these CpGs with respect to a recognised CIMP marker panel demonstrates that mutant-$BRAF^{V600E}$ does not induce a CpG island methylator phenotype in this *in vitro* model system. Furthermore, consistent with the observed lack of a CIMP phenotype in this cell population, and once again in direct contrast to replicative senescence, proliferation arrest induced by $BRAF^{V600E}$ is associated with repression of the *de novo* methyltransferase DNMT3B.

These data must be interpreted with certain caveats: most of which are related to the model system in which these experiments were performed. A primary human fibroblast cell culture model system was selected in order to allow direct comparison of the DNA methylation changes induced by activated oncogenic $BRAF^{V600E}$ and those previously published in replicative senescence in the same model system. This system did however add an additional design constraint to the experiment, as IMR-90 transduced with $BRAF^{V600E}$ for periods of greater than seven days exhibited progressive apoptosis and detachment in culture dishes, and a viable population from which to allow significant quantities of DNA to be extracted for WGBS[17] could not be achieved after the 7 day timepoint. Resultantly, the DNA methylome of $BRAF^{V600E}$ is assayed in the acute setting,

[17] >5μg genomic DNA were required for WGBS at the time these experiments were performed, although recent advances in single-cell sequencing technology mean that sequencing can be performed from as little as 100ng of DNA.

in comparison both to the prolonged period in cell culture associated with the development of replicative senescence, and the prolonged period associated *in vivo* between the development of a pre-neoplastic lesion with an activated *BRAF*^{V600E} oncogene (e.g. hyperplastic polyp or SSA/P) and the subsequent development of a CIMP-high cancer. It is therefore not possible to exclude the possibility that longer-term activation of *BRAF*^{V600E} oncogene is associated with more profound changes in DNA methylation than have been characterised herein: although it is notable that *in vivo*, both CIMP and aberrant CpG island hypermethylation more generally are reported to develop progressively throughout the process of neoplastic transformation [45,125,360].

By contrast, a potential strength of the use of fetal lung fibroblasts as a model system is the avoidance of potentially confounding variables introduced by examining DNA methylation changes induced by an oncogene in cancer cell lines, though notably, the data presented in this chapter would support the findings of a similar, albeit lower coverage, study performed by stable transfection of a colon cancer cell line with mutant-BRAF^{V600E}, which similarly concluded that the latter was insufficient to induce CIMP [362].

The model system employed also means that the observed DNMT3B repression demonstrable on acute BRAF^{V600E} activation should also be interpreted with certain caveats. It has previously been reported that cells arrested in G_0/G_1 express lower levels of mRNA of both DNMT1 and DNMT3B [432]. Whilst the formal possibility that DNMT3B repression is a consequence of cell-cycle arrest and not acute BRAF^{V600E} activation *per se* has not been specifically excluded here, some counterarguments to this alternative hypothesis can be raised. Firstly, it has previously been demonstrated that RAF activation arrests the cell cycle in G_2/M phase rather than G_1, where the reported nadir in DNMT3B mRNA expression is at its lowest [34,432]. Furthermore, in the context of the archetypal proliferation arrest phenotype, cellular senescence, it has been demonstrated that DNMT3B protein expression is in fact elevated [279,281].

4.5 Summary

1. In comparison to replicative senescence which is accompanied by significant CpG hypomethylation, BRAF^{V600E}-induced proliferation arrest is associated with a modest overall gain in CpG methylation.

2. In comparison to replicative senescence however, cells that have undergone BRAF^{V600E} –induced proliferation arrest exhibit far fewer differentially methylated regions.

3. Hypermethylated differentially methylated regions in $BRAF^{V600E}$-induced proliferation arrest show relative enrichment at CpG islands.

4. Despite the apparent enrichment of hypermethylated DMRs at CpG islands associated with $BRAF^{V600E}$; activation of this oncogene is insufficient to induce a CpG island methylator phenotype in primary cells.

5. Acute $BRAF^{V600E}$ activation in primary cells represses DNMT3B expression, which may be consistent with the failure of the former to induce a CpG island methylator phenotype.

5 *In vitro* modelling of functional cooperation between $BRAF^{V600E}$ and DNMT3B

5.1 Rationale

In the previous chapter it was demonstrated that acute $BRAF^{V600E}$ activation in human fetal lung fibroblasts results in downregulation of DNMT3B at the protein level. This result contradicts previous studies, which have functionally linked DNMT3B and activated $BRAF^{V600E}$. In a murine intestinal tumour model induced by activated oncogenic $Braf^{V600E}$, DNMT3B expression is elevated at both the mRNA and protein level upon $Braf^{V600E}$ activation [47]. Furthermore in human colorectal adenocarcinoma, elevated DNMT3B expression has been demonstrated to correlate with CIMP-H, which itself has been closely associated with $BRAF^{V600E}$ mutation status [116,415]. Additionally, mutant-$BRAF^{V600E}$ has been proposed to directly mediate CIMP through DNMT3B [364]. DNMT3B has also been demonstrated to exhibit an oncogenic function in murine intestinal carcinogenesis, although these studies were not performed in the context of an activated *Braf* oncogene [205,433]. Considering the strength of the published data suggesting functional cooperation between activated mutant-$BRAF^{V600E}$ and DNMT3B, and as the repression of DNMT3B consequent upon acute $BRAF^{V600E}$ activation demonstrated in the previous chapter was limited to an *in vitro* model in primary human fetal lung fibroblasts, it is pertinent to investigate functional cooperation between $BRAF^{V600E}$ and DNMT3B. Moreover, as DNMT3B has previously been demonstrated to induce a CIMP-like phenotype in murine intestinal tumours, which exhibits significant commonality with the DNA methylation changes seen in human colorectal adenocarcinoma, this has the dual purpose of modelling a putative oncogenic function of CIMP in the context of an activated BRAF oncogene [434].

5.2 Aims

The specific aims of this chapter are:

(a) To develop an *in vitro* model system to assess functional cooperation between activated oncogenic $BRAF^{V600E}$ and DNMT3B.

(b) To investigate the mechanism of functional cooperation between $BRAF^{V600E}$ and DNMT3B.

(c) To investigate the functional consequences of DNMT3B knockdown in colon cancer cell lines.

5.3 Results

5.3.1 Ectopic expression of DNMT3B suppresses BRAF-induced proliferation arrest

In order to investigate the functional consequences of DNMT3B overexpression together with activated oncogenic $BRAF^{V600E}$, an *in vitro* model system in primary human fetal lung fibroblasts (IMR-90) was employed. Cells were transformed with lentiviral constructs directing ectopic expression of $BRAF^{V600E}$ or DNMT3B. Lentiviral constructs for ectopic DNMT3B1 and DNMT3B3 were characterised in chapter 3 of this thesis, and were designed with a puromycin drug selection marker. The $BRAF^{V600E}$ ectopic expression plasmid used in the previous chapter also includes a puromycin drug selection marker. In order to allow simultaneous transduction of cells with dual-drug selection to confirm double-infection of the transduced cell population, a modified version of the HIV-CS-CG-$BRAF^{V600E}$-puromycin plasmid and its corresponding empty vector were obtained from the Peeper laboratory in which the puromycin resistance gene in the open reading frame is replaced by a blasticidin resistance gene. Four separate conditions were established in order to appropriately control the experimental design, and are summarised in Table 5-1 below.

Table 5-1 Experimental design for double transduction experiments

Condition	HIV-CS-CG-Blasticidin	HIV-CS-CG-$BRAF^{V600E}$-blasticidin	pLenti6-puromycin	pLenti6-DNMT3B1-puromycin
"Double vector"	✔		✔	
"DNMT3B1 only"	✔			✔
"BRAF only"		✔	✔	
"BRAF/DNMT3B1"		✔		✔

Human fetal lung fibroblasts (IMR-90) at low passage number (PD<30) were first transduced with either pLenti6-puromycin or pLenti6-DNMT3B1-puromycin. Twenty-four hours after transduction, cells were drug-selected with culture media supplemented with 1μg/mL puromycin. After passaging, a second transduction was performed with either HIV-CS-CG-blasticidin or HIV-CS-CG-$BRAF^{V600E}$-blasticidin. Twenty-four hours after the second transduction, dual-drug selection was performed by exchange of the culture media for culture media supplemented with 1μg/mL puromycin and 5μg/mL blasticidin. Initial observations of the cells in culture suggested that combined BRAF/DNMT3B1 transduction resulted in an altered BRAF phenotype. Cells transformed with both BRAF and DNMT3B1 did not develop the characteristic "spindle-like" morphology induced by activated oncogenic BRAF in the "BRAF-only" cells, and appeared to continue to proliferate (Figure 5-1). In order to fully characterise this apparent phenotypic difference, protein lysates were generated from cell populations at various time-points post transduction (3 days, 5 days, 7 days and 10 days) for analysis by western blot. Separately, cells were labelled with BrdU and propidium iodide at the same time-points for subsequent cell cycle analysis by FACS. "Double vector" and "DNMT3B1 only" cell populations, which were expected to be "proliferating controls" were assayed in the same fashion at a single time point 48 hours post-transduction, termed "time zero".

Efficient expression of both BRAF and DNMT3B1 was confirmed by western blot at all time-points assessed (Figure 5-2). When expressed on its own, activated mutant-$BRAF^{V600E}$ induced a marked decrease in the percentage of cells in S-phase of the cell cycle, consistent with the previously described ability of this oncogene to induce proliferation arrest in primary cells [30,429]. The decline in cells in S-phase was accompanied by decreased abundance of cell cycle drivers: cyclin A, EZH2, and phosphorylated Rb relative to total Rb. Consistent with the observed phenotype discussed above, combined expression of ectopic DNMT3B1 with $BRAF^{V600E}$ increased the proportion of cells in S-phase at all time-points assayed: an effect also observed in the "DNMT3B only" control. In $BRAF^{V600E}$/DNMT3B1 cells, this increase in S-phase cells was accompanied by increased expression of cyclin A, EZH2 and phosphorylated Rb; and at the 7 day time-point, a reduction in expression of the cell-cycle inhibitor, CDKN1B/$p27^{KIP1}$ (Figure 5-2, Figure 5-3, Figure 5-4).

(a) **IMR-90**
+pL6-Puro
+HIV-BRAF-Blast

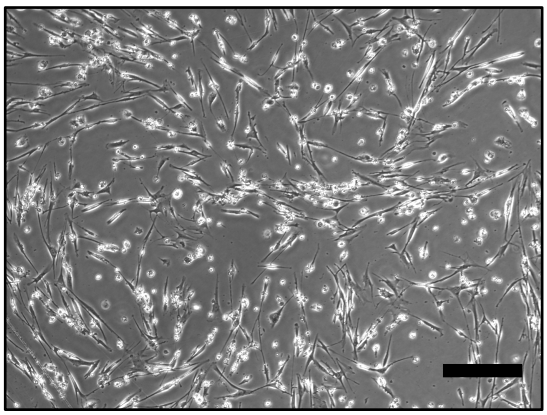

(b) **IMR-90**
+pL6-Dnmt3b1-Puro
+HIV-BRAF-Blast

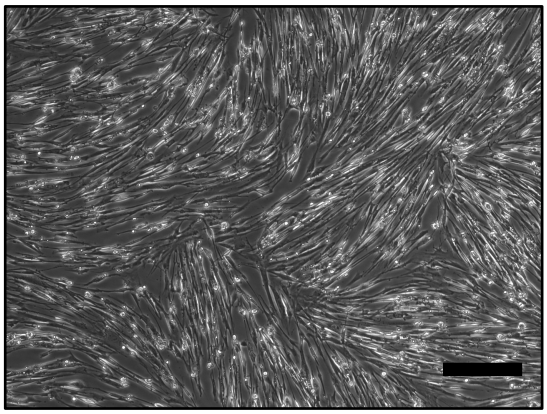

Figure 5-1 Clear morphological differences were noted upon combined ectopic expression of DNMT3B1 and BRAF^{V600E} in human fetal lung fibroblasts compared to BRAF^{V600E} alone

Representative photographs of human fetal lung fibroblasts (IMR-90) seven days following transduction with **(a)** HIV-BRAF^{V600E}-CS-CG-blasticidin + pLenti6-puromycin or **(b)** HIV-BRAF^{V600E}-CS-CG-blasticidin + pLenti6-DNMT3B1-puromycin. Cells transformed with activated oncogenic BRAF^{V600E} and DNMT3B1 **(b)** did not acquire the same spindle-like morphology developed by those expressing BRAF^{V600E} alone **(a)**, and exhibited higher density, consistent with ongoing proliferation. Scale bar = 200μM; n=3 biological replicates.

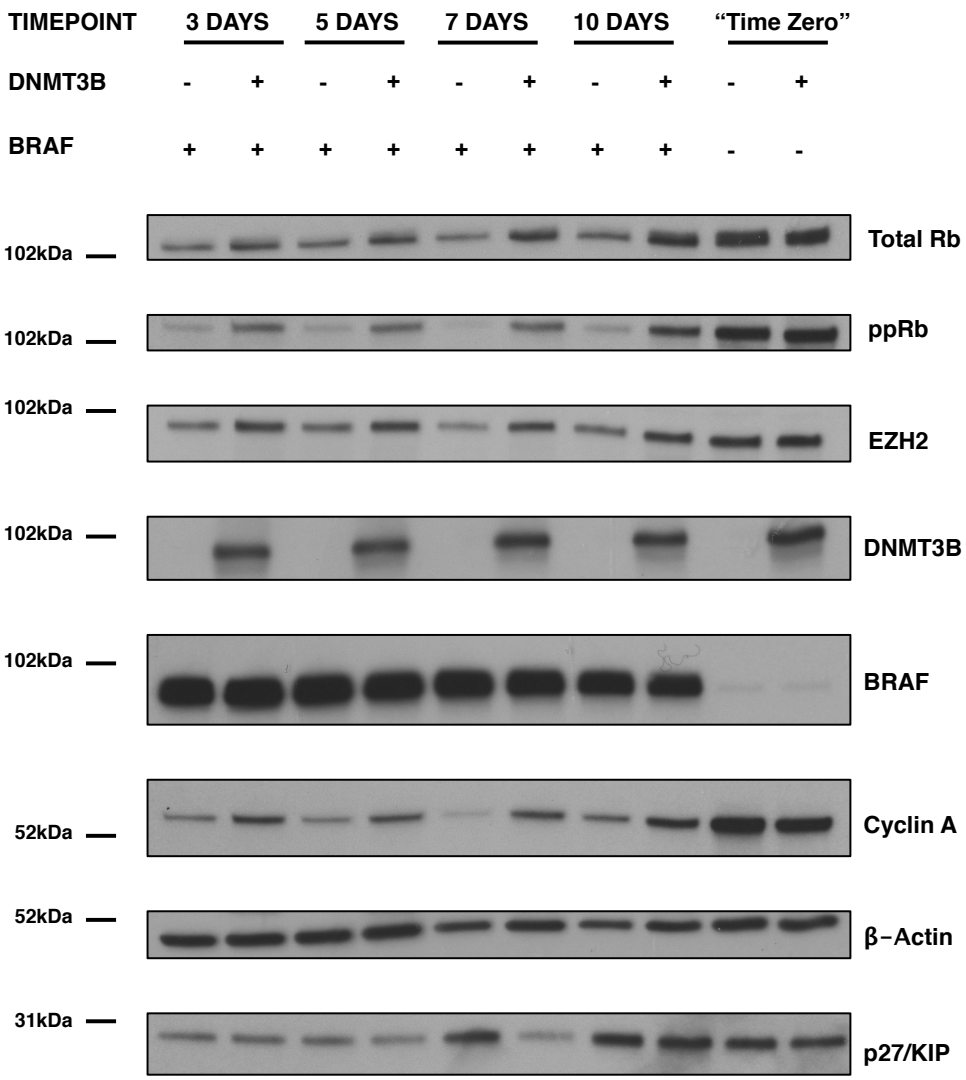

Figure 5-2 Ectopic expression of DNMT3B1 antagonises BRAF^{V600E}-induced proliferation arrest

Western blot of whole cell lysates from human fetal lung fibroblasts (IMR-90) at "time zero", 3, 5, 7 and 10 days following transduction with **(a)** HIV-blasticidin + pLenti6-puromycin **(b)** HIV-blasticidin + pLenti6-DNMT3B1-puromycin **(c)** HIV-BRAF^{V600E}-blasticidin + pLenti6-puromycin or **(d)** HIV-BRAF^{V600E}-blasticidin + pLenti6-DNMT3B1-puromycin. At the seven day time-point, combined DNMT3B1 and BRAF expression resulted in increased expression of the proliferation markers cyclin A, EZH2, and phosphorylated Rb, and repression of the cell-cycle-inhibitor p27^{KIP}/CDKN1B (n=3 biological replicates).

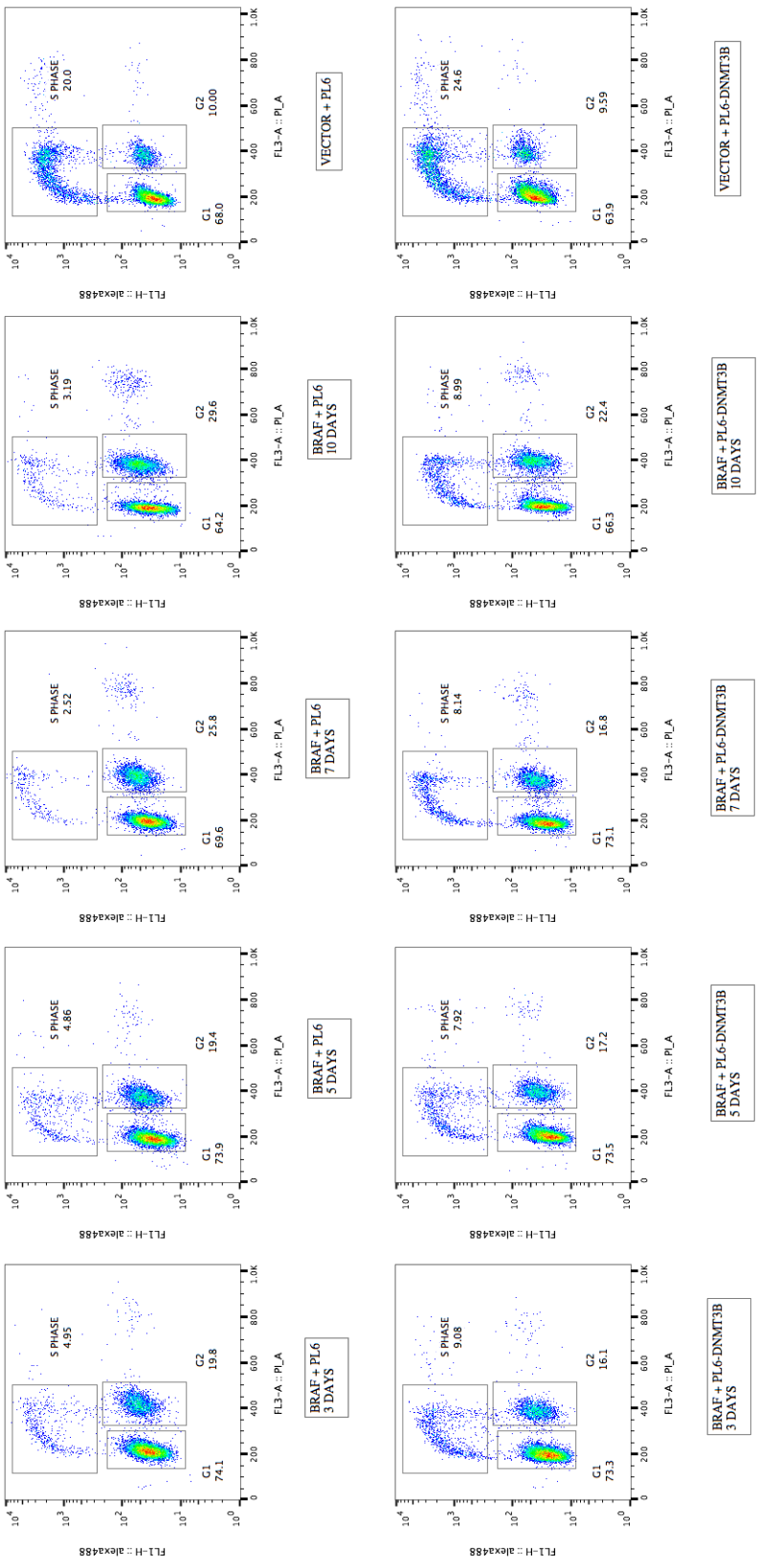

Figure 5-3 Ectopic DNMT3B1 expression impairs BRAF^{V600E}-induced proliferation arrest

BrdU FACS plots of human fetal lung fibroblasts (IMR-90) at “time zero”, 3, 5, 7 and 10 days post-transduction with (1) HIV-blasticidin + pLenti6-puromycin (2) HIV-blasticidin + pLenti6-DNMT3B1-puromycin (3) HIV-BRAF^{V600E}-blasticidin + pLenti6-puromycin or (4) HIV-BRAF^{V600E}-blasticidin + pLenti6-DNMT3B1-puromycin. When expressed on its own, BRAF^{V600E} results in a marked decrease in the percentage of cells in S-phase. Combined DNMT3B1 and BRAF expression resulted in an impaired proliferation arrest phenotype at all time-points examined, with a greater percentage of cells in S-phase (n=1 biological replicate).

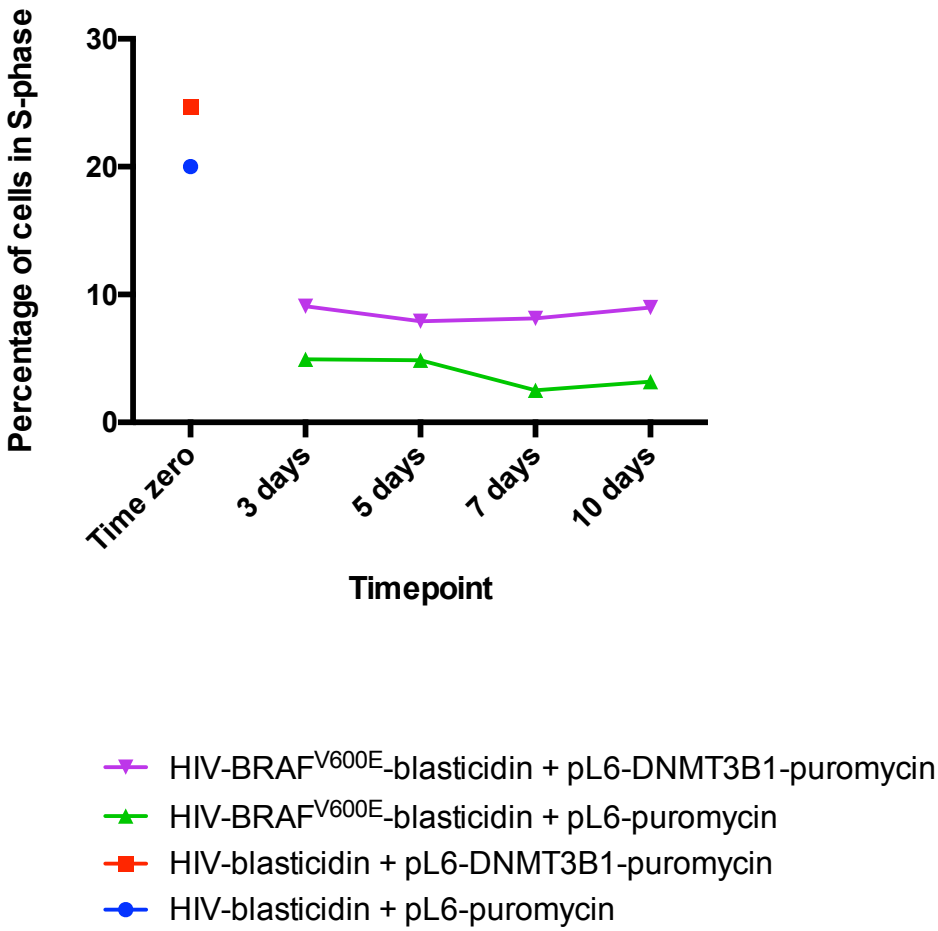

Figure 5-4 Ectopic DNMT3B1 expression impairs BRAF^{V600E}-induced proliferation arrest

Graphical representation of percentage of cells in S-phase at "time zero", 3, 5, 7 and 10 days post-transduction with (1) HIV-blasticidin + pLenti6-puromycin (2) HIV-blasticidin + pLenti6-DNMT3B1-puromycin (3) HIV-BRAF^{V600E}-blasticidin + pLenti6-puromycin or (4) HIV-BRAF^{V600E}-blasticidin + pLenti6-DNMT3B1-puromycin. BrdU FACS analysis was undertaken to assay the percentage of cells in S-phase at "time zero", 3, 5, 7 and 10 days post-transduction for each condition. When expressed on its own, BRAF^{V600E} results in a marked decrease in the percentage of cells in S-phase. Combined DNMT3B1 and BRAF expression resulted in an impaired proliferation arrest phenotype at all time-points examined, with a greater percentage of cells in S-phase (n=1 biological replicate).

As highlighted in the introduction to this thesis, multiple splice isoforms of *DNMT3B* have been characterised, and importantly, some of these have been linked mechanistically to cancer despite lacking an intact catalytic domain [222,435]. DNMT3B3, is one such isoform deplete of an intact C-terminal catalytic domain. Whilst initially characterised as lacking catalytic activity, subsequent studies have suggested that this is an over-simplification, and that DNMT3B3 may have a modest stimulatory effect on DNA methylation, by interaction with other DNA methyltransferases [220,224,225]. In view of the functional evidence linking truncated DNMT3B isoforms and cancer, it was pertinent to explore whether the observed antagonistic effect of DNMT3B1 upon the $BRAF^{V600E}$-induced proliferation arrest program was dependent on its catalytic domain. In view of the reported stimulatory effects of DNMT3B3 on DNA methylation, this experiment does not exclude the possibility of a DNA methylation-mediated mechanism, but does determine whether the catalytic domain is dispensable to the observed DNMT3B phenotype. In chapter 3, a lentivirus construct, pLenti6-DNMT3B3-puromycin, was developed to allow direction of this particular DNMT3B isoform in primary human cells. IMR-90 human fetal lung fibroblasts at low passage number (PD<30) were once again transformed with pLenti6-DNMT3B1-puromycin (DNMT3B1), pLenti6-DNMT3B3-puromycin (DNMT3B3) or the corresponding empty vector (pLenti6-puromycin). Twenty-four hours after transduction, cells were drug-selected with culture media supplemented 1μg/mL puromycin. After passaging, a second transduction was performed with either HIV-CS-CG-blasticidin or HIV-CS-CG-$BRAF^{V600E}$-blasticidin. Twenty-four hours after the second transduction, dual-drug selection was performed by exchange of the culture media for culture media supplemented with 1μg/mL puromycin and 5μg/mL blasticidin.

As the 7 day time-point was assessed to represent the most marked phenotypic dichotomy between "BRAF only" and "BRAF/DNMT3B1" cell populations in the earlier "time-course" experiment, this time-point was selected for analysis. Whole cell lysates were prepared from each condition at 7 days post-transduction, separated by SDS-PAGE, and proliferation genes assessed by Western blot. BrdU FACS analysis was not performed in this experiment. Robust expression of BRAF, DNMT3B1 and DNMT3B3 was confirmed by Western blot. At the 7 day time-point, both "BRAF/DNMT3B1" and "BRAF/DNMT3B3" cells expressed higher levels of the proliferation markers cyclin A, EZH2, and phosphorylated Rb than "BRAF only" controls, suggesting that the antagonistic effect of DNMT3B on $BRAF^{V600E}$-induced proliferation arrest is not dependent on the catalytic domain of the former (Figure 5-5).

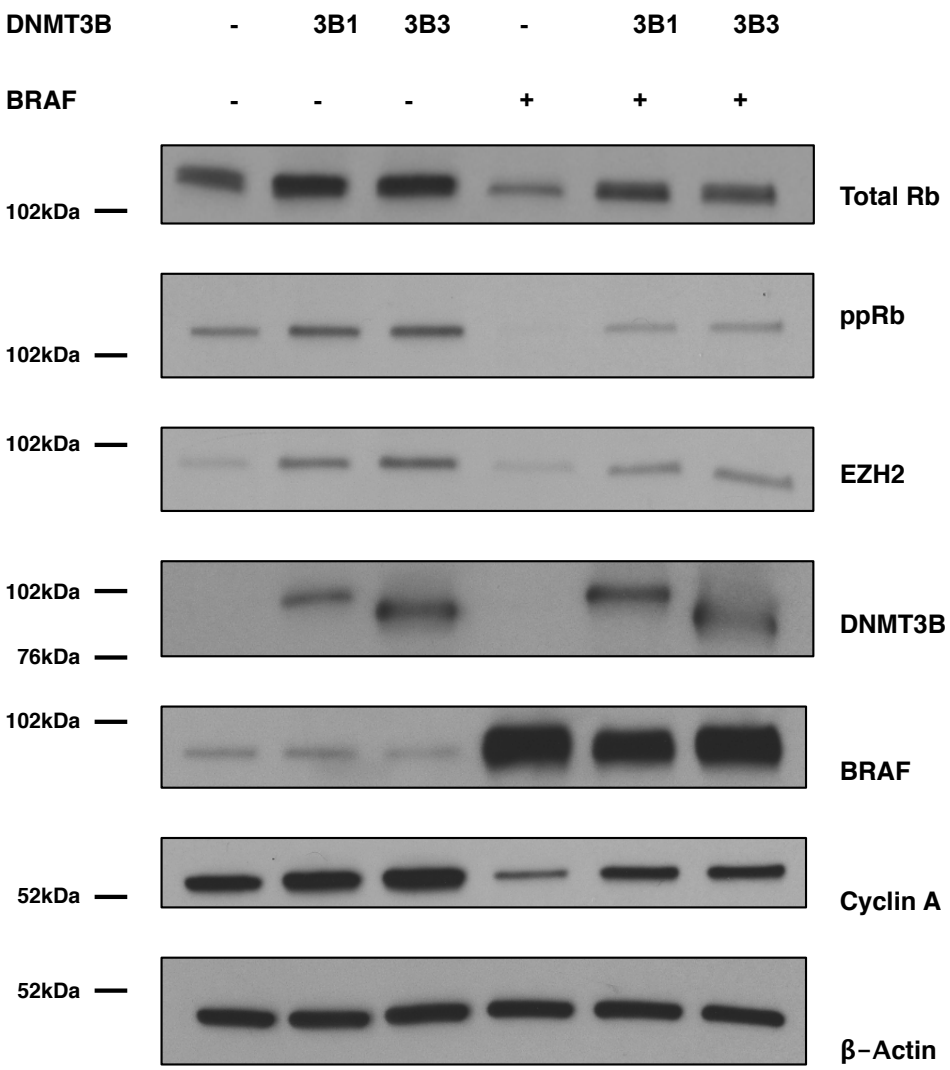

Figure 5-5 The antagonistic effects of DNMT3B on BRAF-induced proliferation arrest may not be related to its catalytic activity

Western blot of whole cell lysates from human fetal lung fibroblasts (IMR-90) seven days following transduction with (1) HIV-blasticidin + pLenti6-puromycin (2) HIV-blasticidin + pLenti6-DNMT3B1-puromycin (3) HIV-blasticidin + pLenti6-DNMT3B3-puromycin (4) HIV-$BRAF^{V600E}$-blasticidin + pLenti6-puromycin (5) HIV-$BRAF^{V600E}$-blasticidin + pLenti6-DNMT3B1-puromycin or (6) HIV-$BRAF^{V600E}$-blasticidin + pLenti6-DNMT3B3-puromycin. Combined DNMT3B1 and BRAF or DNMT3B3 and BRAF expression resulted in increased expression of the proliferation markers cyclin A, EZH2, and phosphorylated Rb, relative to BRAF alone (n=1 biological replicate).

5.3.2 RNA-sequencing

In order to facilitate functional dissection of the mechanisms underlying the antagonistic effects of DNMT3B1 on BRAF-induced proliferation arrest, genome-wide expression analysis was performed on human fetal lung fibroblasts (IMR-90) transduced and drug-selected in an identical fashion to that described in section 5.3.1 above. The decision was made only to examine DNMT3B1 in this experiment. Once again, the 7 day time-point was selected for analysis given the consistent phenotypic dichotomy observed at this time-point in the earlier "time-course". Cells from each of the four previously described conditions ("double vector", "DNMT3B1 only", "BRAF only" and "BRAF/DNMT3B1" (refer Table 5-1) were harvested for RNA 7 days post-transduction in biological triplicate.

Prior to RNA-sequencing, RNA integrity was assessed using the Agilent RNA ScreenTape assay (Figure 5-6). An assessment of RNA quality is summarised using the RNA integrity number (RIN), with an RIN>8 preferred prior to RNA-sequencing [436]. With RNA of sufficient quality for RNA-sequencing confirmed, RNA from each of the three biological replicates for all four conditions was submitted for RNA-sequencing by the Cancer-Research UK sequencing facility at the Beatson Institute for Cancer Research. The RNA-sequencing method has already been discussed in chapter 2.

Processing and analysis of RNA-sequencing data was performed with Mr Neil Robertson, a computational biologist in Professor Peter Adams' lab at the Beatson Institute for Cancer Research, Glasgow. (Alignment data are summarised in chapter 2). Prior to subsequent data analysis, principal component analysis was performed. This confirmed distinct clustering of the biological triplicates for each condition, whilst similarly confirming variation in each of the four conditions assessed (Figure 5-7).

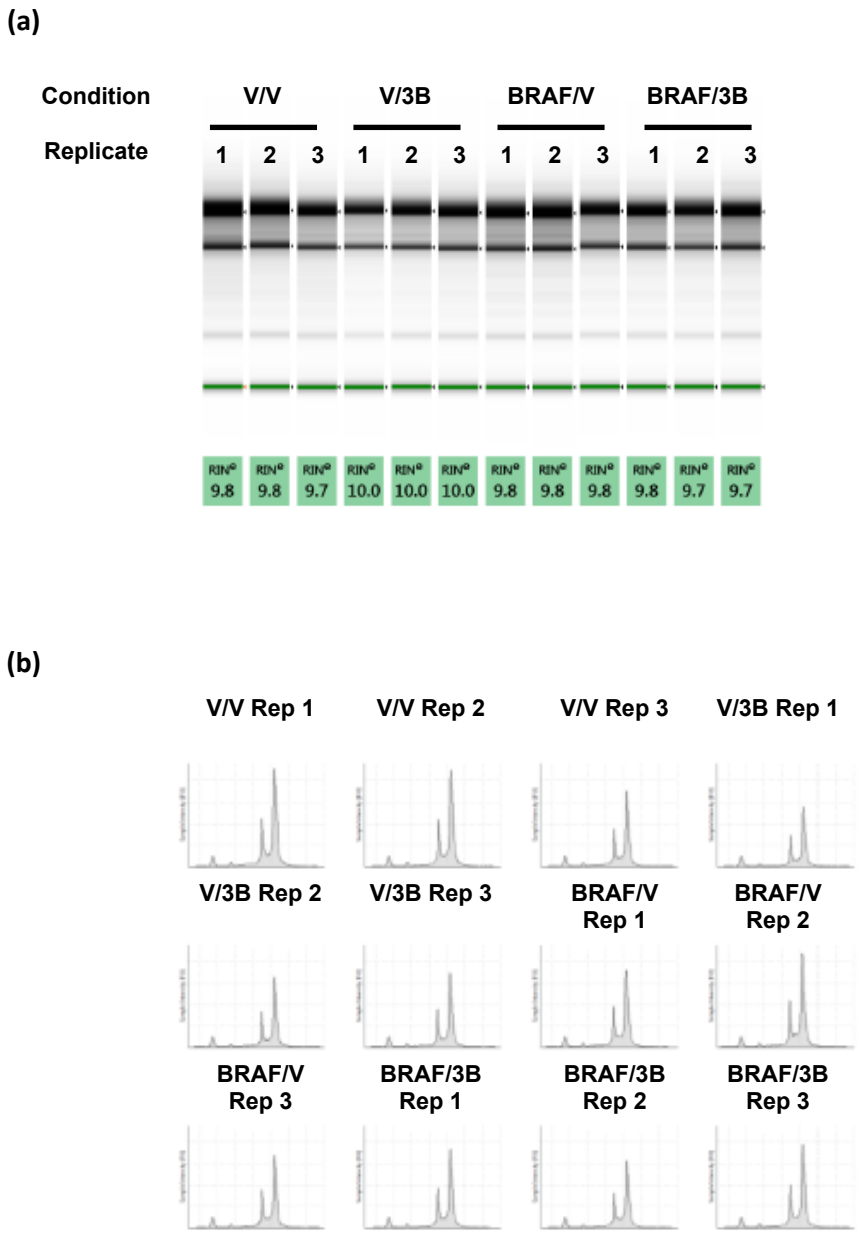

Figure 5-6 Agilent RNA ScreenTape assay for RNA integrity in samples submitted for RNA-sequencing

The Agilent RNA ScreenTape assay was undertaken to assess RNA integrity prior to RNA-sequencing. V/V = “double vector”; V/3B = “DNMT3B1 Only”; BRAF/V = “BRAF only”; BRAF/3B = “BRAF+DNMT3B1. **(a)** An assessment of RNA quality is summarised using the RNA integrity number (RIN), with an RIN>8 preferred prior to RNA-sequencing. All samples had an RIN >8. **(b)** On the histograms, the first peak corresponds to the loading dye. The second peak at 18s corresponds to the small fragment of the ribosome. The third peak at 28s corresponds to the large subunit of the ribosome. Distinct peaks at 18s and 28s are indicative of high quality in tact RNA suitable for sequencing.

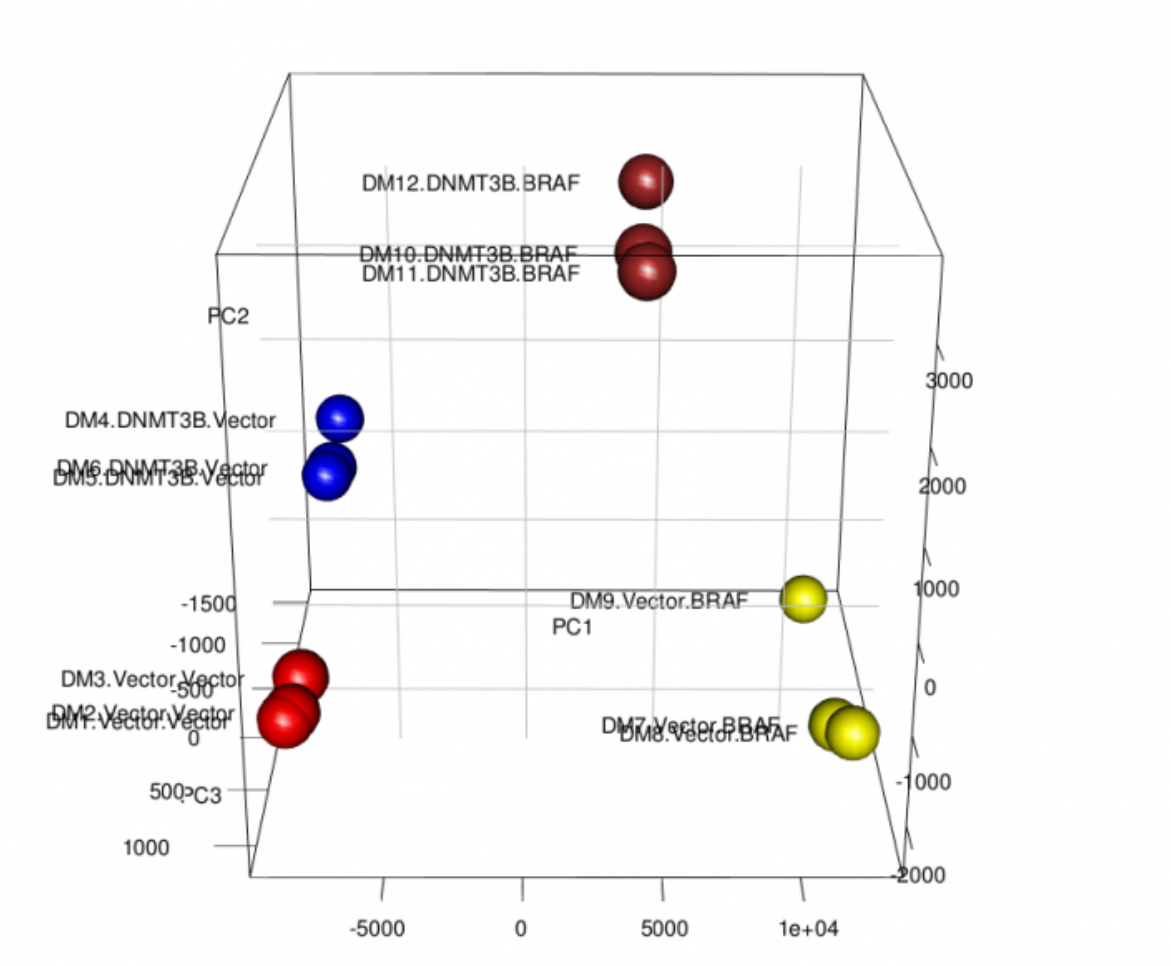

Figure 5-7 Principal component analysis of three independent replicates from each condition examined by RNA-sequencing was performed in order to assess inter-replicate variation

Following initial alignment and processing of RNA-sequencing data, principal component analysis (PCA) was undertaken to compare the variance in the data between each of the four biological conditions examined (“double vector”; “DNMT3B1 only”; “BRAF only”; “BRAF+DNMT3B1”). PCA separates all four biological conditions distinctly, and each of the three replicates from each condition cluster closely, with the first, second and third principal components accounting for 29%, 12.2% and 8.2% of the cumulative variance respectively (n=3 biological replicates).

In furtherance of an explanation for the apparent conflict between the data presented in chapter 4 demonstrating DNMT3B repression upon acute $BRAF^{V600E}$ expression, and the body of evidence in the literature suggesting the contrary, expression of the DNA methyltransferase enzymes and ten-eleven translocation enzymes (TETs) was explicitly examined in the RNA-seq data. Expression of these transcripts was first compared between "double vector" and "BRAF-only" controls, in order to characterise the effects of acute $BRAF^{V600E}$ activation on the "methylation machinery". Perhaps surprisingly, given the relative lack of DNA methylation changes induced by acute $BRAF^{V600E}$ activation in IMR-90 characterised by whole genome bisulfite sequencing in chapter 4, activated oncogenic $BRAF^{V600E}$ results in significant changes in the expression of both DNA methyltransferases and TETs. Compared to proliferating "double vector" controls, "BRAF-only" cells exhibited a significant reduction in DNMT1 and TET1 expression, and a significant upregulation of DNMT3A, TET2 and TET3 expression. Interestingly, DNMT3B mRNA transcript expression was lower in "BRAF only" than "double vector" cells, though this did not reach statistical significance (Figure 5-8). Whilst this lends support to the argument that acute $BRAF^{V600E}$ activation does not upregulate DNMT3B it does not corroborate the protein expression data presented in chapter 4. One possible explanation for this is that the repression of DNMT3B upon $BRAF^{V600E}$ activation demonstrated in chapter 4 might be mediated by a post-translational mechanism.

Given the marked changes in expression of the "methylation machinery" associated with $BRAF^{V600E}$ expression, it was pertinent to address whether ectopic DNMT3B1 expression significantly altered this transcriptome. Expression of each of these transcripts was compared between "BRAF only" and "BRAF-DNMT3B1" populations. Statistical significance was assessed using the CuffDiff method. Ectopic expression of DNMT3B1 did not significantly alter the expression of the other DNA methyltransferases in $BRAF^{V600E}$ expressing cells, however both TET1 and TET3 expression was significantly higher in "DNMT3B1/BRAF" compared to "BRAF-only" cells (Figure 5-9). This latter result is interesting, but perhaps not surprising, given that both TET1 and TET3 are demethylases. Thus, this may simply represent a homeostatic compensatory mechanism in this cell population in an attempt to counter aberrant cytosine methylation induced by DNMT3B ectopic expression.

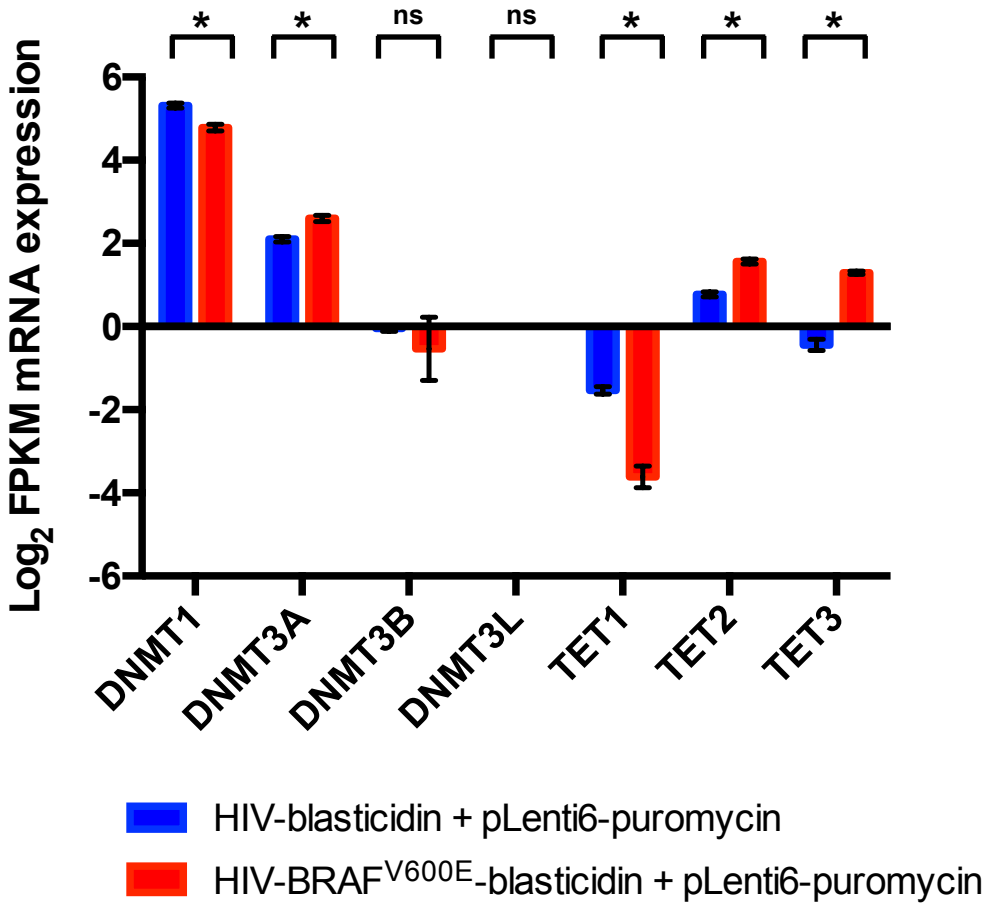

Figure 5-8 Expression changes in DNA methyltransferase and TET mRNA transcripts in BRAF^{V600E}-expressing fibroblasts compared to proliferating controls

Differential expression of the DNA methyltransferase enzymes and ten-eleven translocation enzymes (TETs) was explicitly examined in the RNA-sequencing data to investigate the effects of acute BRAF activation on expression of these transcripts. Bar-chart of Log_2 FPKM mRNA expression of DNMT1, DNMT3A, DNMT3B, DNMT3L and TET1-3 in IMR-90 transformed with either (1) HIV-blasticidin and pLenti6-puromycin or (2) HIV-BRAF^{V600E}-blasticidin and pLenti6-puromycin. Activated oncogenic BRAF^{V600E} results in repression of DNMT1 and TET1 expression, and increased expression of DNMT3A, TET2 and TET3. Whilst a trend to repression of DNMT3B is seen, this did not reach statistical significance. Statistical significance was assessed using the CuffDiff method. DNMT1 q=0.002, DNMT3A q=0.02, DNMT3B q=0.06, TET1 q=0.0001, TET2 q=0.0001, TET3 q=0.0001 (error bars represent SEM; n=3 biological replicates).

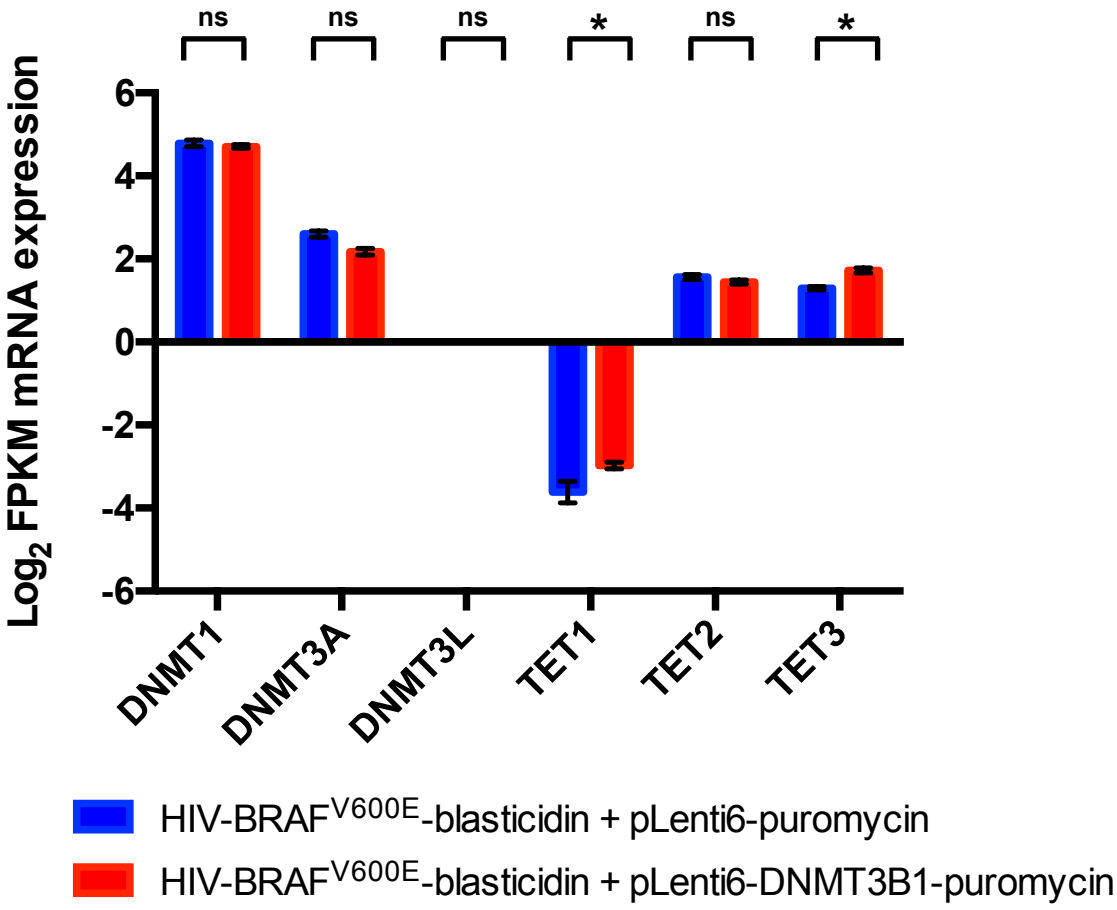

Figure 5-9 Ectopic expression of DNMT3B1 does not significantly alter the expression of the other DNA methylation enzymes, but does alter expression of TET1 and TET3

Differential expression of the DNA methyltransferase enzymes and ten-eleven translocation enzymes (TETs) was explicitly examined in the RNA-sequencing data to investigate the effects of combined BRAF/DNMT3B1 expression on the expression of these transcripts. Bar-chart of Log_2 FPKM mRNA expression of DNMT1, DNMT3A, DNMT3L and TET1-3 in IMR-90 transformed with either (1) HIV-$BRAF^{V600E}$-blasticidin and pLenti6-puromycin or (2) HIV-$BRAF^{V600E}$-blasticidin and pLenti6-DNMT3B1-puromycin. Both TET1 and TET3 expression is significantly increased upon ectopic DNMT3B1 expression. Statistical significance was assessed using the CuffDiff method: DNMT1 q=0.984, DNMT3A q=0.081, TET1 q=0.0003, TET2 q=0.933, TET3 q=0.0003 (error bars represent SEM; n=3 biological replicates).

Consistent with the clear separation of each condition by principal component analysis demonstrated above, further analysis of the RNA-seq data for each of the four conditions tested revealed four distinct transcriptomes, with combined DNMT3B1 and $BRAF^{V600E}$ expression resulting in both positive and negative reversal compared to $BRAF^{V600E}$ alone (Figure 5-10). Significantly changing genes were assessed using the CuffDiff method [413]. Combined DNMT3B1 and $BRAF^{V600E}$ expression resulted in significant upregulation of 4015, and downregulation of 1718 genes compared to "BRAF only" controls. By comparison, "DNMT3B1 only" resulted in the upregulation of 1443 and downregulation of 1245 genes compared to proliferating "double vector" controls (Figure 5-11).

Gene ontology analysis was next performed using gene set enrichment analysis (GSEA) software to identify gene signatures significantly changing between "BRAF only" and "BRAF/DNMT3B1" populations [437,438]. The twenty most positively- and negatively-enriched gene ontologies are summarised in Table 5-2 and Table 5-3 respectively, together with the normalised enrichment scores (NES) and false-discovery rates (FDR). The latter is an estimate of the probability that a particular NES represents a false positive finding. The GSEA software instructions for use suggest that gene sets with an FDR <25% are the most likely to generate hypotheses[18]. Interestingly, the GO-gene sets "cell division", "cell-cycle G2/M phase transition", and "cell cycle transition", all demonstrated positive enrichment in "BRAF/DNMT3B1" compared to "BRAF-only" controls, consistent with the observed phenotype in these cells (Figure 5-12). Perhaps of relevance to the putative role of DNMT3B in intestinal carcinogenesis, the GO-gene set "intestinal cell differentiation" was also enriched in "BRAF/DNMT3B1" compared to "BRAF-only" cells. Gene-ontology analysis of those gene sets most down-regulated in "BRAF/DNMT3B1" cells compared to "BRAF-only" controls, revealed several gene sets of interest: notably "cytokine activity", "chemokine activity" and "chemokine mediated signalling pathway". Given the impaired proliferation-arrest phenotype associated with combined "BRAF/DNMT3B1" compared to "BRAF-only" cells, it was hypothesised that these altered gene sets might be associated with an altered senescence-associated proliferation phenotype, and this hypothesis is explored below.

Given the positive enrichment for cell-cycle GO-gene sets in the GSEA analysis, and the observed proliferation differences characterised earlier between these two cell populations, expression of cell cycle genes and cell cycle inhibitors was compared between "BRAF-

[18] http://software.broadinstitute.org/gsea/doc/GSEAUserGuideFrame.html?_Interpreting_GSEA_Results

only" and "BRAF/DNMT3B1" populations. Consistent with the earlier data from the "time-course" experiment, "BRAF/DNMT3B1" cells expressed higher levels of cyclin A, cyclin D1, cyclin E, PCNA, E2F1 and CDK1. Surprisingly, expression of p21 (CDKN1A) was higher in "BRAF/DNMT3B1" cells than "BRAF-only" cells whereas the expression of other cell cycle inhibitors (CDKN2A, CDKN1B) was not significantly altered (Figure 5-13). Interestingly, and in contrast to CDKN2A, CIMP-high has previously been anticorrelated with p21 repression in colorectal cancer [439].

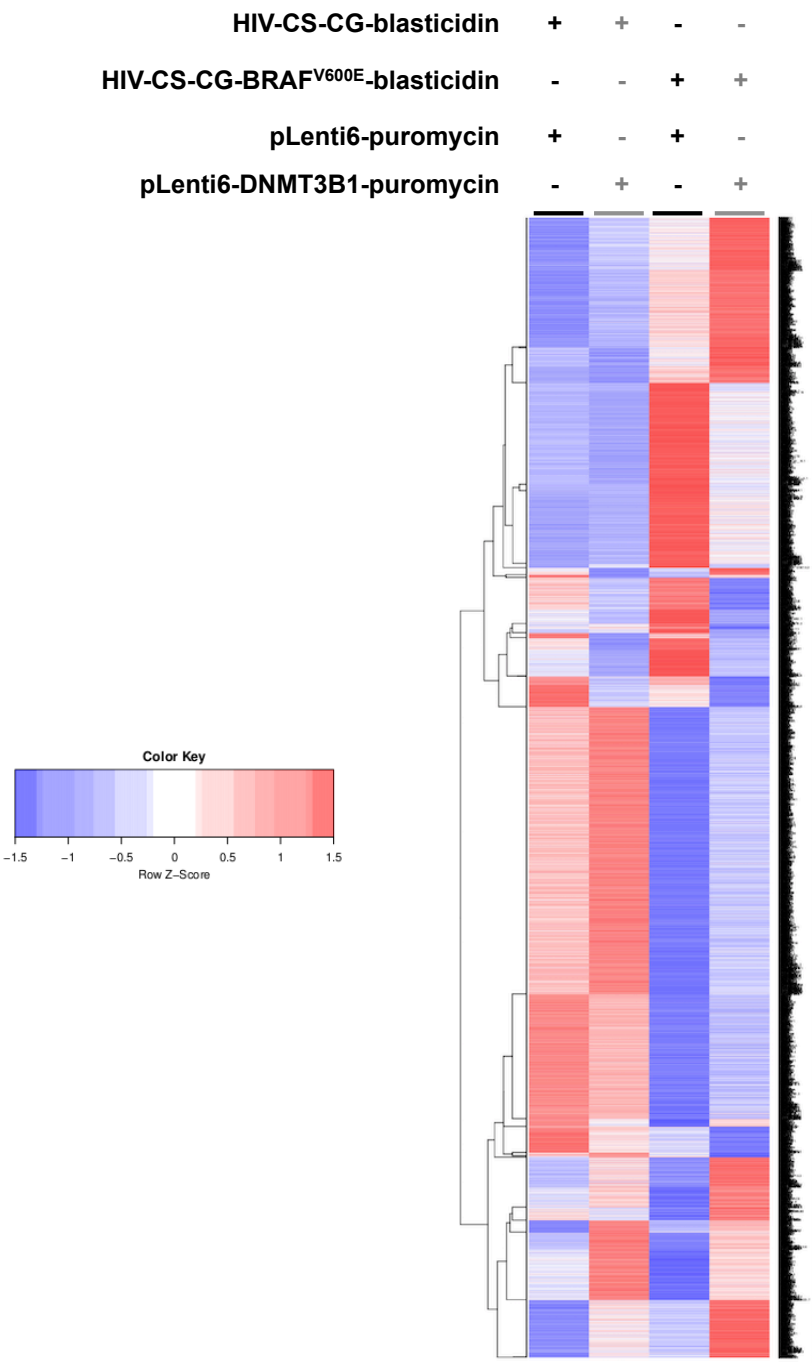

Figure 5-10 Heatmap of gene expression signatures of each condition demonstrates significant transcriptome changes associated with combined BRAF^{V600E} and DNMT3B1 expression

Column-clustered heatmap of significantly changing genes across each of the four biological conditions examined by RNA-sequencing ("double vector"; "DNMT3B1 only"; "BRAF only"; "BRAF+DNMT3B1"). Colour intensity represents row Z-score, where red = high expression, blue = low expression. Four distinct transcriptomes are clearly identifiable: combined DNMT3B1 and BRAF^{V600E} expression results in both positive and negative reversal compared to BRAF^{V600E} alone (n=3 biological replicates).

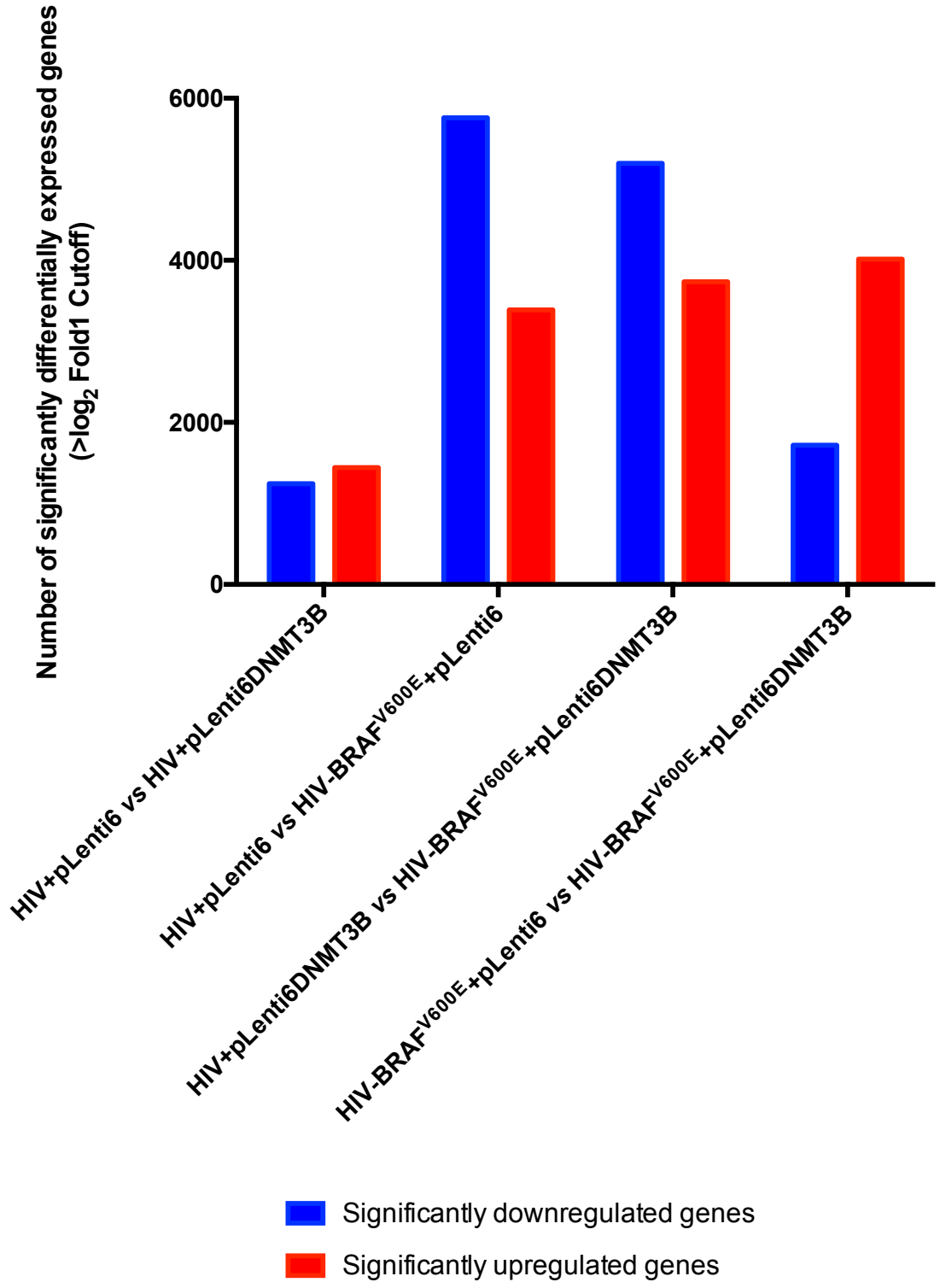

Figure 5-11 Analysis of total number of significantly changing genes comparing different conditions

Bar-chart of number of significantly changing (>$\log_2$ fold1) genes assessed using CuffDiff comparing each of the four biological conditions tested ("double vector"; "DNMT3B1 only"; "BRAF only"; "BRAF+DNMT3B1"). Significantly upregulated genes are in red; significantly downregulated genes are in blue. Combined $BRAF^{V600E}$ and DNMT3B1 ectopic expression resulted in significant upregulation of 4015 and downregulation of 1718 genes compared to $BRAF^{V600E}$ ectopic expression alone (n=3 biological replicates).

Table 5-2 Most upregulated gene sets in "BRAF/DNMT3B1" cells compared to "BRAF-only" controls.

ES = enrichment score, **NES** = normalised enrichment score, **FDR q-value** = false-discovery-rate adjusted p-value.

	GO Gene Set	Number of Genes	ES	NES	FDR q-value
1	Cellular Glucuronidation	22	1.000	1.995	0.000
2	Mitotic Nuclear Division	349	0.645	1.710	0.070
3	Keratin Filament	92	0.691	1.697	0.073
4	Chromosome Condensation	30	0.788	1.689	0.071
5	Acetylcholine Receptor Activity	30	0.796	1.679	0.077
6	Detection Of Chemical Stimulus Involved In Sensory Perception Of Taste	42	0.758	1.676	0.070
7	Nuclear Transcribed mRNA Catabolic Process Nonsense Mediated Decay	118	0.667	1.675	0.062
8	Multi Organism Metabolic Process	137	0.665	1.672	0.058
9	Cell Division	449	0.626	1.665	0.062
10	Cell Cycle G2/M Phase Transition	136	0.653	1.660	0.062
11	Cell Cycle Phase Transition	251	0.628	1.649	0.077
12	Protein Localization to Endoplasmic Reticulum	123	0.653	1.647	0.073
13	Intestinal Epithelial Cell Differentiation	17	0.861	1.642	0.078
14	Kinetochore	113	0.651	1.640	0.075
15	Cytosolic Ribosome	109	0.657	1.637	0.076
16	Midbody	129	0.645	1.626	0.095
17	Sister Chromatid Cohesion	108	0.649	1.624	0.094
18	Establishment of Protein Localization to Endoplasmic Reticulum	104	0.660	1.622	0.092
19	RNA Catabolic Process	222	0.623	1.620	0.093
20	Translational Initiation	143	0.639	1.619	0.090

Table 5-3 Most downregulated gene sets in "BRAF/DNMT3B1" cells compared to "BRAF-only" controls.

ES = enrichment score, **NES** = normalised enrichment score, **FDR q-value** = false-discovery-rate adjusted p-value.

	GO Gene Set	Number of Genes	ES	NES	FDR q-value
1	Olfactory Receptor Activity	379	-0.864	-2.915	0.000
2	Odorant Binding	83	-0.903	-2.698	0.000
3	Positive Regulation of Peptidyl Serine Phosphorylation of STAT Protein	21	-0.962	-2.249	0.000
4	Regulation of Peptidyl Serine Phosphorylation Of STAT Protein	21	-0.962	-2.198	0.000
5	Protein Lipid Complex Remodeling	24	-0.900	-2.157	0.000
6	Macromolecular Complex Remodeling	24	-0.900	-2.147	0.000
7	Plasma Lipoprotein Particle Remodeling	24	-0.900	-2.131	0.001
8	Epoxygenase P450 Pathway	18	-0.920	-2.071	0.002
9	Flavonoid Metabolic Process	28	-0.829	-2.067	0.002
10	Cytokine Activity	216	-0.624	-2.041	0.003
11	Negative Regulation of Catecholamine Secretion	16	-0.924	-2.025	0.004
12	Glutamate Receptor Activity	27	-0.819	-2.014	0.005
13	Negative Regulation of Amine Transport	25	-0.823	-2.009	0.005
14	Regulation of Circadian Sleep Wake Cycle	25	-0.805	-2.006	0.004
15	Neuropeptide Signaling Pathway	93	-0.675	-1.987	0.008
16	Chemokine Activity	48	-0.727	-1.973	0.009
17	Chemokine Mediated Signaling Pathway	68	-0.683	-1.969	0.009
18	Serotonin Receptor Signaling Pathway	18	-0.865	-1.952	0.012
19	Startle Response	25	-0.788	-1.946	0.012
20	High Density Lipoprotein Particle Remodeling	15	-0.896	-1.946	0.012

(a)

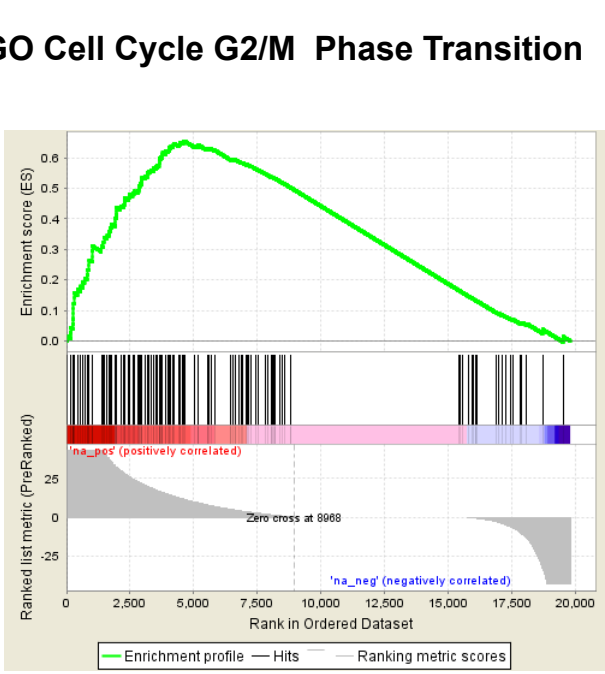

(b)

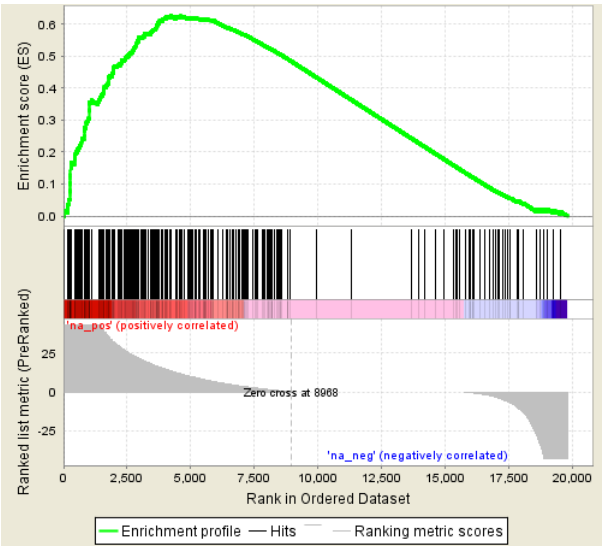

Figure 5-12 Expression changes induced by combined ectopic expression of DNMT3B1 and BRAF^{V600E} demonstrate enrichment for cell cycle genes

GSEA enrichment plots for the GO sets “Cell Cycle G2/M Phase Transition” and “Cell Cycle Phase Transition” created using GSEA. There is significant positive enrichment of cell cycle genes in cells with combined ectopic DNMT3B1/BRAF^{V600E} expression compared to BRAF alone.

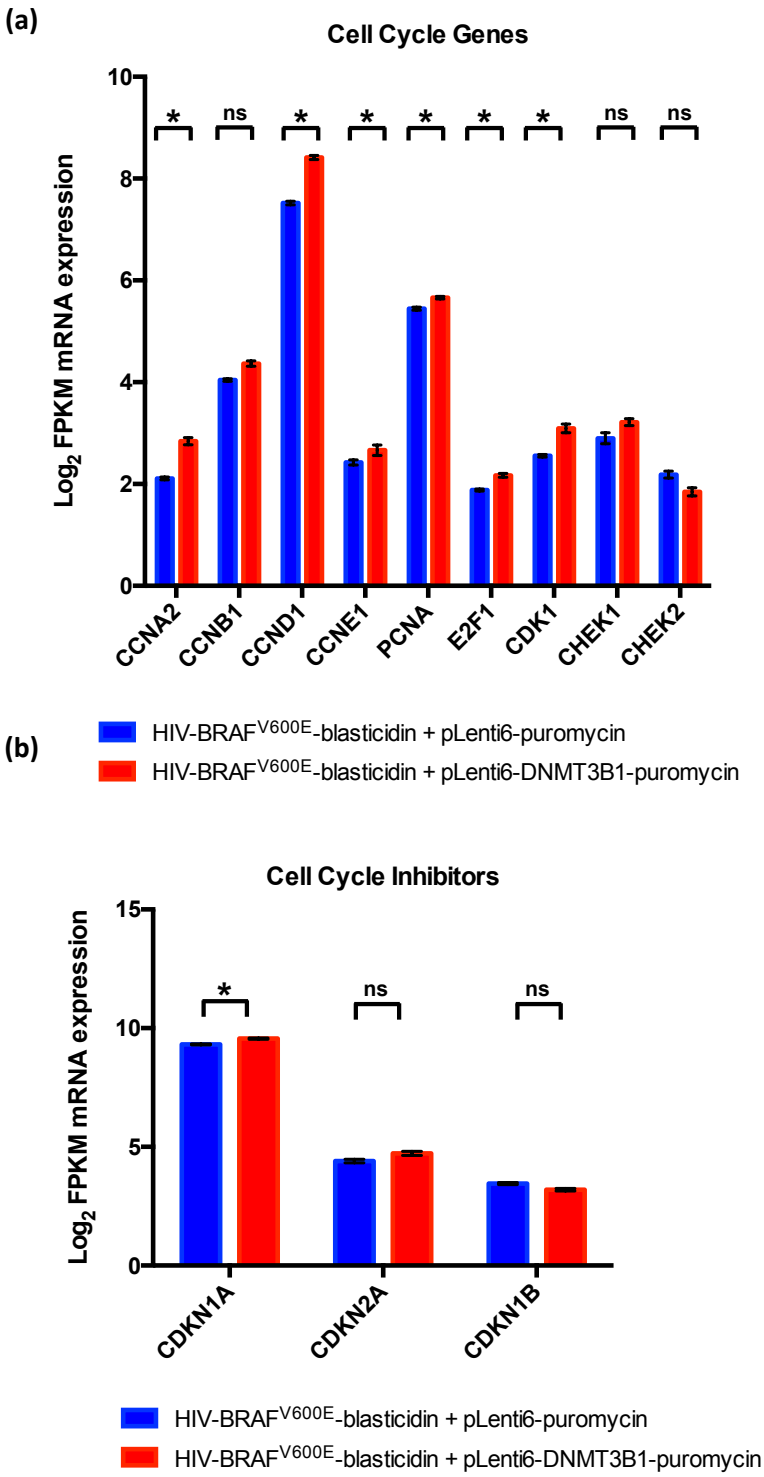

Figure 5-13 Combined ectopic expression of DNMT3B1 and BRAF^{V600E} results in significant changes in cell cycle gene expression but to a lesser extent cell cycle inhibitor gene expression

Cell-cycle transcript analysis was examined in the RNA-seq data comparing "BRAF only" and "BRAF/DNMT3B1". Bar-chart of Log_2 FPKM mRNA expression of **(a)** cell cycle genes and **(b)** cell cycle inhibitor genes in human fetal lung fibroblasts (IMR-90) transformed with either HIV-BRAF^{V600E}-blasticidin and pLenti6-puromycin or HIV-BRAF^{V600E}-blasticidin and pLenti6-DNMT3B1-puromycin. Statistical significance was assessed using CuffDiff, and statistically-significant changes are marked with an asterisk (*). Error bars represent SEM; n=3 biological replicates.

BRAF-mediated oncogene-induced senescence is associated with a senescence-associated secretory phenotype (SASP). Furthermore, the SASP has been demonstrated to reinforce proliferation arrest in a paracrine manner [440]. Given the importance of the SASP to the regulation of proliferation arrest associated with oncogene-induced senescence, it was pertinent to examine how DNMT3B1 ectopic expression might affect expression of SASP transcripts in $BRAF^{V600E}$-expressing cells. Differential expression of SASP transcripts between "BRAF only" and "BRAF/DNMT3B1" populations was explicitly examined using a previously published SASP panel [441]. Consistent with the impaired proliferation-arrest phenotype associated with combined DNMT3B1 and $BRAF^{V600E}$ expression compared to $BRAF^{V600E}$ alone, marked alterations in the SASP-secretome were observed between these two cell populations, suggestive of an impaired SASP associated with combined "BRAF/DNMT3B1" expression. "BRAF/DNMT3B1" cells exhibited lower expression of several key SASP components, including IL1α, IL1β, IL6, IL8, CSF3, MMP3 and MMP9, although whilst the general trend is for an impaired SASP secretome associated with combined "BRAF/DNMT3B1" expression, not all genes follow this trend (Figure 5-14).

As outlined in the introduction to this thesis, Wnt pathway activation has been implicated in the progression of serrated pathway tumourigenesis [19,46,47]. Furthermore, Wnt signalling is also of central importance to the regulation of the oncogene-induced senescence program. Activated canonical Wnt signalling has been demonstrated to impair oncogene-induced senescence in several model systems [429,442]. Furthermore, ectopic DNMT3B1 expression in a murine intestinal tumour model has previously been demonstrated to result in promoter CpG methylation and transcription repression of the Wnt antagonists *Sfrp2*, *Sfrp4* and *Sfrp5* [205,434]. For these reasons, it was appropriate to examine whether combined BRAF/DNMT3B1 expression was associated with alterations in Wnt signalling. Interestingly, "BRAF/DNMT3B1" cells expressed significantly lower levels of the Wnt antagonists AXIN2 and SFRP2. Conversely, "BRAF/DNMT3B1" cells expressed higher levels of DKK1 and SFRP1. Furthermore, "BRAF/DNMT3B1" cells expressed higher levels of several Wnt target genes, including CCND1, CLDN1, SOX9, and MYC, suggesting that the net effect of DNMT3B1 was to accentuate Wnt signalling when combined with $BRAF^{V600E}$ (Figure 5-15).

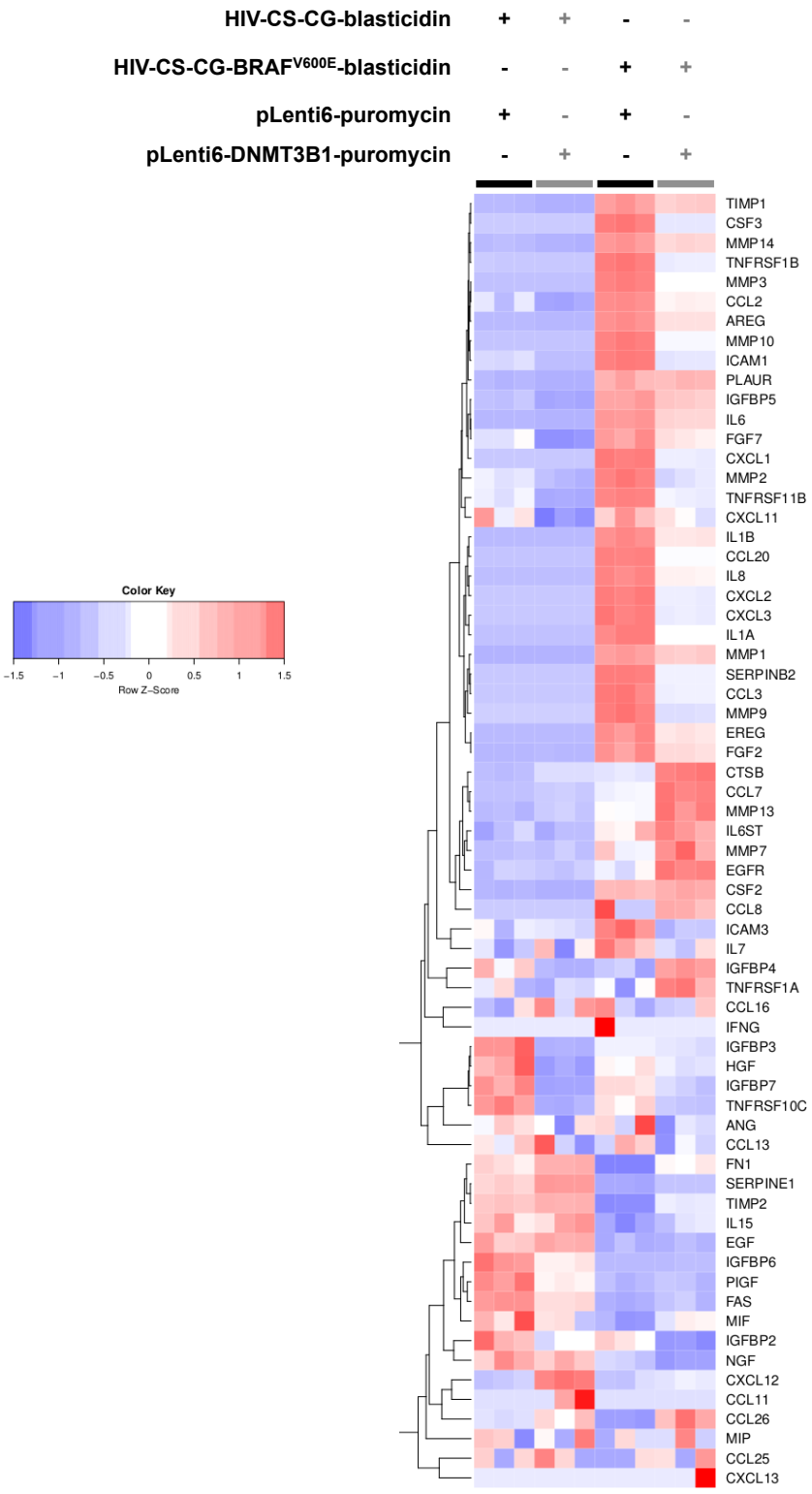

Figure 5-14 Ectopic DNMT3B1 expression may impair the senescence-associated secretory phenotype associated with activated oncogenic BRAF^{V600E}

Column-clustered heatmap of SASP gene[19] expression across all four conditions examined. Colour intensity represents row Z-score, where red = high expression, blue = low expression. Ectopic DNMT3B1 expression alters the SASP profile associated with BRAF^{V600E} expression, with reduced expression of several SASP markers, including IL1α, IL1β, IL6, IL8, CSF3, MMP3 and MMP9, although whilst the general pattern is for an impaired SASP secretome associated with combined "BRAF/DNMT3B1" expression, not all genes follow this trend.

[19] The SASP panel for this analysis was sourced from Correia-Melo et al. [441]. For a full list of SASP genes, the reader is directed to Judith Campisi's comprehensive review [443].

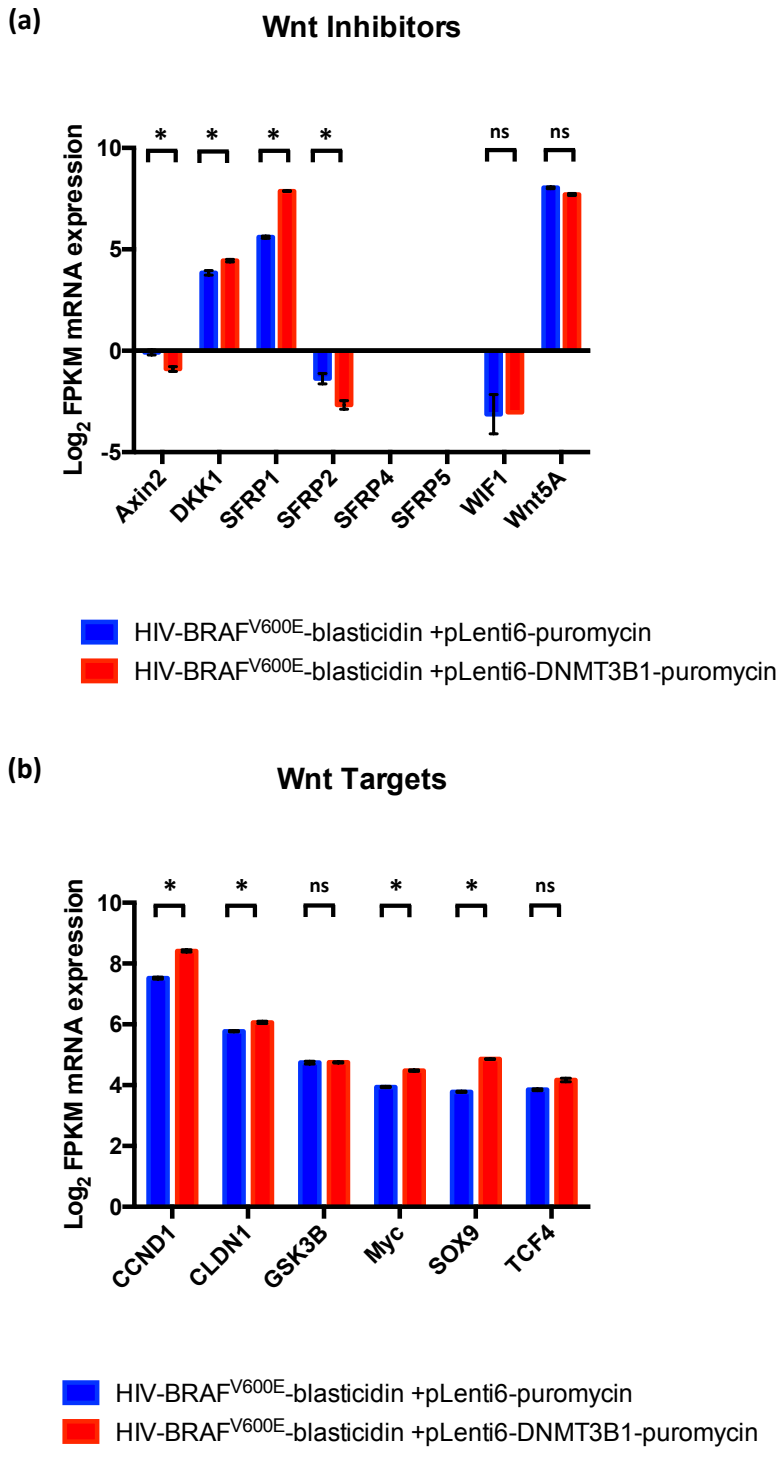

Figure 5-15 Combined ectopic expression of DNMT3B1 and BRAF^{V600E} results in altered expression of Wnt regulators and Wnt target genes

Wnt inhibitor and Wnt target gene expression was explicitly examined in the RNA-seq data comparing "BRAF only" and "BRAF/DNMT3B1". Bar-chart of Log_2 FPKM mRNA expression of **(a)** Wnt inhibitors and **(b)** Wnt target genes in human fetal lung fibroblasts (IMR-90) transformed with either HIV-BRAF^{V600E}-blasticidin and pLenti6-puromycin or HIV-BRAF^{V600E}-blasticidin and pLenti6-DNMT3B1-puromycin. Statistical significance was assessed using CuffDiff, and statistically-significant changes are marked with an asterisk (*). Axin2 q=0.011; DKK1 q=0.0003; SFRP1 q=0.0003; SFRP2 q=0.0067; WIF1 q=1 Wnt5A q=0.247 CCND1 q=0.0003; CLDN1 q=0.0003; GSK3B q=0.518; Myc q=0.0003; Sox9 q=0.0003; TCF4 q=0.08. Error bars represent SEM; n=3 biological replicates.

Finally, given the correlative and mechanistic data linking $BRAF^{V600E}$, DNMT3B and CIMP discussed earlier, it was relevant to examine whether a CIMP-like phenotype was observed upon acute $BRAF^{V600E}$ activation or combined "$BRAF^{V600E}$/DNMT3B1" expression. Matched DNA methylation data were not generated in this experiment, however, as CIMP is associated with transcription repression, RNA-sequencing expression data were examined for changes in expression of CIMP target genes. In addition, the expression of MAFG, which has been proposed as a key driver of $BRAF^{V600E}$-induced CIMP was examined [364]. For this analysis, CIMP target genes were defined using the Weisenberger panel, in addition to *MLH1* and *CDKN2A* [116].

Consistent with the observed lack of a CIMP-phenotype upon acute $BRAF^{V600E}$ activation characterised by whole genome bisulfite sequencing in chapter 4, $BRAF^{V600E}$ expression alone did not induce a "CIMP gene expression signature". Indeed, conversely, expression of CACNA1G, IGF2, RUNX3 and CDKN2A were all increased upon $BRAF^{V600E}$ expression. Significantly however, MAFG expression was elevated upon acute $BRAF^{V600E}$ expression, and this was associated with a small but significant decrease in expression of MLH1 and SOCS1 (Figure 5-16a) In the model proposed by Fang et al. [364], MAFG mRNA expression did not change significantly upon acute $BRAF^{V600E}$ expression, and it was proposed that the observed increase in MAFG expression upon acute $BRAF^{V600E}$ resulted from post-translational modification of the protein. Nevertheless, these data would support an association between $BRAF^{V600E}$ activation and increased expression of MAFG. By contrast however, MLH1 and SOCS1 are the only "CIMP target genes" examined here that show transcription repression associated with acute $BRAF^{V600E}$ expression. By comparison, combined "BRAF/DNMT3B1" expression did not significantly alter the expression of MAFG or MLH1. Furthermore, with the exception of RUNX3, no CIMP target genes demonstrated significant transcription repression in "BRAF/DNMT3B1" compared to "BRAF-only" cells. Indeed, expression of SOCS1 and IGF2 was higher in "BRAF/DNMT3B1" than "BRAF only" cells (Figure 5-16b). Thus neither $BRAF^{V600E}$ alone nor combined "BRAF/DNMT3B1" induces a "CIMP gene expression signature", and the pro-proliferative phenotype characterised in "BRAF/DNMT3B1" compared to "BRAF only" cells does not appear to be associated with the acquisition of a CIMP expression phenotype.

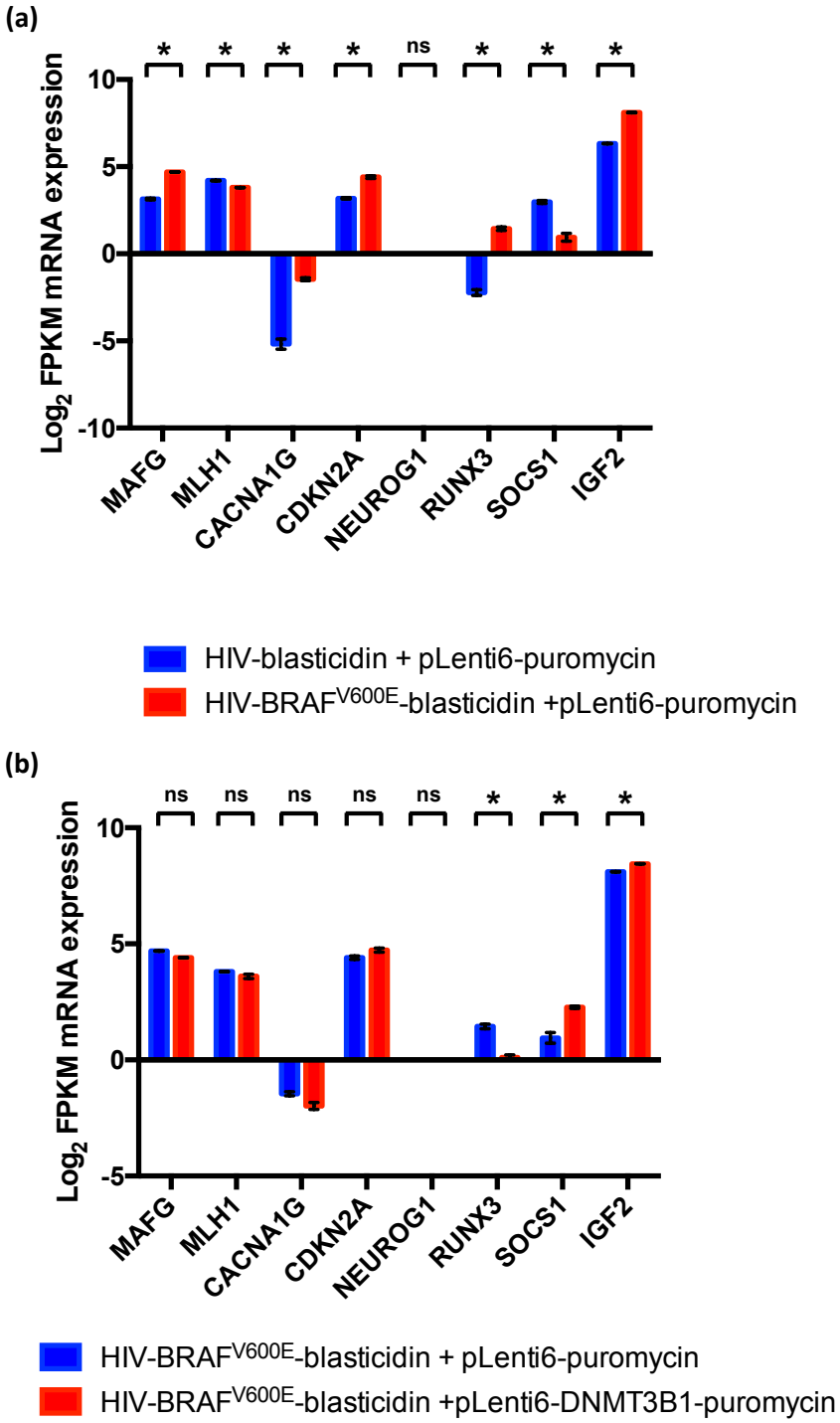

Figure 5-16 Neither "BRAF^{V600E} alone" nor combined "BRAF^{V600E}/DNMT3B1" ectopic expression induces a "CIMP expression signature"

The expression of CIMP target genes was explicitly examined in the RNA-seq data comparing "BRAF only" and "BRAF/DNMT3B1". **(a)** Acute BRAF^{V600E} expression increases mRNA expression of MAFG, and represses MLH1 and SOCS1 expression, but this is not associated with silencing of other CIMP target genes. Indeed, conversely, expression of CACNA1G, CDKN2A, NEUROG1, RUNX3 and IGF2 increase significantly upon acute BRAF^{V600E} activation. Statistical significance was assessed by CuffDiff. MAFG q=0.0001; MLH1 q=0.008; CACNA1G q=0.0001; CDKN2A q=0.01; RUNX3 q=0.0001; SOCS1 q=0.0001 ; IGF2 q=0.0001 **(b)** Combined "BRAF/DNMT3B1" expression does not alter expression of MAFG, or the CIMP target genes MLH1, CACNA1G, CDKN2A, though is associated with repression of RUNX3. Intriguingly however, combined "BRAF/DNMT3B1" expression increases the expression of SOCS1 and IGF2, which are also CIMP targets. Statistical significance was assessed using CuffDiff. MAFG q=0.3; MLH1 q=0.921; CACNA1G q=0.272; CDKN2A q=0.366; RUNX3 q=0.0003 ; SOCS1 q=0.0003; IGF2 q=0.0003. Error bars represent SEM; n=3 biological replicates.

5.3.3 DNMT3B expression in colon cancer cell lines is unrelated to CIMP or *BRAF/KRAS* mutational status

Having demonstrated functional cooperation between activated oncogenic $BRAF^{V600E}$ and DNMT3B in a primary cell model, relationships between $BRAF^{V600E}$, DNMT3B and CIMP were next investigated in a colon-cancer specific context. A panel of colon cancer cell lines were obtained to assess DNMT3B protein expression. In addition to $BRAF^{V600E}$ mutant colon cancer cell lines, a panel of *BRAF* wild-type colon cancer cell lines were tested in order to compare relative DNMT3B expression. The CIMP and $BRAF^{V600E}$ mutational status of these cell lines has previously been described [444]. The colon cancer cell lines employed in this study, together with their CIMP status and *BRAF/KRAS* mutational status are summarised in Table 5-4.

Table 5-4 CIMP, *BRAF*- and *KRAS*-mutational status of colon cancer cell lines employed in this study

Cell Line	*BRAF*	*KRAS*	CIMP
3BKO	WT	G13D	NA
HCT116	WT	G13D	+
DLD-1	WT	G13D	+
SW480	WT	G12V	-
RKO	V600E	WT	+
HT-29	V600E	WT	+
SW1417	V600E	WT	+
LS411N	V600E	WT	+

Following cell line verification (performed by Mr William Clark, sequencing facility, Beatson Institute for Cancer Research, Glasgow) protein lysates were prepared from each cell line, separated by SDS-PAGE, immobilised to PVDF and Western blotting performed for DNMT3B with the validated DNMT3B antibody, SC10236 (Figure 5-17). DNMT3B expression was highest in HCT116 and SW480, which are both *BRAF* wild-type. Lower DNMT3B expression was detectable in DLD-1, RKO, HT-29, SW1417 and LS411N. Although Western blotting is only a semi-quantitative assay, there was no clear relationship between DNMT3B protein expression and CIMP status or *BRAF* mutation status. Of the $BRAF^{V600E}$-mutant lines tested, the highest relative DNMT3B expression was in LS411N.

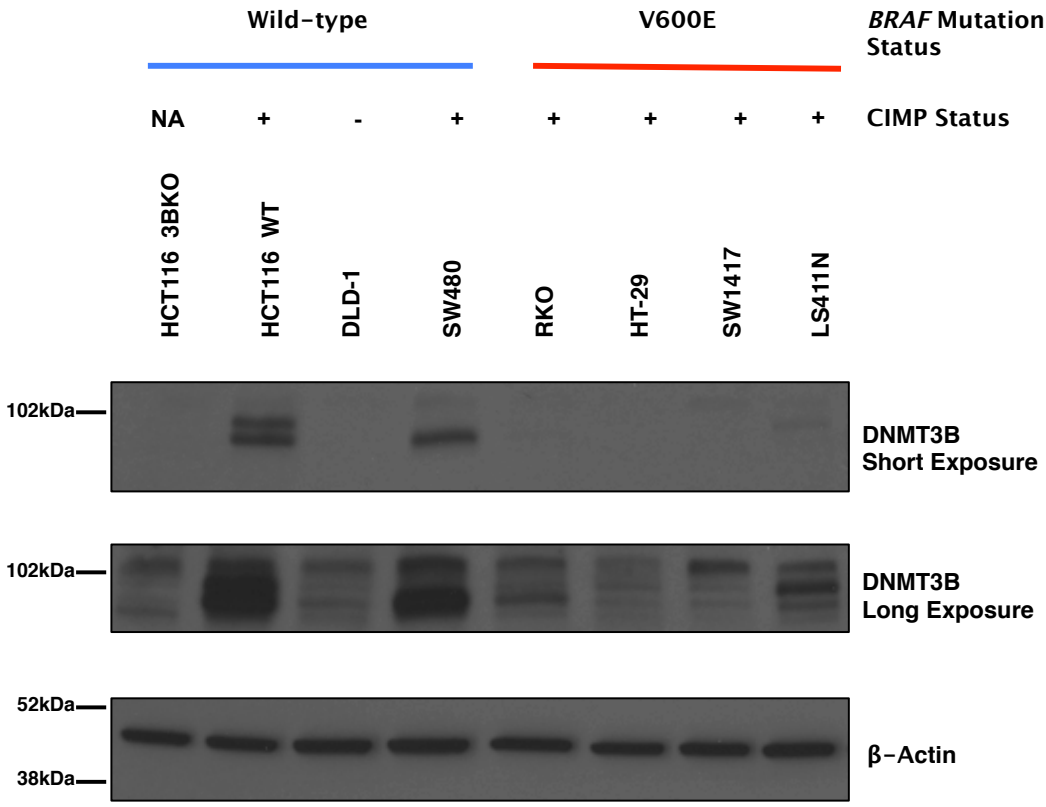

Figure 5-17 DNMT3B expression in colon cancer cell lines is unrelated to *BRAF*^{V600E} mutation or CIMP status

Western blot for DNMT3B (using SC10236 antibody) in whole cell lysates from a panel of colon cancer cell lines annotated by CIMP and *BRAF*^{V600E} mutation status. No clear relationship is observed between relative DNMT3B protein expression and CIMP or *BRAF*^{V600E} mutation status (n=1 biological replicate).

5.3.4 Investigating the functional consequences of DNMT3B knockdown in a *BRAF*-mutant colon cancer cell line

An anti-proliferative and pro-apoptotic phenotype induced by antisense-mediated DNMT3B knockdown has previously been characterised in the *KRAS*-mutant cell line HCT116 [334]. In order to investigate the functional consequences of DNMT3B knockdown in a $BRAF^{V600E}$-mutant context, the colon cancer cell line LS411N was selected given its relatively high levels of DNMT3B protein expression compared to other $BRAF^{V600E}$-mutant lines examined. In chapter 3, both shRNA and CRISPR knockdown systems for DNMT3B were characterised. As only one of the shRNAs tested in this thesis reliably knocked down DNMT3B when tested in HCT116, it was decided to adopt a CRISPR knockdown strategy for these experiments.

LS411N cells were transduced with lentiCRISPRv2-puromycin vector ("vector") lentiCRISPRv2-DNMT3B-sgRNA1-puromycin ("sgRNA1") or lentiCRISPRv2-DNMT3B-sgRNA4-puromycin ("sgRNA4") constructs described in chapter 3. Following drug selection for 7 days with culture media supplemented with 1μg/mL puromycin, cells were harvested for protein lysates. Protein lysates were separated by SDS-PAGE, immobilised to PVDF and Western blotting performed for proliferation markers (cyclin A, ppRB) and the apoptosis marker cleaved PARP. Separately, cells were labelled with BrdU and propidium iodide for cell cycle analysis by FACS.

In contrast to the converse ectopic expression experiments in primary cells, CRISPR-mediated DNMT3B knockdown in LS411N did not significantly affect the proliferation phenotype of these cells. There was no appreciable difference in the expression of the proliferation markers cyclin A or ppRB with either DNMT3B sgRNA construct compared to "vector" controls (Figure 5-18). Similarly, cell cycle analysis by FACS revealed no significant difference in the proportion of cells in S-phase between "vector" and DNMT3B knockdown LS411N (Figure 5-19).

Interestingly, despite the lack of a demonstrable anti-proliferative effect of DNMT3B knockdown, DNMT3B knockdown cells demonstrated upregulation of the apoptosis marker cleaved PARP relative to "vector" controls. (Figure 5-18).

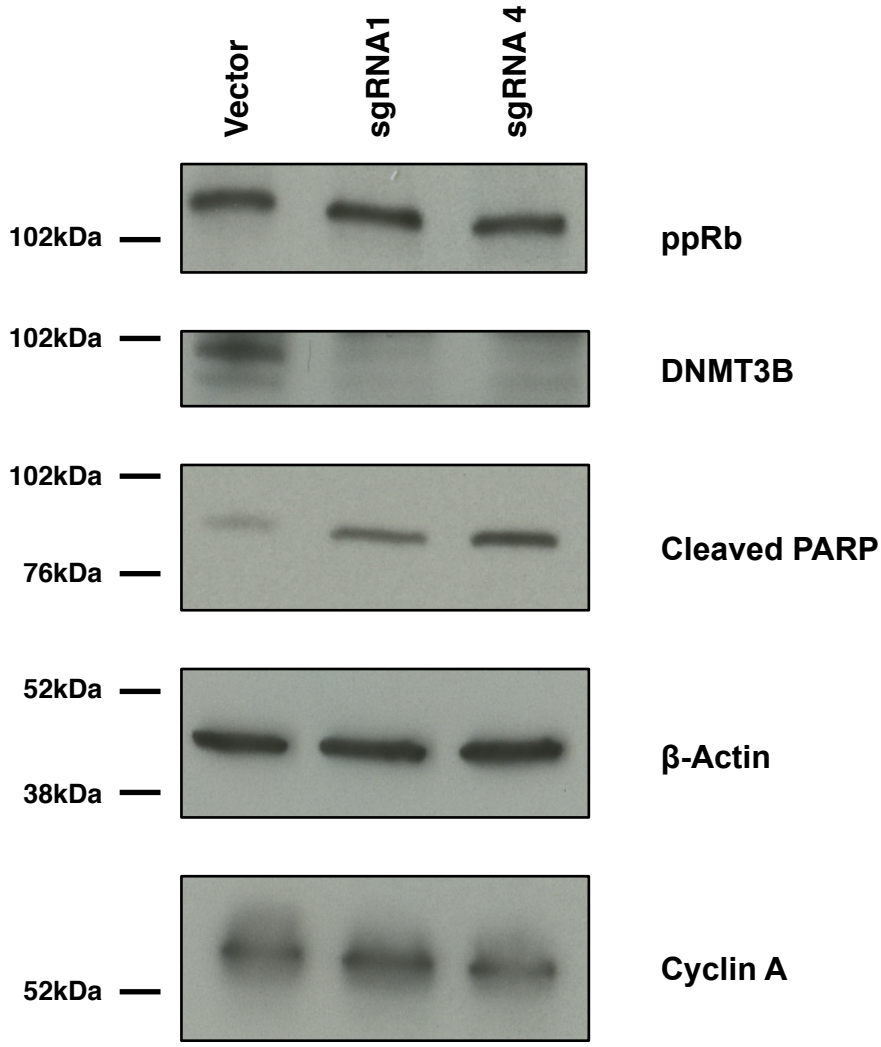

Figure 5-18 DNMT3B CRISPR knockdown in LS411N does not alter proliferation gene protein levels, but may promote apoptosis

Western blot of whole cell lysates from LS411N cells one week following transduction with LentiCRISPRv2-puromycin ("vector") or LentiCRISPRv2-DNMT3B-sgRNA1/4-puromycin ("sgRNA1/4"). Whilst no change is observed in the proliferation markers, cyclin A or ppRb; the apoptosis marker, cleaved PARP demonstrates elevated expression at the protein level (n=2 biological replicates).

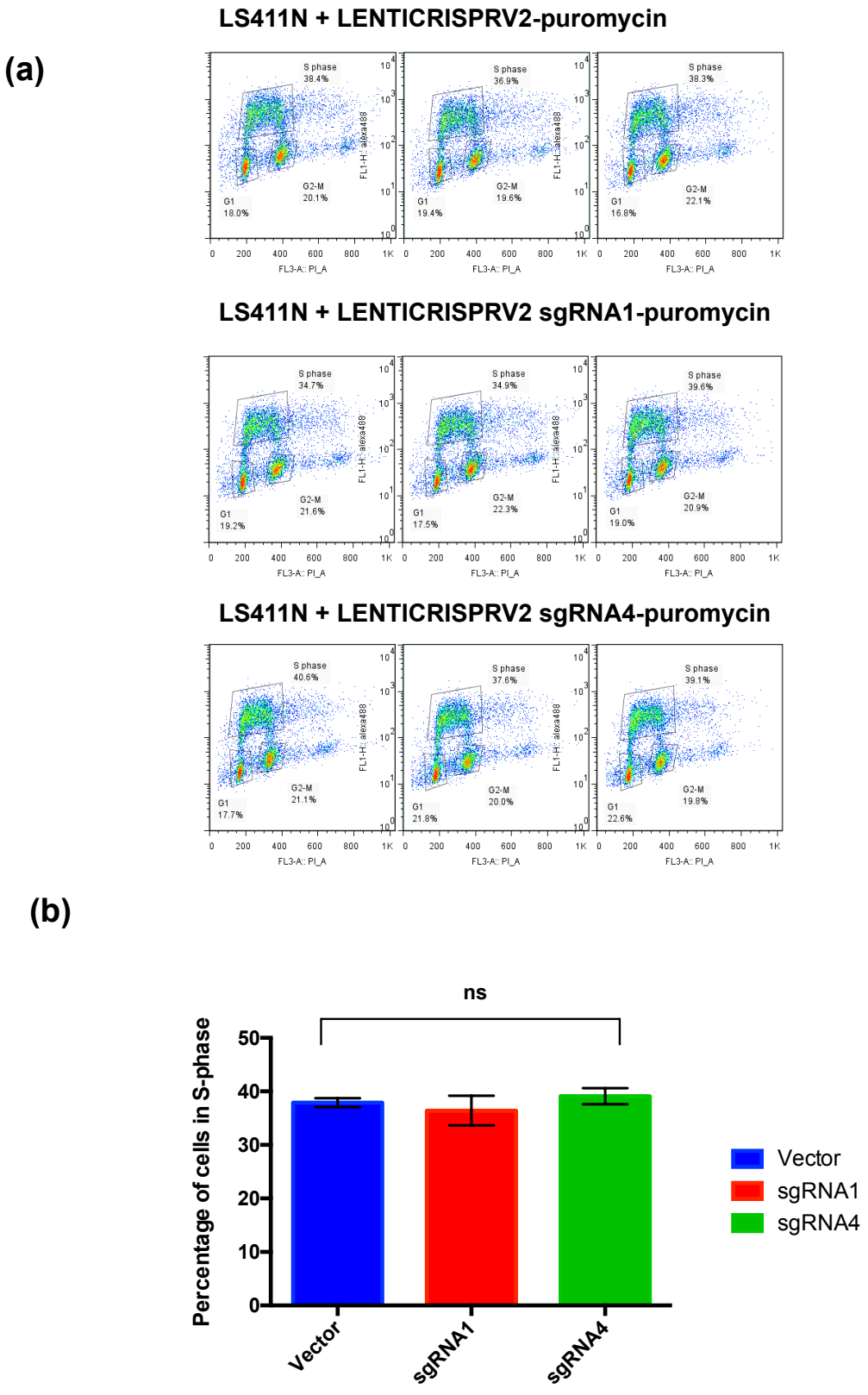

Figure 5-19 DNMT3B knockdown in LS411N does not affect proliferation

(a) BrdU FACS plots from LS411N one week following transduction with LentiCRISPRv2-puromycin (vector) or LentiCRISPRv2-DNMT3B-sgRNA1/4-puromycin. **(b)** Graphical representation of percentage of cells in S-phase with and without DNMT3B knockdown as assayed by BrdU FACS. No significant change in proliferation is observed upon DNMT3B knockdown. Error bars represent SEM. ANOVA with Geisser-Greenhouse correction p=0.3; n=3 biological replicates.

A central question in this thesis is the role played by DNMT3B in establishing CIMP in the context of an activated *BRAF*^{V600E} oncogene. In a recent paper which proposed a mechanism by which mutant-BRAF^{V600E} directly induces CIMP it was reported that shRNA-mediated knockdown of DNMT3B is sufficient to restore expression of the "CIMP marker" MLH1 in colon cancer cell lines [364]. This result is difficult to reconcile with earlier data on the respective roles of DNMT3B and DNMT1 in promoter CpG island methylation in cancer [422,445]. Furthermore, in a murine model of colon cancer, DNMT3B ectopic expression does not result in aberrant promoter methylation of *Mlh1*, which Fang et al. [364] propose to be mediated by DNMT3B in their CIMP model [434]. Given these apparently contradictory data, it was relevant to readdress the consequences of DNMT3B knockdown and ectopic expression on MLH1 expression as a surrogate marker of CIMP.

Whole cell lysates from LS411N transduced with the lentiCRISPRv2-puromycin vector ("vector") lentiCRISPRv2-DNMT3B-sgRNA1-puromycin ("sgRNA1") or lentiCRISPRv2-DNMT3B-sgRNA4-puromycin ("sgRNA4") from the previous experiment were subjected to further Western blotting to assess expression of MLH1. DNMT3B knockdown had already been confirmed (Figure 5-18). In wild-type LS411N cells the *MLH1* promoter is methylated, and expression of MLH1 is repressed, therefore HT-29 lysate was included as a positive control [444]. CRISPR-mediated DNMT3B knockdown did not restore MLH1 expression in LS411N with either DNMT3B sgRNA (Figure 5-20a). In the converse experiment, HT-29 were transduced with pLenti6-puromycin ("vector") or pLenti6-DNMT3B1-puromycin ("DNMT3B1"), and harvested for protein lysates 7 days following drug selection in puromycin-conditioned culture media. MLH1 expression was once again assessed by Western blot. Ectopic expression of DNMT3B1 did not lead to silencing of MLH1 in HT-29 (Figure 5-20b). It should be noted as a caveat that it has not been explicitly demonstrated in the present work that removal of *MLH1* promoter methylation in LS411N will result in re-expression of MLH1, however studies in other cell lines would suggest that this is the case [364]. Furthermore, no formal assessment of *MLH1* promoter methylation was performed in these experiments.

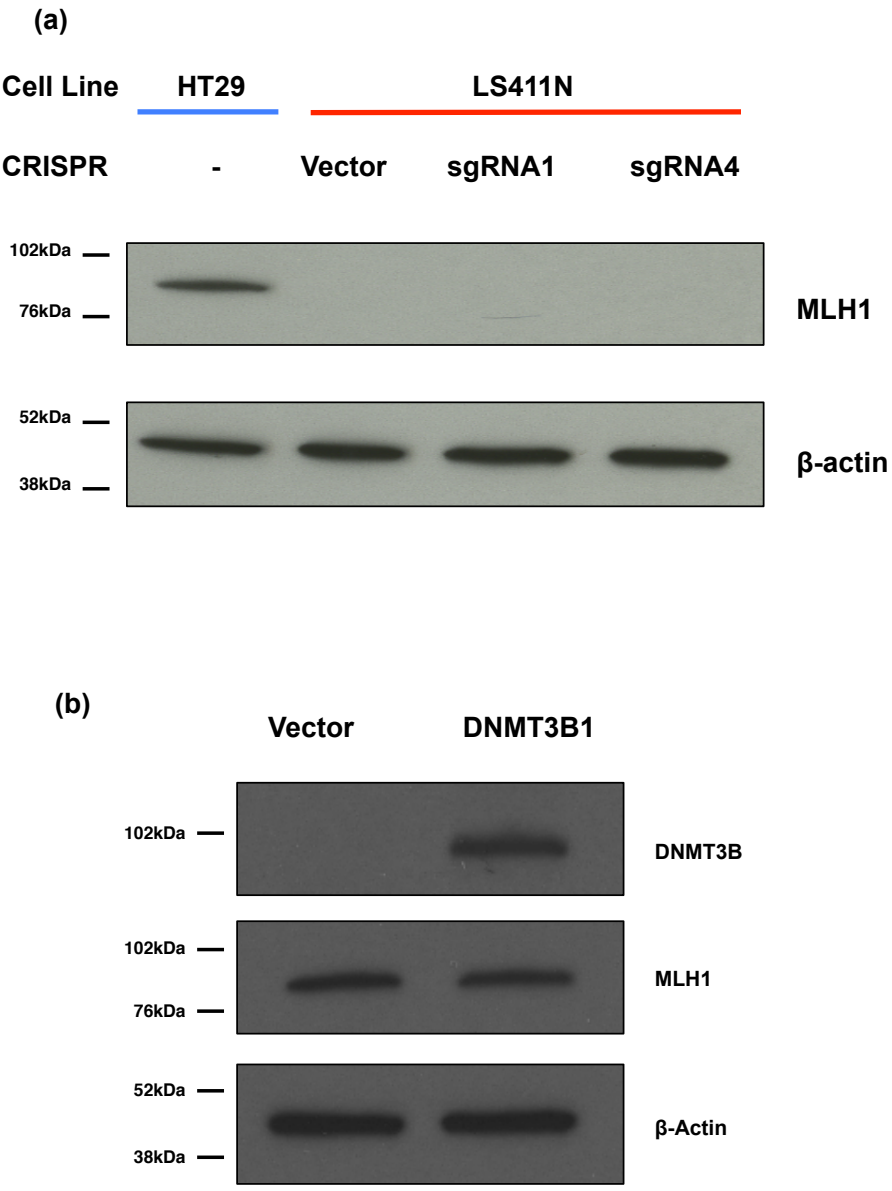

Figure 5-20 DNMT3B knockdown does not restore, and DNMT3B ectopic expression does not silence MLH1 expression in colon cancer cell lines

(a) Western blot of whole cell lysates from LS411N colon cancer cells transduced with LentiCRISPRv2-puromycin ("vector") or LentiCRISPRv2-DNMT3B-sgRNA1/4-puromycin ("sgRNA1/4"). DNMT3B knockdown is confirmed in Figure 5-18. HT-29 lysate is included as a positive control for MLH1. MLH1 expression is unchanged upon DNMT3B knockdown. **(b**) Western blot of whole cell lysates from HT-29 colon cancer cells one week following transduction with either pLenti6-puromycin ("vector") or pLenti6-DNMT3B1-puromycin ("DNMT3B1). DNMT3B1 ectopic expression does not result in silencing of MLH1, a well-characterised "CIMP target gene" (n=2 biological replicates).

5.4 Discussion

In this chapter, functional interactions between $BRAF^{V600E}$ and DNMT3B have been examined in primary human cells and human colon cancer cell lines. It has been demonstrated that combined DNMT3B1 and $BRAF^{V600E}$ expression results in impairment of the proliferation arrest phenotype induced in primary cells by the latter. Furthermore, it has been demonstrated that this effect of DNMT3B1 on $BRAF^{V600E}$-induced proliferation arrest may not be dependent on the catalytic domain of DNMT3B. This is particularly interesting, given the emerging body of data demonstrating expression of truncated *DNMT3B* isoforms in human cancer [222,225]. As the data presented herein are limited by the lack of paired DNA methylation data, and because as discussed earlier, DNMT3B3 may in fact modulate DNA methylation, it cannot be concluded that this represents a DNA methylation-independent function of DNMT3B [224,225]. It does however imply that the catalytic domain may be dispensable to the observed impaired proliferation-arrest phenotype associated with combined DNMT3B and BRAF expression, however this could more accurately be assessed by repeating the experiment using PCR mutagenesis to generate a true "catalytically inactive" DNMT3B point-mutant. Interestingly however, whilst DNMT3B1 ectopic expression in a murine model of colon cancer has been demonstrated to promote intestinal tumourigenesis, the same effect was not observed with ectopic DNMT3B3 expression, though this study was performed in the $Apc^{min/+}$ model, and not in the context of an activated $Braf^{V600E}$ oncogene [205]. It could also be argued that DNMT3B2 might have been a more appropriate isoform to examine in these experiments than DNMT3B1, as previously published human cell-line data suggests that this is the predominant isoform expressed in human cancer cell lines [220].

Further dissection of the mechanism by which DNMT3B1 impairs $BRAF^{V600E}$-induced proliferation arrest was achieved by RNA-sequencing. Consistent with the observed pro-proliferative phenotype, this demonstrated marked differences in the transcriptome of "BRAF/DNMT3B1" compared to "BRAF-only" populations with respect to cell cycle genes. Furthermore, this was supported by gene-ontology analysis. Intriguingly, combined "BRAF/DNMT3B1" expression has also been demonstrated to impair the SASP phenotype. This is particularly relevant given that the SASP has been demonstrated to reinforce the senescence program in certain contexts by promotion of proliferation arrest and immune clearance [440,446]. Furthermore, combined "BRAF/DNMT3B1" expression has also been demonstrated to alter the Wnt signalling pathway associated with $BRAF^{V600E}$ activation. This is a particularly interesting result given that activated Wnt signalling has

previously been demonstrated to impair oncogene-induced senescence [429,442,447]. Whilst the net effect of combined "BRAF/DNMT3B1" activation appears to be Wnt pathway activation (as demonstrated by upregulation of downstream Wnt targets including cyclin D1, Claudin-1, Myc and Sox9), the data with respect to Wnt regulators are more difficult to reconcile. Consistent with a previous report in a murine intestinal tumour model, DNMT3B1 has been demonstrated to decrease the expression of SFRP2. SFRP4 and SFRP5 were not expressed in this cell population (IMR-90 human fetal lung fibroblasts), though have previously been demonstrated to be downregulated by ectopic DNMT3B expression in the murine intestine [205]. Similarly, AXIN2 has also been demonstrated to be repressed by ectopic DNMT3B expression in the present study, and is similarly recognised as a Wnt antagonist which has been implicated in the pathogenesis of colorectal cancer [448]. By contrast, combined BRAF/DNMT3B1 expression results in elevated expression of both SFRP1 and DKK1, which are both considered Wnt antagonists [449-451]. Paradoxically, SFRP1 has also been demonstrated to be a mediator of replicative senescence, and so it is somewhat counterintuitive that its expression should be elevated in "BRAF/DNMT3B1" cells compared to "BRAF-only" cells given the impaired proliferation arrest phenotype in the former [452]. Whilst these results are somewhat paradoxical, the central importance of the Wnt pathway to the pathogenesis of colorectal cancer justify further examination of the relationships between DNMT3B1 and Wnt signalling in an *in vivo* model system of BRAF-induced intestinal tumourigenesis, and this will be addressed in chapter 6.

By contrast, examination of DNMT3B expression in colon cancer cell lines does not reveal an obvious relationship between $BRAF^{V600E}$ mutation status and DNMT3B expression or CIMP status. DNMT3B protein levels are lower in $BRAF^{V600E}$-mutant cell lines than the *RAS*-mutant HCT116 and SW480 cell lines. Although cancer cell lines are a relatively limited and artificial model system, this apparent lack of correlation between DNMT3B expression and either CIMP status or $BRAF^{V600E}$ mutation does not fit particularly well with a model in which BRAF and DNMT3B cooperate to induce CIMP. Interestingly, this corroborates previously published data suggesting no relationship between CIMP status and DNMT3B expression in colon cancer cell lines [334].

Furthermore, whilst ectopic DNMT3B1 expression impairs $BRAF^{V600E}$-induced proliferation arrest, at least in a primary cell culture model, DNMT3B knockdown in $BRAF^{V600E}$ mutant cell line does not have an antiproliferative effect, though may promote apoptosis. This contrasts with previous loss-of-function (RNAi) experiments in the *KRAS*-

mutant cell line HCT116, demonstrating an antiproliferative and pro-apoptotic effect associated with DNMT3B knockdown [334]. It is notable however that HCT116 have been demonstrated in this chapter (and indeed in the aforementioned study) to express very high levels of DNMT3B compared to other colon cancer cell lines, and so the previously-reported antiproliferative effect in this cell line this may simply reflect a degree of "oncogene addiction". Importantly however, in the murine $Apc^{min/+}$ model of colon cancer, *Dnmt3b* knockout has been demonstrated to reduce the number of macroscopic colonic adenomas. Whilst this would be supportive of an oncogenic function for DNMT3B in colon cancer, the $Apc^{min/+}$ mouse is a model of the adenoma-carcinoma pathway, rather than the serrated pathway. It will therefore be appropriate to investigate the effects of *Dnmt3b* knockout in a murine model of $Braf^{V600E}$-induced serrated pathway colon cancer, and this will be addressed in chapter 6 of this thesis.

It is also noteworthy that DNMT3B knockdown in the $BRAF^{V600E}$-mutant cell line LS411N did not reverse silencing of *MLH1*, and conversely, ectopic DNMT3B1 expression in the *MLH1* proficient line HT-29 does not lead to *MLH1* silencing. This directly contradicts some of the data presented by Fang et al. [364] in their recent paper proposing a mechanism by which BRAF directly mediates CIMP. The aforementioned study demonstrated increased MLH1 expression associated with DNMT3B knockdown, and indeed the RNAi screen used in this study to identify candidate drivers of CIMP was designed to identify drivers of *MLH1* silencing. As DNMT3B represents the "final link" in the proposed mechanism of BRAF-induced CIMP, it is perhaps surprising that this result could not be reproduced. This may reflect differences in the sampling interval following DNMT3B knockdown, the choice of cell line, or the fact that MLH1 protein rather than mRNA levels were assayed in the present study. Furthermore, it should be noted as a caveat that no formal assessment of *MLH1* promoter methylation was undertaken in the present work; nor has it been demonstrated that removal of methylation from the *MLH1* promoter in LS411N would result in its re-expression, however this can be inferred from previously published data [115]. Moreover, it is perhaps relevant to note that stable ectopic expression of DNMT3B in the murine intestine does not lead to *Mlh1* promoter hypermethylation [205,434].

5.5 Summary

1. Ectopic expression of DNMT3B1 impairs the ability of activated oncogenic $BRAF^{V600E}$ to induce a robust proliferation arrest phenotype.

2. This effect of ectopic DNMT3B1 expression may not be dependent on its catalytic domain.

3. Ectopic DNMT3B1 expression in association with activated oncogenic $BRAF^{V600E}$ results in upregulation of cell cycle genes, including cyclin A, cyclin E, E2F1 and PCNA.

4. The impaired proliferation arrest phenotype of combined $BRAF^{V600E}$ and DNMT3B1 expression is associated with an altered SASP secretome.

5. Ectopic DNMT3B1 expression in the context of activated mutant-$BRAF^{V600E}$ induces changes in the Wnt pathway activation associated with activation of the latter, with upregulation of Wnt targets including Myc, Cyclin D1, Claudin-1 and SOX9, and downregulation of the Wnt inhibitors, AXIN2 and SFRP2.

6. The impaired proliferation arrest phenotype characterised in "BRAF/DNMT3B1" compared to "BRAF only" cells does not appear to be associated with the acquisition of a CIMP phenotype.

7. In human colon cancer cell lines however, no clear relationship is demonstrable between DNMT3B protein expression and $BRAF^{V600E}$ mutation status or CIMP positivity.

8. Knockdown of DNMT3B in a CIMP-positive colon cancer cell line does not alter proliferation but may promote apoptosis.

9. Knockdown of DNMT3B in CIMP-positive $BRAF^{V600E}$-mutant colon cancer cell line does not lead to reactivation of *MLH1*, which has previously reported to be silenced by CIMP.

10. Ectopic expression of DNMT3B1 in an *MLH1* proficient cell line does not lead to silencing of *MLH1*.

6 *In vivo* modelling of the oncogenic function of DNMT3B in murine models of *Braf*^{V600E}-mediated serrated pathway intestinal carcinogenesis

6.1 Rationale

In the previous chapter it was demonstrated that ectopically expressed DNMT3B impairs the proliferation arrest phenotype induced in primary human cells by activated mutant-BRAF^{V600E}. This effect was associated with upregulation of cell cycle genes, an altered SASP secretome, and altered Wnt signalling. Previous studies have suggested an oncogenic function of DNMT3B in the *Apc*$^{min/+}$ mouse model of intestinal carcinogenesis, with ectopic DNMT3B expression promoting, and conditional knockout suppressing intestinal tumourigenesis [205,433]. Whilst DNMT3B expression has been linked mechanistically and correlatively to the induction of a CpG island methylator phenotype in association with *BRAF*^{V600E}, and with disease progression in a murine model of serrated carcinogenesis; to date, no study has examined the effects of *Dnmt3b* manipulation in murine serrated carcinogenesis driven by an activated *Braf*^{V600E} oncogene [46,47,364,427,453]. It was therefore pertinent to examine the effects of *Dnmt3b* manipulation in *in vivo* models of *Braf*-mediated "serrated pathway" intestinal carcinogenesis.

6.2 Aims

The specific aims of this chapter are:

1. To investigate the effects of DNMT3B ectopic expression on *Braf*^{V600E}-mutant intestinal carcinogenesis

2. To investigate the effects of *Dnmt3b* knockout on *Braf*^{V600E}-mutant intestinal carcinogenesis

3. To determine whether DNMT3B maintains an oncogenic function in the context of activated Wnt signalling

6.3 Results

6.3.1 Initial pilot of conditional *Dnmt3b* knockout in *AhCreEr^{T};^{LSL}Braf^{V600E}* mice

In order to develop an *in vivo* model to investigate the role of DNMT3B in *Braf^{V600E}*-mediated carcinogenesis, a *Dnmt3b* conditional knockout genetically-engineered mouse model (*B6;129S4-Dnmt3b^{tm1Jae}/Mmnc*) was obtained from the MMRRC[20]. In this model, *loxP* sites flank the catalytic domain of *Dnmt3b* (exons 16-19) on chromosome 2 [433]. Heterozygous *Dnmt3b^{tm1jae}* mice were interbred to produce a cohort of *Dnmt3b^{tm1jae} flox/flox* homozygotes (hereafter referred to as *Dnmt3b$^{fl/fl}$*). Separately, the conditional *Braf^{tm1Cpri}* (hereafter referred to as *^{LSL}Braf^{V600E}*) mouse strain, was obtained. In this model, the expression of mutant-BRAF^{V600E} is driven from its endogenous promoter by *Cre* recombinase. The transgenic allele is designed with an LSL-cassette inserted to intron 14 of the *Braf* gene, comprising a mini cDNA encoding exons 15-18 of the *Braf* gene. Furthermore, at the 3' end of the LSL-cassette, the endogenous exon 15 is modified to incorporate the T1799A mutation. The LSL-cassette contains three *loxP* sites. *Cre* recombination results in excision of the *loxP* sites, with resultant expression of mutant *Braf^{V600E}* from its endogenous promoter [454,455]. Heterozygous *^{LSL}Braf^{V600E}* mice were crossed to the *Tg(Cyp1a1-cre/ERT)1Dwi* (hereafter referred to as *AhCreEr^{T}*) strain. In the latter system, tamoxifen- and β-napthoflavone-regulated *Cre* recombination is obtained in the stem cells and transit-amplifying cells of the murine gastrointestinal tract driven by the *Cyp1A1* promoter [456,457]. As outlined in the introduction to this thesis, the resultant *AhCreEr^{T};^{LSL}Braf^{V600E}* model has previously been reported to recapitulate the "serrated pathway" of colorectal carcinogenesis [47]. *AhCreEr^{T};^{LSL}Braf^{V600E}* mice were crossed to *Dnmt3b$^{fl/fl}$* and the offspring interbed to generate *AhCreEr^{T};^{LSL}Braf^{V600E}+/-;Dnmt3b$^{fl/fl}$* cases, and *AhCreEr^{T};^{LSL}Braf^{V600E}+/-;Dnmt3b$^{wt/wt}$* controls.

AhCreEr^{T};^{LSL}Braf^{V600E}+/-;Dnmt3b$^{fl/fl}$ (n=5) and *AhCreEr^{T};^{LSL}Braf^{V600E}+/-;Dnmt3b$^{wt/wt}$* (n=7) mice were induced at 6 weeks of age by intraperitoneal injection of β-napthoflavone (80mg/kg) and tamoxifen (100mg/kg) for four consecutive days. Following induction, mice were closely monitored for clinical signs, including weight loss, abdominal swelling, hunching and pedal pallor (anaemia). Mice were sacrificed when they exhibited >20% weight loss, or exhibited two or more clinical signs of illness. Surprisingly, and in contrast to previous descriptions of these mice, mice in both case and control cohorts had to be

[20] MMRRC = Mutant Mouse Resource and Research Centers (www.mmrrc.org)

culled within 30 days of induction, and there was no statistically significant difference in survival between *Dnmt3b*$^{wt/wt}$ and *Dnmt3b*$^{fl/fl}$ controls (Figure 6-1).

At post-mortem, the small intestine and colon appeared normal with no macroscopic tumours visible and this was confirmed by histology (data not shown). In sharp contrast, all mice exhibited significant gastric hypertrophy, due to the development of large tumours affecting the squamous-lined forestomach (Figure 6-2). The profound forestomach phenotype significantly impaired the potential of this model system to assess the effects of DNMT3B on *Braf*^{V600E}-mediated intestinal carcinogenesis, and thus a different model system was sought.

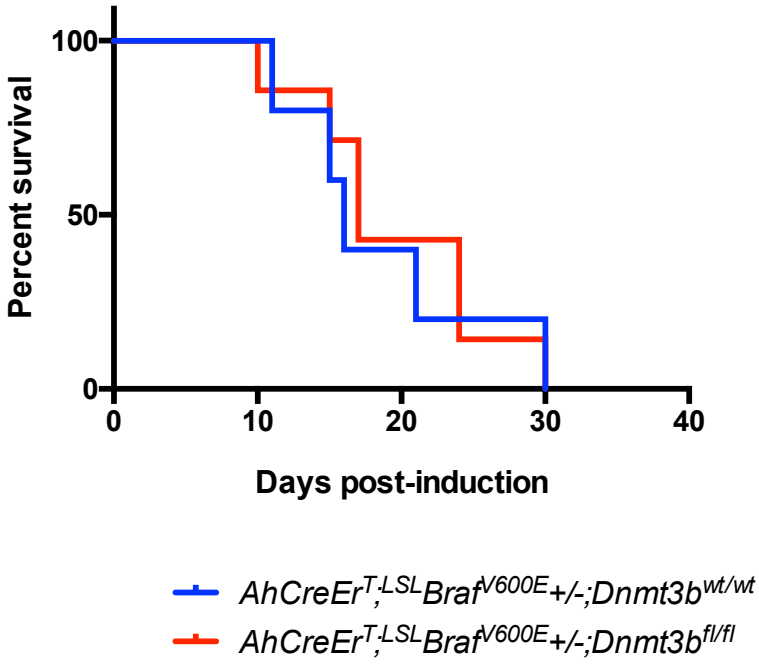

Figure 6-1 Conditional knockout of *Dnmt3b* did not affect survival in an initial pilot cohort of *AhCreER^{T};^{LSL}Braf^{V600E}*+/- mice

Kaplan-Meier curve comparing survival in *AhCreER^{T};^{LSL}Braf^{V600E}+/-;Dnmt3b$^{fl/fl}$* cases and *AhCreER^{T};^{LSL}Braf^{V600E}+/-;Dnmt3b$^{wt/wt}$* controls. *AhCreER^{T};^{LSL}Braf^{V600E}+/-;Dnmt3b$^{fl/fl}$* (n=5) and *AhCreER^{T};^{LSL}Braf^{V600E}+/-;Dnmt3b$^{wt/wt}$* (n=7) mice were induced at 6 weeks of age, and sacrificed at clinical end-point. All mice reached endpoint within 30 days of induction, and there was no statistically significant difference in survival between *Dnmt3b$^{wt/wt}$* and *Dnmt3b$^{fl/fl}$* controls. Log-rank (Mantel-Cox) test p=0.73.

(a)

Forestomach tumour
AhCreEr^{T};^{LSL}Braf^{V600E}+/-;Dnmt3b$^{wt/wt}$

Forestomach tumour
AhCreEr^{T};^{LSL}Braf^{V600E}+/-;Dnmt3b$^{fl/fl}$

(b)

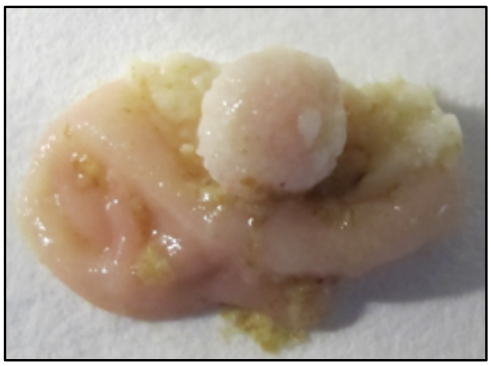

Forestomach tumour
Macroscopic appearance

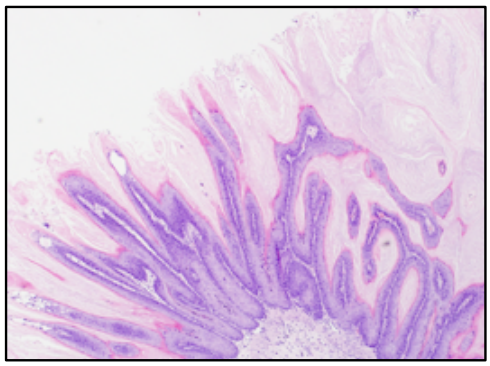

Forestomach tumour
H&E (4x magnification)

Figure 6-2 *AhCreEr^{T};^{LSL}Braf^{V600E}+/-* mice develop forestomach tumours

AhCreEr^{T};^{LSL}Braf^{V600E}+/-;Dnmt3b$^{fl/fl}$ (n=5) and *AhCreEr^{T};^{LSL}Braf^{V600E}+/-;Dnmt3b$^{wt/wt}$* (n=7) mice were induced at 6 weeks of age, and sacrificed at clinical end-point. Tumours of the squamous-lined forestomach develop rapidly in *AhCreEr^{T};^{LSL}Braf^{V600E}+/-* mice regardless of *Dnmt3b* genotype. **(a)** Representative images of the macroscopic appearances of the peritoneal cavity at post-mortem in *Dnmt3b$^{wt/wt}$* and *Dnmt3b$^{fl/fl}$* mice, demonstrating significant gastric hypertrophy due to tumour formation. **(b)** Representative images of macroscopic and microscopic appearances of a forestomach tumour from an *AhCreEr^{T};^{LSL}Braf^{V600E}* mouse.

6.3.2 Ectopic DNMT3B expression accelerates intestinal carcinogenesis in *VilCreER$^{T2\ LSL}$Braf^{V600E}* mice

In order to circumvent the problems associated with the forestomach phenotype associated with the *AhCreEr^{T};^{LSL}Braf^{V600E}* model system, *AhCreEr^{T}* was replaced by *Tg(Vil-cre/ERT2)23Syr* (hereafter termed *VilCreEr^{T2}*), in which *Cre* recombination is achieved almost exclusively in the small intestine and colon [458]. The rationale for this approach was strengthened by a study published during the course of this work in which the intestine-specific expression of *Braf^{V637E}* (the murine homologue of BRAF^{V600E}) in the murine intestine using the constitutive *villin-Cre* system was demonstrated to recapitulate features of serrated pathway colorectal carcinogenesis [46,459]. One potential disadvantage of use of the *VilCreEr^{T2}* model system is the relatively long latency of the intestinal *Braf^{V600E}* phenotype in this model system compared to *AhCreEr^{T2}*. Whilst *AhCreEr^{T2};^{LSL}Braf^{V600E}* mice reportedly develop intestinal tumours 6 weeks after induction, *VilCre;Braf^{V637E}* mice develop dysplastic lesions at 2-3 months and invasive carcinoma in some mice at 10 months [46,47].

In chapter 5 it was demonstrated that combined DNMT3B1 and BRAF^{V600E} expression in human fetal lung fibroblasts impaired the proliferation arrest phenotype normally associated with the activation of the latter in primary human cells. Furthermore, in a previously published study in *AhCreEr^{T};^{LSL}Braf^{V600E}* mice, it was demonstrated that BRAF^{V600E} expression in the murine intestine induces an initial period of hyperproliferation, followed by crypt senescence. Crypt senescence was however transient, and followed by the development of intestinal tumours, which were associated with silencing of *p16^{Ink4a}* and upregulation of DNMT3B. It was therefore hypothesised that ectopic DNMT3B expression would accelerate intestinal tumourigenesis in *VilCreEr^{T2};^{LSL}Braf^{V600E}* mice. In order to test this hypothesis, the *B6.Cg-Col1a1$^{tm9(tet0-DNMT3b_i1)Jae}$/J* (hereafter referred to as *Col1a1-tetO-Dnmt3b1*) *and B6.Cg-Gt(ROSA)26Sor$^{tm1(rtTA*M2)Jae}$/J* (hereafter referred to as *R26-M2-rtTA*) transgenic alleles were obtained from the Jackson laboratory. *Col1a1-tetO-Dnmt3b1* has previously been demonstrated to direct ectopic, tetracycline-inducible DNMT3B1 expression in the murine intestine [205]. Doubly heterozygous *R26-M2-rtTA;Col1a1-tetO-Dnmt3b1* mice were obtained and crossed to *VilCreEr^{T2};^{LSL}Braf^{V600E}+/-* mice, and the offspring interbred to generate *VilCreEr^{T2};^{LSL}Braf^{V600E}+/-;R26-M2-rtTA+/-;Col1a1-tetO-Dnmt3b1+/-* mice. All alleles were maintained on an inbred C57BL/6 genetic background. Prior to comparison between these cohorts, intestinal DNMT3B ectopic expression was first confirmed in *R26-M2-rtTA+/-;Col1a1-tetO-Dnmt3b1+/-* mice by induction for two weeks with doxycycline,

with subsequent harvest for intestinal tissues for DNMT3B protein analysis by western blot and immunohistochemistry. Ectopic DNMT3B expression was demonstrable in both the small intestine and colon of *R26-M2-rtTA+/-;Col1a1-tetO-Dnmt3b1+/-* mice induced with doxycycline but not in *Dnmt3b* wild-type controls (Figure 6-3).

VilCreEr^{T2};^{LSL}Braf^{V600E}+/-;R26-M2-rtTA+/-;Col1a1-tetO-Dnmt3b1+/- cases (n=13) were induced by a single intraperitoneal injection of 80mg/kg tamoxifen and 0.5mg/mL of doxycycline hyclate in 1% sucrose (administered *ad libitum* in the drinking water and changed three times weekly). Wild-type DNMT3B (i.e. endogenous expression) controls (n=26) for this experiment were either of the same genotype as cases (i.e. *VilCreEr^{T2};^{LSL}Braf^{V600E}+/-;R26-M2-rtTA+/-;Col1a1-tetO-Dnmt3b1+/-*), or wild-type for either *R26-M2-rtTA* or *Col1a1-tetO-Dnmt3b1*. Control mice were induced by a single intraperitoneal injection of 80mg/kg tamoxifen, but were administered 1% sucrose in the drinking water without the addition of doxycyline. As additional controls, "DNMT3B only" mice (n=31) were also generated. "DNMT3B only" controls were a mixture of *VilCreEr^{T2};R26-M2-rtTA+/-;Col1a1-tetO-Dnmt3b1+/-*, induced in the same fashion as cases and *VilCreEr^{T2};^{LSL}Braf^{V600E}+/-;R26-M2-rtTA+/-;Col1a1-tetO-Dnmt3b1+/-* mice, induced with doxycycline but not tamoxifen. Both "DNMT3B only" control genotypes were therefore "*Braf* wild type". Mice were monitored for clinical signs of illness, including weight loss, hunching and pedal pallor (anaemia). Mice were sacrificed when they exhibited >20% weight loss, or exhibited two or more clinical signs of illness.

Strikingly, combined ectopic DNMT3B1 expression together with activated *Braf^{V600E}* in the murine intestine resulted in a marked decrease in overall survival compared to *Braf^{V600E}* alone. Median post-survival induction in *Dnmt3b* wild-type mice was 489 days, compared to 289 in mice with ectopic DNMT3B1. "DNMT3B only" mice however, did not develop any clinical signs of illness up until 377 days following induction, and were culled at this timepoint (Figure 6-4). All but five (wild-type DNMT3B n=4; ectopic DNMT3B n=1) *VilCreEr^{T2};^{LSL}Braf^{V600E}+/-* mice had developed intestinal tumours at clinical end-point. These were exclusively located in the small intestine, and no colonic tumours were identifiable in any mice examined. By comparison, and consistent with the lack of clinical signs of illness in this control cohort, no intestinal tumours were identified in "DNMT3B only" mice. Interestingly, and despite the marked acceleration of the *Braf^{V600E}* phenotype induced by ectopic DNMT3B expression, no significant difference in total intestinal tumour number was demonstrable between wild-type DNMT3B controls and ectopic DNMT3B cases (Figure 6-5).

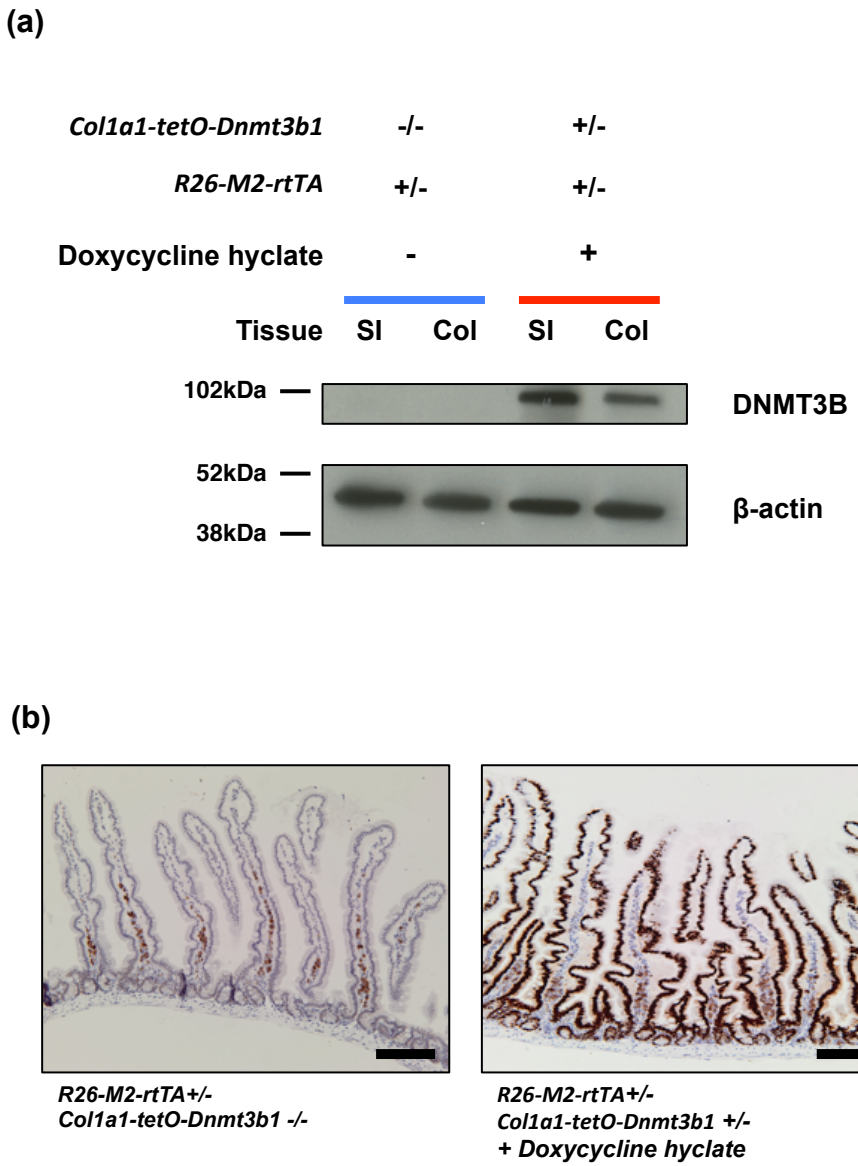

Figure 6-3 Intestinal DNMT3B ectopic expression was confirmed upon induction of the *Col1a1-tetO-Dnmt3b1* transgene by doxycycline hyclate

R26-M2-rtTA+/-;Col1a1-tetO-Dnmt3b1+/- cases and *R26-M2-rtTA+/-;Col1a1-tetO-Dnmt3b1-/-* controls were induced for two weeks by the addition of doxycycline hyclate (cases) or sucrose (controls) to the drinking water, with subsequent harvest for intestinal tissues for DNMT3B protein analysis by western blot and immunohistochemistry. **(a)** Western blot of whole cell lysate from small intestine (SI) and colon (Col) of *R26-M2-rtTA+/-;Col1a1-tetO-Dnmt3b1+/-* case and *R26-M2-rtTA+/-;Col1a1-tetO-Dnmt3b1-/-* control. Ectopic expression of DNMT3B is demonstrated in both the small intestine and colon of the *R26-M2-rtTA+/-;Col1a1-tetO-Dnmt3b1+/-* case mouse upon induction with doxycyline hyclate, but not in the *R26-M2-rtTA+/-;Col1a1-tetO-Dnmt3b1-/-* control (*n*=1 biological replicate). **(b)** Representative immunohistochemistry images from small intestine of *R26-M2-rtTa+/-;Col1a1-tetO-Dnmt3b1+/-* case and *R26-M2-rtTA+/-;Col1a1-tetO-Dnmt3b1-/-* control, demonstrating robust ectopic expression of DNMT3B upon transgene induction with doxycycline hyclate in *R26-M2-rtTA+/-;Col1a1-tetO-Dnmt3b1+/-* cases, but not in *R26-M2-rtTA+/-;Col1a1-tetO-Dnmt3b1-/-* controls (n=3 *vs* 3 biological replicates).

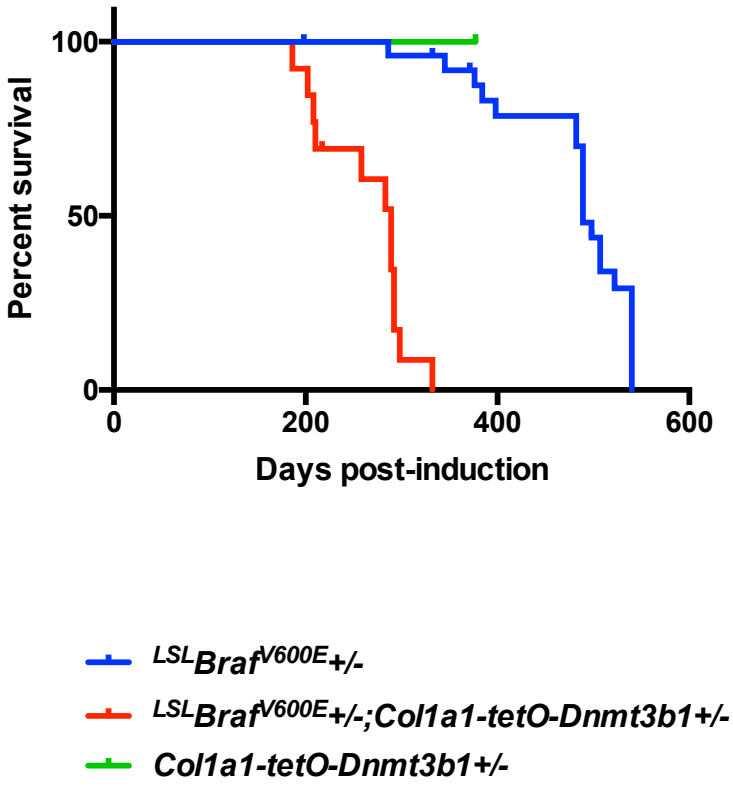

Figure 6-4 Intestinal ectopic DNMT3B1 expression significantly reduces survival in *VilCreErT2;LSLBrafV600E* mice.

Kaplan-Meier curve comparing survival in *VilCreER^{T2};^{LSL}Braf^{V600E}* transgenic mice with and without intestinal DNMT3B1 ectopic expression. *VilCreER^{T2};^{LSL}Braf^{V600E}+/-;R26-M2-rtTA+/-;Col1a1-tetO-Dnmt3b1+/-* cases (n=13) were induced by a single intraperitoneal injection of 80mg/kg tamoxifen and 0.5mg/mL of doxycycline hyclate in 1% sucrose. Wild-type DNMT3B controls (n=26) were induced by a single intraperitoneal injection of 80mg/kg tamoxifen, but were administered 1% sucrose in the drinking water without the addition of doxycyline. Wild-type DNMT3B controls were a mix of *VilCreER^{T2};^{LSL}Braf^{V600E}+/-;R26-M2-rtTA+/-;Col1a1-tetO-Dnmt3b1+/-*, *VilCreER^{T2};^{LSL}Braf^{V600E}+/-;R26-M2-rtTA+/-;Col1a1-tetO-Dnmt3b1-/- and VilCreER^{T2};^{LSL}Braf^{V600E}+/-;R26-M2-rtTA-/-;Col1a1-tetO-Dnmt3b1+/-*. Mice were sacrificed at clinical end-point. As additional controls, "DNMT3B only" mice (*Col1a1-tetO-Dnmt3b1*+/-; n=31*)* were induced. Median post-survival induction in wild-type DNMT3B mice was 489 days, compared to 289 in mice with ectopic DNMT3B1. "DNMT3B only" mice did not develop any clinical signs of illness up until 377 days following induction, at which timepoint they were culled with no evidence of intestinal tumour formation. Log-rank (Mantel-Cox) test $p<0.0001$.

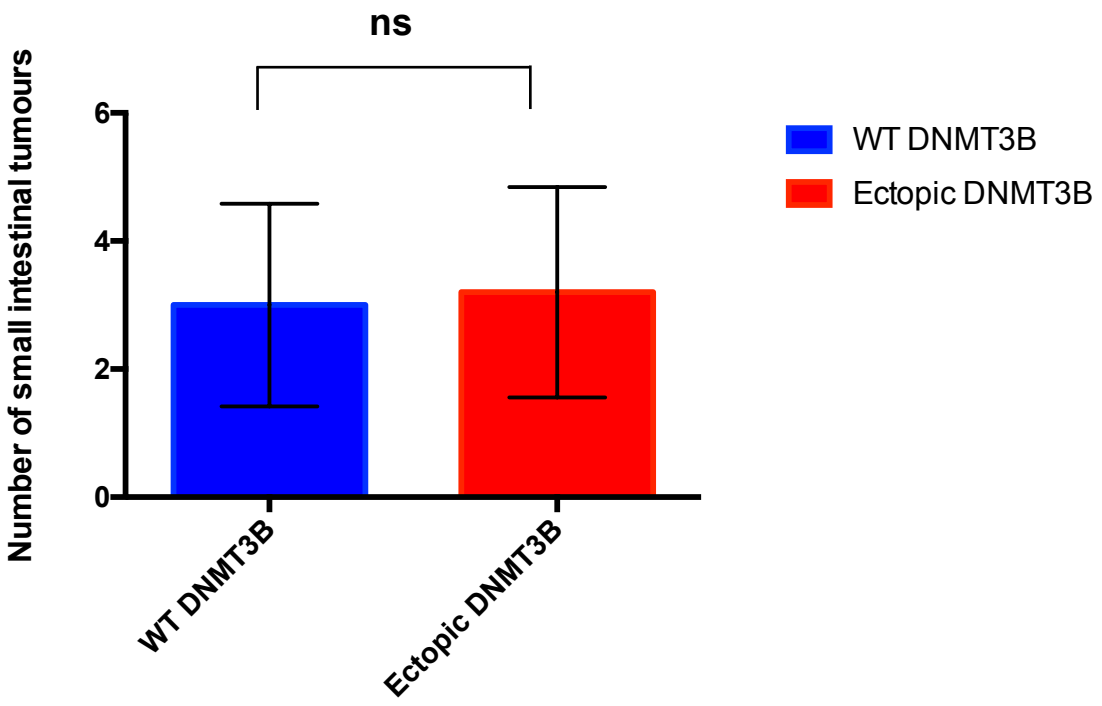

Figure 6-5 Comparison of small intestinal tumour number in *VilCreEr^{T2};^{LSL}Braf^{V600E} mice* with and without ectopic DNMT3B1 expression

Bar-chart of small intestinal tumour number at clinical end-point in *VilCreEr^{T2};^{LSL}Braf^{V600E}*+/- with wild-type (control) or ectopic (cases) DNMT3B1. No statistically significant difference in small intestinal tumour number is demonstrable in mice expressing ectopic DNMT3B (n=5) compared to wild-type DNMT3B controls (n=5). Error bars represent SEM. Mann Whitney test p=0.98 (ns).

As ectopic DNMT3B1 expression accelerates carcinogenesis in *VilCreEr^{T2}; ^{LSL}Braf^{V600E}* mice, but does not alter tumour number at clinical endpoint, it was relevant to further dissect aspects of carcinogenesis in this model. It has previously been reported that *Braf^{V600E}* activation in the murine intestine induces transient crypt senescence at six-weeks post-induction [47]. In chapter 5, DNMT3B was demonstrated to impair the proliferation arrest induced by BRAF^{V600E} *in vitro*, and so it was pertinent to address whether the acceleration induced by ectopic DNMT3B expression observed in this model was mediated by an impaired crypt senescence program. Wholemount intestinal sections from mice at clinical endpoint (n=3 ectopic DNMT3B and n=3 wild-type DNMT3B) were stained with several markers associated with a senescence phenotype: Ki67, p21, γH2AX, and IL1α. Interestingly, whilst scattered positivity for p21, γH2AX, and IL1α was demonstrable in the intestinal crypts (which have all individually been associated with a senescence phenotype), the crypts were highly proliferative, as demonstrated by strong, uniform staining for the proliferation marker Ki67. This phenotype was not altered in mice expressing ectopic DNMT3B (Figure 6-6). Similarly, tumours in *VilCreEr^{T2}; ^{LSL}Braf^{V600E}* were highly proliferative as assessed by strong Ki67 positivity, which was also unaffected by ectopic DNMT3B expression. Interestingly, despite being highly proliferative, tumours from *VilCreEr^{T2}; ^{LSL}Braf^{V600E}* mice exhibited strong staining for the cell-cycle repressor p21, though this was also unaffected by DNMT3B ectopic expression (Figure 6-7). It has previously been reported that both murine and human serrated lesions demonstrate p53 positivity, and that this is correlated with disease progression [46,74]. The observed p21 staining in the tumours of *VilCreEr^{T2}; ^{LSL}Braf^{V600E}* mice may therefore represent p53 pathway activation.

As combined BRAF^{V600E} and DNMT3B expression *in vitro* had been demonstrated to alter Wnt signalling in primary cells expressing BRAF^{V600E} in the previous chapter, and given the central importance of this pathway to intestinal carcinogenesis, it was relevant to examine whether Wnt signalling was altered by ectopic DNMT3B expression in the murine intestine. Wholemount intestinal sections from *VilCreEr^{T2}; ^{LSL}Braf^{V600E}* mice at clinical endpoint (n=3 ectopic DNMT3B and n=3 wild-type DNMT3B) were stained for the Wnt targets Sox9, Cyclin D1 and the Wnt effector, β-catenin. The crypts of *VilCreEr^{T2}; ^{LSL}Braf^{V600E}* mice demonstrated exclusively membranous β-catenin staining, though did exhibit positivity for the Wnt targets Sox9 and Cyclin D1. This was unaffected by DNMT3B ectopic expression (Figure 6-8). By contrast, in tumours, there was more convincing evidence for Wnt pathway activation, with strong staining for Sox9 and Cyclin

D1, in association with nuclear and cytoplasmic β-catenin staining, though once again, this appeared to be independent of, and unaltered by DNMT3B ectopic expression (Figure 6-9).

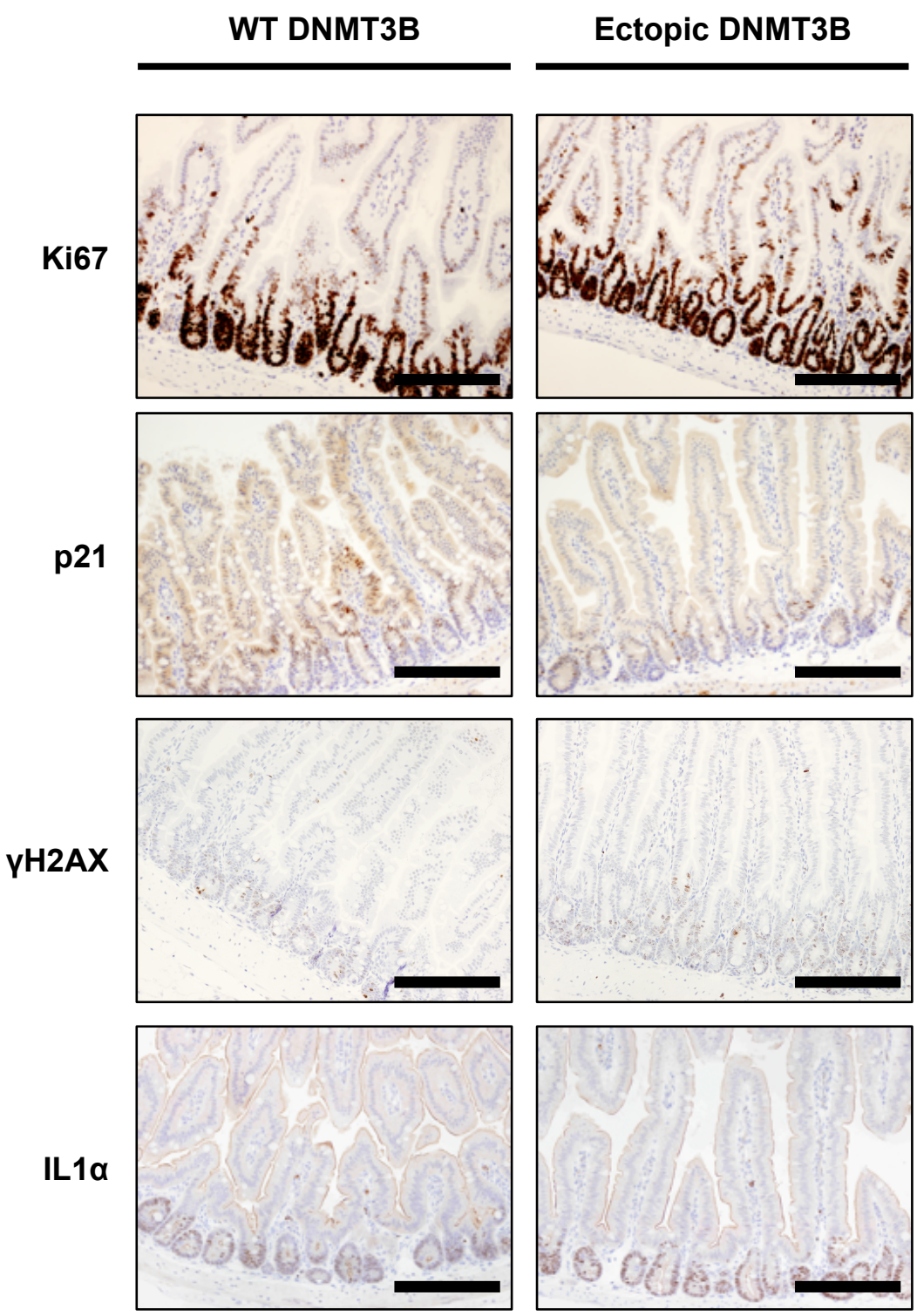

Figure 6-6 Whilst some features of a "senescence phenotype" are observed in the intestinal crypts of *VilCreEr$^{T2;LSL}$Braf^{V600E}* mice, they are highly proliferative and this is independent of DNMT3B expression status

Representative immunohistochemistry images for Ki67, p21, γH2AX and IL1α in the small intestine of *VilCreEr$^{T2;LSL}$Braf^{V600E}+/-;R26-M2-rtTA+/-;Col1a1-tetO-Dnmt3b1+/-* ("Ectopic DNMT3B") cases and *VilCreEr$^{T2;LSL}$Braf^{V600E}+/-;R26-M2-rtTA+/-;Col1a1-tetO-Dnmt3b1-/-* ("WT DNMT3B") controls at clinical end-point. Intestinal crypts are highly proliferative, as identified by strong staining for Ki67. Scattered crypt positivity for p21 and γH2AX is however detectable as is positivity for the SASP marker Il1α. No difference is observed between the crypt phenotype of wild-type or ectopic DNMT3B mice. Scale-bar = 200μM; n=3 *vs* 3 biological replicates.

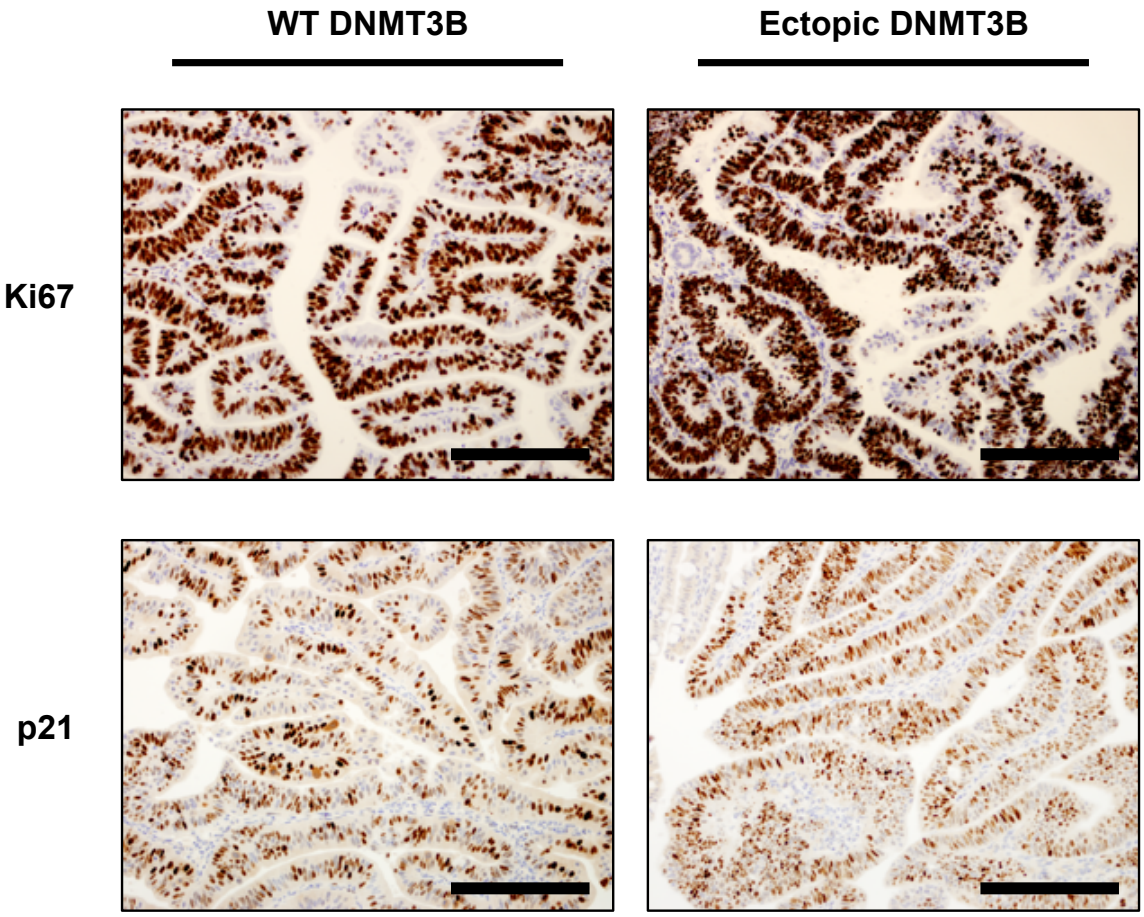

Figure 6-7 Tumours of *VilCreEr^{T2};^{LSL}Braf^{V600E}* mice are highly proliferative but exhibit prominent p21 staining, though this is independent of DNMT3B status

Representative immunohistochemistry images for Ki67 and p21 in the small intestinal tumours of *VilCreEr^{T2};^{LSL}Braf^{V600E}+/-;R26-M2-rtTA+/-;Col1a1-tetO-Dnmt3b1+/-* ("Ectopic DNMT3B") cases and *VilCreEr^{T2};^{LSL}Braf^{V600E}+/-;R26-M2-rtTA+/-;Col1a1-tetO-Dnmt3b1-/-* ("WT DNMT3B") controls at clinical end-point. Both genotypes develop highly proliferative tumours, which paradoxically express high levels of p21. Scale-bar = 200μM; n=3 *vs* 3 biological replicates.

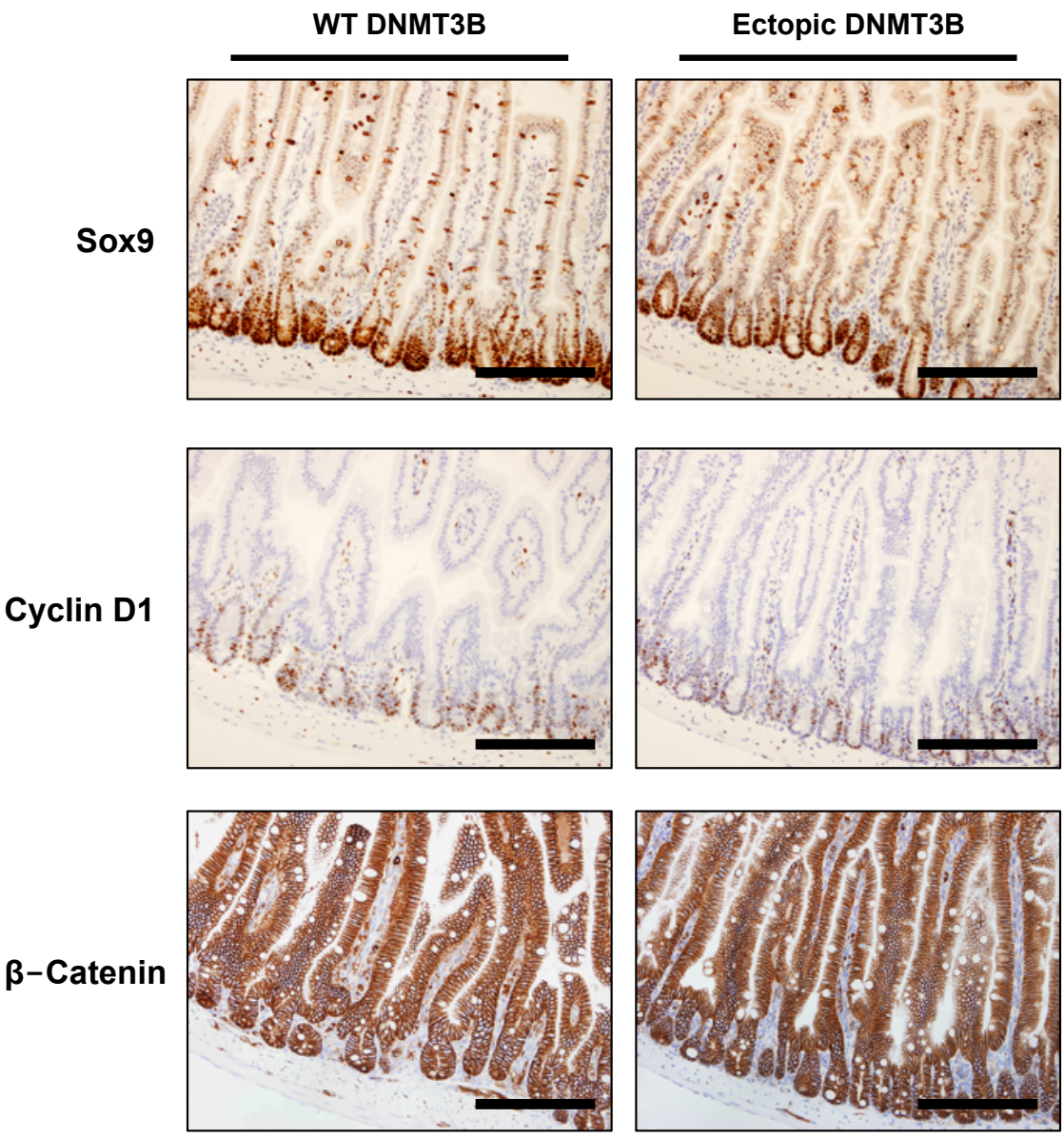

Figure 6-8 The crypts of *VilCreEr$^{T2;LSL}$Braf^{V600E}* mice exhibit membranous β-catenin staining but demonstrate marked positivity for the Wnt targets Cyclin D1 and Sox9, though this is independent of DNMT3B expression status

Representative immunohistochemistry images for Sox9, Cyclin D1 and β-catenin in in the small intestine of *VilCreEr$^{T2;LSL}$Braf^{V600E}+/-;R26-M2-rtTA+/-;Col1a1-tetO-Dnmt3b1+/-* ("Ectopic DNMT3B") cases and *VilCreEr$^{T2;LSL}$Braf^{V600E}+/-;R26-M2-rtTA+/-;Col1a1-tetO-Dnmt3b1-/-* ("WT DNMT3B") controls at clinical end-point. *VilCreEr$^{T2;LSL}$Braf^{V600E}* mice exhibit membranous β-catenin staining in the crypts, though staining for the Wnt targets Cyclin D1 and Sox9 is demonstrable in the crypts. This is unaltered upon, and does not require ectopic DNMT3B expression. Scale-bar = 200μM; n=3 *vs* 3 biological replicates.

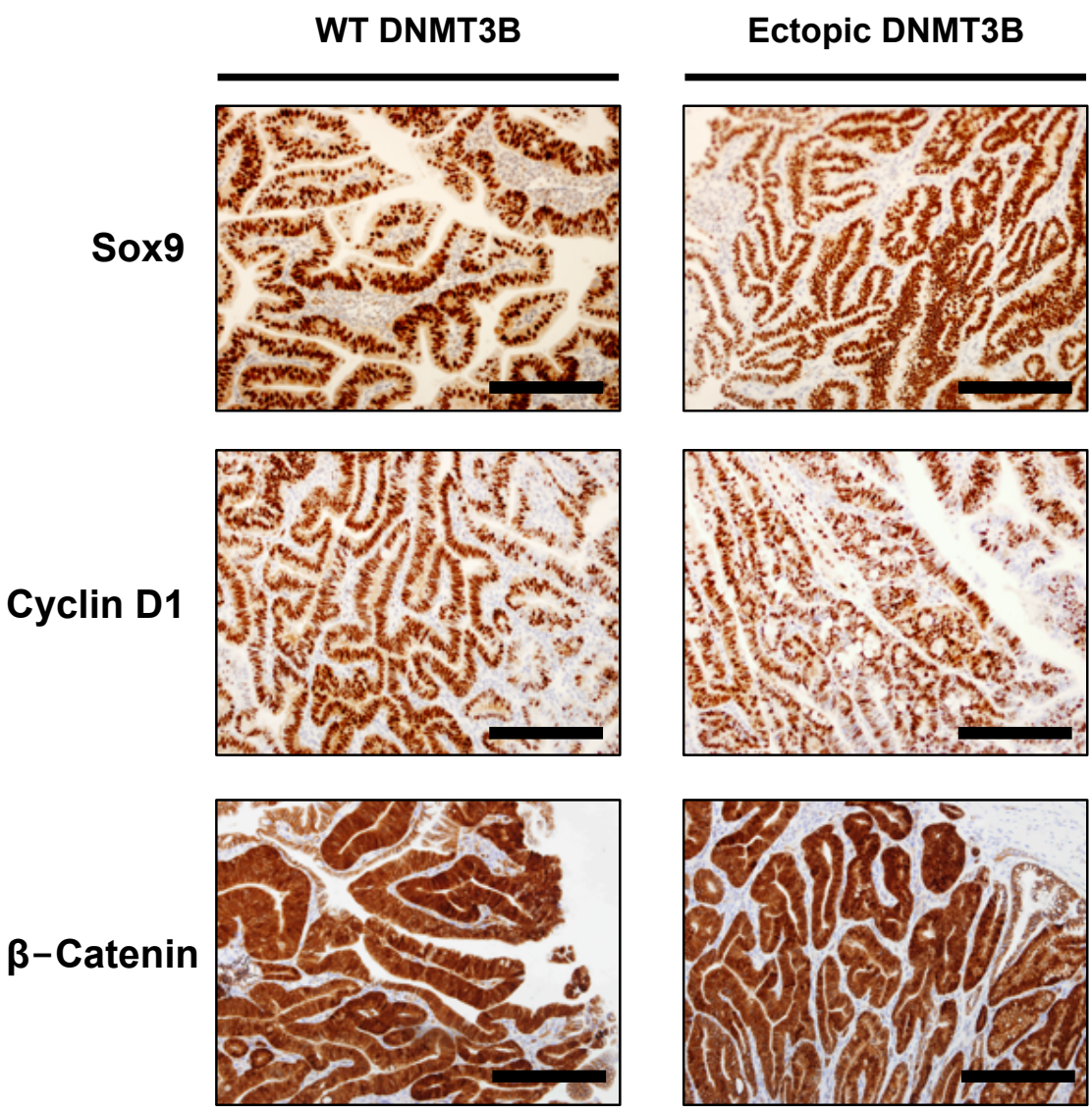

Figure 6-9 Wnt pathway activation is demonstrable in the tumours of *VilCreEr^{T2};^{LSL}Braf^{V600E}* mice but is not affected by DNMT3B ectopic expression

Representative immunohistochemistry images for Sox9, Cyclin D1 and β-catenin in the small intestinal tumours of *VilCreEr^{T2};^{LSL}Braf^{V600E}+/-;R26-M2-rtTA+/-;Col1a1-tetO-Dnmt3b1+/-* ("Ectopic DNMT3B") cases and *VilCreEr^{T2};^{LSL}Braf^{V600E}+/-;R26-M2-rtTA+/-;Col1a1-tetO-Dnmt3b1-/-* ("WT DNMT3B") controls at clinical end-point. Tumours from *VilCreEr^{T2};^{LSL}Braf^{V600E}* mice demonstrate nuclear and cytoplasmic β-catenin staining, and strongly positive Sox9 and Cyclin D1 expression, though this is unaltered by, and does not require DNMT3B ectopic expression. Scale-bar = 200μM; n=3 *vs* 3 biological replicates.

6.3.3 Conditional intestine-specific knockout of *Dnmt3b* impairs intestinal carcinogenesis in *VilCreER^{T2}; ^{LSL}Braf^{V600E}* mice

Given the striking acceleration of *Braf^{V600E}*-mediated intestinal tumourigenesis associated with ectopic DNMT3B expression, the converse experiment was performed, with intestine-specific deletion of *Dnmt3b* achieved using the *Dnmt3b$^{fl/fl}$* transgenic allele described above. *VilCreEr^{T2}; ^{LSL}Braf^{V600E}*+/- mice were crossed to the *Dnmt3b$^{fl/fl}$* strain, and the resultant offspring intercrossed to generate cohorts of *VilCreEr^{T2};^{LSL}Braf^{V600E}*+/-*;Dnmt3b$^{fl/fl}$* cases, and *VilCreEr^{T2};^{LSL}Braf^{V600E}*+/-*;Dnmt3b$^{wt/wt}$* controls. As the *Dnmt3b$^{fl/fl}$* allele was on a mixed (B6;129S4) genetic background, littermates were used as controls. Efficient *Dnmt3b* floxing was first confirmed by Western blotting of intestinal protein lysates from induced *Dnmt3b$^{fl/fl}$* and *Dnmt3b$^{wt/wt}$* mice (Figure 6-10).

VilCreEr^{T2};^{LSL}Braf^{V600E}+/-*;Dnmt3b$^{fl/fl}$* cases (n=14), and *VilCreEr^{T2};^{LSL}Braf^{V600E}*+/-*;Dnmt3b$^{wt/wt}$* controls (n=12) were induced by a single intraperitoneal injection of 80mg/kg tamoxifen, and monitored for clinical signs of illness, including weight loss, hunching and pedal pallor (anaemia). Mice were sacrificed when they exhibited >20% weight loss, or exhibited two or more clinical signs of illness.

Significantly, and complementing the data generated in the converse experiment, combined *Dnmt3b* deletion together with activated *Braf^{V600E}* in the murine intestine resulted in increased overall survival compared to *Braf^{V600E}* alone. Median post-survival induction in *Dnmt3b* wild-type mice was 522.5 days, compared to 609 days in mice with intestine-specific *Dnmt3b* deletion (Figure 6-11). Both *VilCreEr^{T2};^{LSL}Braf^{V600E}*+/-*;Dnmt3b$^{fl/fl}$* mice and *VilCreEr^{T2};^{LSL}Braf^{V600E}*+/-*;Dnmt3b$^{wt/wt}$* controls developed small intestinal but not colonic tumours. Mirroring the situation in the converse experiment however, *Dnmt3b* deletion did not significantly alter the total number of intestinal tumours in *VilCreEr^{T2};^{LSL}Braf^{V600E}*+/- mice (Figure 6-12). As an additional control to ensure that this observed result was not influenced by the mixed genetic background of this strain, survival and total intestinal tumour number were compared between *VilCreEr^{T2};^{LSL}Braf^{V600E}*+/-*;Dnmt3b$^{wt/wt}$* mice and *VilCreEr^{T2};^{LSL}Braf^{V600E}*+/- controls (i.e. wild-type, "endogenous" *Dnmt3b*) from the ectopic expression experiment, which were on an inbred C57BL/6 background. No significant difference in survival or total number of intestinal tumours was demonstrable between these two cohorts (median survival in C57BL/6 mice was 489 days compared to 522.5 in B6;129S4 mixed-background mice) implying that the survival advantage conferred by *Dnmt3b* deletion in *VilCreEr^{T2};^{LSL}Braf^{V600E}*+/- mice was not influenced by the mixed genetic background of this strain (Figure 6-13).

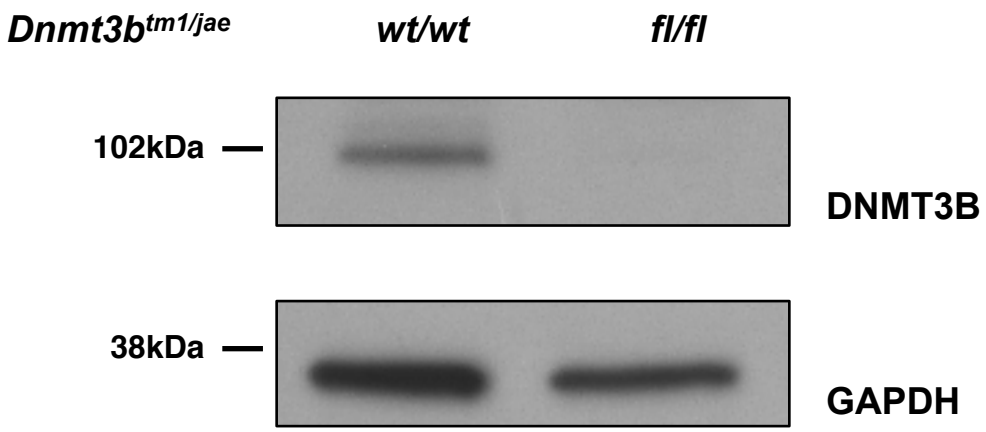

Figure 6-10 Efficient *Dnmt3b* intestinal floxing was confirmed by Western blot

Western blot of whole cell lysates from mouse intestine from a *Dnmt3b*$^{fl/fl}$ case and wild-type control. *VilCreEr*^{T2}*;Dnmt3b*$^{fl/fl}$, and *VilCreEr*^{T2}*;Dnmt3b*$^{wt/wt}$ mice were induced by a single intraperitoneal injection of 80mg/kg tamoxifen and harvested for intestinal tissue for protein lysate. Protein lysates were separated by SDS-PAGE, blotted to PVDF, and probed for DNMT3B with IMG184A. Efficient knockdown of DNMT3B is demonstrated in the *Dnmt3b*$^{fl/fl}$ specimen (n=1 biological replicate).

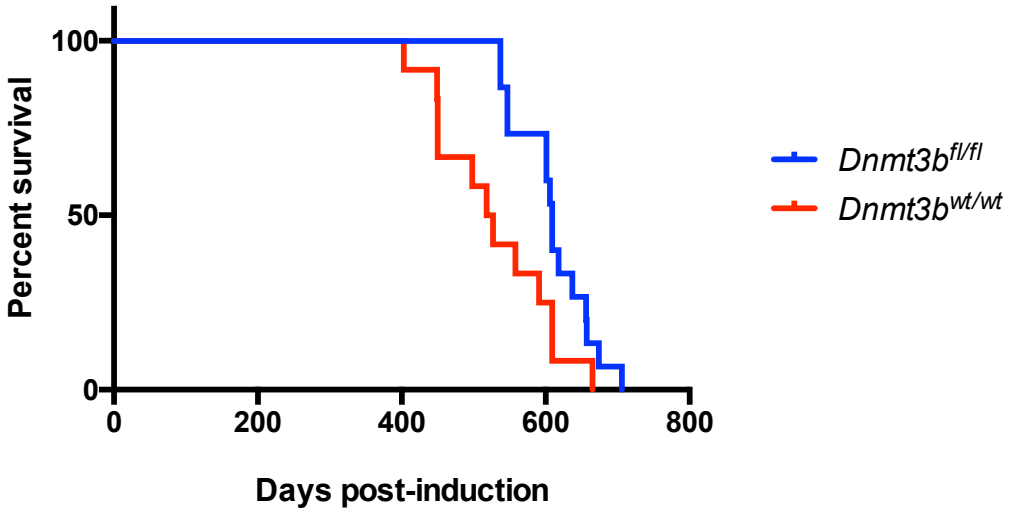

Figure 6-11 *Dnmt3b* knockout prolongs survival in *VilCreER^{T2};^{LSL}Braf^{V600E}* mice

Kaplan-Meier curve comparing survival in *VilCreER^{T2};^{LSL}Braf^{V600E}* mice with wild-type or floxed *Dnmt3b*. *VilCreER^{T2};^{LSL}Braf^{V600E}+/-;Dnmt3b$^{fl/fl}$* cases (n=14), and *VilCreER^{T2};^{LSL}Braf^{V600E}+/-;Dnmt3b$^{wt/wt}$* controls (n=12) were induced by a single intraperitoneal injection of 80mg/kg tamoxifen, and sacrificed at clinical end-point. A significant survival advantage is conferred by intestine-specific *Dnmt3b* deletion: median post-survival induction in *Dnmt3b* wild-type mice was 522.5 days, compared to 609 days in mice with intestine-specific *Dnmt3b* deletion. Log-Rank (Mantel-Cox) test p=0.02.

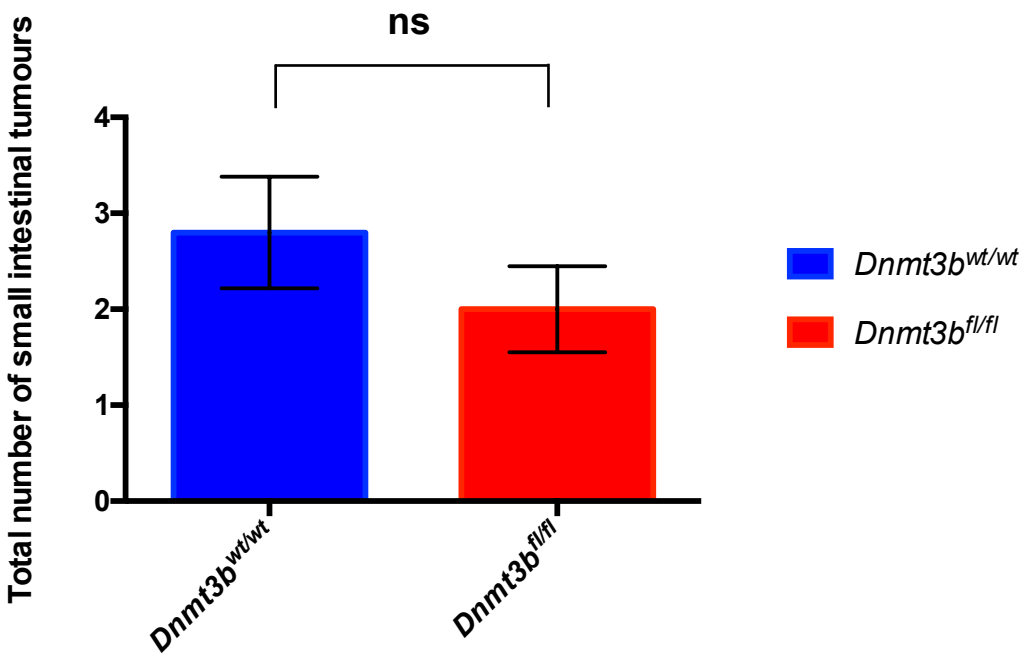

Figure 6-12 Total small intestinal tumour number is unaltered in *VilCreEr^{T2};^{LSL}Braf^{V600E}* mice upon deletion of *Dnmt3b*

Bar-chart of small intestinal tumour number at clinical end-point in *VilCreEr^{T2};^{LSL}Braf^{V600E};Dnmt3b$^{fl/fl}$* cases and *VilCreEr^{T2};^{LSL}Braf^{V600E};Dnmt3b$^{wt/wt}$* controls. The total number of small intestinal tumours does not differ significantly between cohorts. Error bars represent SEM. Mann Whitney test p=0.42; n=5 *vs* 5 biological replicates.

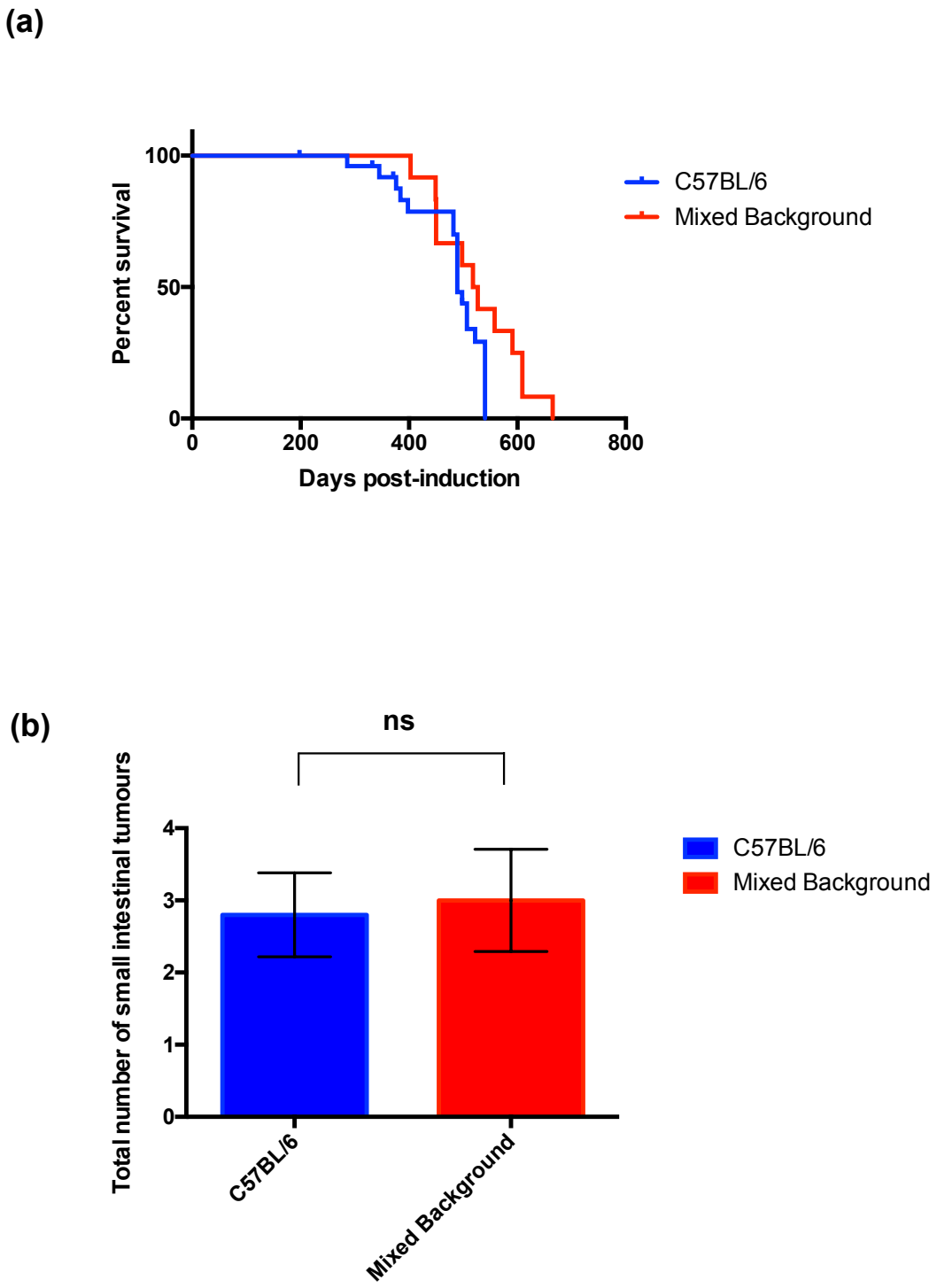

Figure 6-13 A mixed genetic background does not significantly alter survival or total intestinal tumour number in *VilCreEr^{T2};^{LSL}Braf^{V600E}* mice

Survival and total small intestinal tumour number were compared between *VilCreEr^{T2};^{LSL}Braf^{V600E}* mice on inbred C57Bl6 and mixed B6;129S4 genetic backgrounds. **(a)** Kaplan-Meier curve comparing survival in *VilCreEr^{T2};^{LSL}Braf^{V600E}* mice from an inbred C57BL/6 background (n=25) and mixed B6;129S4 (n=12) genetic background. No statistically-significant difference in survival is demonstrated: median survival in C57BL/6 mice was 489 days compared to 522.5 in B6;129S4 mixed-background mice. Log Rank (Mantel Cox) test p=0.063. (**b**) Comparison of total small intestinal tumour number at clinical endpoint in *VilCreEr^{T2};^{LSL}Braf^{V600E}* mice from an inbred C57BL/6 background (n=5) and mixed B6;129S4 (n=5) genetic background. No statistically-significant difference in tumour number is observed. Error bars represent SEM; Mann Whitney test p=0.992.

6.3.4 The effects of DNMT3B on survival are abrogated in the context of activated Wnt signalling

In chapter 5, it was demonstrated that ectopic DNMT3B1 expression in the context of activated oncogenic $BRAF^{V600E}$ alters the expression of several Wnt regulators and target genes. Furthermore, in the $Apc^{Min/+}$ model, ectopic DNMT3B expression has been demonstrated to promote intestinal tumourigenesis associated with silencing of the secreted Wnt antagonists *Sfrp2*, *Sfrp4* and *Sfrp5* [205]. Furthermore, as demonstrated above, *Dnmt3b* knockout in $VilCreEr^{T2};^{LSL}Braf^{V600E}$+/- mice delays the development of intestinal tumours in this model. In chapter 5 however, it was demonstrated that DNMT3B knockdown in a $BRAF^{V600E}$-mutant colon cancer cell line, LS411N (which harbours an *APC* mutation and exhibits activated Wnt signalling) did not affect proliferation. As outlined in the introduction to this thesis, Wnt signalling is activated in both murine and human serrated neoplasia. It was therefore pertinent to address whether the apparent oncogenic function of DNMT3B in $Braf^{V600E}$-mediated murine intestinal carcinogenesis was maintained in the context of activated Wnt signalling.

To model the effects of activated Wnt signalling in $Braf^{V600E}$–mediated intestinal carcinogenesis, additional mouse models were generated. The Apc^{tm1Tno} strain (hereafter referred to as $Apc^{fl/wt}$) was obtained on an inbred C57BL/6 background from the Sansom laboratory. In this model, *loxP* sites are located within introns 13 and 14 of the *Apc* gene, and *Cre* recombination results in a frameshift mutation at codon 580, and results in a non-functioning protein [460]. Heterozygous $Apc^{fl/wt}$ mice were crossed to $VilCreEr^{T2};^{LSL}Braf^{V600E}$+/- mice to generate $VilCreEr^{T2};^{LSL}Braf^{V600E}$+/-;$Apc^{fl/wt}$ cohorts.

Survival was first compared between $VilCreEr^{T2};^{LSL}Braf^{V600E}$+/- (n=17) and $VilCreEr^{T2};^{LSL}Braf^{V600E}$+/-;$Apc^{fl/wt}$ (n=34) cohorts. Mice were induced by a single intraperitoneal injection of 80mg/kg tamoxifen, and monitored for clinical signs of illness, including weight loss, hunching, rectal prolapse, and pedal pallor (anaemia). Mice were sacrificed when they exhibited >20% weight loss, or exhibited two or more clinical signs of illness. $VilCreEr^{T2};^{LSL}Braf^{V600E}$+/-;$Apc^{fl/wt}$ mice exhibited a drastically-accelerated intestinal tumour phenotype, reaching clinical endpoint at a median of 76 days post-induction, compared to 498 days post-induction for $VilCreEr^{T2};^{LSL}Braf^{V600E}$+/- controls (Figure 6-14). Consistent with this drastic acceleration of the $Braf^{V600E}$ model, $VilCreEr^{T2};^{LSL}Braf^{V600E}$+/-;$Apc^{fl/wt}$ mice developed significantly more intestinal tumours, and unlike "$Braf^{V600E}$-only" controls, developed tumours in both the small intestine and colon (Figure 6-15).

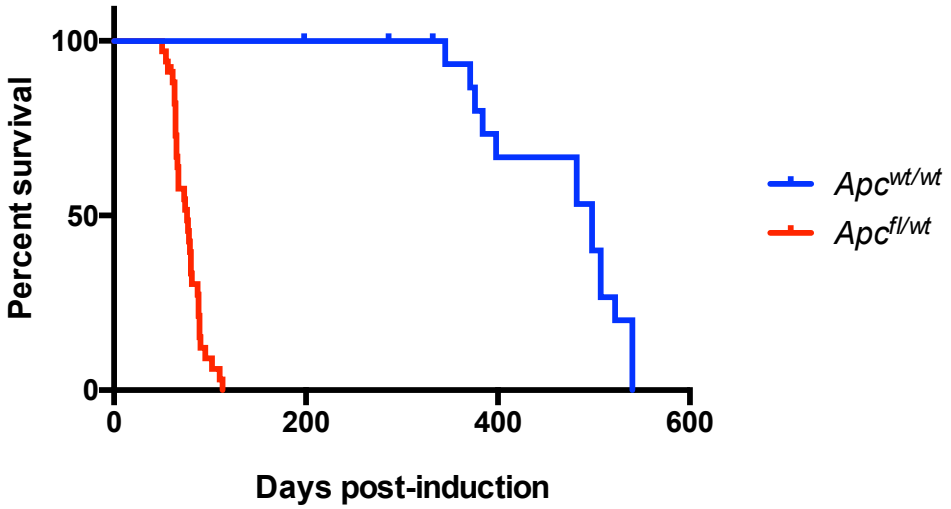

Figure 6-14 Activated Wnt signalling dramatically decreases survival in *VilCreEr^{T2};^{LSL}Braf^{V600E}* mice

Kaplan-Meier curve comparing survival in *VilCreEr^{T2};^{LSL}Braf^{V600E}* and *VilCreEr^{T2};^{LSL}Braf^{V600E};Apc$^{fl/wt}$* mice. *VilCreEr^{T2};^{LSL}Braf^{V600E}+/-;Apc$^{fl/wt}$* cases (*n*=17) and *VilCreEr^{T2};^{LSL}Braf^{V600E}+/-* controls (*n*=34) were induced by a single intraperitoneal injection of 80mg/kg tamoxifen and harvested at clinical endpoint. A significant reduction in survival is seen in mice with the *Apc$^{fl/wt}$* allele compared to those with wild-type *Apc*. Median post-induction survival in *VilCreEr^{T2};^{LSL}Braf^{V600E}+/-;Apc$^{fl/wt}$* mice was 76 days compared to 498 days post-induction for *VilCreEr^{T2};^{LSL}Braf^{V600E}+/-* controls. Log-rank (Mantel-Cox) test p<0.0001.

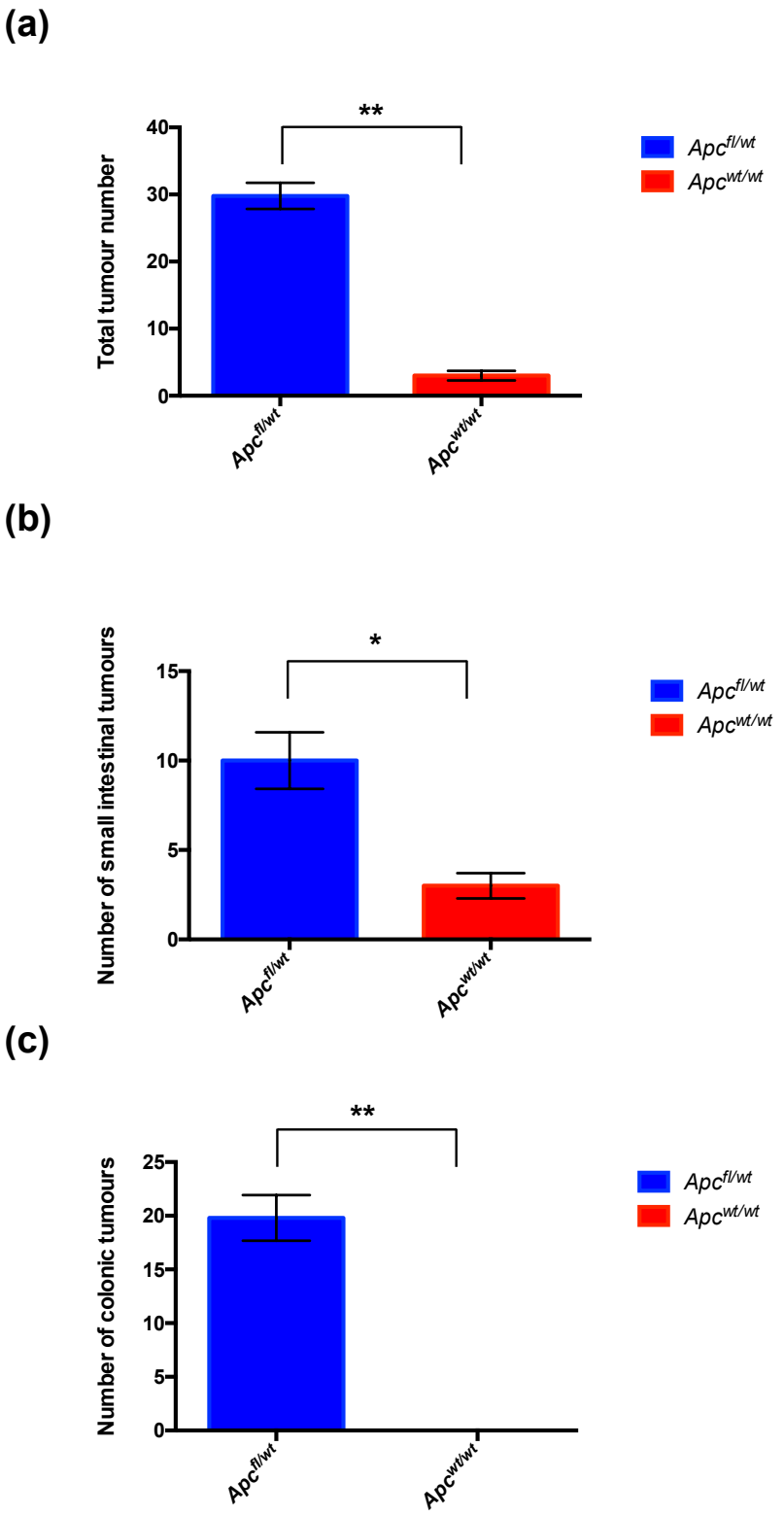

Figure 6-15 Activated Wnt signalling significantly alters the phenotype of *VilCreEr^{T2};^{LSL}Braf^{V600E}* mice

Bar-charts comparing **(a)** total intestinal tumour number **(b)** small intestinal tumour number and **(c)** colonic tumour number at clinical endpoint in *VilCreEr^{T2};^{LSL}Braf^{V600E};Apc$^{fl/wt}$* cases (n=5) and *VilCreEr^{T2};^{LSL}Braf^{V600E}* controls (n=5). Error bars represent SEM. In comparison to *VilCreEr^{T2};^{LSL}BRAF^{V600E};Apc$^{wt/wt}$* controls, *VilCreEr^{T2};^{LSL}BRAF^{V600E};Apc$^{fl/wt}$* mice develop significantly more tumours overall (Mann Whitney test p=0.008); in the small intestine (Mann Whitney test p=0.023); and in the colon (Mann Whitney test p=0.008).

In order to examine the effects of DNMT3B ectopic expression on *Braf*^{V600E}-mediated serrated neoplasia in the context of activated Wnt signalling, *VilCreEr*^{T2}*;*^{LSL}*Braf*^{V600E}*+/-;Apc*$^{fl/wt}$ mice were crossed to *VilCreEr*^{T2}*;* ^{LSL}*Braf*^{V600E}*+/-;R26-M2-rtTA+/-;Col1a1-tetO-Dnmt3b1+/-* cohorts, and the resultant offspring interbred to generate *VilCreEr*^{T2}*;*^{LSL}*Braf*^{V600E}*+/-;R26-M2-rtTA+/-;Col1a1-tetO-Dnmt3b1+/-;Apc*$^{fl/wt}$ mice ("cases"). Cases were induced by a single intraperitoneal injection of 80mg/kg tamoxifen and 0.5mg/mL of doxycycline hyclate in 1% sucrose (administered *ad libitum* in the drinking water and changed three times weekly). Control mice for this experiment were either the same genotype as cases (n=6), or wild-type for either the *R26-M2-rtTA* (n=18) or *Col1a1-tetO-Dnmt3b1* (n=5) or both (n=4) alleles. All mice were on an inbred C57BL/6 background. Controls were induced by a single intraperitoneal injection of 80mg/kg tamoxifen, but were administered 1% sucrose in the drinking water without the addition of doxycyline. Following induction, mice were monitored for clinical signs of disease and sacrificed when they exhibited >20% weight loss, or exhibited two or more clinical signs of illness. Strikingly, and in notable contrast to *VilCreEr*^{T2}*;*^{LSL}*Braf*^{V600E} mice, ectopic DNMT3B expression did not significantly alter survival in *VilCreEr*^{T2}*;*^{LSL}*Braf*^{V600E}*+/-;Apc*$^{fl/wt}$ mice. Median post-induction survival in case mice (i.e. ectopic DNMT3B) was 71 days compared to 76 days in wild-type DNMT3B controls (Figure 6-16). Perhaps somewhat surprisingly however, *VilCreEr*^{T2}*;*^{LSL}*Braf*^{V600E}*+/-;R26-M2-rtTA+/-;Col1a1-tetO-Dnmt3b1+/-;Apc*$^{fl/wt}$ cases developed significantly more tumours than *Dnmt3b* wild-type controls, although whilst the total tumour burden was increased, the increase in tumour number was limited to the small intestine (Figure 6-17).

In the converse experiment, *VilCreEr*^{T2}*;*^{LSL}*Braf*^{V600E}*+/-;Apc*$^{fl/wt}$ mice were crossed to *VilCreEr*^{T2}*;*^{LSL}*Braf*^{V600E}*+/-;Dnmt3b*$^{fl/fl}$ cohorts, and the resultant offspring interbred to produce *VilCreEr*^{T2}*;*^{LSL}*Braf*^{V600E}*+/-;Apc*$^{fl/wt}$*;Dnmt3b*$^{fl/fl}$ cases (n=16) and *VilCreEr*^{T2}*;*^{LSL}*Braf*^{V600E}*+/-;Apc*$^{fl/wt}$*;Dnmt3B*$^{wt/wt}$ controls (n=9). As these mice were on a mixed genetic background, littermate controls were used. Cases and controls were induced by a single intraperitoneal injection of 80mg/kg tamoxifen, and monitored for clinical signs of illness. Mirroring the converse experiment above, *Dnmt3b* knockout did not alter survival in *VilCreEr*^{T2}*;*^{LSL}*Braf*^{V600E}*+/-;Apc*$^{fl/wt}$ mice. Median survival post-induction was 95 days in *Dnmt3b*$^{fl/fl}$ mice compared to 92 days in *Dnmt3b*$^{wt/wt}$ controls (Figure 6-18). In contrast to the ectopic expression experiment however, *Dnmt3b* knockout did not significantly alter the number of intestinal tumours in *VilCreEr*^{T2}*;*^{LSL}*Braf*^{V600E}*+/-;Apc*$^{fl/wt}$ mice (Figure 6-19).

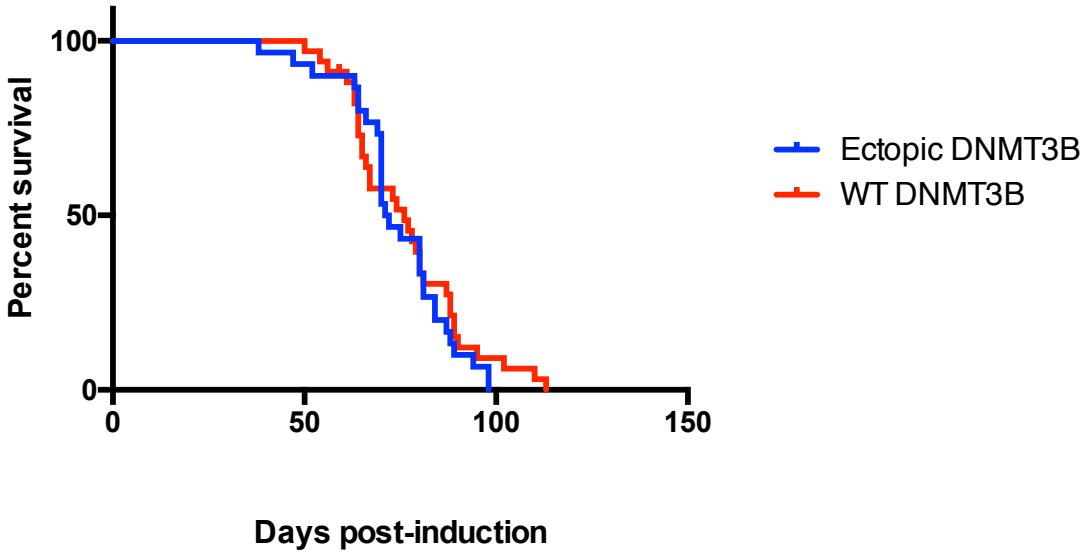

Figure 6-16 Ectopic expression of DNMT3B does not alter survival in *VilCreEr^{T2};^{LSL}Braf^{V600E};Apc$^{fl/wt}$* mice

Kaplan-Meier curve comparing survival in *VilCreEr^{T2};^{LSL}BRAF^{V600E};Apc$^{fl/wt}$* mice with and without ectopically expressed DNMT3B. *VilCreEr^{T2};^{LSL}Braf^{V600E}+/-;R26-M2-rtTA+/-;Col1a1-tetO-Dnmt3b1+/-;Apc$^{fl/wt}$* cases (n=30) and controls (n=33) were induced, and sacrificed at clinical endpoint. Control mice were either the same genotype as cases (n=6), or wild-type for either the *R26-M2-rtTA* (n=18) or *Col1a1-tetO-Dnmt3b1* (n=5) or both (n=4) alleles. Cases were induced by a single intraperitoneal injection of 80mg/kg tamoxifen and 0.5mg/mL of doxycycline hyclate in 1% sucrose administered *ad libitum* in the drinking water. Controls were induced by a single intraperitoneal injection of 80mg/kg tamoxifen, but were administered 1% sucrose in the drinking water without the addition of doxycyline. No significant difference is seen in survival between cohorts. Median post-induction survival in case mice (i.e. ectopic DNMT3B) was 71 days compared to 76 days in wild-type DNMT3B controls. Log-rank (Mantel-Cox) test p=0.84.

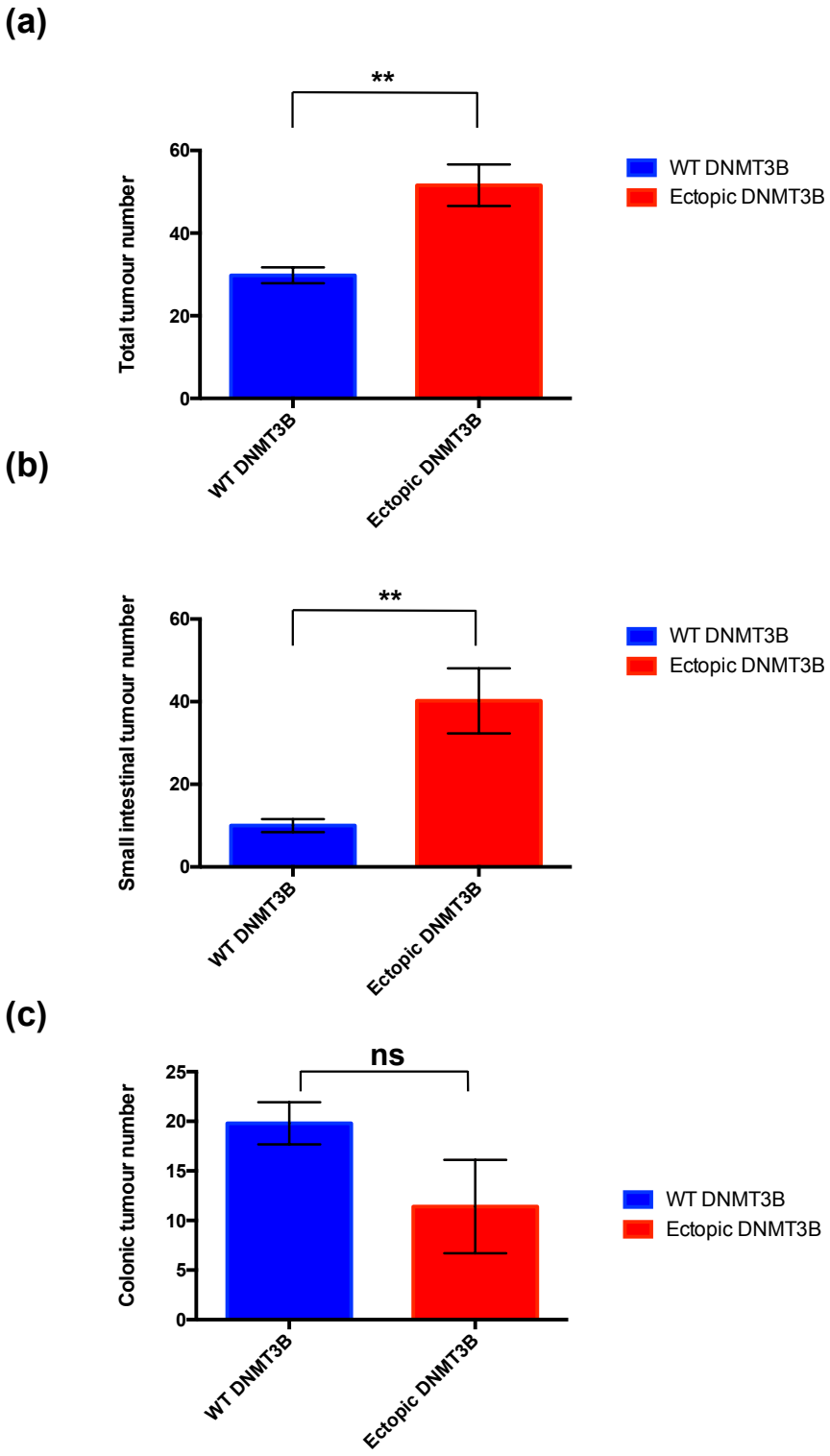

Figure 6-17 Ectopic DNMT3B expression increases the tumour burden in *VilCreEr^{T2};^{LSL}Braf^{V600E};Apc$^{fl/wt}$* mice

Bar-charts comparing **(a)** total intestinal tumour number **(b)** small intestinal tumour number and **(c)** colonic tumour number in *VilCreEr^{T2};^{LSL}Braf^{V600E};Apc$^{fl/wt}$* with ectopic DNMT3B (cases; n=5) or wild-type DNMT3B (controls; n=5) at clinical endpoint. Error bars represent SEM. In comparison to wild-type DNMT3B controls, *VilCreEr^{T2};^{LSL}Braf^{V600E};Apc$^{fl/wt}$* mice with ectopically-expressed DNMT3B develop significantly more intestinal tumours (Mann-Whitney test p=0.008), and small intestinal tumours (Mann-Whitney test p=0.008). Colonic tumour number is unaffected by ectopic DNMT3B expression (Mann-Whitney test p=0.134).

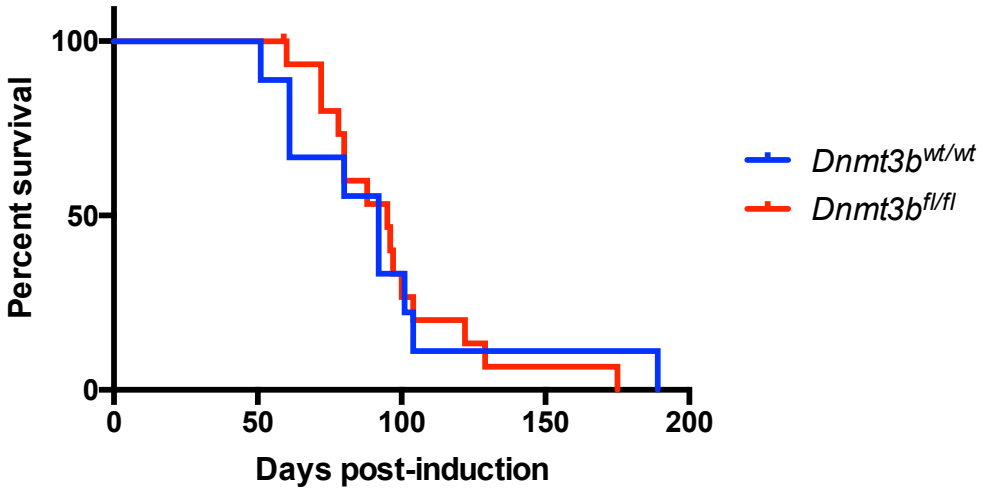

Figure 6-18 *Dnmt3b* knockout does not alter survival in *VilCreEr^{T2};^{LSL}Braf^{V600E};Apc$^{fl/wt}$* mice

Kaplan-Meier curve comparing survival between *VilCreEr^{T2};^{LSL}Braf^{V600E};Apc$^{fl/wt}$;Dnmt3b$^{fl/fl}$* cases (n=16) and *VilCreEr^{T2};^{LSL}Braf^{V600E};Apc$^{fl/wt}$;Dnmt3b$^{wt/wt}$* controls (n=9). Cases and controls were induced by a single intraperitoneal injection of 80mg/kg tamoxifen, and sacrificed at clinical endpoint. No significant difference is seen in survival between cohorts. Median survival post-induction was 95 days in *Dnmt3b$^{fl/fl}$* mice compared to 92 days in *Dnmt3b$^{wt/wt}$* controls. Log-rank (Mantel-Cox) test p=0.995.

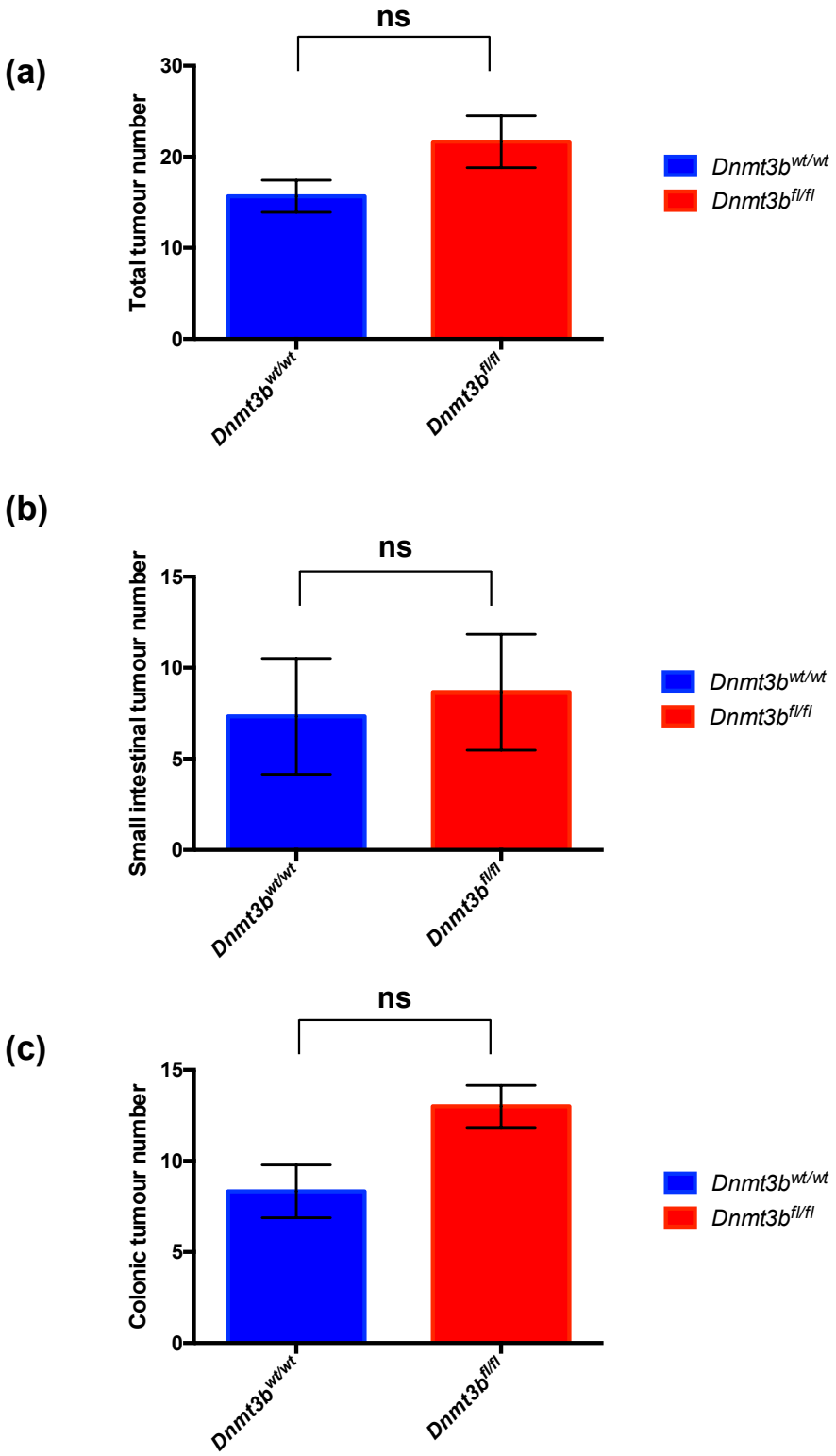

Figure 6-19 *Dnmt3b* knockout does not alter tumour burden in *VilCreEr^{T2}; ^{LSL}Braf^{V600E};Apc$^{fl/wt}$* mice

Bar-charts comparing **(a)** total intestinal tumour number **(b)** small intestinal tumour number and **(c)** colonic tumour number between *VilCreEr^{T2};^{LSL}Braf^{V600E};Apc$^{fl/wt}$;Dnmt3b$^{fl/fl}$* cases (n=3) and *VilCreEr^{T2};^{LSL}Braf^{V600E};Apc$^{fl/wt}$;Dnmt3b$^{wt/wt}$* controls (n=3). Error bars represent SEM. Intestine-specific *Dnmt3b* knockout does not significantly alter total, (Mann-Whitney test p=0.25) small intestinal, (Mann Whitney test p=0.7) or colonic (Mann Whitney test p=0.2) tumour number in *VilCreEr^{T2};^{LSL}BRAF^{V600E};Apc$^{fl/wt}$* mice.

6.4 Discussion

In this chapter, the effects of DNMT3B ectopic expression and *Dnmt3b* knockout have been examined in novel murine models of serrated pathway colon cancer driven by an activated $Braf^{V600E}$ oncogene. Significantly, ectopic DNMT3B expression in $VilCreEr^{T2};^{LSL}Braf^{V600E}$+/- mice has been demonstrated to accelerate intestinal tumourigenesis associated with intestine-specific activation of this oncogene. This acceleration is however not associated with an increased tumour burden. Whilst this probably reflects consistency in the clinical criteria used to assess end-point in this model, it raises questions about the mechanism underlying the acceleration of the $Braf^{V600E}$-induced intestinal phenotype. It has previously been demonstrated that ectopic DNMT3B expression promotes tumourigenesis in the $Apc^{Min/+}$ model. Interestingly, and in contrast to the data presented herein, this study did not examine the survival implications of ectopic DNMT3B in this model, but did demonstrate a significant increase in small intestinal and colonic tumour numbers in association with DNMT3B ectopic expression [205].

As DNMT3B was demonstrated in the previous chapter to impair BRAF-induced proliferation arrest, and as a senescence-barrier has been implicated in serrated pathway carcinogenesis, intestinal sections from mice at clinical endpoint were examined for an altered proliferation phenotype in both intestinal crypts and tumours [47,48]. In contrast to the findings of Carragher et al. [47] and in agreement with Rad et al. [46] a crypt senescence phenotype was not observed in $VilCreEr^{T2};^{LSL}Braf^{V600E}$+/- mice. The intestinal crypts of $VilCreEr^{T2};^{LSL}Braf^{V600E}$+/- mice stained strongly and uniformly for the proliferation marker Ki67, and this was unaltered by ectopic DNMT3B expression. It is possible that the failure to observe a crypt senescence phenotype in the current model system is due to differences in the sampling protocol. Whilst mice in the present study were examined at clinical endpoint, Carragher et al. [47] reported crypt senescence at 6 weeks post-induction. It may therefore be relevant to re-examine crypt proliferation at timepoints following induction in the $VilCreEr^{T2};^{LSL}Braf^{V600E}$+/- model. However, as the latency of this model is longer than that reported in the $AhCreEr^{T};^{LSL}Braf^{V600E}$ model, this would necessitate a time-course experiment.

In chapter 5, the impaired proliferation arrest associated with combined expression of DNMT3B and mutant-$BRAF^{V600E}$ was demonstrated to be associated with altered Wnt pathway signalling. Wnt pathway activation has previously been demonstrated to impair the induction of oncogene-induced senescence [429,442,447]. Furthermore, activated Wnt

signalling is a feature of serrated pathway carcinogenesis, and is associated with neoplastic transformation [19,46,47,81]. Finally, DNMT3B has been demonstrated to reduce the expression of secreted Wnt antagonists in the *Apc*$^{Min/+}$ model. There was therefore a strong rationale to examine whether the observed acceleration of *Braf*^{V600E}-mediated intestinal tumourigenesis was associated with altered Wnt signalling. To an extent, the data presented herein are somewhat paradoxical. Whilst no DNMT3B-dependent differences in Wnt effector or target gene (Sox9, Cyclin D1 and β-catenin) expression were demonstrable in the crypts or tumours of *VilCreEr*^{T2}*;*^{LSL}*Braf*^{V600E}+/- mice, the acceleration of *Braf*^{V600E}-mediated intestinal tumourigenesis mediated by ectopic DNMT3B expression was abrogated in the context of combined *Braf*^{V600E} and activated Wnt signalling in the *VilCreEr*^{T2}*;*^{LSL}*Braf*^{V600E}*+/-;Apc*$^{fl/wt}$ model. These somewhat paradoxical findings might be explained by the choice of Wnt targets examined by IHC. Cyclin D1 expression for example is increased by activated BRAF^{V600E}, and indeed it has also been argued that it is not a direct target of Wnt signalling pathway [455,461].

As Wnt pathway activation is associated with neoplastic transformation of sessile serrated lesions, it is possible to speculate that DNMT3B exerts a pro-tumourigenic stimulus at the earlier stages of neoplastic transformation, perhaps mediated in part by altered Wnt signalling, but that this pro-tumourigenic effect is then nullified upon activation of Wnt signalling, reflecting the primacy of this signalling pathway in intestinal tumourigenesis. Whilst by no means explicitly confirmed by these data, this model is perhaps supported by the loss-of-function experiments performed in murine serrated-pathway cancer models in this chapter. Mirroring the converse ectopic expression experiments described above, intestine-specific inactivation of *Dnmt3b* in *VilCreEr*^{T2}*;*^{LSL}*Braf*^{V600E}+/- mice significantly delayed intestinal tumourigenesis and increased survival. As in the ectopic expression mice, and once again contrary to the published data in the *Apc*$^{min/+}$ model, this survival advantage was not associated with a decreased tumour burden [433]. Strikingly however, the delayed intestinal tumourigenesis and survival advantage conferred by *Dnmt3b* inactivation in *VilCreEr*^{T2}*;*^{LSL}*Braf*^{V600E}+/- was not observed in the context of combined *Braf*^{V600E} activation and Wnt signalling in the *VilCreEr*^{T2}*,*^{LSL}*Braf*^{V600E}*+/-;Apc*$^{fl/wt}$ model. Clearly, in order to further this hypothesis, additional experimental work would be required, and might include RNA-sequencing of intestinal crypts from *VilCreEr*^{T2}*,*^{LSL}*Braf*^{V600E}+/- mice with and without DNMT3B ectopic expression, coupled with reduced-representation bisulfite sequencing to determine whether the effect is methylation-dependent. DNMT3B ChIP-seq would also allow assessment of interactions between DNMT3B and Wnt pathway regulators and targets. Functional experiments in

intestinal organoids derived from *VilCreEr^{T2};^{LSL}Braf^{V600E}*+/- by contrast would likely not help with dissection of this mechanism, as activated Wnt signalling is required to maintain intestinal organoids in culture [462].

6.5 Summary

1. Combined ectopic expression of DNMT3B and mutant-BRAF^{V600E} in the mouse intestine significantly accelerates the tumourigenesis associated with activated BRAF^{V600E} but does not alter the overall tumour burden.

2. DNMT3B ectopic expression alone does not lead to intestinal tumourigenesis.

3. A crypt-senescence phenotype is not observed in *VilCreEr^{T2};^{LSL}Braf^{V600E}* mice, and DNMT3B ectopic expression does not affect the crypt proliferation phenotype.

4. Intestine-specific knockout of *Dnmt3b* impairs intestinal tumourigenesis associated with activated oncogenic BRAF^{V600E} and prolongs survival, but without significantly affecting the tumour burden.

5. Intestinal carcinogenesis in *VilCreEr^{T2};^{LSL}Braf^{V600E}* mice with activated Wnt signalling (modelled by crossing to the *Apc$^{fl/wt}$* strain) significantly accelerates intestinal tumourigenesis induced by an activated *Braf^{V600E}* oncogene.

6. The effects of DNMT3B ectopic expression and *Dnmt3b* knockout on survival are lost when *Braf^{V600E}* mutation is combined with activated Wnt signalling.

7. Despite the abrogation of survival effect associated with activated Wnt signalling, ectopic DNMT3B expression increases the total tumour burden in *VilCreEr^{T2};^{LSL}Braf^{V600E}*+/-;*Apc$^{fl/wt}$* mice; though *Dnmt3b* knockout does not have the converse effect.

7 *In silico* analysis of relationships between BRAF, DNMT3B and CIMP in human colorectal adenocarcinoma

7.1 Rationale

In the previous chapters evidence has been presented that mutant-BRAF^{V600E} represses DNMT3B expression and does not directly induce a CpG island methylator phenotype (CIMP). The data presented thusfar herein therefore do not fit with the multitude of correlative data reporting a tight association between *BRAF^{V600E}* mutation and CIMP positivity, and effectively contradict the recently described model that proposes that activated oncogenic BRAF^{V600E} directly induces the CpG island methylator phenotype, and that this may be directly modulated through DNMT3B [40,113,116,355,364]. Paradoxically however, DNMT3B ectopic expression has been demonstrated to exhibit an oncogenic function and/or pro-proliferative function in the context of an activated *BRAF^{V600E}* oncogene in both *in vitro* and *in vivo* model systems. Furthermore, in colon cancer cell lines, no relationship could be demonstrated between DNMT3B expression and BRAF^{V600E} mutation or CIMP positivity, and inactivation of DNMT3B in a CIMP positive cell line did not reverse gene-silencing characteristic of CIMP. Together, these data would be supportive of an oncogenic function for DNMT3B that is independent of CIMP. As the data presented thusfar are limited to the *in vitro* and *in vivo* contexts, it was pertinent to explore the relationships between BRAF^{V600E}, DNMT3B and CIMP in human colorectal adenocarcinoma in order to resolve these apparent conflicts and/or shed new light on the oncogenic function of DNMT3B in human colorectal cancer.

7.2 Aims

The specific aims of this chapter are:

1. To characterise alterations in DNMT3B in human colorectal adenocarcinoma.

2. To investigate the relationship between *BRAF^{V600E}* mutations and aberrant DNA methyltransferase expression in human colorectal adenocarcinoma.

3. To investigate the relationship between *BRAF^{V600E}* mutation and the CpG island methylator phenotype in human colorectal adenocarcinoma.

4. To investigate the relationship between aberrant DNA methyltransferase expression and the CpG island methylator phenotype in human colorectal adenocarcinoma.

5. To investigate the prognostic implications of *BRAF*^{V600E} mutation, CIMP status and DNMT3B overexpression on survival in human colorectal adenocarcinoma.

7.3 Results

7.3.1 DNMT3B expression is higher in tumours without the *BRAF*^{V600E} mutation

In order to investigate how DNMT3B is altered in human colorectal adenocarcinoma, recently-published TCGA data on human colorectal adenocarcinoma were first analysed for *DNMT3B* mutation using the cBioPortal[21] platform in 633 patients [40,463,464]. Recurrent mutations of *DNMT3A* (most commonly at amino acid R882) have recently been described in acute myeloid leukaemia [209]. Surprisingly, given the wealth of data supporting an oncogenic function of DNMT3B in colorectal cancer, *DNMT3B* mutation was infrequent in human colorectal adenocarcinoma. Only 18 (2.84%) of colorectal adenocarcinomas in the TCGA cohort harboured a mutation in the *DNMT3B* gene (Figure 7-1a). Furthermore, no "hot-spot" mutations were identified in the observed *DNMT3B* mutations, and no mutations associated with ICF syndrome (A766P and R840Q) were identified [465]. This contrasts sharply with *DNMT3A* mutations in the leukaemia context, and would favour these *DNMT3B* point mutations representing passenger rather than driver mutations (Table 7-1). Despite the relative paucity of *DNMT3B* mutations in the TCGA cohort, the relationship between *BRAF*^{V600E} mutation was formally explored. *BRAF*^{V600E} mutation data were extrapolated from the human colorectal adenocarcinoma TCGA data set. Paired *BRAF* and *DNMT3B* mutation data were available for 266 patients. No statistically significant relationship was demonstrable between *BRAF*^{V600E} mutation and *DNMT3B* mutation (Fisher's exact test p=0.625) (Figure 7-1b).

[21] http://www.cbioportal.org/index.do

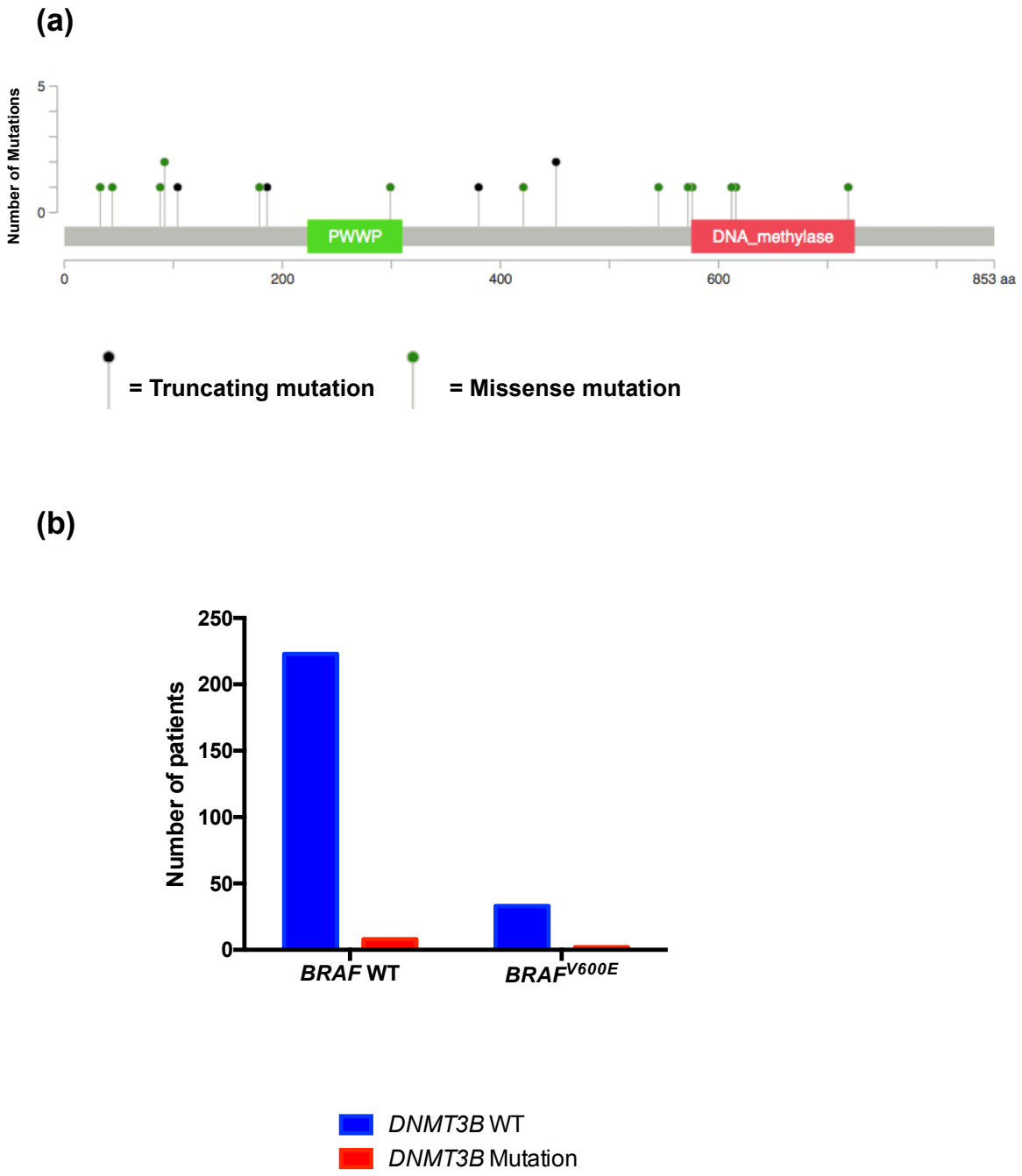

Figure 7-1 *DNMT3B* is infrequently mutated in human colorectal adenocarcinoma and *DNMT3B* mutations do not overlap significantly with *BRAF*^{V600E} mutation

(a) Schematic diagram of the *DNMT3B* gene annotated with *DNMT3B* mutations. *DNMT3B* mutations in human colorectal adenocarcinoma were interrogated in the TCGA cohort using the cBioPortal cancer genomic analysis platform. Mutations in *DNMT3B* are detected in 18 (2.84%) of the sequenced tumours (n=633 patients; plot created using www.cbioportal.org) **(b)** Bar-chart of *DNMT3B* and *BRAF* mutation status in the TCGA human colorectal adenocarcinoma cohort. There is no significant relationship between *BRAF*^{V600E} mutation and *DNMT3B* mutation in human colorectal adenocarcinoma (n=266 patients; Fisher's exact test p=0.625).

Table 7-1 *DNMT3B* mutations in human colorectal adenocarcinoma (TCGA cohort)

TCGA Sample ID	Amino Acid Change	Classification
TCGA-CM-6162-01	V616M	Missense
TCGA-AZ-4315-01	R576Q	Missense
TCGA-G4-6309-01	Y188Tfs*4	Frame-shift deletion
TCGA-AU-6004-01	L454Sfs*136	Frame-shift deletion
TCGA-AA-3492-01	L454Sfs*136	Frame-shift deletion
TCGA-AA-3986-01	R380*	Nonsense
TCGA-AA-3710-01	P44L	Missense
TCGA-AA-3818-01	R92W	Missense
TCGA-AG-3583-01	R92W	Missense
TCGA-AG-3892-01	A421T	Missense
TCGA-AG-A002-01	R299Q	Missense
TCGA-AG-A002-01	D33N	Missense
TCGA-A6-5666-01	R545C	Missense
TCGA-AZ-4315-01	R104*	Nonsense
TCGA-D5-6536-01	V719A	Missense
TCGA-D5-6924-01	R572S	Missense
TCGA-F4-6807-01	G179V	Missense
TCGA-F4-6809-01	P88L	Missense
TCGA-CL-5917-01	A612T	Missense

Examination of expression data for DNMT3B from the TCGA colorectal cancer cohort was next performed. RNA-seq expression data for DNMT3B were available for 459 tumour samples and 41 normal colon mucosa samples. DNMT3B mRNA FPKM expression data from both tumour and normal tissue was first tested for Gaussian distribution using both the D'agostino & Pearson omnibus and Shapiro-Wilk normality tests. Both approaches demonstrated that the DNMT3B mRNA data were not normally distributed. In order to compare expression between cohorts therefore, a non-parametric test was appropriate. A highly significant increase was demonstrated in median DNMT3B FPKM mRNA expression in tumour relative to normal tissue (Mann Whitney test $p<0.0001$) (Figure 7-2a). Furthermore, frequency distribution analysis revealed tight clustering of DNMT3B FPKM mRNA expression in normal colon tissue compared to much more dispersed expression in tumour samples (Figure 7-2b).

Given the highly significant difference in DNMT3B expression observed between tumour and normal tissue, the relationship between $BRAF^{V600E}$ mutation and DNMT3B expression was next explored. Paired *BRAF* mutation data and DNMT3B expression data were available for 207 patients. Median-centred DNMT3B expression was first plotted against *BRAF* mutation status (V600E *versus* wild-type), revealing an apparent clustering of *BRAF* mutation and low DNMT3B expression (Figure 7-3a). Median DNMT3B expression was then explicitly compared between $BRAF^{V600E}$ mutant and *BRAF* wild-type tumours. Median DNMT3B expression was significantly higher in *BRAF* wild-type tumours than $BRAF^{V600E}$ mutant tumours (Mann Whitney test $p=0.0002$) (Figure 7-3b).

Given the strong evidence reviewed earlier functionally linking $BRAF^{V600E}$ mutation and CIMP, and as DNMT3B expression was significantly lower in $BRAF^{V600E}$ than *BRAF* wild-type tumour populations, it was relevant to examine how expression of other members of the "DNA methylation machinery" varied between these two cohorts. RNA-seq expression data were therefore compared for DNMT1, DNMT3A, DNMT3L, TET1, TET2 and TET3. Data were once again compared for 207 patients for whom paired expression data and $BRAF^{V600E}$ mutation data were available. Expression data were once again tested for normality using both the D'agostino & Pearson omnibus and Shapiro-Wilk normality tests. Both approaches demonstrated a lack of normal distribution in all data sets, necessitating non-parametric analysis. Surprisingly given the significant difference in DNMT3B expression observed between $BRAF^{V600E}$ mutant and *BRAF* wild-type tumours, no statistically significant difference in median expression of DNMT1, DNMT3A, DNMT3L, TET1 or TET3 was demonstrable between $BRAF^{V600E}$ mutant and *BRAF* wild-type tumours

(Mann Whitney test DNMT1 p=0.1172; DNMT3A p=0.263; DNMT3L p=0.402; TET1 p=0.479; TET3 p=0.627). By comparison, TET2 expression was significantly elevated in $BRAF^{V600E}$ mutant tumours relative to BRAF wild-type tumours (Mann Whitney test p=0.021) (Figure 7-4).

Given the lack of absolute expression changes in DNMT1 and DNMT3A associated with $BRAF^{V600E}$ mutation, the ratio of DNMT3A and DNMT3B to DNMT1 expression was compared between $BRAF^{V600E}$ mutant and wild-type tumours. Interestingly, a significant reduction in the DNMT3B:DNMT1 ratio, DNMT3A:DNMT1 and DNMT3B:DNMT3A ratio was observed in $BRAF^{V600E}$ mutant tumours relative to wild-type tumours (Mann Whitney test DNMT3A:DNMT1 p=0.03; DNMT3B:DNMT1 p<0.0001; DNMT3B:DNMT3A p=0.0013) (Figure 7-5). This is of particular interest given aberrant cell-cycle mediated expression of DNMTs has previously been described in cancer cell lines and postulated to be an alternative to individual DNMT overexpression as an explanation for the aberrant methylation demonstrated in cancer [432].

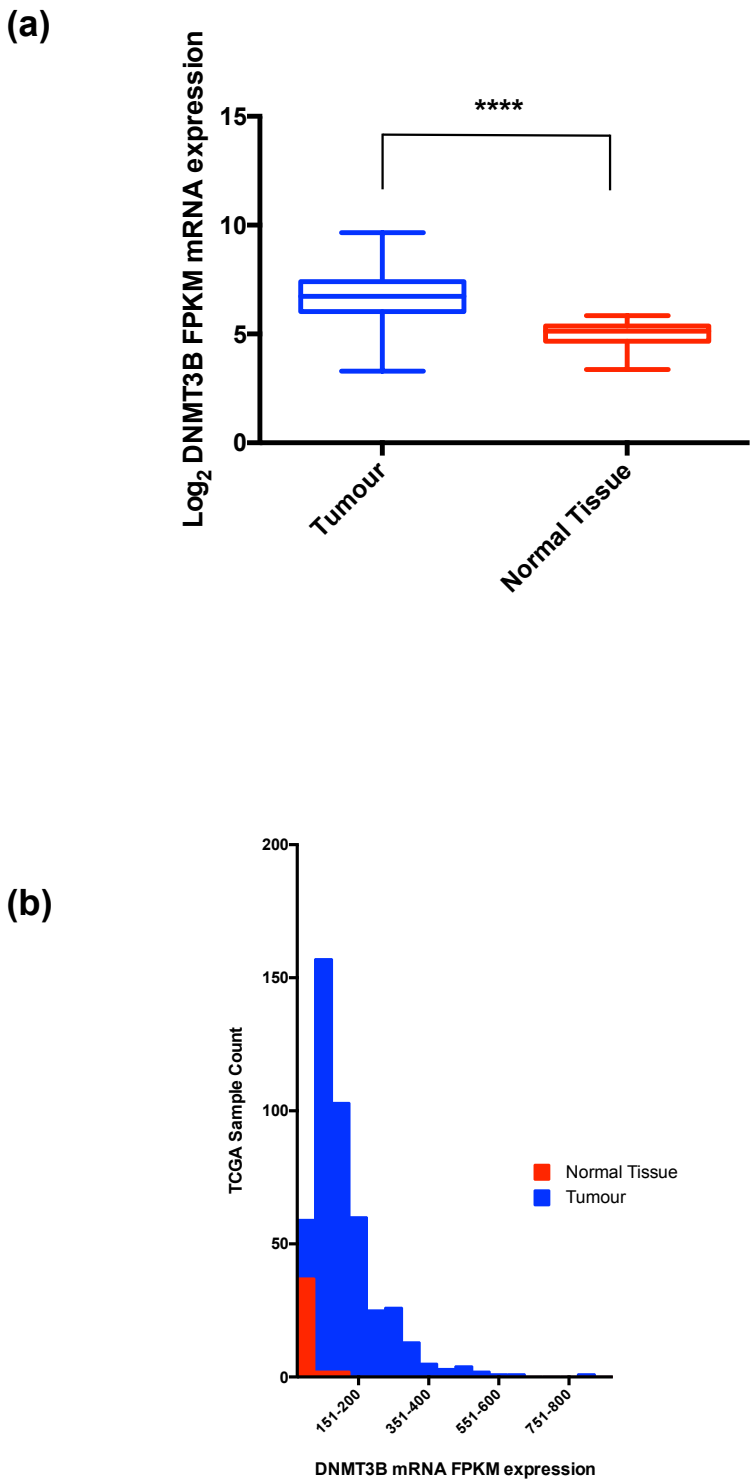

Figure 7-2 DNMT3B is frequently overexpressed in human colorectal adenocarcinoma

(a) Boxplot of DNMT3B mRNA expression (FPKM) in human colorectal adenocarcinoma and corresponding normal colon tissues from the TCGA data set. RNA-seq expression data for DNMT3B were analysed for 459 tumour samples and 41 normal colon mucosa samples. Significantly higher DNMT3B expression is demonstrated in tumour tissue compared to normal tissue. Mann Whitney test $p<0.0001$. **(b)** Frequency distribution histogram of DNMT3B mRNA expression in 459 colorectal tumours and 41 normal colon mucosa samples from the TCGA data set confirming tight clustering of DNMT3B expression within the normal tissue category, compared to more dispersed mRNA expression in the tumour samples.

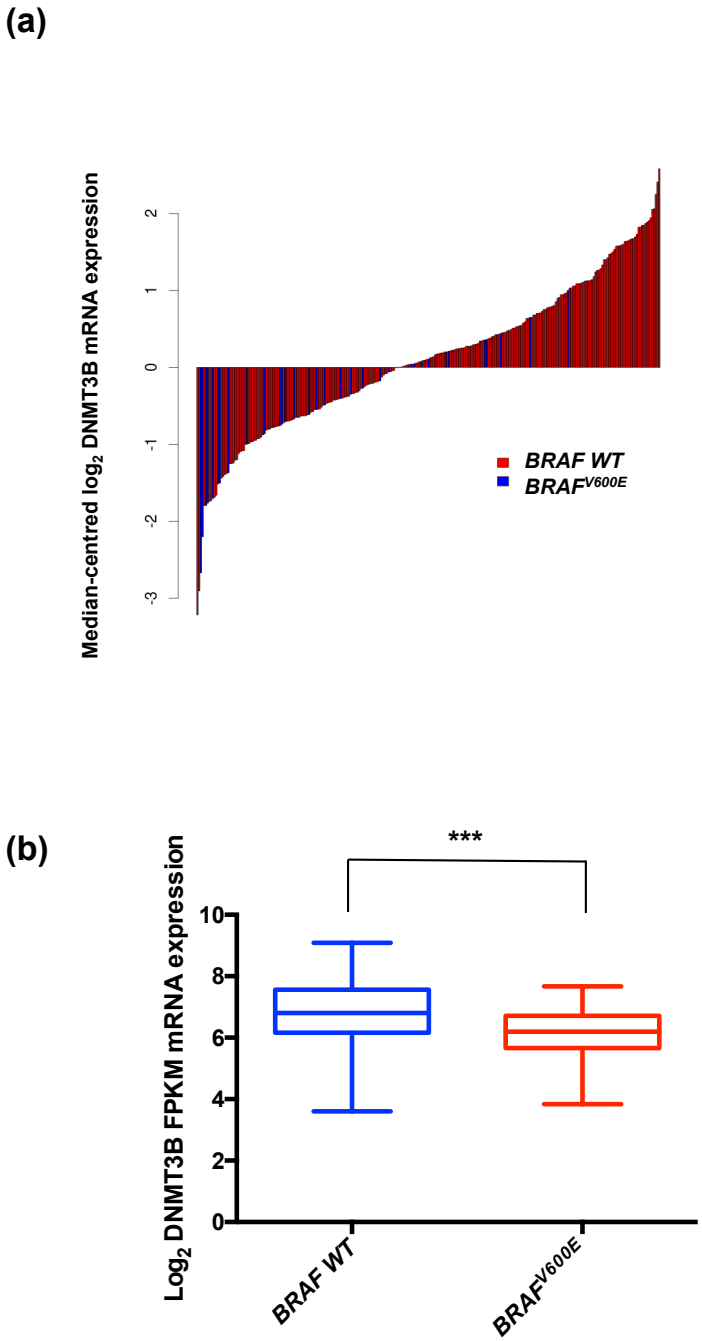

Figure 7-3 DNMT3B mRNA expression is higher in tumours with wild-type *BRAF* than in those with *BRAF*^{V600E} mutation

(a) Bar-chart of median centered log_2 DNMT3B mRNA expression from 207 human colorectal adenocarcinoma samples from the TCGA cohort annotated with *BRAF* mutation status. *BRAF*^{V600E} mutations cluster with low DNMT3B mRNA expression. **(b)** Boxplot of log_2 DNMT3B FPKM mRNA expression and *BRAF*^{V600E} mutation status from 207 human colorectal adenocarcinoma samples from the TCGA cohort. DNMT3B mRNA expression is significantly lower in *BRAF*^{V600E} mutant samples compared to wild-type samples (Mann Whitney test p=0.0002).

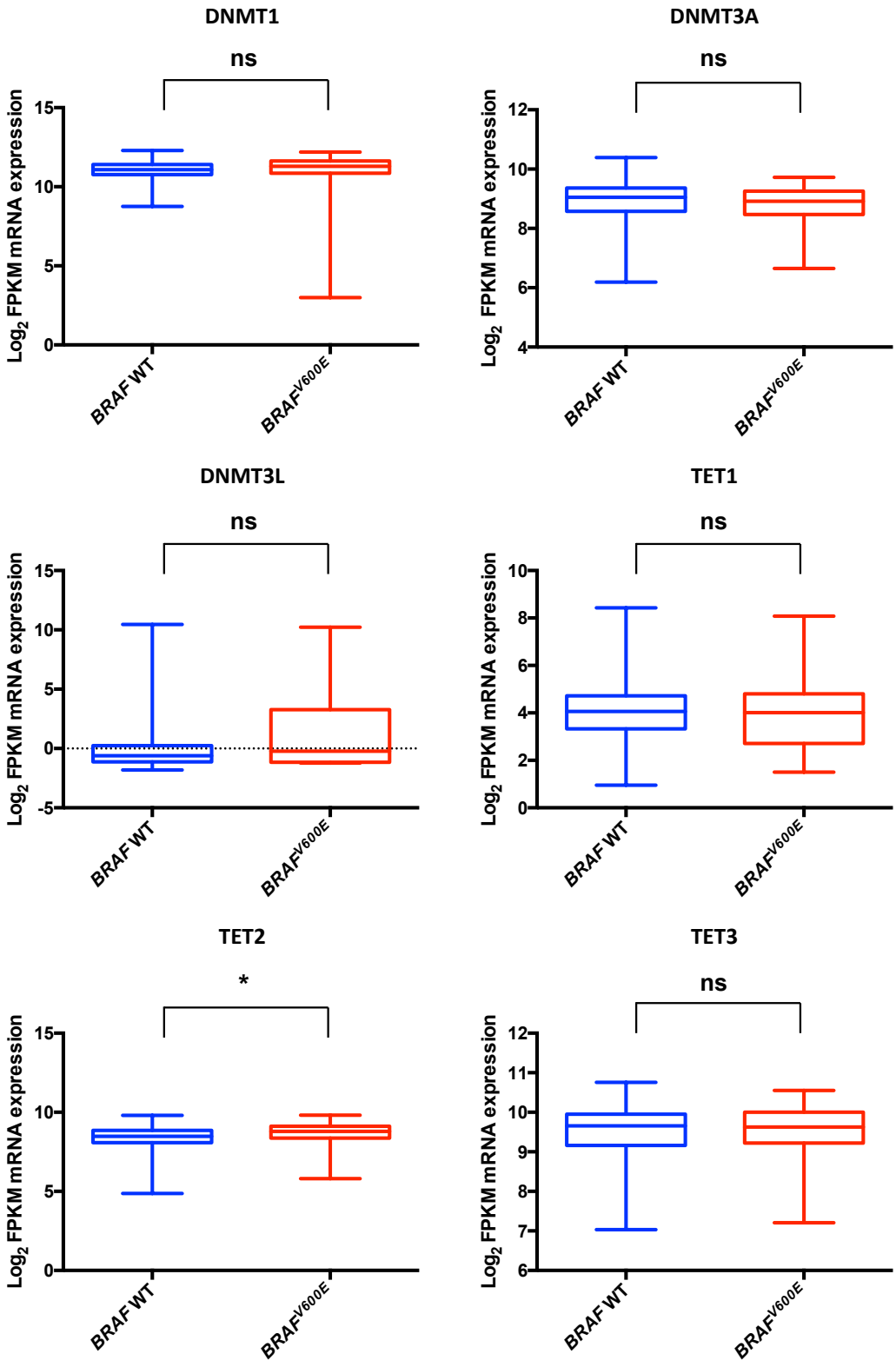

Figure 7-4 Expression of TET2, but not DNMT1, DNMT3A, DNMT3L, TET1 or TET3 is significantly altered in *BRAF*^{V600E} mutant tumours compared to *BRAF* wild-type tumours

Boxplots of Log_2 FPKM mRNA expression of DNMT1, DNMT3A, DNMT3L, TET1, TET2 and TET3 in *BRAF* wild-type and *BRAF*^{V600E} mutant tumour samples from the TCGA cohort of human colorectal adenocarcinoma (n=207 patients). The expression of TET2 is significantly higher in *BRAF*^{V600E} mutant tumours than *BRAF* wild-type tumours. Mann-Whitney p=0.021. DNMT1, DNMT3A, DNMT3L TET1 and TET3 exhibit no significant difference in mean mRNA expression between *BRAF* wild-type and *BRAF*^{V600E} mutant samples. Mann Whitney test for DNMT1= 0.1172; DNMT3A= 0.263; DNMT3L= 0.402; TET1= 0.479; TET3 = 0.627.

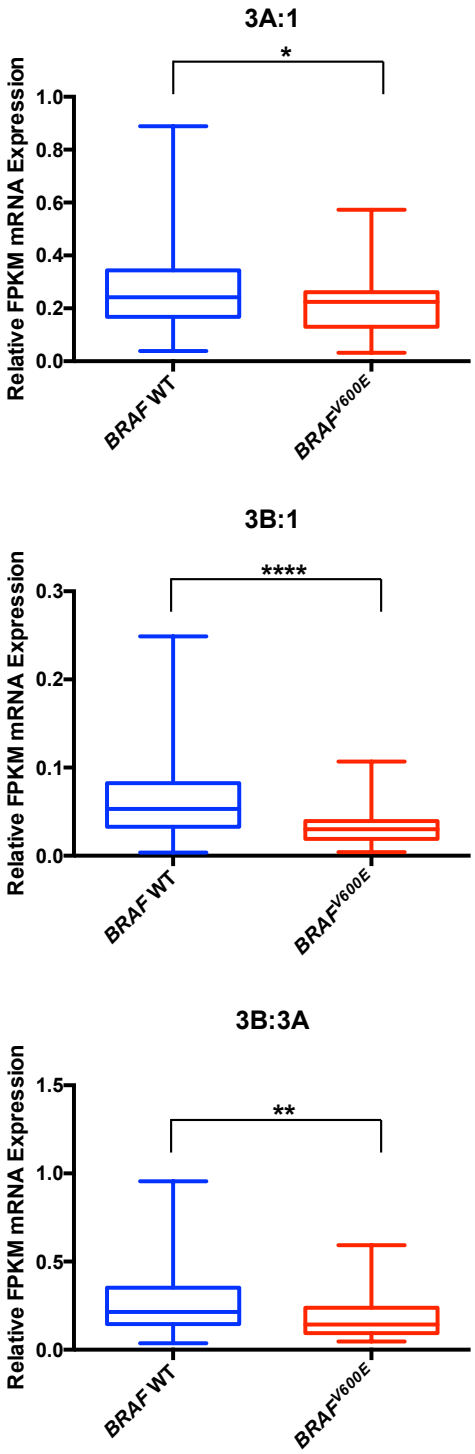

Figure 7-5 The stoichiometry of DNA methyltransferase expression is significantly altered in tumours harbouring an activated *BRAF*^{V600E} mutation

Boxplots of relative FPKM DNMT mRNA expression in *BRAF*^{V600E} mutant tumours and *BRAF* wild-type tumours from the TCGA cohort (n=207 patients). Whilst individual DNMT enzymes do not exhibit significant expression changes in *BRAF*^{V600E} mutant tumours, the stoichiometry of DNA methyltransferase enzyme expression is significantly altered in *BRAF*^{V600E} mutant tumours relative to *BRAF* wild-type tumours. The DNMT3A:DNMT1, DNMT3B:DNMT1 and DNMT3B:DNMT3A ratio are all significantly lower in *BRAF*^{V600E} mutant tumours than *BRAF* wild-type tumours. Mann-Whitney test DNMT3A:DNMT1 p=0.03; DNMT3B:DNMT1 p<0.0001; DNMT3B:DNMT3A p=0.0013.

7.3.2 *BRAF*^{V600E} is neither necessary nor sufficient to induce CIMP in human colorectal adenocarcinoma

In order to test the relationship between CIMP status and *BRAF*^{V600E} mutation, it was necessary to define a CIMP positive cohort in the TCGA data set. This was performed by analysis of the Infinium 450K methylation array data available through the TCGA portal. A consensus on the definition of CIMP is hard to define, and as outlined in the introduction to this thesis, multiple CIMP panels have been proposed. The TCGA colorectal cancer study used a pragmatic unbiased approach to define CIMP patients by performing unsupervised clustering based on the most variable 1403 probes at promoters in the methylation array data [40]. Such an unbiased approach was felt to represent the most objective fashion in which to identify a CIMP positive cohort. A hierarchical clustered heatmap representing all variable (STD-dev >0.2) CpG island CpGs was generated from the 450K array data for 207 patients in the TCGA colon cancer cohort by Mr Neil Robertson, a computational biologist in the Adams' lab at the Beatson Institute for Cancer research. As an additional validation of this approach, a second hierarchical clustered heatmap representing all variable (STD-dev >0.2) "CIMP panel gene" (combining the Ogino and Weisenberger panels) CpG island CpGs was generated, and demonstrated to identify the same cohort of patients as CIMP positive (Figure 7-6). Finally, CpG island mean beta methylation was compared between CIMP positive and CIMP negative patients, confirming that the cohort defined as CIMP positive exhibited the highest CpG island methylation (Figure 7-7). This strategy identified a cohort of 61 patients (29.5%) as CIMP positive. This is broadly within the range previously described in the literature [113,116,309,310,317].

With a cohort of CIMP positive patients defined, the relationship between *BRAF*^{V600E} mutation and CIMP status was next examined. The association between *BRAF*^{V600E} mutation and CIMP status was first examined by contingency. In keeping with previously published data, a highly significant association was demonstrated between *BRAF*^{V600E} mutation and CIMP positivity (χ^2 test $p<0.0001$). Despite this clear association, 67.2% (n=41) of CIMP-positive patients are *BRAF* wild-type, and 42.8% (n=20) of *BRAF*^{V600E} mutant patients are CIMP-negative, implying that *BRAF*^{V600E} is neither necessary nor sufficient to induce CIMP (Figure 7-8).

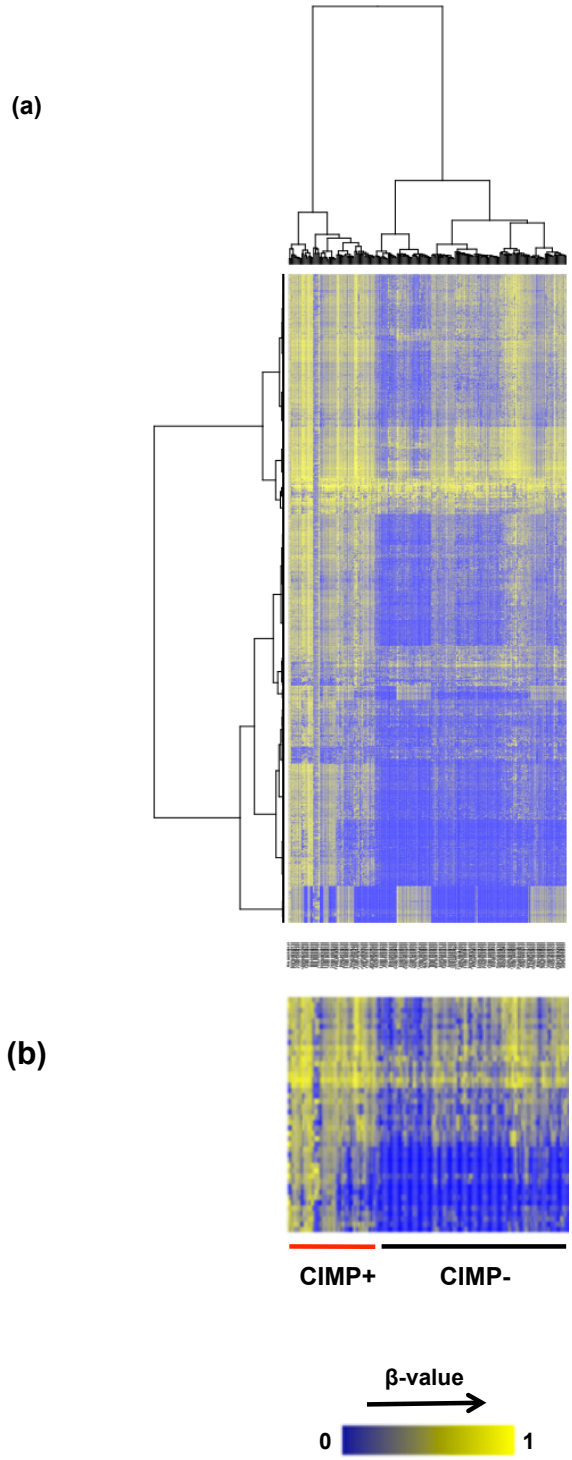

Figure 7-6 CIMP patients within the TCGA cohort were identified by unbiased analysis of 450K methylation array data[22]

Unsupervised clustering was performed to identify CIMP positive and CIMP negative cohorts by analysis of promoter CpG methylation data from the TCGA 450K array data (n=207 patients). Hierarchical clustered heatmaps of the DNA methylation β-values of **(a)** all variable (STD-dev >0.2) CpG island CpGs **(b)** all variable (STD-dev >0.2) CIMP-gene (*CACNA1G, CDKN2A, CRABP1, MLH1, NEUROG1, IGF2, SOCS1, RUNX3*) CpG islands in human colorectal adenocarcinoma from TCGA 450K array data. A cohort of CIMP positive patients can clearly be identified.

[22] Figure generated by Mr Neil Robertson, Beatson Institute for Cancer Research, Glasgow.

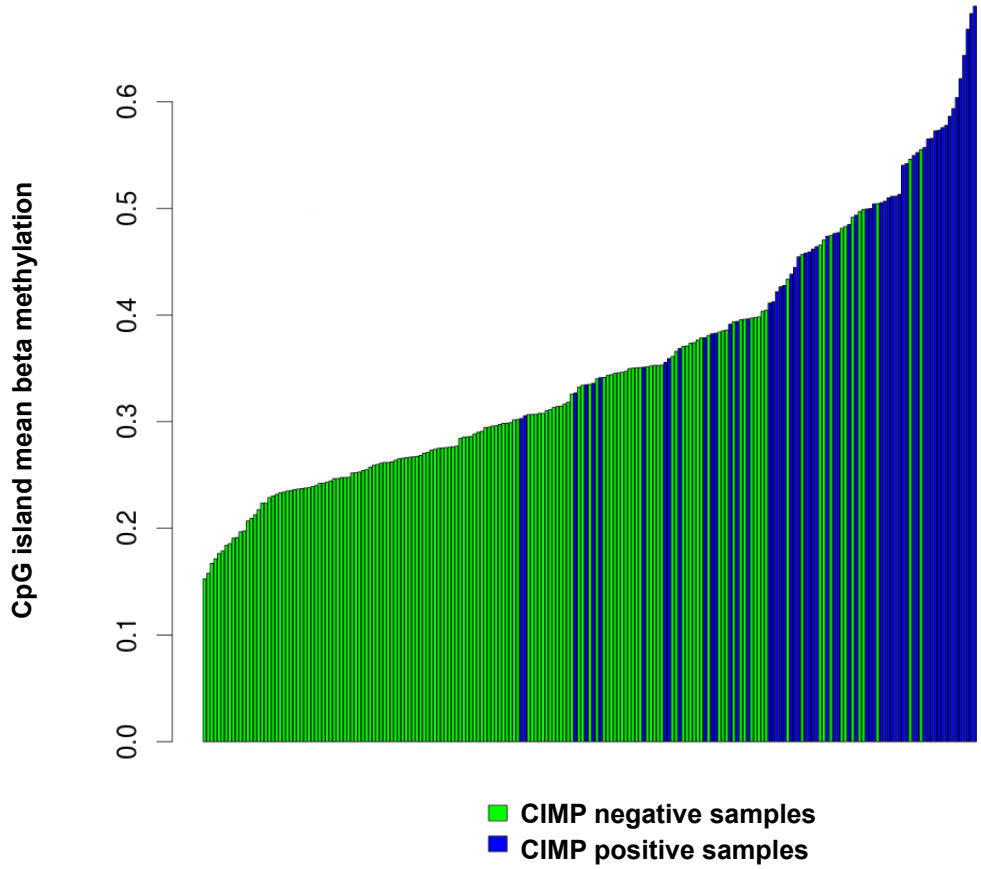

Figure 7-7 CpG island mean beta methylation is greater in CIMP positive than CIMP negative samples[23]

CpG island mean beta methylation was compared in patients categorised as CIMP positive and CIMP negative in the TCGA colorectal cancer cohort (n=207 patients). Bar chart of mean CpG island beta methylation, demonstrating higher CpG island mean beta methylation in patients classified as CIMP positive compared to those classified as CIMP negative; confirming the validity of the use of this approach to identify a CIMP positive cohort.

[23] Figure generated by Mr Neil Robertson, Beatson Institute for Cancer Research Glasgow.

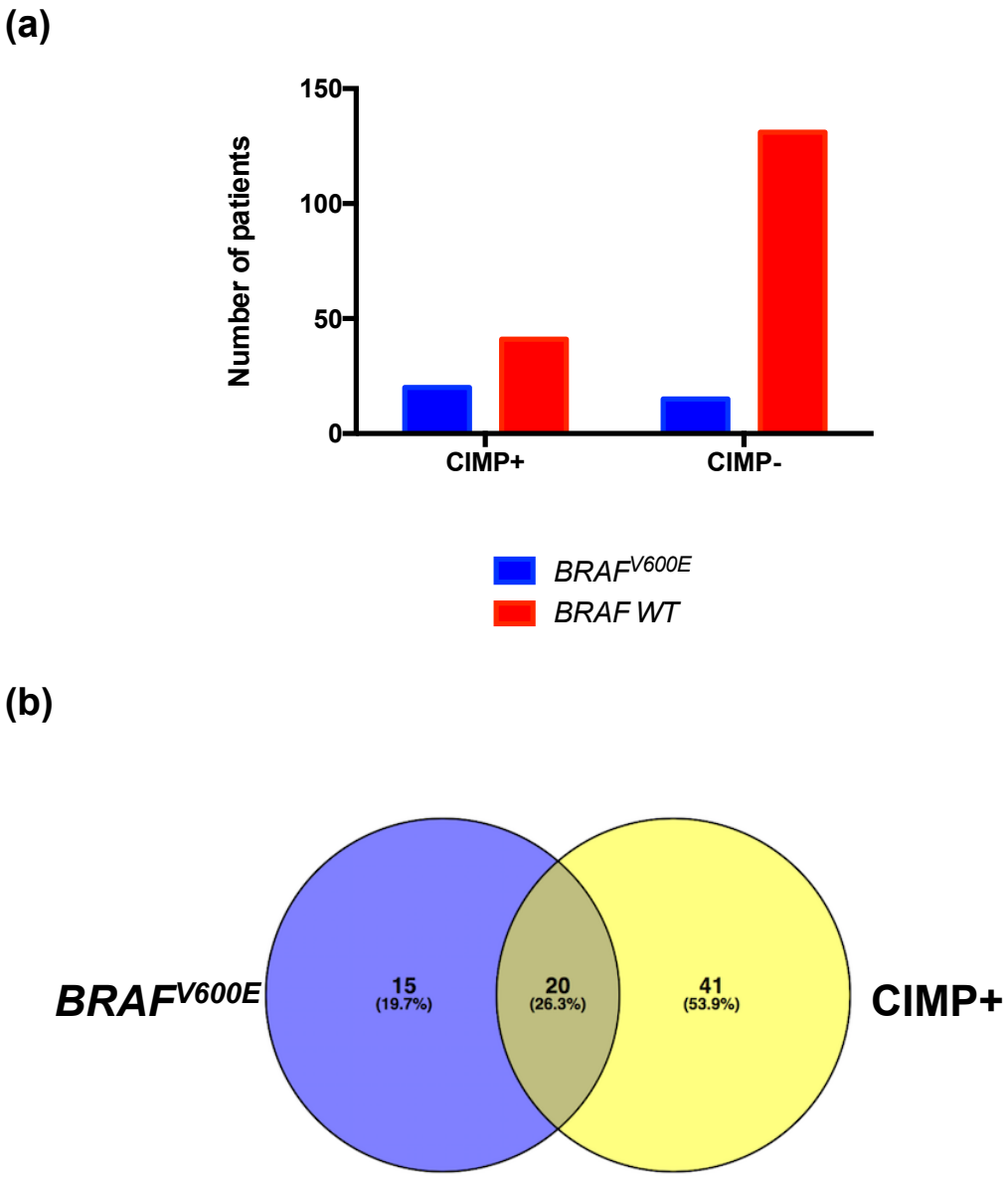

Figure 7-8 *BRAF*^{V600E} is strongly associated with, but is neither necessary nor sufficient to induce CIMP

The relationship between *BRAF*^{V600E} mutation status and CIMP positivity was examined, and tested by contingency (n=207 patients). **(a)** Bar-chart of relationship between *BRAF* mutation status and CIMP positivity. 67.2% (n=41) of CIMP+ patients are *BRAF* wild-type, and 42.8% (n=20) of *BRAF*^{V600E} mutant patients are CIMP-negative (χ^2 test p<0.0001) **(b)** Venn diagram of *BRAF*^{V600E} mutation and CIMP status in colorectal cancer patients from the TCGA data set. Only 57.14% (n=20) of *BRAF*^{V600E} mutant patients are CIMP positive: thus *BRAF*^{V600E} mutation alone is insufficient to induce CIMP.

7.3.3 DNMT3B mRNA expression is not related to CIMP positivity in human colorectal adenocarcinoma

The relationship between DNMT3B expression and CIMP was next examined. As outlined in the introduction to this thesis, two papers have previously suggested a direct relationship between DNMT3B protein expression and CIMP positivity in human colorectal adenocarcinoma [427,428]. As the antibody used to assay DNMT3B in both of these studies (clone 52A1018) was demonstrated in chapter 3 of this thesis to detect murine but not human DNMT3B, the relationship between DNMT3B mRNA expression and CIMP status was examined in the TCGA data set. Paired expression data and CIMP data were available for 207 patients.

Median DNMT3B FPKM mRNA expression was first compared between CIMP-positive and CIMP-negative tumours. Instead of being elevated in CIMP-positive tumours, median DNMT3B expression was in fact modestly, but significantly lower in CIMP-positive than CIMP-negative samples (Mann Whitney test p=0.001), and a frequency distribution histogram showed distinct clustering of DNMT3B expression between CIMP-positive and CIMP-negative tumours (Figure 7-9a, Figure 7-9b). To further explore the apparently inverse relationship between DNMT3B mRNA expression and CIMP status, DNMT3B FPKM mRNA expression levels for tumours were further clustered, and reanalysed with respect to CIMP status. Clustering of expression data into "DNMT3B over-expressing" (defined as any sample with a DNMT3B FPKM mRNA expression greater than the highest normal tissue DNMT3B FPKM mRNA expression value) and "DNMT3B unaltered" cohorts as well as clustering into centiles was performed. Clustering of DNMT3B expression into "over-expressing" and "unaltered" cohorts demonstrated an anticorrelation with CIMP (Fisher's exact test p=0.037). Clustering of DNMT3B expression into two cohorts of (a) $>75^{th}$ centile and (b) $<75^{th}$ centile FPKM mRNA expression confirmed this anticorrelation with CIMP (Fisher's exact test p=0.013) (Figure 7-9c, Figure 7-9d). Therefore, in all permutations, CIMP positivity is anticorrelated with DNMT3B expression.

Given the apparent anticorrelation between DNMT3B expression and CIMP status, it was pertinent to examine how expression of other members of the "DNA methylation machinery" varied between these two cohorts. The mRNA expression data for DNMT1, DNMT3A, DNMT3L TET1, TET2 and TET3 were therefore examined in the CIMP-positive and CIMP-negative cohorts.

Intriguingly, median FPKM mRNA expression of the other candidate *de novo* methyltransferase, DNMT3A, was also significantly lower in CIMP-positive compared to CIMP-negative tumours (Mann Whitney test p=0.0009) whereas DNMT1 and DNMT3L expression did not differ significantly between CIMP-positive and CIMP-negative cohorts (Mann Whitney test DNMT1 p=0.058; DNMT3L p=0.643). Notably, TET1 expression was significantly lower in CIMP-positive than CIMP-negative tumours (Mann Whitney test p=0.025). Interestingly, this corroborates a recent study, which associated aberrant TET1 methylation with CIMP positivity in human colorectal adenocarcinoma [350]. By comparison, expression of TET2 and TET3 was not significantly altered between CIMP-positive and CIMP-negative cohorts (Mann Whitney test TET2 p=0.061; TET3 p=0.554) (Figure 7-10).

As absolute expression of both candidate *de novo* DNA methyltransferase enzymes was lower in CIMP-positive compared to CIMP-negative tumours, the relative expression of the DNMTs was again assessed between cohorts. Interestingly, the DNMT3A:DNMT1 and DNMT3B:DNMT1 ratio was significantly lower in CIMP-positive compared to CIMP-negative tumours (Mann Whitney test DNMT3A:DNMT1 p<0.0001; DNMT3B:DNMT1 p<0.0001), mirroring the pattern associated with $BRAF^{V600E}$ mutation, which has previously been closely associated with CIMP-positivity (Figure 7-11). In contrast to the $BRAF^{V600E}$ data however, the DNMT3A:DNMT3B ratio is unaltered when CIMP-positive and CIMP-negative tumours are compared (Mann Whitney test p=0.326).

Finally, the relationship between *DNMT3B* mutations and CIMP status was examined. Paired *DNMT3B* mutation and CIMP data were available for 207 patients. A Fisher's exact test demonstrated no significant relationship (p=0.727) between CIMP-positivity and *DNMT3B* mutation (Figure 7-12).

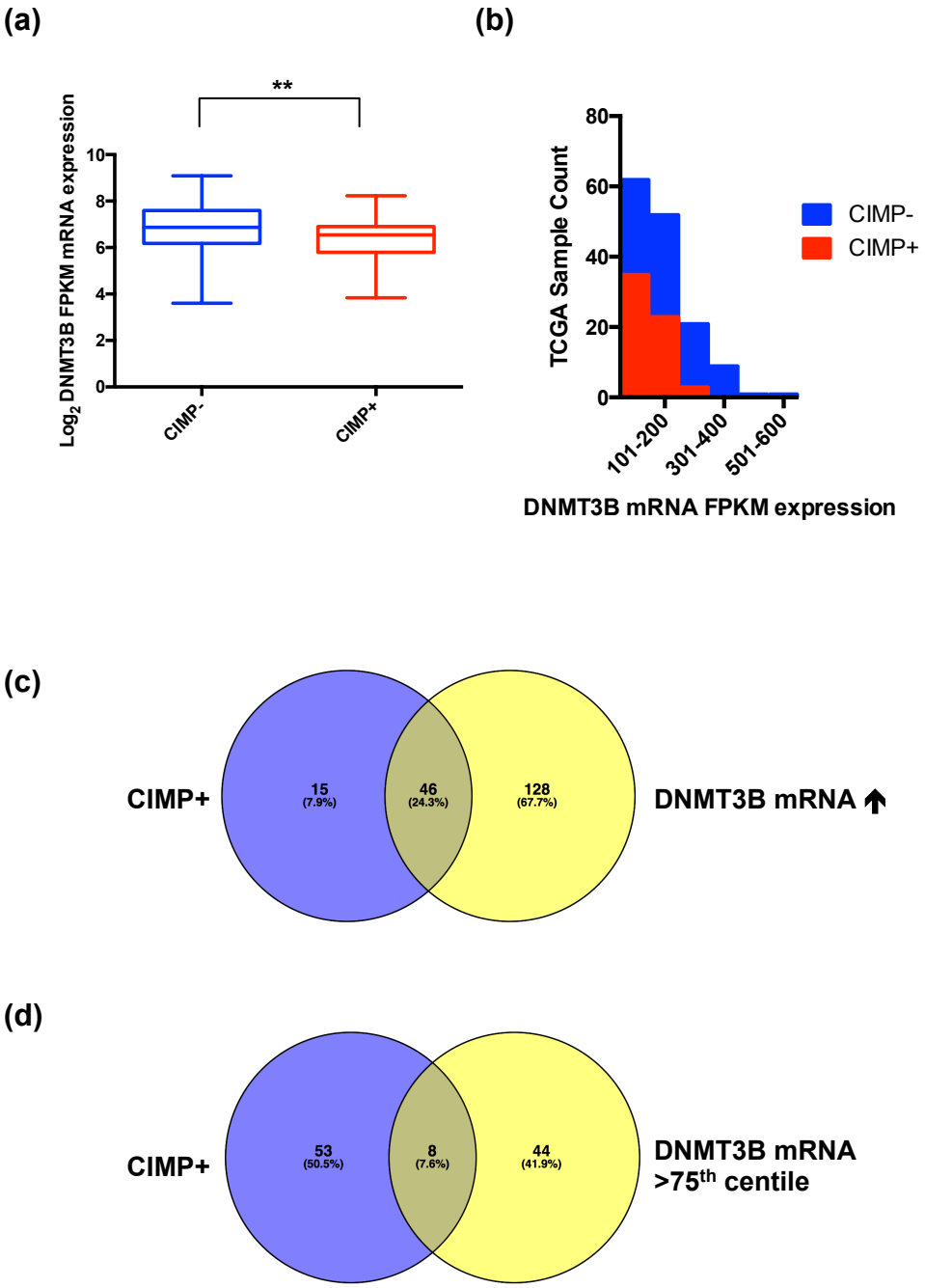

Figure 7-9 DNMT3B mRNA expression is not related to CIMP positivity in human colorectal adenocarcinoma

The relationship between DNMT3B mRNA expression and CIMP positivity in human colorectal adenocarcinoma was explored in the TCGA cohort (n=207 patients). **(a)** Boxplot of DNMT3B Log_2 FPKM mRNA expression in human colorectal carcinoma TCGA patients subdivided by CIMP status. CIMP negative patients have a higher mean DNMT3B mRNA expression than CIMP positive patients. (Mann Whitney test p=0.001) **(b)** Frequency distribution histogram of DNMT3B mRNA FPKM expression in CIMP positive and CIMP negative patients demonstrating lower DNMT3B expression in CIMP positive compared to CIMP negative patients **(c)** Venn diagram demonstrating overlap between CIMP positive and DNMT3B overexpressing (compared to normal tissue) patients. DNMT3B overexpression is demonstrably anticorrelated with CIMP (Fisher's exact test p=0.037) **(d)** Venn diagram demonstrating overlap between CIMP positive and DNMT3B mRNA expression >75th centile. DNMT3B overexpression is anticorrelated with CIMP (Fisher's exact test p=0.013).

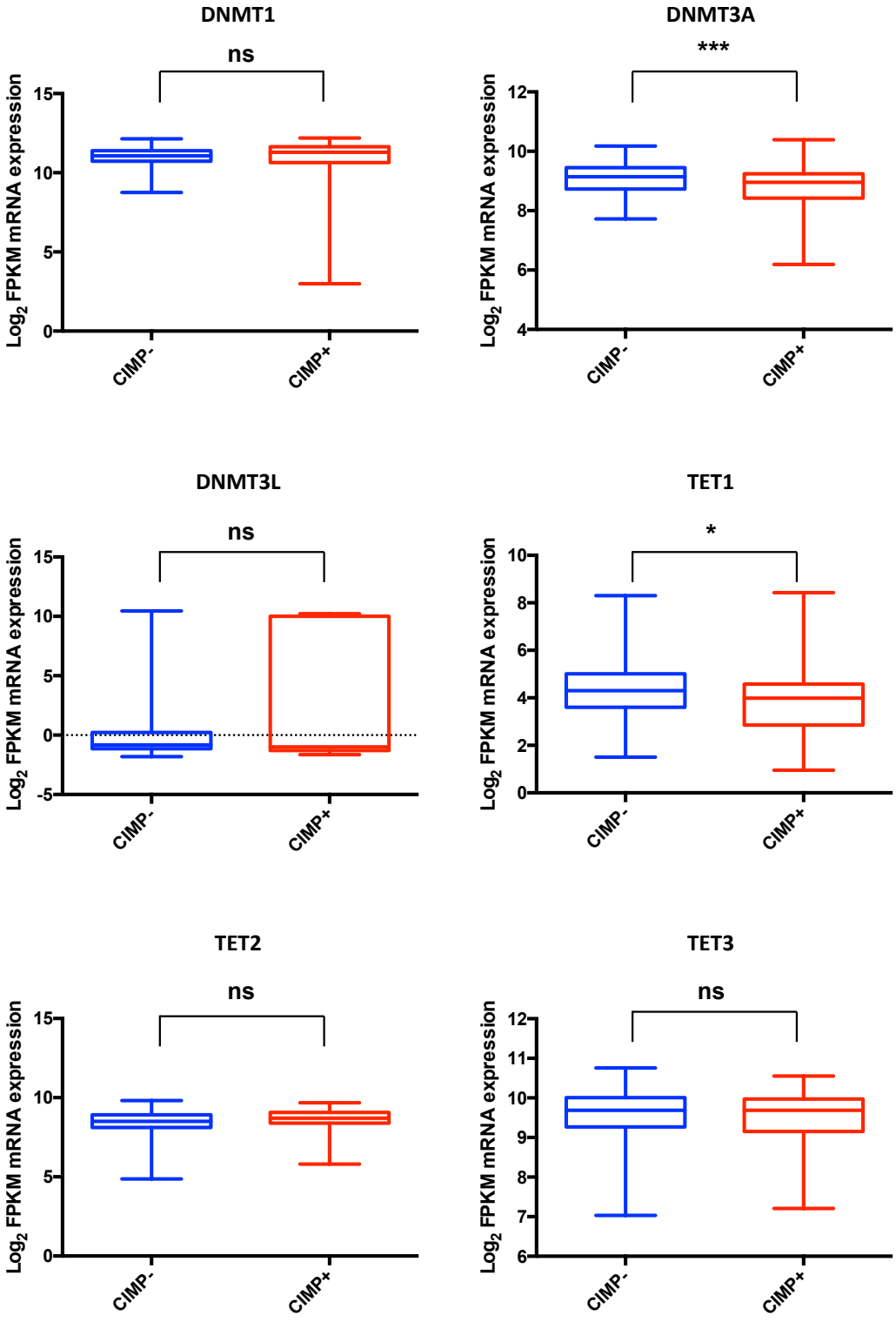

Figure 7-10 Both DNMT3A and TET1 expression is significantly lower in CIMP positive tumours than CIMP negative tumours

The mRNA expression of DNMT1, DNMT3A, DNMT3L, TET1, TET2 and TET3 were compared between CIMP+ and CIMP- tumour samples from the TCGA colorectal human adenocarcinoma cohort (n=207 patients). Both DNMT3A and TET1 mRNA levels were significantly lower in CIMP+ than CIMP negative tumours (Mann Whitney test DNMT3A p=0.0009; TET1 p=0.025). By contrast, the mRNA expression of DNMT1, DNMT3L, TET1, TET2 and TET3 exhibited no statistically significant difference between CIMP+ and CIMP- samples. Mann Whitney test DNMT1 p=0.058; DNMT3L p=0.643; TET2 p=0.061; TET3 p=0.554.

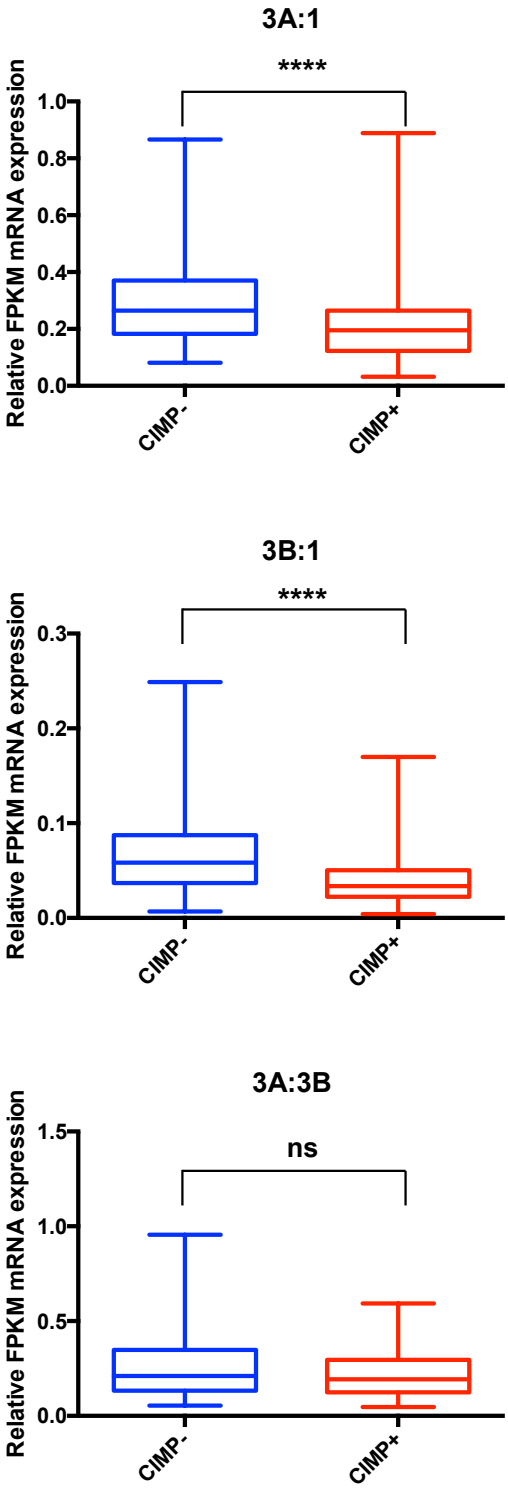

Figure 7-11 DNMT3B:DNMT1 and DNMT3A:DNMT1 ratio is lower in CIMP positive patients than CIMP negative patients

Boxplots of DNMT3A:DNMT1; DNMT3B:DNMT1 and DNMT3A:DNMT3B mRNA expression ratio in CIMP positive and CIMP negative patients. The ratio of DNMT3B:DNMT1 and DNMT3A:DNMT1 mRNA expression is significantly lower in CIMP positive than CIMP negative tumours (Mann-Whitney test DNMT3A:DNMT1 $p<0.0001$; DNMT3B:DNMT1 $p<0.0001$;). By contrast, the DNMT3A:DNMT3B ratio is unaltered between CIMP positive and CIMP negative tumours (Mann Whitney $p=0.326$).

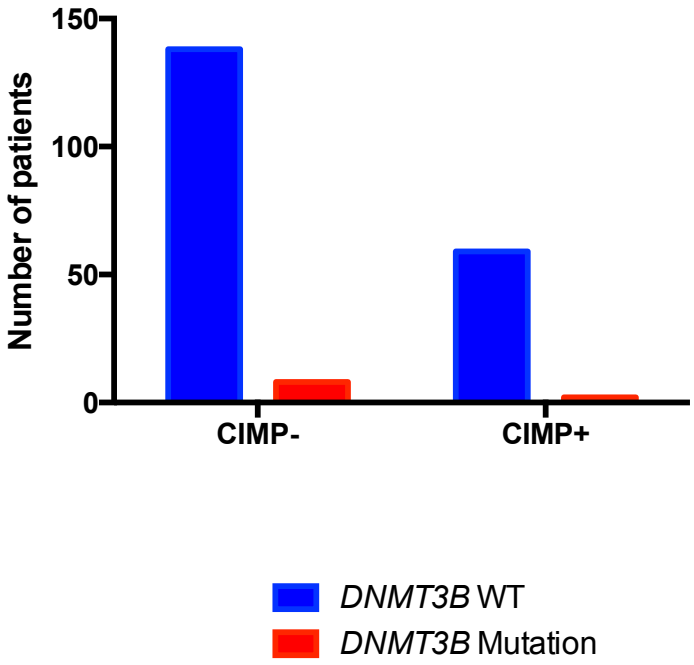

Figure 7-12 *DNMT3B* mutation is not significantly linked to CIMP positivity in human colorectal adenocarcinoma

The relationship between *DNMT3B* mutation and CIMP positivity was examined in the TCGA cohort (n=207 patients). Bar-chart of relationship between CIMP status and *DNMT3B* mutation status in the TCGA human colorectal adenocarcinoma cohort. There is no significant relationship between CIMP status and *DNMT3B* mutation status (Fisher's exact test p=0.727).

7.3.4 *DNMT3B* is frequently amplified in human colorectal adenocarcinoma

As neither DNMT3B mRNA expression nor mutation exhibited positive correlation with CIMP or BRAF mutational status, the relationship between these variables and *DNMT3B* gene copy number was explored. Interestingly, chromosome 20q (where the *DNMT3B* gene is located) was identified by the cancer genome atlas as a common site of gene amplification [40]. *DNMT3B* somatic copy number amplification (SCNA) was assessed using the GISTIC method. Copy number data were obtained from the TCGA portal, and analysed by Neil Robertson and Gintare Sendzikaite, computational biologists at the Beatson Institute for cancer research. In the TCGA copy number dataset an estimated copy number mean for particular genomic segments is specified and is log based (tumour intensity:normal intensity). Therefore an estimated copy number of zero is indicative of diploid copy number. By contrast, a segment mean of >0.2 is defined as an amplification [466]. Using this approach, *DNMT3B* copy number alterations were detectable in 67.4% of patients in the TCGA cohort. Strikingly, there was a very clear relationship between DNMT3B mRNA expression and *DNMT3B* amplification (Figure 7-13). To assess the significance of differences in DNMT3B expression between amplified and non-amplified *DNMT3B* patient samples, a t-test was performed on the normalised expression levels between the two groups, confirming a highly significant association between high DNMT3B expression and *DNMT3B* amplification (p=0.0026).

The relationship between *DNMT3B* copy number and both CIMP status and *BRAF* mutation status was next assessed. Both CIMP and *BRAF* mutation status (as defined earlier) were plotted against *DNMT3B* relative copy number, revealing an anticorrelation between both CIMP and $BRAF^{V600E}$ mutation and *DNMT3B* copy number amplification (Figure 7-14a, Figure 7-14b). This result is perhaps not surprising for a number of reasons. Firstly, given the extremely strong relationship between DNMT3B mRNA expression and copy number amplification, it would have been surprising to see positive correlation between *DNMT3B* SCNA and $BRAF^{V600E}$ mutation status or CIMP positivity. Moreover, frequent SCNA is a feature of consensus-molecular subtype 2 (canonical) and 4 (mesenchymal) colorectal cancer, which are typically CIMP-negative. By contrast, consensus-molecular subtypes 1 (“MSI immune”) and 3 (“metabolic”), which are characterised by a CIMP-phenotype, exhibit a low frequency of SCNA [27].

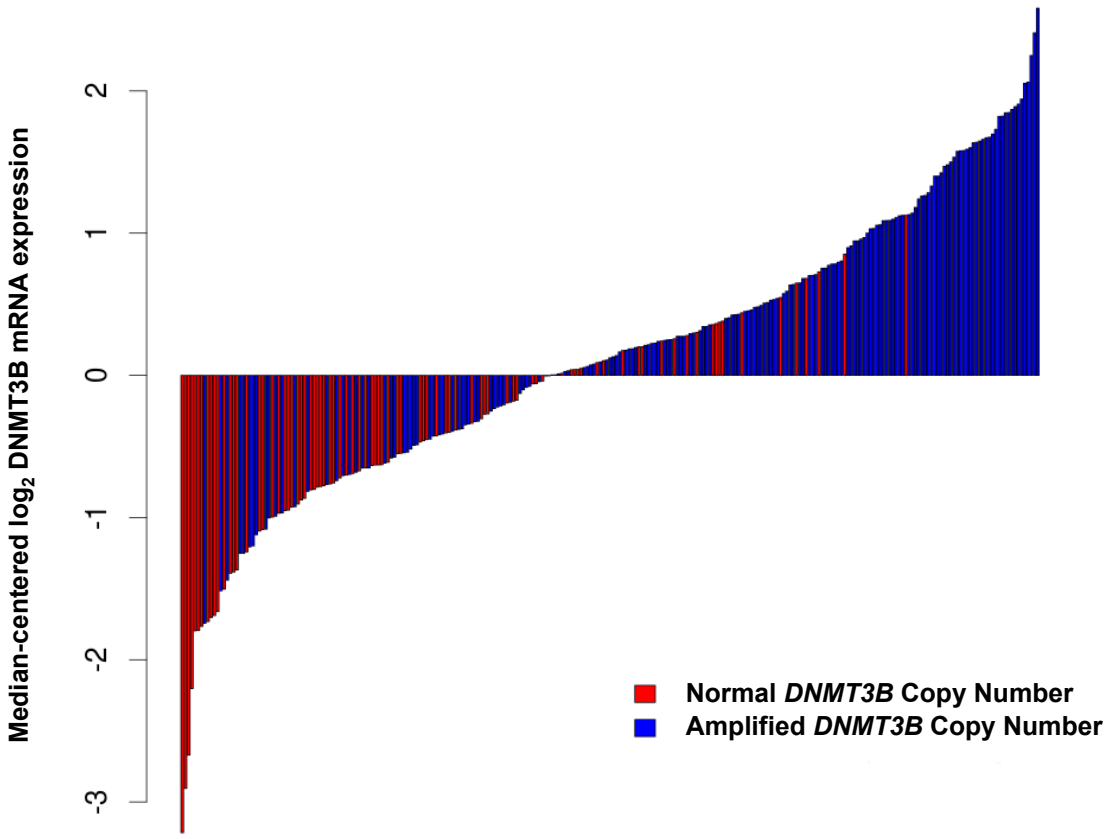

Figure 7-13 *DNMT3B* is frequently amplified in human colorectal adenocarcinoma and SCNA is associated with mRNA upregulation[24]

Median centred log_2 DNMT3B mRNA expression plot annotated by *DNMT3B* copy number status. *DNMT3B* somatic copy number amplification (SCNA) was assessed using the GISTIC method, and plotted together with DNMT3B log_2 FPKM mRNA expression. A clear association is demonstrable between *DNMT3B* SCNA and high DNMT3B expression (n=215 patients; t-test p=0.0026).

[24] Figure generated by Mr Neil Robertson and Ms Gintare Sendzikaite, Beatson Institute for Cancer Research, Glasgow.

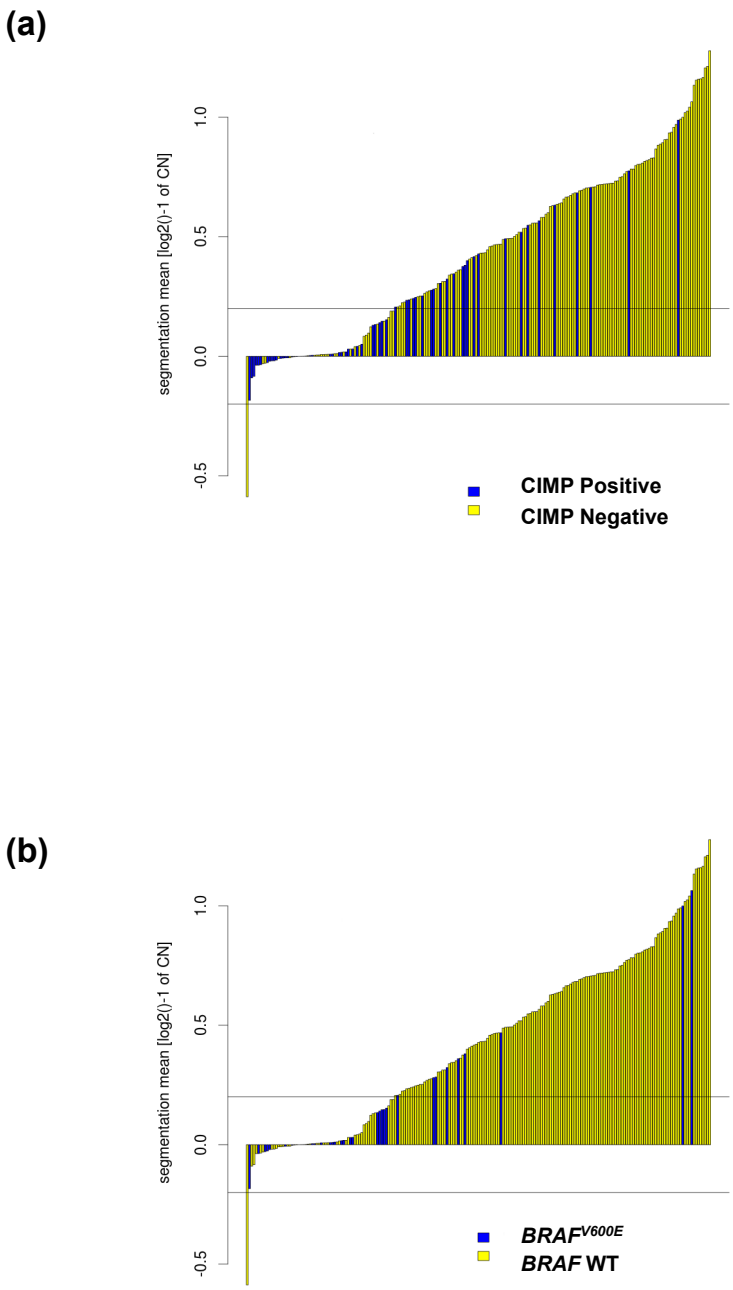

Figure 7-14 Both CIMP positivity and *BRAF*^{V600E} mutation status are anticorrelated with *DNMT3B* SCNA in human colorectal adenocarcinoma[25]

Segmentation mean plots of *DNMT3B* copy number annotated by **(a)** CIMP status and **(b)** *BRAF* mutational status. *DNMT3B* somatic copy number amplification (SCNA) was assessed using the GISTIC method. **(a)** A clear anticorrelation between CIMP-positivity and *DNMT3B* SCNA is demonstrable (permutation test p= 0.00078) **(b)** An anticorrelation between *DNMT3B* SCNA and *BRAF*^{V600E} mutation is demonstrable (permutation test p=0.012).

[25] Figure generated by Mr Neil Robertson and Ms Gintare Sendzikaite, Beatson Institute for Cancer Research, Glasgow.

7.3.5 Neither DNMT3B expression, CIMP nor *BRAF* mutation correlate with survival in human colorectal adenocarcinoma

Elevated DNMT3B expression has been shown to correlate with poor survival in malignant melanoma, renal cell carcinoma, oesophageal squamous cell carcinoma, testicular seminoma, and hepatocellular carcinoma [231,467-470]. One study has examined DNMT3B expression in colorectal cancer and found no correlation with DNMT3B expression and survival. As outlined previously however, this study used the 52A1018 clone DNMT3B antibody which appears not to detect human DNMT3B [427]. In chapter 6, in murine models of serrated pathway carcinogenesis, DNMT3B ectopic expression was demonstrated to reduce overall survival in a model driven by activated $Braf^{V600E}$ mutation and *Dnmt3b* knockout had the converse effect. Conversely, these effects on survival were abrogated in the context of activated Wnt signalling modelled by crossing the $^{LSL}Braf^{V600E}$ allele to the $Apc^{fl/wt}$ model. It was therefore relevant to assess the effects of DNMT3B expression on survival in human colorectal adenocarcinoma.

The TCGA data set includes both overall survival and disease-free survival data for patients. These data were accessed using the cBioPortal platform [463,464]. Survival data were then integrated using individual TCGA sample IDs with the mRNA expression data analysed earlier. As DNMT3B mRNA expression had been demonstrated to be closely correlated to SCNA, these data were also correlated with survival. As median DNMT3B mRNA FPKM expression in the TCGA cohort is elevated in tumour tissue relative to normal tissue in 84% of samples, the decision was made to define elevated DNMT3B expression as DNMT3B mRNA FPKM >75th centile, an approach validated by a recent study in the context of melanoma [231]. Interestingly, neither elevated DNMT3B expression nor somatic copy number amplification are independently associated with overall or disease-specific survival in the TCGA cohort (Log Rank test overall survival by elevated DNMT3B mRNA expression p=0.16; disease-free survival by elevated DNMT3B mRNA expression p=0.88; overall survival by *DNMT3B* SCNA p=0.14, disease-free survival by *DNMT3B* SCNA p=0.87) (Figure 7-15).

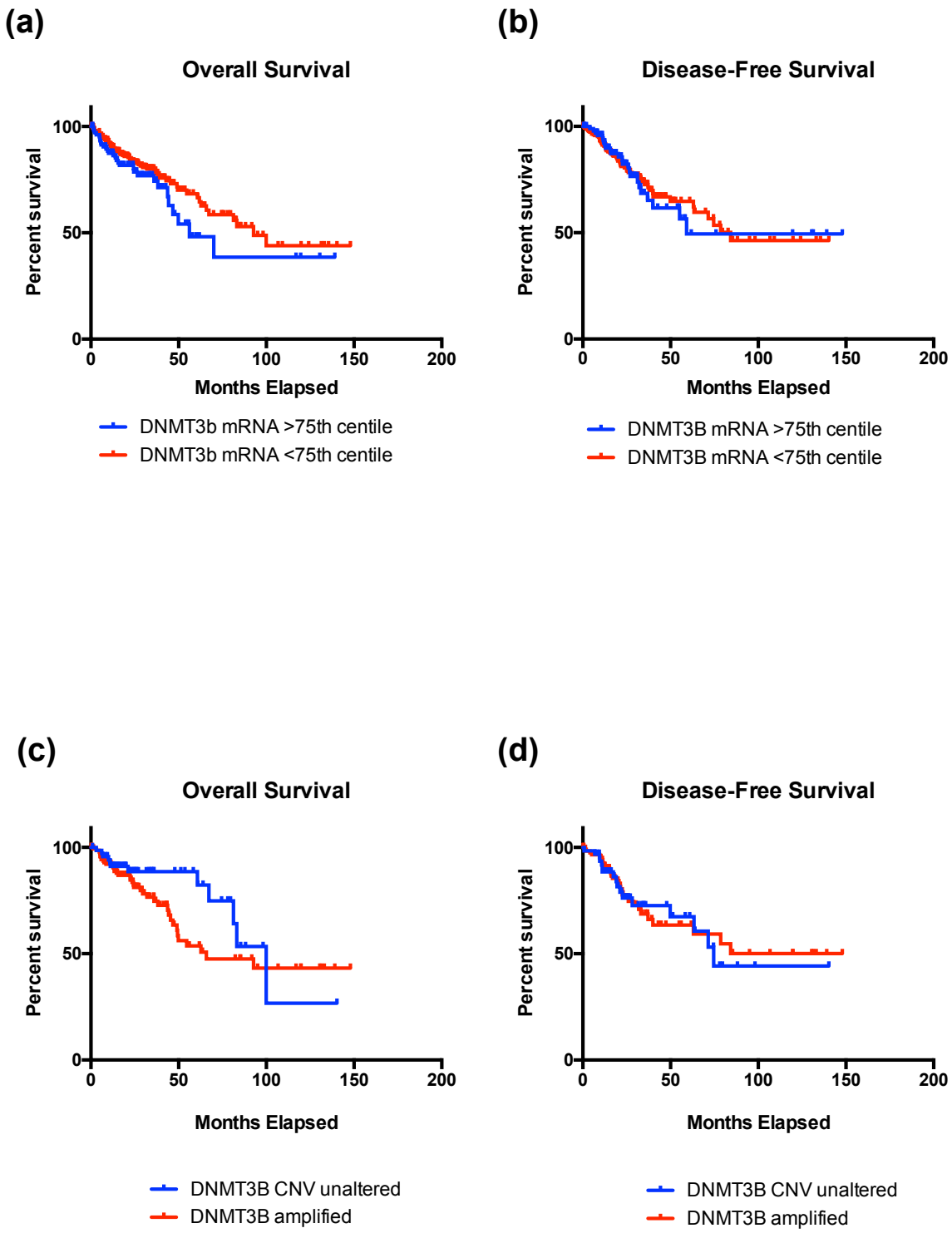

Figure 7-15 Neither *DNMT3B* SCNA nor mRNA expression correlate with overall or disease-free survival in human colorectal adenocarcinoma

The effects of DNMT3B mRNA expression and SCNA alteration were assessed in the TCGA cohort. **(a)** Kaplan-Meier curve of overall survival stratified by DNMT3B mRNA expression. DNMT3B overexpression does not affect overall survival. Log-Rank (Mantel-Cox) test p=0.16 **(b)** Kaplan-Meier curve of disease-free survival stratified by DNMT3B mRNA expression. DNMT3B overexpression does not affect disease-free survival. Log-Rank (Mantel-Cox) test p=0.88 **(c)** Kaplan-Meier curve of overall survival stratified by *DNMT3B* CNV status. *DNMT3B* SCNA does not affect survival. Log-Rank (Mantel-Cox) test p=0.14 **(d)** Kaplan-Meier curve of disease-free stratified by *DNMT3B* CNV status. *DNMT3B* SCNA does not affect disease-free survival. Log-Rank (Mantel-Cox) test p=0.87.

The relationship between CIMP status and survival in human colorectal adenocarcinoma remains controversial. Several studies have associated CIMP with adverse clinical outcomes, though inconsistent and conflicting data have been published [319,355,471-473]. A recent meta-analysis of the prognostic implications of CIMP in colon cancer included 19 separate studies and concluded that CIMP was independently associated with worse prognosis in human colorectal adenocarcinoma [474]. One of the fundamental problems in assessing the relationship of CIMP status to survival is the heterogeneity of the classification systems used to define CIMP positivity. A significant advantage of the approach taken to classify CIMP in the present study was the unbiased approach (compared to candidate gene approach often used to define CIMP) used to define a CIMP positive cohort. It was therefore of interest to compare survival between the CIMP-positive and CIMP-negative populations defined in the TCGA data. Overall survival and disease-specific survival data were once again compared between CIMP-positive and CIMP-negative patient cohorts. No independent significant difference in overall (Log-rank p=0.62) or disease-specific (Log-rank p=0.86) survival was demonstrable in CIMP-positive compared to CIMP-negative patients (Figure 7-16).

Finally, survival data were compared for $BRAF^{V600E}$ mutant and *BRAF* wild-type cohorts within the TCGA dataset. $BRAF^{V600E}$ mutation has previously been demonstrated to correlate with poorer survival in microsatellite stable but not microsatellite unstable cancers [355,475,476]. Microsatellite stability data were not analysed in the present study, which must be taken as a caveat to the interpretation of these data. Surprisingly, no significant difference in overall survival (Log-rank p=0.29) or disease-specific (Log-rank p=0.65) survival was demonstrable between $BRAF^{V600E}$ mutant and *BRAF* wild-type patients in the TCGA cohort (Figure 7-17).

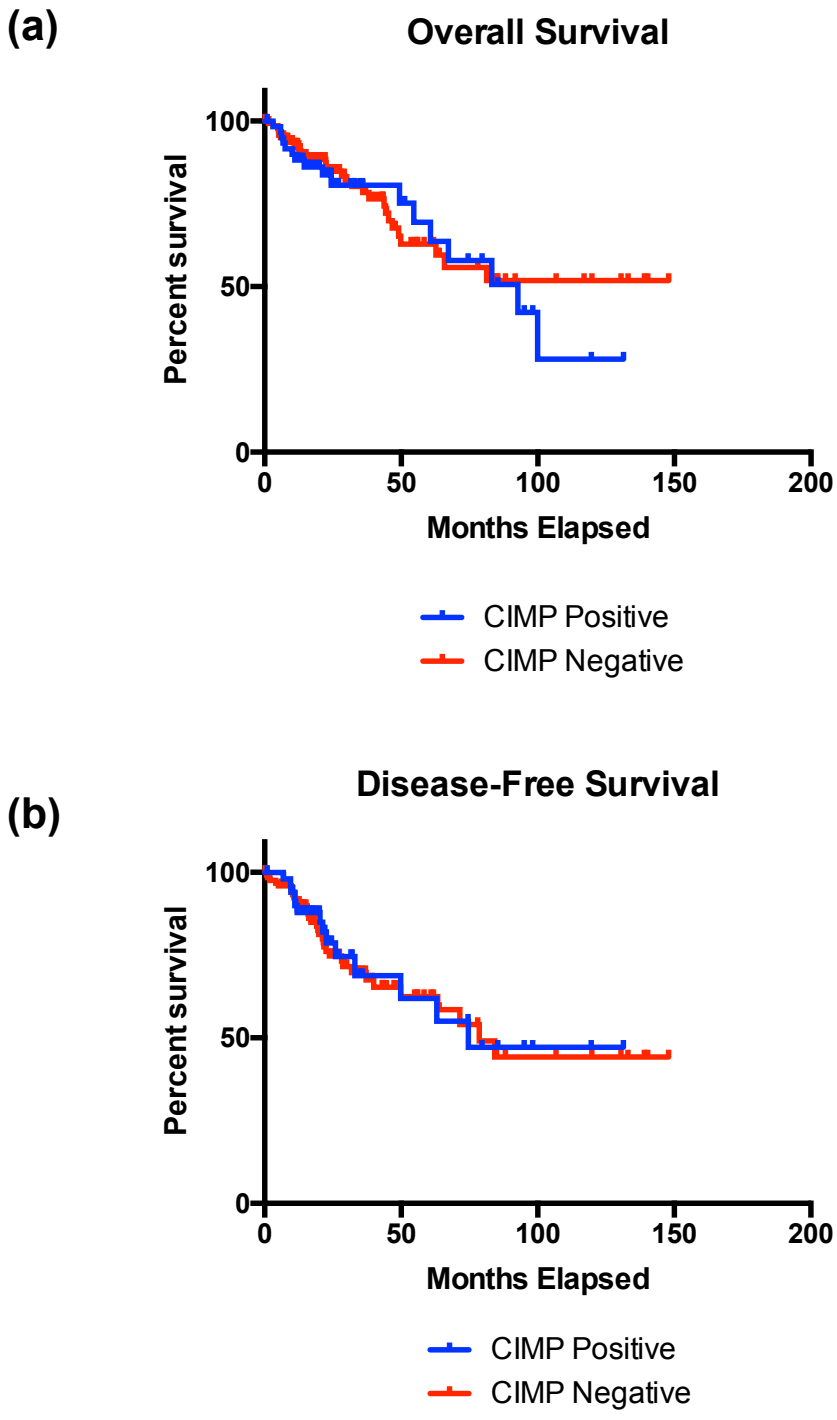

Figure 7-16 CIMP is not an independent predictor of survival in human colorectal adenocarcinoma

The effects of CIMP positivity on survival in human colorectal adenocarcinoma were assessed in the TCGA cohort. **(a)** Kaplan-Meier curve of overall survival stratified by CIMP status. CIMP-positivity does not affect overall survival. Log-Rank (Mantel-Cox) test p=0.62 **(b)** Kaplan-Meier curve of disease-free survival stratified by CIMP status. CIMP positivity does not affect disease-free survival. Log-Rank (Mantel-Cox) test p=0.86.

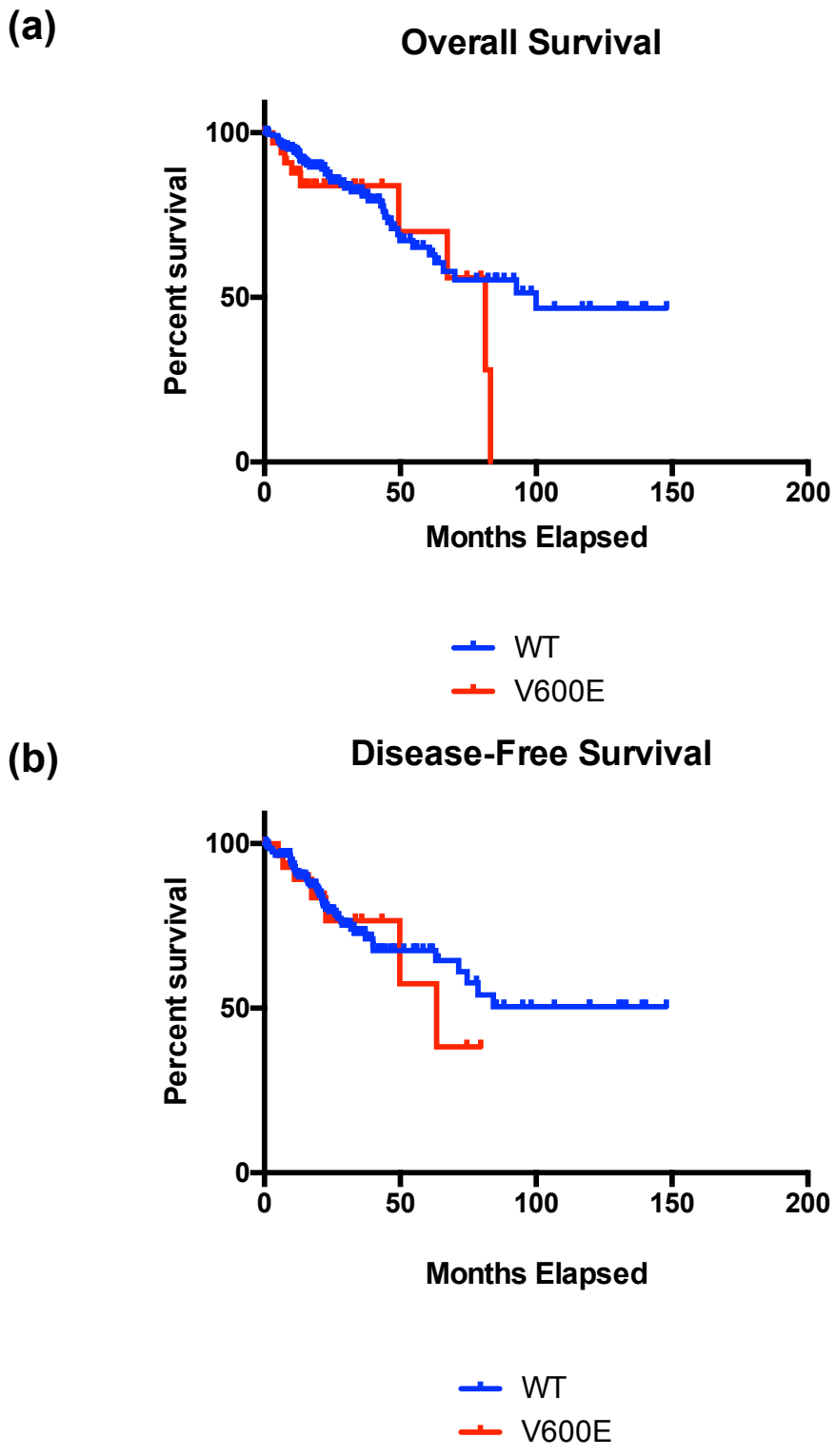

Figure 7-17 *BRAF*^{V600E} mutation status is not an independent predictor of survival in human colorectal adenocarcinoma

The effects of *BRAF*^{V600E} mutation on survival in human colorectal adenocarcinoma were assessed in the TCGA cohort. **(a)** Kaplan-Meier curve of overall survival stratified by *BRAF*^{V600E} mutation status. *BRAF*^{V600E} mutation does not affect overall survival. Log-rank (Mantel-Cox) p=0.29 **(b)** Kaplan-Meier curve of disease-free survival stratified by *BRAF*^{V600E} mutation status. *BRAF*^{V600E} mutation does not affect disease-free survival. Log-rank (Mantel-Cox) test p=0.65.

7.4 Discussion

Together, the data presented in this chapter corroborate some of the earlier data presented in this thesis. Specifically they address a number of areas of conflict between the data presented thusfar herein and the published data regarding the relationships between DNMT3B, BRAF and CIMP in human colorectal adenocarcinoma. *DNMT3B* mutation has been demonstrated to be an infrequent event in human colorectal adenocarcinoma. Conversely, frequent upregulation of DNMT3B mRNA expression has been demonstrated in the majority of colorectal cancers, and has been demonstrated to be closely related to a high frequency of *DNMT3B* copy-number amplifications also observed in this cohort. Importantly, a clear and unambiguous inverse relationship has been demonstrated between $BRAF^{V600E}$ mutation and DNMT3B expression, which is supportive of the *in vitro* DNMT3B protein expression data presented in chapter 4. Furthermore, whilst $BRAF^{V600E}$ mutation has been confirmed to be statistically very closely associated with CIMP in this cohort, it is also clear that $BRAF^{V600E}$ mutation is neither necessary nor sufficient to induce CIMP in human colorectal adenocarcinoma. This is in keeping with the observed lack of a CpG island methylator phenotype upon acute $BRAF^{V600E}$ activation demonstrated in chapter 4. One caveat to these conclusions, is the method used to identify a CIMP positive cohort in this study. Specifically, rather than employing a 'candidate gene' approach as used in the widely-published CIMP panel studies, a non-biased hierarchical-based clustering approach has been used to identify a CIMP-positive cohort. The rationale for this is supported by the recent TCGA[40] analysis of human colorectal carcinoma, which employed a similar approach and it has been further demonstrated (Figure 7-6) that this approach identifies patients with hypermethylation of previously published "CIMP panel" genes. Furthermore, unlike several other studies, the present work did not subclassify CIMP patients into CIMP-high and CIMP-low. Taken together, these data cast doubt on the viability of a model which proposes a direct link between $BRAF^{V600E}$ mutation and CIMP mediated by DNMT3B as proposed by Fang et al. [364].

Finally, despite an apparent pro-proliferative and oncogenic function of DNMT3B in the *in vitro*, and *in vivo* contexts respectively (at least in the absence of activated Wnt signalling), DNMT3B expression is not independently associated with disease-specific or overall survival in human colorectal adenocarcinoma. Similarly, neither CIMP-positivity nor $BRAF^{V600E}$ mutation have been demonstrated to affect disease-specific or overall survival in human colorectal adenocarcinoma. As discussed above, these latter two conclusions differ from some previously published studies. There are a number of possible

explanations for this. Firstly, the number of patients assessed in this study was relatively modest. Secondly, the survival data from TCGA are not yet "mature" (mean follow-up =31.25 months), and it is feasible that if repeated with more "mature" survival data, a survival impact of DNMT3B overexpression, CIMP-positivity or $BRAF^{V600E}$ mutation might be demonstrable. Furthermore, a negative prognostic impact of $BRAF^{V600E}$ mutation in particular has been demonstrated only in the context of MSS stage II and stage III tumours, but not in MSI positive tumours [477]. As the survival data in the present study were stratified neither for TNM stage nor MSI status, this nuanced effect of $BRAF^{V600E}$ on survival may have been missed.

7.5 Summary

1. *DNMT3B* is infrequently mutated in human colorectal adenocarcinoma, and no "hot-spot" mutations are identified

2. *DNMT3B* mutation is not significantly associated with $BRAF^{V600E}$ mutation or CIMP status.

3. DNMT3B is highly overexpressed in human colorectal adenocarcinoma tissue compared to corresponding normal tissues.

4. DNMT3B expression is significantly lower in tumours harbouring a $BRAF^{V600E}$ mutation relative to those with wild-type *BRAF*.

5. The absolute expression of DNMT1, DNMT3A, DNMT3L, TET1 and TET3 does not significantly vary between $BRAF^{V600E}$ mutant and wild-type tumours, though TET2 expression is higher in $BRAF^{V600E}$ mutant tumours than *BRAF* wild-type tumours.

6. By comparison, the relative expression of DNMT enzymes is significantly altered in $BRAF^{V600E}$ mutant tumours compared to *BRAF* wild-type tumours, with significant reductions in the DNMT3A:DNMT1, DNMT3B:DNMT1 and DNMT3B:DNMT3A ratio.

7. $BRAF^{V600E}$ mutation is strongly associated with but is neither necessary nor sufficient to induce CIMP.

8. DNMT3B, DNMT3A and TET1 expression is significantly lower in CIMP positive tumours than CIMP negative tumours.

9. The DNMT3B:DNMT1 and DNMT3A:DNMT1 ratio are significantly lower in CIMP positive tumours than CIMP negative tumours, though the DNMT3A:DNMT3B ratio is unaltered.

10. *DNMT3B* mutation is not significantly associated with CIMP status in human colorectal adenocarcinoma.

11. *DNMT3B* copy number is frequently altered in human colorectal adenocarcinoma, but is not associated with CIMP status.

12. Neither DNMT3B expression, CIMP status nor $BRAF^{V600E}$ mutation status individually correlate with disease-specific or overall survival in human colorectal adenocarcinoma.

8 Discussion

8.1 Summary

Approximately 10-20% of human colorectal cancers harbour a *BRAF*^{V600E} mutation, which has been demonstrated to act as a founder mutation for an alternative serrated pathway of colorectal carcinogenesis [39-43,46,47]. Conversely, activating *BRAF*^{V600E} mutations are detectable in 62-70% of hyperplastic colonic polyps: lesions traditionally considered to harbour no oncogenic potential [10,11]. Paradoxically, both *in vitro* and *in vivo*, activated oncogenic *BRAF*^{V600E} induces a stable proliferation arrest: oncogene-induced senescence, an established tumour-suppressive mechanism [30,46,47,478]. Furthermore, the existence of an oncogene-induced senescence barrier in human serrated pathway carcinogenesis is supported by the published *in situ* data [48]. It is clear, therefore, that additional genetic and epigenetic events are required to promote neoplastic transformation in the serrated pathway, which if untreated (e.g. by endoscopic polypectomy) eventually culminates in the development of invasive carcinoma. The CpG island methylator phenotype (CIMP) is thought to promote tumourigenesis by bypass of tumour-suppressor mechanisms, such as silencing of *CDKN2A/INK4A* [47,48]. It has been recognised for some time that there is an extremely close relationship between *BRAF*^{V600E} mutations and CIMP positivity in human colorectal cancer, and indeed disease progression is associated with progressive development of a CIMP phenotype [45,116,355,357,425]. Whilst this association was initially correlative, it has recently been proposed that *BRAF*^{V600E} can directly induce CIMP through the *de novo* methyltransferase, DNMT3B [364]. Separately, elevated DNMT3B expression has previously been linked to the development of CIMP in both murine and human colorectal neoplasia [47,427,434,453]. Furthermore, DNMT3B has been demonstrated to have an oncogenic function in murine colon cancer [205,433].

Thus, the emerging dogma is supportive of a model in which neoplastic transformation in *BRAF*^{V600E}-mutant colorectal serrated lesions may be contributed to by the ability of this oncogene to induce a CpG island methylator phenotype, mediated by DNMT3B. There are however, several obvious paradoxes. Firstly, only a minority of colorectal lesions harbouring an activating *BRAF*^{V600E} mutation eventually progress to invasive carcinoma. Secondly, CIMP develops gradually with serrated pathway progression [45]. Thirdly, as many as 40% of CIMP-high tumours do not harbour an activating *BRAF*^{V600E} mutation, and finally, approximately 10% of patients with an activating *BRAF*^{V600E} mutation are CIMP-low or CIMP-negative [355]. Thus a simple, linear model by which *BRAF*^{V600E} directly

induces CIMP cannot be fully reconciled with the disease biology. In this thesis therefore, the relationships between an activated *BRAF*^{V600E} oncogene, DNMT3B and CIMP in colorectal cancer have been comprehensively explored by multiple approaches.

In chapter 3, a panel of commercially-available DNMT3B antibodies was characterised and validated using a combination of ectopic DNMT3B expression, DNMT3B knockdown (using lentivirus encoded shRNAs and CRISPRs) and a *DNMT3B*-null cell line. Surprisingly, only one of the putative DNMT3B antibodies tested (SC10236) could confidently be determined to exhibit sensitivity and specificity for human DNMT3B, highlighting the importance of rigorous validation procedures prior to the use of antibodies for further experimental work. Intriguingly, and of fundamental importance to the subject matter of this thesis, IMG184A (52A1018) was demonstrated to react with murine but not human DNMT3B. Both published immunohistochemical studies linking DNMT3B expression to CIMP in human colorectal cancer were performed using this antibody, thus raising considerable questions about the validity of the conclusions made in these studies linking elevated DNMT3B expression and CIMP [427,453]. Whilst this might explain an apparent conflict with other studies which have demonstrated no relationship between DNMT3B mRNA expression and CIMP status in human colorectal cancer, it does not help to resolve the apparent conflict with data from murine models, which have demonstrated a clear relationship between DNMT3B expression and a CIMP-like phenotype [47,337,434,445].

In chapter 4, experiments were designed to test the hypothesis that an activated *BRAF*^{V600E} oncogene alone is sufficient to induce a CpG island methylator phenotype. A primary cell culture model was designed to characterise the DNA methylation changes induced by activated oncogenic BRAF^{V600E}, at single base pair resolution using whole-genome bisulfite sequencing: to date the most comprehensive such assessment of the DNA methylation changes induced by an activated *BRAF*^{V600E} oncogene. Furthermore, as expression of mutant-BRAF^{V600E} in primary cells results in oncogene-induced senescence (OIS), and as the latter has been implicated as a critical tumour-suppressive barrier in serrated pathway colorectal cancer, it was pertinent to compare the methylation changes induced by mutant-BRAF^{V600E} to those recently characterised in replicative senescence [30,47,281]. This was particularly relevant in light of a previous report of a CIMP-like phenotype in cells that have undergone replicative senescence, which was furthermore demonstrated to be associated with elevated DNMT3B expression [281]. Intriguingly, and unexpectedly, it was demonstrated that in comparison to replicative-senescence,

$BRAF^{V600E}$-induced proliferation arrest results in only very modest changes in DNA methylation. In comparison to replicative senescence, which is associated with a significant overall global reduction in DNA methylation, $BRAF^{V600E}$-induced proliferation arrest was associated with a small overall gain in DNA methylation. Interestingly however, the relatively small number of hypermethylated DMRs associated with mutant-$BRAF^{V600E}$ expression did demonstrate relative enrichment at CpG islands. Significantly, and in agreement with a more limited study by a previous group (who expressed mutant-$BRAF^{V600E}$ in a CIMP-negative colon cancer cell line) however, it was demonstrated that despite an apparent enrichment for CpG island DMRs, stable expression of activated mutant-$BRAF^{V600E}$ is insufficient to induce CIMP *in vitro* [479]. Furthermore, and in keeping with the failure to induce a CIMP phenotype, it was also demonstrated that acute $BRAF^{V600E}$ activation represses the expression of DNMT3B. In combination therefore, these data do not support a linear $BRAF^{V600E}$ – DNMT3B – CIMP pathway, as has previously been proposed [364].

As previous studies had linked elevated DNMT3B expression and $BRAF^{V600E}$ mutation in colorectal cancer, an *in vitro* model system was developed in chapter 5 in which to further examine the functional interactions between $BRAF^{V600E}$ and DNMT3B [47]. Remarkably, this demonstrated that combined expression of $BRAF^{V600E}$ and DNMT3B significantly impaired the ability of the former to induce a proliferation arrest phenotype, which was associated with increased expression of cell cycle drivers, including cyclin A, phosphorylated pRb and EZH2 [480]. Intriguingly, it was also demonstrated that this pro-proliferative function of DNMT3B might not be dependent on its catalytic domain. This latter result is interesting in light of previous studies which have demonstrated expression of truncated DNMT3B isoforms in cancer [222,225].

In order to further investigate the mechanism underlying the attenuated proliferation arrest phenotype driven by DNMT3B, expression-profiling was performed, comparing control, "DNMT3B only", "BRAF-only" and "BRAF/DNMT3B" cell populations using RNA-sequencing. Consistent with the observed pro-proliferative phenotype associated with combined BRAF/DNMT3B expression, this cell population exhibited significantly altered expression of cell cycle drivers (including cyclin A, cyclin D1, cyclin E, PCNA and E2F1). Interestingly, a recent meta-analysis has confirmed a relationship between elevated cyclin D1 expression and poor prognosis in human colorectal cancer [481]. A significant enrichment for cell cycle genes was also noted on GSEA gene-ontology analysis of those genes whose expression changed upon combined "BRAF/DNMT3B" expression compared

to “BRAF only”. Intriguingly, closer analysis of the RNA-sequencing data demonstrated that combined “BRAF/DNMT3B” expression also resulted in an impaired senescence-associated secretory phenotype (SASP). This is particularly notable given that the SASP has been demonstrated to promote proliferation arrest and immune clearance: both tumour-suppressive features of senescence [440,446]. Furthermore, combined “BRAF/DNMT3B” expression also resulted in significant changes in Wnt signalling, with “BRAF/DNMT3B” cells expressing higher levels of the Wnt targets Cyclin D1, Sox9, Claudin 1 and Myc, which have all previously been implicated in colorectal carcinogenesis [482-485]. Moreover, consistent with the observed phenotype in these cell culture experiments, activated Wnt signalling has been demonstrated to impair oncogene-induced senescence [429,442,447]. In summary, DNMT3B impairs, although does not completely bypass or prevent, the proliferation arrest phenotype induced by an activated $BRAF^{V600E}$ oncogene.

In light of the observation that DNMT3B impairs the proliferation arrest phenotype induced by an activated $BRAF^{V600E}$ oncogene, and in view of the previously published murine data supportive of an oncogenic function of DNMT3B in murine models of colon cancer, in chapter 6, the oncogenic function of DNMT3B was explored in a number of murine models of serrated pathway carcinogenesis, driven by activated $Braf^{V600E}$ by generating mice with both $Braf^{V600E}$ mutation and ectopic or absent DNMT3B expression. Remarkably, ectopic DNMT3B expression in $VilCreEr^{T2};^{LSL}Braf^{V600E}$+/- mice (a murine model of $BRAF^{V600E}$-driven serrated pathway cancer) led to a significant reduction in overall survival. In contrast to previously published data in the $Apc^{Min/+}$ model, this phenotypic acceleration was not associated with an increase in tumour number [205]. Moreover, in contrast to a previous report, an oncogene-induced senescence phenotype could not be characterised in this model system: though this may simply reflect differences in the sampling timepoint and protocol [47]. Furthermore, and in contrast to the *in vitro* data, ectopic DNMT3B expression did not noticeably alter the proliferation phenotype of intestinal crypts or tumours. Interestingly, whilst evidence of activated Wnt signalling was demonstrable in murine tumours driven by $Braf^{V600E}$, there was not a demonstrable difference between “BRAF-only” and “BRAF-DNMT3B” mice in this regard. Intriguingly however, the acceleration of BRAF-mediated carcinogenesis associated with DNMT3B ectopic expression was abrogated when combined with activated Wnt signalling in the $VilCreEr^{T2};^{LSL}Braf^{V600E}$+/-;$Apc^{fl/wt}$ model. Conversely, intestine-specific *Dnmt3b* knockout in a murine model of $Braf^{V600E}$-mediated intestinal carcinogenesis, increased survival, and mirroring the converse experiment did not affect tumour number. In keeping with the ectopic expression experiments however, the survival advantage of *Dnmt3b* deletion was

immediately abrogated when combined with activated Wnt signalling. Whilst no demonstrable difference in Wnt signalling could be ascertained by immunohistochemistry between *VilCreEr^{T2};^{LSL}Braf^{V600E}+/-* and *VilCreEr^{T2};^{LSL}Braf^{V600E}+/-;R26-M2-rtTA+/-;Col1a1-tetO-Dnmt3b1+/-* mice, this is a rather limited fashion in which to assess Wnt signalling, which may fail to detect subtle differences. Overall, when considered in light of the *in vitro* RNA-sequencing data generated in chapter 5, and data from previous studies in murine intestinal tumour models demonstrating altered expression of SFRP proteins in association with DNMT3B ectopic expression, it is tempting to conclude that altered Wnt signalling may be a significant contributing mechanism underlying the effects of DNMT3B on survival in *BRAF^{V600E}*-driven murine colorectal neoplasia [205]. Clearly, additional experiments would be required to further this hypothesis, and might include RNA-sequencing of intestinal crypts from *VilCreEr^{T2};^{LSL}Braf^{V600E}+/-* and *VilCreEr^{T2};^{LSL}Braf^{V600E}+/-;R26-M2-rtTA+/-;Col1a1-tetO-Dnmt3b1+/-* mice, or intercrossing to a Wnt reporter transgene [486].

Having established (at least in an *in vitro* model system) that mutant-BRAF^{V600E} represses DNMT3B expression, and is insufficient to induce a CpG island methylator phenotype, but that together BRAF^{V600E} and DNMT3B appear to exhibit oncogenic cooperation, it was appropriate to examine relationships between DNMT3B and BRAF in human colorectal cancer. Initial experiments in colon cancer cell lines in chapter 5 were supportive of the data generated in earlier chapters: failing to reveal a clear relationship between DNMT3B expression and *BRAF* mutation or CIMP status in colon cancer cell lines. Furthermore, whilst ectopic DNMT3B expression has been demonstrated to impair BRAF^{V600E}-induced proliferation arrest, and accelerate murine intestinal tumourigenesis driven by an activated *Braf^{V600E}* oncogene (at least in the absence of activated Wnt signalling), DNMT3B knockdown in a BRAF^{V600E}-mutant colon cancer cell line (LS411N) did not demonstrably affect proliferation. Interestingly, LS411N harbours an *APC* mutation, and active Wnt signalling [487]. Thus to an extent, this *in vitro* result mirrors the data generated in the *VilCreEr^{T2};^{LSL}Braf^{V600E}+/-;Apc$^{fl/wt}$* model, and may add further weight to the proposed Wnt-status dependency of DNMT3B's oncogenic function. Furthermore, in direct conflict with the model presented by Fang et al. [364], it was demonstrated that DNMT3B knockdown in a *BRAF^{V600E}*-mutant cell line does not restore expression of the CIMP-target gene *MLH1*. Similarly, ectopic expression of DNMT3B in an *MLH1* proficient, microsatellite stable cell line (HT-29) failed to induce silencing of *MLH1*: a key CIMP-marker, and a proposed target of the *BRAF^{V600E}*-mediated MAFG-BACH1-CHD8-DNMT3B complex described by Fang et al. [364]. Significantly, the data presented in this

thesis are consistent with the previously published murine data, which did not demonstrate *Mlh1* methylation in association with ectopic DNMT3B expression [205,434].

Taken together, the data summarised herein argue against a simple BRAF-DNMT3B-CIMP pathway. As the data thusfar were limited to the *in vitro* and *in vivo* contexts, it was appropriate to further explore relationships between BRAF, DNMT3B and CIMP in human colorectal cancer. In chapter 7, the human colorectal adenocarcinoma Cancer Genome Atlas (TCGA) data was utilised to characterise these relationships. Significantly, whilst *DNMT3B* mutations were demonstrated to be very uncommon in human colorectal cancer, DNMT3B was demonstrated to be frequently overexpressed in colorectal cancer tissue relative to normal colonic tissue, consistent with a potential oncogenic function as characterised above and in previous studies [205,433]. Furthermore, *DNMT3B* copy number was demonstrated to be frequently amplified in colorectal cancer, and demonstrated a strong association with DNMT3B mRNA expression.

Significantly, explicit examination of the relationship between $BRAF^{V600E}$ mutation and DNMT3B expression revealed a striking anticorrelation between $BRAF^{V600E}$ mutation and elevated DNMT3B expression in human colorectal cancer, consistent with the earlier *in vitro* data demonstrating repression of DNMT3B by activated $BRAF^{V600E}$. As it had earlier been demonstrated that mutant-$BRAF^{V600E}$ expression alone is insufficient to induce CIMP, this hypothesis was examined in the TCGA data. Importantly, whilst a statistically significant overlap between $BRAF^{V600E}$ mutation and CIMP-positivity was evident, $BRAF^{V600E}$ was neither necessary nor sufficient to induce CIMP. Furthermore, DNMT3B mRNA expression was significantly lower in CIMP-positive than CIMP-negative tumours, and interestingly this was also the case for the other candidate *de novo* methyltransferase, DNMT3A. Intriguingly however, and consistent with a previous report, TET1 expression was lower in CIMP-positive than CIMP-negative tumours [350]. Finally, it was demonstrated that elevated DNMT3B expression does not independently predict overall or disease-free survival in human colorectal cancer. Interestingly, this is in keeping with the murine data in which the survival effects of *Dnmt3b* manipulation are abrogated upon activated Wnt signalling. Together these data might suggest that DNMT3B's oncogenic function is most relevant at the earlier stages of neoplastic transformation, and is superseded by the progressive development of more powerful oncogenic stimuli (such as activated Wnt signalling) accompanying neoplastic transformation.

In summary, the data presented in this thesis directly challenge the current model of relationships between BRAF, DNMT3B and CIMP in human colorectal cancer, whereby DNMT3B contributes to CIMP in association with *BRAF*^{V600E} mutation and, in the most extreme form of the model, that mutant-BRAF^{V600E} drives CIMP via DNMT3B. By multiple approaches, it has been demonstrated that *BRAF*^{V600E} mutation is associated with repression of DNMT3B and is neither necessary nor sufficient to induce CIMP. Furthermore, it has been demonstrated that whilst DNMT3B overexpression and somatic copy number amplification are common features of human colorectal cancer, that they are inversely correlated with CIMP. Conversely, ectopic DNMT3B expression results in impaired *BRAF*^{V600E}-induced proliferation arrest, and promotes murine serrated pathway intestinal tumourigenesis driven by an activated *Braf*^{V600E} oncogene. Thus, whilst BRAF^{V600E} and DNMT3B both harbour oncogenic potential, they do not appear to cooperate to induce CIMP, and do not appear to cooperate frequently in human colorectal cancer by any mechanism.

8.2 Further Work

The data presented in this thesis do not support the existence of a linear BRAF-DNMT3B-CIMP pathway, nor the hypothesis that DNMT3B directly induces CIMP. The data do however support a possible oncogenic function of DNMT3B in colorectal carcinoma, and further work should explore further the potential mechanisms underlying this putative oncogenic function. One potential mechanism that has been developed in the present work is an interaction between DNMT3B and the Wnt signalling pathway. Further experiments both *in vitro* and *in vivo* would allow further dissection of this relationship. It would be of interest to repeat the combined DNMT3B/BRAF ectopic experiments presented in chapter 5 in the presence of small molecular inhibitor of Wnt to determine whether Wnt pathway inhibition abolishes the pro-proliferative phenotype associated with combined BRAF/DNMT3B ectopic expression. This relationship could also be explored *in vivo* by performing RNA-sequencing of intestinal crypts from *VilCreEr*^{T2}*;*^{LSL}*Braf*^{V600E}*+/-* and *VilCreEr*^{T2}*;*^{LSL}*Braf*^{V600E}*+/-;R26-M2-rtTA+/-;Col1a1-tetO-Dnmt3b1+/-* mice and specifically interrogating these data for Wnt pathway components. Furthermore, intercrossing *R26-M2-rtTA+/-;Col1a1-tetO-Dnmt3b1+/-* mice to a Wnt reporter transgene would allow direct assessment of whether DNMT3B ectopic expression alone is sufficient to activate the Wnt signalling pathway [486].

Whilst in this thesis, activated oncogenic $BRAF^{V600E}$ has not been demonstrated to induce a CpG island methylator phenotype (and this is supported by the later *in situ* data), there are certain caveats to this conclusion. Notably, the model used to assess the effects of activated mutant-$BRAF^{V600E}$ on DNA methylation was an *in vitro* primary human cell culture model system in fetal lung fibroblasts. Furthermore, the inability to maintain these cells in culture for a prolonged period meant that the effects of activated oncogenic $BRAF^{V600E}$ on DNA methylation were assayed in the "acute setting" rather than the prolonged period *in vivo* between the development of a pre-neoplastic lesion with an activating $BRAF^{V600E}$ mutation (e.g. hyperplastic polyp, SSA/P) and the subsequent development of a CIMP-high cancer. Furthermore, whilst ectopic BRAF expression was confirmed *in vitro*, downstream targets of its signalling pathway (to confirm MAPK pathway activation) were not formally assessed, though this could be addressed by the addition of phospho-ERK and phospho-MEK western blots. In order to resolve this limitation of the *in vitro* system, it would be of interest to assess the effects of activated oncogenic $BRAF^{V600E}$ on DNA methylation by undertaking whole-genome bisulfite sequencing of crypts (and/or tumours) isolated at an appropriate timepoint (e.g. >365 days post-induction) in $VilCreEr^{T2};{}^{LSL}Braf^{V600E}$+/- mice and $VilCreEr^{T2};{}^{LSL}Braf^{V600E}$-/- controls. This experiment would be more "physiological" than the *in vitro* model used in the present work, and would thus allow a more definitive conclusion to be drawn regarding the ability of activated oncogenic $BRAF^{V600E}$ to induce a CIMP phenotype.

References

1. Fearon ER, Vogelstein B. A genetic model for colorectal tumorigenesis. Cell. 1990 Jun 1;61(5):759–67.

2. Jass JR. Classification of colorectal cancer based on correlation of clinical, morphological and molecular features. Histopathology. 2007 Jan;50(1):113–30.

3. Longacre TA, Fenoglio-Preiser CM. Mixed hyperplastic adenomatous polyps/serrated adenomas. A distinct form of colorectal neoplasia. Am J Surg Pathol. 1990 Jun;14(6):524–37.

4. Wong NACS, Hunt LP, Novelli MR, Shepherd NA, Warren BF. Observer agreement in the diagnosis of serrated polyps of the large bowel. Histopathology. 2009 Jul;55(1):63–6.

5. Vakiani E, Yantiss RK. Pathologic features and biologic importance of colorectal serrated polyps. Adv Anat Pathol. 2009 Mar;16(2):79–91.

6. Bateman AC. Pathology of serrated colorectal lesions. J Clin Pathol. 2014 Oct;67(10):865–74.

7. Imperiale TF, Wagner DR, Lin CY, Larkin GN, Rogge JD, Ransohoff DF. Results of screening colonoscopy among persons 40 to 49 years of age. N Engl J Med. 2002 Jun 6;346(23):1781–5.

8. Lieberman DA, Prindiville S, Weiss DG, Willett W, VA Cooperative Study Group 380. Risk factors for advanced colonic neoplasia and hyperplastic polyps in asymptomatic individuals. JAMA. 2003 Dec 10;290(22):2959–67.

9. Estrada RG, Spjut HJ. Hyperplastic polyps of the large bowel. Am J Surg Pathol. 1980 Apr;4(2):127–33.

10. Yang S, Farraye FA, Mack C, Posnik O, O'Brien MJ. BRAF and KRAS Mutations in hyperplastic polyps and serrated adenomas of the colorectum: relationship to histology and CpG island methylation status. Am J Surg Pathol. 2004 Nov;28(11):1452–9.

11. Mesteri I, Bayer G, Meyer J, Capper D, Schoppmann SF, Deimling von A, et al. Improved molecular classification of serrated lesions of the colon by immunohistochemical detection of BRAF V600E. Modern Pathology. 2014 Jan;27(1):135–44.

12. Pollock PM, Harper UL, Hansen KS, Yudt LM, Stark M, Robbins CM, et al. High frequency of BRAF mutations in nevi. Nat Genet. 2003 Jan;33(1):19–20.

13. Rex DK, Ahnen DJ, Baron JA, Batts KP, Burke CA, Burt RW, et al. Serrated lesions of the colorectum: review and recommendations from an expert panel. 2012. pp. 1315–29.

14. Bettington M, Walker N, Clouston A, Brown I, Leggett B, Whitehall V. The serrated pathway to colorectal carcinoma: current concepts and challenges. Histopathology. 2013 Jan 22;62(3):367–86.

15. Spring KJ, Zhao ZZ, Karamatic R, Walsh MD, Whitehall VLJ, Pike T, et al. High

prevalence of sessile serrated adenomas with BRAF mutations: a prospective study of patients undergoing colonoscopy. Gastroenterology. 2006 Nov;131(5):1400–7.

16. Lash RH, Genta RM, Schuler CM. Sessile serrated adenomas: prevalence of dysplasia and carcinoma in 2139 patients. J Clin Pathol. 2010 Aug;63(8):681–6.

17. Fujita K, Yamamoto H, Matsumoto T, Hirahashi M, Gushima M, Kishimoto J, et al. Sessile serrated adenoma with early neoplastic progression: a clinicopathologic and molecular study. Am J Surg Pathol. 2011 Feb;35(2):295–304.

18. Torlakovic E, Skovlund E, Snover DC, Torlakovic G, Nesland JM. Morphologic reappraisal of serrated colorectal polyps. Am J Surg Pathol. 2003 Jan;27(1):65–81.

19. Bettington M, Walker N, Rosty C, Brown I, Clouston A, McKeone D, et al. Clinicopathological and molecular features of sessile serrated adenomas with dysplasia or carcinoma. Gut. 2017 Jan;66(1):97–106.

20. Jass JR. Serrated route to colorectal cancer: back street or super highway? J Pathol. 2001 Mar;193(3):283–5.

21. Sheridan TB, Fenton H, Lewin MR, Burkart AL, Iacobuzio-Donahue CA, Frankel WL, et al. Sessile serrated adenomas with low- and high-grade dysplasia and early carcinomas: an immunohistochemical study of serrated lesions "caught in the act". Am J Clin Pathol. 2006 Oct;126(4):564–71.

22. Buda A, De Bona M, Dotti I, Piselli P, Zabeo E, Barbazza R, et al. Prevalence of different subtypes of serrated polyps and risk of synchronous advanced colorectal neoplasia in average-risk population undergoing first-time colonoscopy. Clin Transl Gastroenterol. 2012 Jan 5;3(1):e6.

23. Torlakovic EE, Gomez JD, Driman DK, Parfitt JR, Wang C, Benerjee T, et al. Sessile serrated adenoma (SSA) vs. traditional serrated adenoma (TSA). Am J Surg Pathol. 2008 Jan;32(1):21–9.

24. Kim K-M, Lee EJ, Kim Y-H, Chang DK, Odze RD. KRAS mutations in traditional serrated adenomas from Korea herald an aggressive phenotype. Am J Surg Pathol. 2010 May;34(5):667–75.

25. Mäkinen MJ, George SM, Jernvall P, Mäkelä J, Vihko P, Karttunen TJ. Colorectal carcinoma associated with serrated adenoma--prevalence, histological features, and prognosis. J Pathol. 2001 Mar;193(3):286–94.

26. De Sousa E Melo F, Wang X, Jansen M, Fessler E, Trinh A, de Rooij LPMH, et al. Poor-prognosis colon cancer is defined by a molecularly distinct subtype and develops from serrated precursor lesions. Nature Medicine. 2013 May;19(5):614–8.

27. Guinney J, Dienstmann R, Wang X, de Reyniès A, Schlicker A, Soneson C, et al. The consensus molecular subtypes of colorectal cancer. Nature Medicine. 2015 Nov;21(11):1350–6.

28. Davies H, Bignell GR, Cox C, Stephens P, Edkins S, Clegg S, et al. Mutations of the BRAF gene in human cancer. Nature. 2002 Jun 27;417(6892):949–54.

29. Garnett MJ, Marais R. Guilty as charged. Cancer Cell. 2004 Oct;6(4):313–9.

30. Michaloglou C, Vredeveld LCW, Soengas MS, Denoyelle C, Kuilman T, van der Horst CMAM, et al. BRAFE600-associated senescence-like cell cycle arrest of human naevi. Nature. 2005 Aug 4;436(7051):720–4.

31. Wellbrock C, Karasarides M, Marais R. The RAF proteins take centre stage. Nat Rev Mol Cell Biol. 2004 Nov;5(11):875–85.

32. Wan PTC, Garnett MJ, Roe SM, Lee S, Niculescu-Duvaz D, Good VM, et al. Mechanism of activation of the RAF-ERK signaling pathway by oncogenic mutations of B-RAF. Cell. 2004 Mar 19;116(6):855–67.

33. Mercer K, Giblett S, Green S, Lloyd D, DaRocha Dias S, Plumb M, et al. Expression of endogenous oncogenic V600EB-raf induces proliferation and developmental defects in mice and transformation of primary fibroblasts. Cancer Research. 2005 Dec 15;65(24):11493–500.

34. Zhu J, Woods D, McMahon M, Bishop JM. Senescence of human fibroblasts induced by oncogenic Raf. Genes & Development. 1998 Oct 1;12(19):2997–3007.

35. Gray-Schopfer VC, Cheong SC, Chong H, Chow J, Moss T, Abdel-Malek ZA, et al. Cellular senescence in naevi and immortalisation in melanoma: a role for p16? British Journal of Cancer. 2006 Aug 21;95(4):496–505.

36. Dhomen N, Reis-Filho JS, da Rocha Dias S, Hayward R, Savage K, Delmas V, et al. Oncogenic Braf induces melanocyte senescence and melanoma in mice. Cancer Cell. 2009 Apr 7;15(4):294–303.

37. Kambara T, Simms LA, Whitehall VLJ, Spring KJ, Wynter CVA, Walsh MD, et al. BRAF mutation is associated with DNA methylation in serrated polyps and cancers of the colorectum. Gut. 2004 Aug;53(8):1137–44.

38. Chan TL, Zhao W, Leung SY, Yuen ST, Cancer Genome Project. BRAF and KRAS mutations in colorectal hyperplastic polyps and serrated adenomas. Cancer Research. 2003 Aug 15;63(16):4878–81.

39. Rajagopalan H, Bardelli A, Lengauer C, Kinzler KW, Vogelstein B, Velculescu VE. Tumorigenesis: RAF/RAS oncogenes and mismatch-repair status. Nature. 2002 Aug 29;418(6901):934–4.

40. Network TCGA. Comprehensive molecular characterization of human colon and rectal cancer. Nature. 2012 Jul 10;487(7407):330–7.

41. Fransén K, Klintenäs M, Osterström A, Dimberg J, Monstein H-J, Söderkvist P. Mutation analysis of the BRAF, ARAF and RAF-1 genes in human colorectal adenocarcinomas. Carcinogenesis. 2004 Apr;25(4):527–33.

42. Vaughn CP, Zobell SD, Furtado LV, Baker CL, Samowitz WS. Frequency of KRAS, BRAF, and NRAS mutations in colorectal cancer. Genes Chromosomes Cancer. 2011 May;50(5):307–12.

43. Giannakis M, Mu XJ, Shukla SA, Qian ZR, Cohen O, Nishihara R, et al. Genomic Correlates of Immune-Cell Infiltrates in Colorectal Carcinoma. Cell Reports. Elsevier; 2016 Oct 18;17(4):1206.

44. Yuen ST, Davies H, Chan TL, Ho JW, Bignell GR, Cox C, et al. Similarity of the

phenotypic patterns associated with BRAF and KRAS mutations in colorectal neoplasia. Cancer Research. 2002 Nov 15;62(22):6451–5.

45. Inoue A, Okamoto K, Fujino Y, Nakagawa T, Muguruma N, Sannomiya K, et al. B-RAF mutation and accumulated gene methylation in aberrant crypt foci (ACF), sessile serrated adenoma/polyp (SSA/P) and cancer in SSA/P. British Journal of Cancer. 2015 Jan 20;112(2):403–12.

46. Rad R, Cadiñanos J, Rad L, Varela I, Strong A, Kriegl L, et al. A Genetic Progression Model of BrafV600E-Induced Intestinal Tumorigenesis Reveals Targets for Therapeutic Intervention. Cancer Cell. 2013 Jul 8;24(1):15–29.

47. Carragher LAS, Snell KR, Giblett SM, Aldridge VSS, Patel B, Cook SJ, et al. V600EBraf induces gastrointestinal crypt senescence and promotes tumour progression through enhanced CpG methylation of p16INK4a. EMBO Mol Med. 2010 Oct 13;2(11):458–71.

48. Kriegl L, Neumann J, Vieth M, Greten FR, Reu S, Jung A, et al. Up and downregulation of p16Ink4a expression in BRAF-mutated polyps/adenomas indicates a senescence barrier in the serrated route to colon cancer. Modern Pathology. 2011 Mar 18;24(7):1015–22.

49. Bettington ML, Walker NI, Rosty C, Brown IS, Clouston AD, McKeone DM, et al. A clinicopathological and molecular analysis of 200 traditional serrated adenomas. Modern Pathology. 2015 Mar;28(3):414–27.

50. Bond CE, Umapathy A, Ramsnes I, Greco SA, Zhen Zhao Z, Mallitt K-A, et al. p53 mutation is common in microsatellite stable, BRAF mutant colorectal cancers. Int J Cancer. 2012 Apr 1;130(7):1567–76.

51. Gala MK, Mizukami Y, Le LP, Moriichi K, Austin T, Yamamoto M, et al. Gastroenterology. 2013 Oct 24;146(2):1–57.

52. Parada LF, Tabin CJ, Shih C, Weinberg RA. Human EJ bladder carcinoma oncogene is homologue of Harvey sarcoma virus ras gene. Nature. 1982 Jun 10;297(5866):474–8.

53. Der CJ, Krontiris TG, Cooper GM. Transforming genes of human bladder and lung carcinoma cell lines are homologous to the ras genes of Harvey and Kirsten sarcoma viruses. Proceedings of the National Academy of Sciences. 1982 Jun;79(11):3637–40.

54. Santos E, Tronick SR, Aaronson SA, Pulciani S, Barbacid M. T24 human bladder carcinoma oncogene is an activated form of the normal human homologue of BALB- and Harvey-MSV transforming genes. Nature. 1982 Jul 22;298(5872):343–7.

55. Spandidos DA, Kerr IB. Elevated expression of the human ras oncogene family in premalignant and malignant tumours of the colorectum. British Journal of Cancer. 1984 Jun;49(6):681–8.

56. Shimizu K, Goldfarb M, Suard Y, Perucho M, Li Y, Kamata T, et al. Three human transforming genes are related to the viral ras oncogenes. Proceedings of the National Academy of Sciences. 1983 Apr;80(8):2112–6.

57. Karnoub AE, Weinberg RA. Ras oncogenes: split personalities. Nat Rev Mol Cell Biol. 2008 Jul;9(7):517–31.

58. Newbold RF, Overell RW. Fibroblast immortality is a prerequisite for transformation by EJ c-Ha-ras oncogene. Nature. 1983 Aug;304(5927):648–51.

59. Land H, Parada LF, Weinberg RA. Tumorigenic conversion of primary embryo fibroblasts requires at least two cooperating oncogenes. Nature. 1983 Aug;304(5927):596–602.

60. Ruley HE. Adenovirus early region 1A enables viral and cellular transforming genes to transform primary cells in culture. Nature. 1983 Aug;304(5927):602–6.

61. Rhim JS, Jay G, Arnstein P, Price FM, Sanford KK, Aaronson SA. Neoplastic transformation of human epidermal keratinocytes by AD12-SV40 and Kirsten sarcoma viruses. Science. 1985 Mar 8;227(4691):1250–2.

62. Yoakum GH, Lechner JF, Gabrielson EW, Korba BE, Malan-Shibley L, Willey JC, et al. Transformation of human bronchial epithelial cells transfected by Harvey ras oncogene. Science. 1985 Mar 8;227(4691):1174–9.

63. Serrano M, Lin AW, McCurrach ME, Beach D, Lowe SW. Oncogenic ras provokes premature cell senescence associated with accumulation of p53 and p16INK4a. Cell. 1997 Mar 7;88(5):593–602.

64. Papp T, Pemsel H, Zimmermann R, Bastrop R, Weiss DG, Schiffmann D. Mutational analysis of the N-ras, p53, p16INK4a, CDK4, and MC1R genes in human congenital melanocytic naevi. J Med Genet. 1999 Aug;36(8):610–4.

65. Carr J, Mackie RM. Point mutations in the N-ras oncogene in malignant melanoma and congenital naevi. Br J Dermatol. 1994 Jul;131(1):72–7.

66. Bennecke M, Kriegl L, Bajbouj M, Retzlaff K, Robine S, Jung A, et al. Ink4a/Arf and Oncogene-Induced Senescence Prevent Tumor Progression during Alternative Colorectal Tumorigenesis. Cancer Cell. 2010 Aug;18(2):135–46.

67. Poynter JN, Elder JT, Fullen DR, Nair RP, Soengas MS, Johnson TM, et al. BRAF and NRAS mutations in melanoma and melanocytic nevi. Melanoma Res. 2006 Aug;16(4):267–73.

68. Otori K, Oda Y, Sugiyama K, Hasebe T, Mukai K, Fujii T, et al. High frequency of K-ras mutations in human colorectal hyperplastic polyps. Gut. 1997 May 1;40(5):660–3.

69. Janssen K-P, Marjou el F, Pinto D, Sastre X, Rouillard D, Fouquet C, et al. Targeted expression of oncogenic K-ras in intestinal epithelium causes spontaneous tumorigenesis in mice. Gastroenterology. 2002 Aug;123(2):492–504.

70. Sansom OJ, Meniel V, Wilkins JA, Cole AM, Oien KA, Marsh V, et al. Loss of Apc allows phenotypic manifestation of the transforming properties of an endogenous K-ras oncogene in vivo. Proceedings of the National Academy of Sciences. 2006 Sep 19;103(38):14122–7.

71. Haigis KM, Kendall KR, Wang Y, Cheung A, Haigis MC, Glickman JN, et al. Differential effects of oncogenic K-Ras and N-Ras on proliferation, differentiation

and tumor progression in the colon. Nat Genet. 2008 May;40(5):600–8.

72. Trobridge P, Knoblaugh S, Washington MK, Munoz NM, Tsuchiya KD, Rojas A, et al. TGF-beta receptor inactivation and mutant Kras induce intestinal neoplasms in mice via a beta-catenin-independent pathway. Gastroenterology. 2009 May;136(5):1680–7.

73. Bennecke M, Kriegl L, Bajbouj M, Retzlaff K, Robine S, Jung A, et al. Ink4a/Arf and Oncogene-Induced Senescence Prevent Tumor Progression during Alternative Colorectal Tumorigenesis. Cancer Cell. 2010 Aug 17;18(2):135–46.

74. Bettington M, Walker N, Rosty C, Brown I, Clouston A, McKeone D, et al. Serrated tubulovillous adenoma of the large intestine. Histopathology. 2016 Mar;68(4):578–87.

75. Riemer P, Sreekumar A, Reinke S, Rad R, Schäfer R, Sers C, et al. Transgenic expression of oncogenic BRAF induces loss of stem cells in the mouse intestine, which is antagonized by β-catenin activity. Oncogene. 2014 Aug 11;34(24):3164–75.

76. Iacopetta B, Grieu F, Li W, Ruszkiewicz A, Caruso M, Moore J, et al. APC gene methylation is inversely correlated with features of the CpG island methylator phenotype in colorectal cancer. Int J Cancer. 2006 Nov 15;119(10):2272–8.

77. Samowitz WS, Slattery ML, Sweeney C, Herrick J, Wolff RK, Albertsen H. APC mutations and other genetic and epigenetic changes in colon cancer. Molecular Cancer Research. 2007 Feb;5(2):165–70.

78. Dehari R. Infrequent APC mutations in serrated adenoma. Tohoku J Exp Med. 2001 Mar;193(3):181–6.

79. Yamamoto T, Konishi K, Yamochi T, Makino R, Kaneko K, Shimamura T, et al. No major tumorigenic role for beta-catenin in serrated as opposed to conventional colorectal adenomas. British Journal of Cancer. 2003 Jul 7;89(1):152–7.

80. Wu JM, Montgomery EA, Iacobuzio-Donahue CA. Frequent beta-catenin nuclear labeling in sessile serrated polyps of the colorectum with neoplastic potential. Am J Clin Pathol. 2008 Mar;129(3):416–23.

81. Yachida S, Mudali S, Martin SA, Montgomery EA, Iacobuzio-Donahue CA. Beta-catenin nuclear labeling is a common feature of sessile serrated adenomas and correlates with early neoplastic progression after BRAF activation. Am J Surg Pathol. 2009 Dec;33(12):1823–32.

82. Sandmeier D, Benhattar J, Martin P, Bouzourene H. Serrated polyps of the large intestine: a molecular study comparing sessile serrated adenomas and hyperplastic polyps. Histopathology. 2009 Aug;55(2):206–13.

83. Yachida S, Mudali S, Martin SA, Montgomery EA, Iacobuzio-Donahue CA. Beta-catenin nuclear labeling is a common feature of sessile serrated adenomas and correlates with early neoplastic progression after BRAF activation. Am J Surg Pathol. 2009 Dec;33(12):1823–32.

84. Fujita K, Yamamoto H, Matsumoto T, Hirahashi M, Gushima M, Kishimoto J, et al. Sessile serrated adenoma with early neoplastic progression: a clinicopathologic

and molecular study. Am J Surg Pathol. 2011 Feb;35(2):295–304.

85. de Vogel S, Weijenberg MP, Herman JG, Wouters KAD, de Goeij AFPM, van den Brandt PA, et al. MGMT and MLH1 promoter methylation versus APC, KRAS and BRAF gene mutations in colorectal cancer: indications for distinct pathways and sequence of events. Ann Oncol. 2009 Jul;20(7):1216–22.

86. Panarelli NC, Vaughn CP, Samowitz WS, Yantiss RK. Sporadic microsatellite instability-high colon cancers rarely display immunohistochemical evidence of Wnt signaling activation. Am J Surg Pathol. 2015 Mar;39(3):313–7.

87. Suzuki H, Watkins DN, Jair K-W, Schuebel KE, Markowitz SD, Chen WD, et al. Epigenetic inactivation of SFRP genes allows constitutive WNT signaling in colorectal cancer. Nat Genet. 2004 Apr;36(4):417–22.

88. Fu X, Li J, Li K, Tian X, Zhang Y. Hypermethylation of APC promoter 1A is associated with moderate activation of Wnt signalling pathway in a subset of colorectal serrated adenomas. Histopathology. 2009 Nov;55(5):554–63.

89. Rawson JB, Manno M, Mrkonjic M, Daftary D, Dicks E, Buchanan DD, et al. Promoter methylation of Wnt antagonists DKK1 and SFRP1 is associated with opposing tumor subtypes in two large populations of colorectal cancer patients. Carcinogenesis. 2011 May;32(5):741–7.

90. Ying J, Li H, Yu J, Ng KM, Poon FF, Wong SCC, et al. WNT5A exhibits tumor-suppressive activity through antagonizing the Wnt/beta-catenin signaling, and is frequently methylated in colorectal cancer. Clinical Cancer Research. 2008 Jan 1;14(1):55–61.

91. Rawson JB, Mrkonjic M, Daftary D, Dicks E, Buchanan DD, Younghusband HB, et al. Promoter methylation of Wnt5a is associated with microsatellite instability and BRAF V600E mutation in two large populations of colorectal cancer patients. Br J Cancer. 2011 Jun 7;104(12):1906–12.

92. Murakami T, Mitomi H, Saito T, Takahashi M, Sakamoto N, Fukui N, et al. Distinct WNT/β-catenin signaling activation in the serrated neoplasia pathway and the adenoma-carcinoma sequence of the colorectum. Modern Pathology. 2015 Jan;28(1):146–58.

93. Dhir M, Yachida S, Van Neste L, Glöckner SC, Jeschke J, Pappou EP, et al. Sessile serrated adenomas and classical adenomas: an epigenetic perspective on premalignant neoplastic lesions of the gastrointestinal tract. Int J Cancer. 2011 Oct 15;129(8):1889–98.

94. Kohonen-Corish MRJ, Sigglekow ND, Susanto J, Chapuis PH, Bokey EL, Dent OF, et al. Promoter methylation of the mutated in colorectal cancer gene is a frequent early event in colorectal cancer. Oncogene. 2007 Jun 28;26(30):4435–41.

95. Koinuma K, Yamashita Y, Liu W, Hatanaka H, Kurashina K, Wada T, et al. Epigenetic silencing of AXIN2 in colorectal carcinoma with microsatellite instability. Oncogene. 2006 Jan 5;25(1):139–46.

96. Sakai E, Fukuyo M, Ohata K, Matsusaka K, Doi N, Mano Y, et al. Genetic and epigenetic aberrations occurring in colorectal tumors associated with serrated pathway. Int J Cancer. 2016 Apr 1;138(7):1634–44.

97. Giannakis M, Hodis E, Jasmine Mu X, Yamauchi M, Rosenbluh J, Cibulskis K, et al. RNF43 is frequently mutated in colorectal and endometrial cancers. Nat Genet. 2014 Dec;46(12):1264–6.

98. Koo B-K, Spit M, Jordens I, Low TY, Stange DE, van de Wetering M, et al. Tumour suppressor RNF43 is a stem-cell E3 ligase that induces endocytosis of Wnt receptors. Nature. 2012 Aug 30;488(7413):665–9.

99. Tsukiyama T, Fukui A, Terai S, Fujioka Y, Shinada K, Takahashi H, et al. Molecular Role of RNF43 in Canonical and Noncanonical Wnt Signaling. Mol Cell Biol. 2015 Jun 1;35(11):2007–23.

100. Loregger A, Grandl M, Mejías-Luque R, Allgäuer M, Degenhart K, Haselmann V, et al. The E3 ligase RNF43 inhibits Wnt signaling downstream of mutated β-catenin by sequestering TCF4 to the nuclear membrane. Sci Signal. 2015 Sep 8;8(393):ra90–0.

101. Sekine S, Yamashita S, Tanabe T, Hashimoto T, Yoshida H, Taniguchi H, et al. Frequent PTPRK-RSPO3 fusions and RNF43 mutations in colorectal traditional serrated adenoma. J Pathol. 2016 Jun;239(2):133–8.

102. Tsai J-H, Liau J-Y, Yuan C-T, Lin Y-L, Tseng L-H, Cheng M-L, et al. RNF43 Is an Early and Specific Mutated Gene in the Serrated Pathway, With Increased Frequency in Traditional Serrated Adenoma and Its Associated Malignancy. Am J Surg Pathol. 2016 Oct;40(10):1352–9.

103. Yan HHN, Lai JCW, Ho SL, Leung WK, Law WL, Lee JFY, et al. RNF43 germline and somatic mutation in serrated neoplasia pathway and its association with BRAF mutation. Gut. 2016 Jun 21;:gutjnl–2016–311849.

104. Boland CR, Goel A. Microsatellite Instability in Colorectal Cancer. Gastroenterology. 2010 May 1;138(6):2073–3.

105. Boland CR, Thibodeau SN, Hamilton SR, Sidransky D, Eshleman JR, Burt RW, et al. A National Cancer Institute Workshop on Microsatellite Instability for cancer detection and familial predisposition: development of international criteria for the determination of microsatellite instability in colorectal cancer. Cancer Research. 1998. pp. 5248–57.

106. Umar A, Boland CR, Terdiman JP, Syngal S, la Chapelle de A, Rüschoff J, et al. Revised Bethesda Guidelines for hereditary nonpolyposis colorectal cancer (Lynch syndrome) and microsatellite instability. J Natl Canc Inst. 2004. pp. 261–8.

107. Nardon E, Glavač D, Benhattar J, Groenen PJTA, Höfler G, Höfler H, et al. A multicenter study to validate the reproducibility of MSI testing with a panel of 5 quasimonomorphic mononucleotide repeats. Diagn Mol Pathol. 2010 Dec;19(4):236–42.

108. Peltomäki P, Lothe RA, Aaltonen LA, Pylkkänen L, Nyström-Lahti M, Seruca R, et al. Microsatellite instability is associated with tumors that characterize the hereditary non-polyposis colorectal carcinoma syndrome. Cancer Research. 1993 Dec 15;53(24):5853–5.

109. Lynch HT, Lynch PM, Harris RE. Minimal genetic findings and their cancer control implications. A family with the cancer family syndrome. JAMA. 1978 Aug

11;240(6):535–8.

110. Hampel H, Frankel WL, Martin E, Arnold M, Khanduja K, Kuebler P, et al. Screening for the Lynch syndrome (hereditary nonpolyposis colorectal cancer). N Engl J Med. 2005 May 5;352(18):1851–60.

111. Thibodeau SN, Bren G, Schaid D. Microsatellite instability in cancer of the proximal colon. Science. 1993 May 7;260(5109):816–9.

112. Ionov Y, Peinado MA, Malkhosyan S, Shibata D, Perucho M. Ubiquitous somatic mutations in simple repeated sequences reveal a new mechanism for colonic carcinogenesis. Nature. 1993 Jun 10;363(6429):558–61.

113. Toyota M, Ahuja N, Ohe-Toyota M, Herman JG, Baylin SB, Issa JP. CpG island methylator phenotype in colorectal cancer. Proceedings of the National Academy of Sciences. 1999 Jul 20;96(15):8681–6.

114. Kane MF, Loda M, Gaida GM, Lipman J, Mishra R, Goldman H, et al. Methylation of the hMLH1 promoter correlates with lack of expression of hMLH1 in sporadic colon tumors and mismatch repair-defective human tumor cell lines. Cancer Research. 1997 Mar 1;57(5):808–11.

115. Veigl ML, Kasturi L, Olechnowicz J, Ma AH, Lutterbaugh JD, Periyasamy S, et al. Biallelic inactivation of hMLH1 by epigenetic gene silencing, a novel mechanism causing human MSI cancers. Proceedings of the National Academy of Sciences. 1998 Jul 21;95(15):8698–702.

116. Weisenberger DJ, Siegmund KD, Campan M, Young J, Long TI, Faasse MA, et al. CpG island methylator phenotype underlies sporadic microsatellite instability and is tightly associated with BRAF mutation in colorectal cancer. Nat Genet. 2006 Jun 25;38(7):787–93.

117. Koinuma K, Shitoh K, Miyakura Y, Furukawa T, Yamashita Y, Ota J, et al. Mutations of BRAF are associated with extensive hMLH1 promoter methylation in sporadic colorectal carcinomas. Int J Cancer. 2004 Jan 10;108(2):237–42.

118. Wang L, Cunningham JM, Winters JL, Guenther JC, French AJ, Boardman LA, et al. BRAF mutations in colon cancer are not likely attributable to defective DNA mismatch repair. Cancer Research. 2003 Sep 1;63(17):5209–12.

119. Jass JR, Biden KG, Cummings MC, Simms LA, Walsh M, Schoch E, et al. Characterisation of a subtype of colorectal cancer combining features of the suppressor and mild mutator pathways. J Clin Pathol. 1999 Jun;52(6):455–60.

120. Hawkins NJ, Ward RL. Sporadic colorectal cancers with microsatellite instability and their possible origin in hyperplastic polyps and serrated adenomas. J Natl Cancer Inst. 2001 Sep 5;93(17):1307–13.

121. Tuppurainen K, Mäkinen JM, Junttila O, Liakka A, Kyllönen AP, Tuominen H, et al. Morphology and microsatellite instability in sporadic serrated and non-serrated colorectal cancer. J Pathol. 2005 Nov;207(3):285–94.

122. Iino H, Jass JR, Simms LA, Young J, Leggett B, Ajioka Y, et al. DNA microsatellite instability in hyperplastic polyps, serrated adenomas, and mixed polyps: a mild mutator pathway for colorectal cancer? J Clin Pathol. 1999

Jan;52(1):5–9.

123. Hiyama T, Yokozaki H, Shimamoto F, Haruma K, Yasui W, Kajiyama G, et al. Frequent p53 gene mutations in serrated adenomas of the colorectum. J Pathol. 1998 Oct 1;186(2):131–9.

124. Sawyer EJ, Cerar A, Hanby AM, Gorman P, Arends M, Talbot IC, et al. Molecular characteristics of serrated adenomas of the colorectum. Gut. 2002 Aug;51(2):200–6.

125. O'Brien MJ, Yang S, Mack C, Xu H, Huang CS, Mulcahy E, et al. Comparison of microsatellite instability, CpG island methylation phenotype, BRAF and KRAS status in serrated polyps and traditional adenomas indicates separate pathways to distinct colorectal carcinoma end points. Am J Surg Pathol. 2006 Dec;30(12):1491–501.

126. Matos P, Oliveira C, Velho S, Gonçalves V, da Costa LT, Moyer MP, et al. B-RafV600E Cooperates With Alternative Spliced Rac1b to Sustain Colorectal Cancer Cell Survival. Gastroenterology. 2008 Sep;135(3):899–906.

127. Silva A-L, Carmo F, Bugalho MJ. RAC1b overexpression in papillary thyroid carcinoma: a role to unravel. Eur J Endocrinol. 2013 Jun;168(6):795–804.

128. Matos P, Jordan P. Expression of Rac1b stimulates NF-kappaB-mediated cell survival and G1/S progression. Experimental Cell Research. 2005 May 1;305(2):292–9.

129. Matos P, Jordan P. Increased Rac1b expression sustains colorectal tumor cell survival. Molecular Cancer Research. American Association for Cancer Research; 2008 Jul;6(7):1178–84.

130. Alonso-Espinaco V, Cuatrecasas M, Alonso V, Escudero P, Marmol M, Horndler C, et al. RAC1b overexpression correlates with poor prognosis in KRAS/BRAF WT metastatic colorectal cancer patients treated with first-line FOLFOX/XELOX chemotherapy. Eur J Cancer. 2014 Jul;50(11):1973–81.

131. Henriques AFA, Barros P, Moyer MP, Matos P, Jordan P. Expression of tumor-related Rac1b antagonizes B-Raf-induced senescence in colorectal cells. Cancer Lett. 2015 Dec 28;369(2):368–75.

132. Buongiorno P, Pethe VV, Charames GS, Esufali S, Bapat B. Rac1 GTPase and the Rac1 exchange factor Tiam1 associate with Wnt-responsive promoters to enhance beta-catenin/TCF-dependent transcription in colorectal cancer cells. Mol Cancer. 2008 Sep 30;7(1):73.

133. Bapat B. Rac1b recruits Dishevelled and β-catenin to Wnt target gene promoters independent of Wnt3A stimulation. Int J Oncol. 2011 Jun 6;:1–6.

134. Esufali S, Charames GS, Pethe VV, Buongiorno P, Bapat B. Activation of tumor-specific splice variant Rac1b by dishevelled promotes canonical Wnt signaling and decreased adhesion of colorectal cancer cells. Cancer Research. 2007 Mar 15;67(6):2469–79.

135. Bourgeois M, Holliday R, Pugh J, Brush J, Douglas N, Khayum R, et al. DNA modification mechanisms and gene activity during development. Science.

1975;187(4173):226–32.

136. Vardimon L, Kressmann A, Cedar H, Maechler M, Doerfler W. Expression of a cloned adenovirus gene is inhibited by in vitro methylation. Proceedings of the National Academy of Sciences. 1982 Feb 1;79(4):1073–7.

137. Stein R, Razin A, Cedar H. In vitro methylation of the hamster adenine phosphoribosyltransferase gene inhibits its expression in mouse L cells. Proceedings of the National Academy of Sciences. 1982 Jun;79(11):3418–22.

138. Ramsahoye BH, Biniszkiewicz D, Lyko F, Clark V, Bird AP, Jaenisch R. Non-CpG methylation is prevalent in embryonic stem cells and may be mediated by DNA methyltransferase 3a. Proceedings of the National Academy of Sciences. 2000 May 9;97(10):5237–42.

139. Lister R, Pelizzola M, Dowen RH, Hawkins RD, Hon G, Tonti-Filippini J, et al. Human DNA methylomes at base resolution show widespread epigenomic differences. Nature. 2009 Nov 19;462(7271):315–22.

140. Saxonov S, Berg P, Brutlag DL. A genome-wide analysis of CpG dinucleotides in the human genome distinguishes two distinct classes of promoters. Proceedings of the National Academy of Sciences. 2006 Jan 31;103(5):1412–7.

141. Bird AP. CpG-rich islands and the function of DNA methylation. Nature. 1986 May 15;321(6067):209–13.

142. Weber M, Davies JJ, Wittig D, Oakeley EJ, Haase M, Lam WL, et al. Chromosome-wide and promoter-specific analyses identify sites of differential DNA methylation in normal and transformed human cells. Nat Genet. 2005 Aug 1;37(8):853–62.

143. Lock LF, Takagi N, Martin GR. Methylation of the Hprt gene on the inactive X occurs after chromosome inactivation. Cell. 1987 Jan 16;48(1):39–46.

144. Li E, Beard C, Jaenisch R. Role for DNA methylation in genomic imprinting. Nature. 1993 Dec 25;366(6453):362–5.

145. Takeshima H, Yamashita S, Shimazu T, Niwa T, Ushijima T. The presence of RNA polymerase II, active or stalled, predicts epigenetic fate of promoter CpG islands. Genome Research. 2009 Nov;19(11):1974–82.

146. Landolin JM, Johnson DS, Trinklein ND, Aldred SF, Medina C, Shulha H, et al. Sequence features that drive human promoter function and tissue specificity. Genome Research. 2010 Jul;20(7):890–8.

147. Barski A, Cuddapah S, Cui K, Roh T-Y, Schones DE, Wang Z, et al. High-resolution profiling of histone methylations in the human genome. Cell. 2007 May 18;129(4):823–37.

148. Kelly TK, Miranda TB, Liang G, Berman BP, Lin JC, Tanay A, et al. H2A.Z maintenance during mitosis reveals nucleosome shifting on mitotically silenced genes. Molecular Cell. 2010 Sep 24;39(6):901–11.

149. Ooi SKT, Qiu C, Bernstein E, Li K, Jia D, Yang Z, et al. DNMT3L connects unmethylated lysine 4 of histone H3 to de novo methylation of DNA. Nature. 2007

Aug 9;448(7154):714–7.

150. Lee J-H, Tate CM, You J-S, Skalnik DG. Identification and characterization of the human Set1B histone H3-Lys4 methyltransferase complex. Journal of Biological Chemistry. 2007 May 4;282(18):13419–28.

151. Thomson JP, Skene PJ, Selfridge J, Clouaire T, Guy J, Webb S, et al. CpG islands influence chromatin structure via the CpG-binding protein Cfp1. Nature. 2010 Apr 15;464(7291):1082–6.

152. Hendrich B, Bird A. Identification and characterization of a family of mammalian methyl-CpG binding proteins. Molecular and Cellular Biology. 1998 Nov;18(11):6538–47.

153. Klose RJ, Bird AP. Genomic DNA methylation: the mark and its mediators. Trends in Biochemical Sciences. 2006 Feb;31(2):89–97.

154. Lin JC, Jeong S, Liang G, Takai D, Fatemi M, Tsai YC, et al. Role of nucleosomal occupancy in the epigenetic silencing of the MLH1 CpG island. Cancer Cell. 2007 Nov;12(5):432–44.

155. Fahrner JA, Eguchi S, Herman JG, Baylin SB. Dependence of histone modifications and gene expression on DNA hypermethylation in cancer. Cancer Research. 2002 Dec 15;62(24):7213–8.

156. Mohn F, Weber M, Rebhan M, Roloff TC, Richter J, Stadler MB, et al. Lineage-specific polycomb targets and de novo DNA methylation define restriction and potential of neuronal progenitors. 2008 Jun 20;30(6):755–66.

157. Ohm JE, McGarvey KM, Yu X, Cheng L, Schuebel KE, Cope L, et al. A stem cell-like chromatin pattern may predispose tumor suppressor genes to DNA hypermethylation and heritable silencing. Nat Genet. 2007 Feb;39(2):237–42.

158. Viré E, Brenner C, Deplus R, Blanchon L, Fraga M, Didelot C, et al. The Polycomb group protein EZH2 directly controls DNA methylation. Nature. 2006 Feb 16;439(7078):871–4.

159. Yoder JA, Walsh CP, Bestor TH. Cytosine methylation and the ecology of intragenomic parasites. Trends in Genetics. 1997 Aug;13(8):335–40.

160. Laurent L, Wong E, Li G, Huynh T, Tsirigos A, Ong CT, et al. Dynamic changes in the human methylome during differentiation. Genome Research. 2010 Mar;20(3):320–31.

161. Shukla S, Kavak E, Gregory M, Imashimizu M, Shutinoski B, Kashlev M, et al. CTCF-promoted RNA polymerase II pausing links DNA methylation to splicing. Nature. Nature Research; 2011 Nov 3;479(7371):74–9.

162. Maunakea AK, Nagarajan RP, Bilenky M, Ballinger TJ, D'Souza C, Fouse SD, et al. Conserved role of intragenic DNA methylation in regulating alternative promoters. Nature. 2010 Jul 8;466(7303):253–7.

163. Yang X, Han H, De Carvalho DD, Lay FD, Jones PA, Liang G. Gene Body Methylation Can Alter Gene Expression and Is a Therapeutic Target in Cancer. Cancer Cell. 2014 Sep 23;26(4):1–14.

164. Baubec T, Colombo DF, Wirbelauer C, Schmidt J, Burger L, Krebs AR, et al. Genomic profiling of DNA methyltransferases reveals a role for DNMT3B in genic methylation. Nature. 2015 Apr 9;520(7546):243–7.

165. Neri F, Rapelli S, Krepelova A, Incarnato D, Parlato C, Basile G, et al. Intragenic DNA methylation prevents spurious transcription initiation. Nature. 2017 Mar 2;543(7643):72–7.

166. Stadler MB, Murr R, Burger L, Ivanek R, Lienert F, Schöler A, et al. DNA-binding factors shape the mouse methylome at distal regulatory regions. Nature. 2011 Dec 14;480(7378):490–5.

167. Schmidl C, Klug M, Boeld TJ, Andreesen R, Hoffmann P, Edinger M, et al. Lineage-specific DNA methylation in T cells correlates with histone methylation and enhancer activity. Genome Research. 2009 Jul;19(7):1165–74.

168. Bock C, Beerman I, Lien W-H, Smith ZD, Gu H, Boyle P, et al. DNA methylation dynamics during in vivo differentiation of blood and skin stem cells. Molecular Cell. 2012 Aug 24;47(4):633–47.

169. Aran D, Sabato S, Hellman A. DNA methylation of distal regulatory sites characterizes dysregulation of cancer genes. Genome Biol. 2013;14(3):R21.

170. Blattler A, Yao L, Witt H, Guo Y, Nicolet CM, Berman BP, et al. Global loss of DNA methylation uncovers intronic enhancers in genes showing expression changes. Genome Biol. 2014 Sep 20;15(9):469.

171. Barau J, Teissandier A, Zamudio N, Roy S, Nalesso V, Hérault Y, et al. The DNA methyltransferase DNMT3C protects male germ cells from transposon activity. Science. 2016 Nov 18;354(6314):909–12.

172. Bestor T, Laudano A, Mattaliano R, Ingram V. Cloning and sequencing of a cDNA encoding DNA methyltransferase of mouse cells. The carboxyl-terminal domain of the mammalian enzymes is related to bacterial restriction methyltransferases. J Mol Biol. 1988 Oct 20;203(4):971–83.

173. Gruenbaum Y, Cedar H, Razin A. Substrate and sequence specificity of a eukaryotic DNA methylase. Nature. 1982 Feb 18;295(5850):620–2.

174. Chuang LS. Human DNA-(Cytosine-5) Methyltransferase-PCNA Complex as a Target for p21WAF1. Science. 1997 Sep 26;277(5334):1996–2000.

175. Leonhardt H, Page AW, Weier HU, Bestor TH. A targeting sequence directs DNA methyltransferase to sites of DNA replication in mammalian nuclei. Cell. 1992 Nov 27;71(5):865–73.

176. Sharif J, Muto M, Takebayashi S-I, Suetake I, Iwamatsu A, Endo TA, et al. The SRA protein Np95 mediates epigenetic inheritance by recruiting Dnmt1 to methylated DNA. Nature. 2007 Dec 6;450(7171):908–12.

177. Spada F, Haemmer A, Kuch D, Rothbauer U, Schermelleh L, Kremmer E, et al. DNMT1 but not its interaction with the replication machinery is required for maintenance of DNA methylation in human cells. J Cell Biol. 2007 Feb 26;176(5):565–71.

178. Li E, Bestor TH, Jaenisch R. Targeted mutation of the DNA methyltransferase gene results in embryonic lethality. Cell. 1992 Jun 12;69(6):915–26.

179. Liao J, Karnik R, Gu H, Ziller MJ, Clement K, Tsankov AM, et al. Targeted disruption of DNMT1, DNMT3A and DNMT3B in human embryonic stem cells. Nat Genet. 2015 May 1;47(5):469–78.

180. Tsumura A, Hayakawa T, Kumaki Y, Takebayashi S-I, Sakaue M, Matsuoka C, et al. Maintenance of self-renewal ability of mouse embryonic stem cells in the absence of DNA methyltransferases Dnmt1, Dnmt3a and Dnmt3b. Genes Cells. 2006 Jul;11(7):805–14.

181. Barra V, Schillaci T, Lentini L, Costa G, Di Leonardo A. Bypass of cell cycle arrest induced by transient DNMT1 post-transcriptional silencing triggers aneuploidy in human cells. Cell Div. 2012 Feb 3;7(1):2.

182. Jackson-Grusby L, Beard C, Possemato R, Tudor M, Fambrough D, Csankovszki G, et al. Loss of genomic methylation causes p53-dependent apoptosis and epigenetic deregulation. Nat Genet. 2001 Jan;27(1):31–9.

183. Eden A, Gaudet F, Waghmare A, Jaenisch R. Chromosomal instability and tumors promoted by DNA hypomethylation. Science. 2003 Apr 18;300(5618):455–5.

184. Gaudet F, Hodgson JG, Eden A, Jackson-Grusby L, Dausman J, Gray JW, et al. Induction of tumors in mice by genomic hypomethylation. Science. 2003 Apr 18;300(5618):489–92.

185. Laird PW, Jackson-Grusby L, Fazeli A, Dickinson SL, Jung WE, Li E, et al. Suppression of intestinal neoplasia by DNA hypomethylation. Cell. 1995 Apr 21;81(2):197–205.

186. Cormier RT, Dove WF. Dnmt1N/+ Reduces the Net Growth Rate and Multiplicity of Intestinal Adenomas in C57BL/6-Multiple Intestinal Neoplasia (Min)/+ Mice Independently of p53 but Demonstrates Strong Synergy with the Modifier of Min 1AKR Resistance Allele. Cancer Research. 2000 Jul 15;60(14):3965–70.

187. Yoder JA, Bestor TH. A candidate mammalian DNA methyltransferase related to pmt1p of fission yeast. Human Molecular Genetics. 1998 Feb;7(2):279–84.

188. Okano M, Xie S, Li E. Dnmt2 is not required for de novo and maintenance methylation of viral DNA in embryonic stem cells. Nucleic Acids Research. 1998 Jun 1;26(11):2536–40.

189. Raddatz G, Guzzardo PM, Olova N, Fantappié MR, Rampp M, Schaefer M, et al. Dnmt2-dependent methylomes lack defined DNA methylation patterns. Proc Natl Acad Sci USA. 2013 May 21;110(21):8627–31.

190. Goll MG, Kirpekar F, Maggert KA, Yoder JA, Hsieh C-L, Zhang X, et al. Methylation of tRNAAsp by the DNA methyltransferase homolog Dnmt2. Science. 2006 Jan 20;311(5759):395–8.

191. Choi SH, Heo K, Byun HM, An W, Lu W, Yang AS. Identification of preferential target sites for human DNA methyltransferases. Nucleic Acids Research. 2011 Jan 6;39(1):104–18.

192. Lei H, Oh SP, Okano M, Jüttermann R, Goss KA, Jaenisch R, et al. De novo DNA cytosine methyltransferase activities in mouse embryonic stem cells. Development. 1996 Oct;122(10):3195–205.

193. Okano M, Xie S, Li E. Cloning and characterization of a family of novel mammalian DNA (cytosine-5) methyltransferases. Nat Genet. 1998 Jul 1;19(3):219–20.

194. Hsieh CL. In vivo activity of murine de novo methyltransferases, Dnmt3a and Dnmt3b. Molecular and Cellular Biology. 1999 Dec;19(12):8211–8.

195. Robertson KD, Uzvolgyi E, Liang G, Talmadge C, Sumegi J, Gonzales FA, et al. The human DNA methyltransferases (DNMTs) 1, 3a and 3b: coordinate mRNA expression in normal tissues and overexpression in tumors. Nucleic Acids Res. 1999 Jun 1;27(11):2291–8.

196. Xie S, Wang Z, Okano M, Nogami M, Li Y, He WW, et al. Cloning, expression and chromosome locations of the human DNMT3 gene family. Gene. 1999 Aug 5;236(1):87–95.

197. Okano M, Bell DW, Haber DA, Li E. DNA methyltransferases Dnmt3a and Dnmt3b are essential for de novo methylation and mammalian development. Cell. 1999 Oct 29;99(3):247–57.

198. Weisenberger DJ, Velicescu M, Preciado-Lopez MA, Gonzales FA, Tsai YC, Liang G, et al. Identification and characterization of alternatively spliced variants of DNA methyltransferase 3a in mammalian cells. Gene. 2002 Sep 18;298(1):91–9.

199. Chen T, Ueda Y, Xie S, Li E. A novel Dnmt3a isoform produced from an alternative promoter localizes to euchromatin and its expression correlates with active de novo methylation. Journal of Biological Chemistry. 2002 Oct 11;277(41):38746–54.

200. Deng T, Kuang Y, Wang L, Li J, Wang Z, Fei J. An essential role for DNA methyltransferase 3a in melanoma tumorigenesis. Biochemical and Biophysical Research Communications. 2009 Sep 25;387(3):611–6.

201. Cao X-Y. DNA methyltransferase3a expression is an independent poor prognostic indicator in gastric cancer. WJG. 2014;20(25):8201–9.

202. Cui H, Zhao C, Gong P, Wang L, Wu H, Zhang K, et al. DNA methyltransferase 3A promotes cell proliferation by silencing CDK inhibitor p18INK4C in gastric carcinogenesis. Sci Rep. 2015 Aug 27;:1–13.

203. Schmidt WM, Sedivy R, Forstner B, Steger GG, Zöchbauer-Müller S, Mader RM. Progressive up-regulation of genes encoding DNA methyltransferases in the colorectal adenoma-carcinoma sequence. Mol Carcinog. 2007 Sep;46(9):766–72.

204. Weis B, Schmidt J, Maamar H, Raj A, Lin H, Tóth C, et al. Inhibition of intestinal tumor formation by deletion of the DNA methyltransferase 3a. Oncogene. Nature Publishing Group; 2014 May 19;0(14):1822–30.

205. Linhart HG, Lin H, Yamada Y, Moran E, Steine EJ, Gokhale S, et al. Dnmt3b promotes tumorigenesis in vivo by gene-specific de novo methylation and

transcriptional silencing. Genes & Development. 2007 Dec 1;21(23):3110–22.

206. Samuel MS, Suzuki H, Buchert M, Putoczki TL, Tebbutt NC, Lundgren May T, et al. Elevated Dnmt3a Activity Promotes Polyposis in *Apc*^{Min} Mice by Relaxing Extracellular Restraints on Wnt Signaling. Gastroenterology. 2009 Sep;137(3):902–11.

207. Gao Q, Steine EJ, Barrasa MI, Hockemeyer D, Pawlak M, Fu D, et al. Deletion of the de novo DNA methyltransferase Dnmt3a promotes lung tumor progression. Proc Natl Acad Sci USA. 2011 Nov 1;108(44):18061–6.

208. Raddatz G, Gao Q, Bender S, Jaenisch R, Lyko F. Dnmt3a protects active chromosome domains against cancer-associated hypomethylation. PLoS Genet. 2012;8(12):e1003146.

209. Ley TJ, Ding L, Walter MJ, McLellan MD, Lamprecht T, Larson DE, et al. DNMT3A mutations in acute myeloid leukemia. N Engl J Med. 2010 Dec 16;363(25):2424–33.

210. Russler-Germain DA, Spencer DH, Young MA, Lamprecht TL, Miller CA, Fulton R, et al. The R882H DNMT3A mutation associated with AML dominantly inhibits wild-type DNMT3A by blocking its ability to form active tetramers. Cancer Cell. 2014 Apr 14;25(4):442–54.

211. Jeong M, Sun D, Luo M, Huang Y, Challen GA, Rodriguez B, et al. Large conserved domains of low DNA methylation maintained by Dnmt3a. Nat Genet. 2014 Jan 1;46(1):17–23.

212. Challen GA, Sun D, Jeong M, Luo M, Jelinek J, Berg JS, et al. Dnmt3a is essential for hematopoietic stem cell differentiation. 2011 Dec 4;44(1):23–31.

213. Spencer DH, Russler-Germain DA, Ketkar S, Helton NM, Lamprecht TL, Fulton RS, et al. CpG Island Hypermethylation Mediated by DNMT3A Is a Consequence of AML Progression. Cell. 2017 Feb;168(5):801–13.

214. Bachman KE, Rountree MR, Baylin SB. Dnmt3a and Dnmt3b are transcriptional repressors that exhibit unique localization properties to heterochromatin. J Biol Chem. 2001 Aug 24;276(34):32282–7.

215. Chen T, Tsujimoto N, Li E. The PWWP domain of Dnmt3a and Dnmt3b is required for directing DNA methylation to the major satellite repeats at pericentric heterochromatin. Molecular and Cellular Biology. 2004 Oct;24(20):9048–58.

216. Gopalakrishnan S, Sullivan BA, Trazzi S, Valle Della G, Robertson KD. DNMT3B interacts with constitutive centromere protein CENP-C to modulate DNA methylation and the histone code at centromeric regions. Human Molecular Genetics. 2009 Aug 7;18(17):3178–93.

217. Smeets DF, Moog U, Weemaes CM, Vaes-Peeters G, Merkx GF, Niehof JP, et al. ICF syndrome: a new case and review of the literature. Hum Genet. 1994 Sep;94(3):240–6.

218. Heyn H, Vidal E, Sayols S, Sanchez-Mut JV, Moran S, Medina I, et al. Whole-genome bisulfite DNA sequencing of a DNMT3B mutant patient. epigenetics. 2012 Jun 1;7(6):542–50.

219. Tiedemann RL, Putiri EL, Lee J-H, Hlady RA, Kashiwagi K, Ordog T, et al. Acute Depletion Redefines the Division of Labor among DNA Methyltransferases in Methylating the Human Genome. Cell Reports. 2014 Nov 20;9(4):1554–66.

220. Weisenberger DJ, Velicescu M, Cheng JC, Gonzales FA, Liang G, Jones PA. Role of the DNA methyltransferase variant DNMT3b3 in DNA methylation. Molecular Cancer Research. 2004 Jan;2(1):62–72.

221. Wang J, Walsh G, Liu DD, Lee JJ, Mao L. Expression of Delta DNMT3B variants and its association with promoter methylation of p16 and RASSF1A in primary non-small cell lung cancer. Cancer Research. 2006 Sep 1;66(17):8361–6.

222. Ostler KR, Davis EM, Payne SL, Gosalia BB, Expósito-Céspedes J, Beau MML, et al. Cancer cells express aberrant DNMT3B transcripts encoding truncated proteins. Oncogene. 2007 Mar 12;26(38):5553–63.

223. Gopalakrishnan S, Van Emburgh BO, Shan J, Su Z, Fields CR, Vieweg J, et al. A novel DNMT3B splice variant expressed in tumor and pluripotent cells modulates genomic DNA methylation patterns and displays altered DNA binding. Molecular Cancer Research. 2009 Oct;7(10):1622–34.

224. Gordon CA, Hartono SR, Chédin F. Inactive DNMT3B Splice Variants Modulate De Novo DNA Methylation. PLoS ONE. 2013 Jul 22;8(7):e69486.

225. Duymich CE, Charlet J, Yang X, Jones PA, Liang G. DNMT3B isoforms without catalytic activity stimulate gene body methylation as accessory proteins in somatic cells. Nature Communications. 2016 Apr 21;7:1–9.

226. Beaulieu N. An Essential Role for DNA Methyltransferase DNMT3B in Cancer Cell Survival. Journal of Biological Chemistry. 2002 May 15;277(31):28176–81.

227. Soejima K, Fang W, Rollins BJ. DNA methyltransferase 3b contributes to oncogenic transformation induced by SV40T antigen and activated Ras. Oncogene. 2003 Jul 24;22(30):4723–33.

228. Lin H, Yamada Y, Nguyen S, Linhart H, Jackson-Grusby L, Meissner A, et al. Suppression of intestinal neoplasia by deletion of Dnmt3b. Mol Cell Biol. 2006 Apr;26(8):2976–83.

229. Linhart HG, Lin H, Yamada Y, Moran E, Steine EJ, Gokhale S, et al. Dnmt3b promotes tumorigenesis in vivo by gene-specific de novo methylation and transcriptional silencing. Genes & Development. 2007 Dec 1;21(23):3110–22.

230. Huidobro C, Urdinguio RG, Rodríguez RM, Mangas C, Calvanese V, Martínez-Camblor P, et al. A DNA methylation signature associated with aberrant promoter DNA hypermethylation of DNMT3B in human colorectal cancer. Eur J Cancer. 2012 Sep;48(14):2270–81.

231. Micevic G, Muthusamy V, Damsky W, Theodosakis N, Liu X, Meeth K, et al. DNMT3b Modulates Melanoma Growth by Controlling Levels of mTORC2 Component RICTOR. Cell Reports. 2016 Mar 8;14(9):2180–92.

232. Venza M, Visalli M, Biondo C, Lentini M, Catalano T, Teti D, et al. Epigenetic regulation of p14ARF and p16INK4A expression in cutaneous and uveal melanoma. Biochim Biophys Acta. 2015 Mar;1849(3):247–56.

233. Hlady RA, Novakova S, Opavska J, Klinkebiel D, Peters SL, Bies J, et al. Loss of Dnmt3b function upregulates the tumor modifier Ment and accelerates mouse lymphomagenesis. J Clin Invest. 2012 Jan 3;122(1):163–77.

234. Haney SL, Hlady RA, Opavska J, Klinkebiel D, Pirruccello SJ, Dutta S, et al. Methylation-independent repression of Dnmt3b contributes to oncogenic activity of Dnmt3a in mouse MYC-induced T-cell lymphomagenesis. Oncogene. 2015 Oct;34(43):5436–46.

235. Vasanthakumar A, Lepore JB, Zegarek MH, Kocherginsky M, Singh M, Davis EM, et al. Dnmt3b is a haploinsufficient tumor suppressor gene in Myc-induced lymphomagenesis. Blood. 2013 Mar 14;121(11):2059–63.

236. Amara K, Ziadi S, Hachana M, Soltani N, Korbi S, Trimeche M. DNA methyltransferase DNMT3b protein overexpression as a prognostic factor in patients with diffuse large B cell lymphomas. Cancer Sci. 2010 Jul 1;101(7):1722–30.

237. Schulze I, Rohde C, Scheller-Wendorff M, Bäumer N, Krause A, Herbst F, et al. Increased DNA methylation of Dnmt3b targets impairs leukemogenesis. Blood. 2016 Mar 24;127(12):1575–86.

238. Zheng Y, Zhang H, Wang Y, Li X, Lu P, Dong F, et al. Loss of Dnmt3b accelerates MLL-AF9 leukemia progression. Leukemia. 2016 Dec;30(12):2373–84.

239. Peters SL, Hlady RA, Opavska J, Klinkebiel D, Pirruccello SJ, Talmon GA, et al. Tumor suppressor functions of Dnmt3a and Dnmt3b in the prevention of malignant mouse lymphopoiesis. Leukemia. 2014 May;28(5):1138–42.

240. Hayette S, Thomas X, Jallades L, Chabane K, Charlot C, Tigaud I, et al. High DNA methyltransferase DNMT3B levels: a poor prognostic marker in acute myeloid leukemia. PLoS ONE. 2012;7(12):e51527.

241. Niederwieser C, Kohlschmidt J, Volinia S, Whitman SP, Metzeler KH, Eisfeld A-K, et al. Prognostic and biologic significance of DNMT3B expression in older patients with cytogenetically normal primary acute myeloid leukemia. Leukemia. 2015 Mar;29(3):567–75.

242. Aapola U, Shibuya K, Scott HS, Ollila J, Vihinen M, Heino M, et al. Isolation and Initial Characterization of a Novel Zinc Finger Gene, DNMT3L, on 21q22.3, Related to the Cytosine-5- Methyltransferase 3 Gene Family. Genomics. 2000 May;65(3):293–8.

243. Bourc'his D, Xu GL, Lin CS, Bollman B, Bestor TH. Dnmt3L and the establishment of maternal genomic imprints. Science. 2001 Dec 21;294(5551):2536–9.

244. Aapola U, Mäenpää K, Kaipia A, Peterson P. Epigenetic modifications affect Dnmt3L expression. Biochem J. 2004 Jun 15;380(Pt 3):705–13.

245. Hata K, Okano M, Lei H, Li E. Dnmt3L cooperates with the Dnmt3 family of de novo DNA methyltransferases to establish maternal imprints in mice. Development. 2002 Apr;129(8):1983–93.

246. Chédin F, Lieber MR, Hsieh C-L. The DNA methyltransferase-like protein DNMT3L stimulates de novo methylation by Dnmt3a. Proceedings of the National Academy of Sciences. 2002 Dec 24;99(26):16916–21.

247. Gowher H, Liebert K, Hermann A, Xu G, Jeltsch A. Mechanism of stimulation of catalytic activity of Dnmt3A and Dnmt3B DNA-(cytosine-C5)-methyltransferases by Dnmt3L. Journal of Biological Chemistry. 2005 Apr 8;280(14):13341–8.

248. Kareta MS, Botello ZM, Ennis JJ, Chou C, Chédin F. Reconstitution and mechanism of the stimulation of de novo methylation by human DNMT3L. Journal of Biological Chemistry. 2006 Sep 8;281(36):25893–902.

249. Neri F, Krepelova A, Incarnato D, Maldotti M, Parlato C, Galvagni F, et al. Dnmt3L antagonizes DNA methylation at bivalent promoters and favors DNA methylation at gene bodies in ESCs. Cell. 2013 Sep 26;155(1):121–34.

250. Minami K, Chano T, Kawakami T, Ushida H, Kushima R, Okabe H, et al. DNMT3L is a novel marker and is essential for the growth of human embryonal carcinoma. Clinical Cancer Research. 2010 May 15;16(10):2751–9.

251. Sen GL, Reuter JA, Webster DE, Zhu L, Khavari PA. DNMT1 maintains progenitor function in self-renewing somatic tissue. Nature. 2010 Jan 28;463(7280):563–7.

252. Cheng H, Bjerknes M. Cell production in mouse intestinal epithelium measured by stathmokinetic flow cytometry and Coulter particle counting. Anat Rec. 1983 Nov;207(3):427–34.

253. Totafurno J, Bjerknes M, Cheng H. The crypt cycle. Crypt and villus production in the adult intestinal epithelium. Biophys J. 1987 Aug;52(2):279–94.

254. Sheaffer KL, Kim R, Aoki R, Elliott EN, Schug J, Burger L, et al. DNA methylation is required for the control of stem cell differentiation in the small intestine. Genes & Development. 2014 Mar 17;28(6):652–64.

255. Georgia S, Kanji M, Bhushan A. DNMT1 represses p53 to maintain progenitor cell survival during pancreatic organogenesis. Genes & Development. 2013 Feb 15;27(4):372–7.

256. Fan G, Beard C, Chen RZ, Csankovszki G, Sun Y, Siniaia M, et al. DNA hypomethylation perturbs the function and survival of CNS neurons in postnatal animals. J Neurosci. 2001 Feb 1;21(3):788–97.

257. Elliott EN, Sheaffer KL, Schug J, Stappenbeck TS, Kaestner KH. Dnmt1 is essential to maintain progenitors in the perinatal intestinal epithelium. Development. 2015 Jun 15;142(12):2163–72.

258. Yu D-H, Gadkari M, Zhou Q, Yu S, Gao N, Guan Y, et al. Postnatal epigenetic regulation of intestinal stem cells requires DNA methylation and is guided by the microbiome. Genome Biol. 2015 Sep 30;16(1):211.

259. Elliott EN, Sheaffer KL, Kaestner KH. The “de novo” DNA methyltransferase Dnmt3b compensates the Dnmt1-deficient intestinal epithelium. eLife. 2016 Jan 25;5:27.

260. Kaaij LTJ, van de Wetering M, Fang F, Decato B, Molaro A, van de Werken HJG, et al. DNA methylation dynamics during intestinal stem cell differentiation reveals enhancers driving gene expression in the villus. Genome Biol. 2013 May 28;14(5):R50.

261. Issa JP, Ottaviano YL, Celano P, Hamilton SR, Davidson NE, Baylin SB. Methylation of the oestrogen receptor CpG island links ageing and neoplasia in human colon. Nat Genet. 1994 Aug;7(4):536–40.

262. Ahuja N, Li Q, Mohan AL, Baylin SB, Issa JP. Aging and DNA methylation in colorectal mucosa and cancer. Cancer Research. 1998 Dec 1;58(23):5489–94.

263. Maegawa S, Hinkal G, Kim HS, Shen L, Zhang L, Zhang J, et al. Widespread and tissue specific age-related DNA methylation changes in mice. Genome Research. 2010 Mar;20(3):332–40.

264. Steegenga WT, de Wit NJ, Boekschoten MV, IJssennagger N, Lute C, Keshtkar S, et al. Structural, functional and molecular analysis of the effects of aging in the small intestine and colon of C57BL/6J mice. BMC Medical Genomics; 2012 Aug 28;5(1):1–1.

265. Hannum G, Guinney J, Zhao L, Zhang L, Hughes G, Sadda S, et al. Genome-wide methylation profiles reveal quantitative views of human aging rates. Molecular Cell. 2013 Jan 24;49(2):359–67.

266. Horvath S. DNA methylation age of human tissues and cell types. Genome Biol. 2013;14(10):R115.

267. Bork S, Pfister S, Witt H, Horn P, Korn B, Ho AD, et al. DNA methylation pattern changes upon long-term culture and aging of human mesenchymal stromal cells. Aging Cell. 2010 Feb;9(1):54–63.

268. Rakyan VK, Down TA, Maslau S, Andrew T, Yang T-P, Beyan H, et al. Human aging-associated DNA hypermethylation occurs preferentially at bivalent chromatin domains. Genome Research. 2010 Apr;20(4):434–9.

269. Teschendorff AE, Menon U, Gentry-Maharaj A, Ramus SJ, Weisenberger DJ, Shen H, et al. Age-dependent DNA methylation of genes that are suppressed in stem cells is a hallmark of cancer. Genome Research. 2010 Apr;20(4):440–6.

270. Noreen F, Röösli M, Gaj P, Pietrzak J, Weis S, Urfer P, et al. Modulation of age- and cancer-associated DNA methylation change in the healthy colon by aspirin and lifestyle. J Natl Cancer Inst. 2014 Jul;106(7):161–1.

271. Kamiyama H, Suzuki K, Maeda T, Koizumi K, Miyaki Y, Okada S, et al. DNA demethylation in normal colon tissue predicts predisposition to multiple cancers. Oncogene. 2012 Nov 29;31(48):5029–37.

272. Hayflick L. The limited in vitro lifetime of human diploid cell strains. Experimental Cell Research. 1965 Mar;37:614–36.

273. Jeyapalan JC, Ferreira M, Sedivy JM, Herbig U. Accumulation of senescent cells in mitotic tissue of aging primates. Mechanisms of Ageing and Development. 2007 Jan;128(1):36–44.

274. Waaijer MEC, Gunn DA, Adams PD, Pawlikowski JS, Griffiths CEM, van Heemst D, et al. P16INK4a Positive Cells in Human Skin Are Indicative of Local Elastic Fiber Morphology, Facial Wrinkling, and Perceived Age. J Gerontol. 2016 Aug;71(8):1022–8.

275. Childs BG, Baker DJ, Wijshake T, Conover CA, Campisi J, van Deursen JM. Senescent intimal foam cells are deleterious at all stages of atherosclerosis. Science. 2016 Oct 28;354(6311):472–7.

276. Choi J, Shendrik I, Peacocke M, Peehl D, Buttyan R, Ikeguchi EF, et al. Expression of senescence-associated beta-galactosidase in enlarged prostates from men with benign prostatic hyperplasia. Urology. 2000 Jul;56(1):160–6.

277. Price JS, Waters JG, Darrah C, Pennington C, Edwards DR, Donell ST, et al. The role of chondrocyte senescence in osteoarthritis. Aging Cell. 2002 Oct;1(1):57–65.

278. Campisi J. Senescent cells, tumor suppression, and organismal aging: good citizens, bad neighbors. Cell. 2005 Feb 25;120(4):513–22.

279. Zhang W, Ji W, Yang J, Yang L, Chen W, Zhuang Z. Comparison of global DNA methylation profiles in replicative versus premature senescence. Life Sciences. 2008 Sep 26;83(13-14):475–80.

280. Wilson VL, Jones PA. DNA methylation decreases in aging but not in immortal cells. Science. 1983 Jun 3;220(4601):1055–7.

281. Cruickshanks HA, McBryan T, Nelson DM, Van der Kraats ND, Shah PP, van Tuyn J, et al. Senescent cells harbour features of the cancer epigenome. Nat Cell Biol. 2013 Nov 24;15(12):1495–506.

282. Franzen J, Zirkel A, Blake J, Rath B, Benes V, Papantonis A, et al. Senescence-associated DNA methylation is stochastically acquired in subpopulations of mesenchymal stem cells. Aging Cell. 2016 Oct 26.

283. Koch CM, Reck K, Shao K, Lin Q, Joussen S, Ziegler P, et al. Pluripotent stem cells escape from senescence-associated DNA methylation changes. Genome Research. 2013 Feb;23(2):248–59.

284. Beggs AD, Jones A, El-Bahwary M, Abulafi M, Hodgson SV, Tomlinson IP. Whole-genome methylation analysis of benign and malignant colorectal tumours. J Pathol. 2013 Jan 24;229(5):697–704.

285. Feinberg AP, Vogelstein B. Hypomethylation distinguishes genes of some human cancers from their normal counterparts. Nature. 1983 Jan 6;301(5895):89–92.

286. Feinberg AP, Gehrke CW, Kuo KC, Ehrlich M. Reduced genomic 5-methylcytosine content in human colonic neoplasia. Cancer Research. 1988 Mar 1;48(5):1159–61.

287. Berman BP, Weisenberger DJ, Aman JF, Hinoue T, Ramjan Z, Liu Y, et al. Regions of focal DNA hypermethylation and long-range hypomethylation in colorectal cancer coincide with nuclear lamina-associated domains. Nat Genet. 2012 Jan;44(1):40–6.

288. Bhave MR, Wilson MJ, Poirier LA. c-H-ras and c-K-ras gene hypomethylation in

the livers and hepatomas of rats fed methyl-deficient, amino acid-defined diets. Carcinogenesis. 1988 Mar;9(3):343–8.

289. Tao L, Yang S, Xie M, Kramer PM, Pereira MA. Hypomethylation and overexpression of c-jun and c-myc protooncogenes and increased DNA methyltransferase activity in dichloroacetic and trichloroacetic acid-promoted mouse liver tumors. Cancer Letters. 2000 Oct 1;158(2):185–93.

290. Howard G, Eiges R, Gaudet F, Jaenisch R, Eden A. Activation and transposition of endogenous retroviral elements in hypomethylation induced tumors in mice. Oncogene. 2008 Jan 10;27(3):404–8.

291. Chen RZ, Pettersson U, Beard C, Jackson-Grusby L, Jaenisch R. DNA hypomethylation leads to elevated mutation rates. Nature. 1998 Sep 3;395(6697):89–93.

292. Holm TM, Jackson-Grusby L, Brambrink T, Yamada Y, Rideout WM, Jaenisch R. Global loss of imprinting leads to widespread tumorigenesis in adult mice. Cancer Cell. 2005 Oct;8(4):275–85.

293. Baylin SB, Höppener JW, de Bustros A, Steenbergh PH, Lips CJ, Nelkin BD. DNA methylation patterns of the calcitonin gene in human lung cancers and lymphomas. Cancer Research. 1986 Jun;46(6):2917–22.

294. Ottaviano YL, Issa JP, Parl FF, Smith HS, Baylin SB, Davidson NE. Methylation of the estrogen receptor gene CpG island marks loss of estrogen receptor expression in human breast cancer cells. Cancer Research. 1994 May 15;54(10):2552–5.

295. Merlo A, Herman JG, Mao L, Lee DJ, Gabrielson E, Burger PC, et al. 5' CpG island methylation is associated with transcriptional silencing of the tumour suppressor p16/CDKN2/MTS1 in human cancers. Nature Medicine. 1995 Jul;1(7):686–92.

296. Barekati Z, Radpour R, Kohler C, Zhang B, Toniolo P, Lenner P, et al. Methylation profile of TP53 regulatory pathway and mtDNA alterations in breast cancer patients lacking TP53 mutations. Hum Mol Genet. 2010 Aug 1;19(15):2936–46.

297. Bachman KE, Park BH, Rhee I, Rajagopalan H, Herman JG, Baylin SB, et al. Histone modifications and silencing prior to DNA methylation of a tumor suppressor gene. Cancer Cell. 2003 Jan;3(1):89–95.

298. Raynal NJM, Si J, Taby RF, Gharibyan V, Ahmed S, Jelinek J, et al. DNA Methylation Does Not Stably Lock Gene Expression but Instead Serves as a Molecular Mark for Gene Silencing Memory. Cancer Research. 2012 Mar 1;72(5):1170–81.

299. Pruitt K, Zinn RL, Ohm JE, McGarvey KM, Kang S-HL, Watkins DN, et al. Inhibition of SIRT1 reactivates silenced cancer genes without loss of promoter DNA hypermethylation. PLoS Genet. 2006 Mar;2(3):e40.

300. Irizarry RA, Ladd-Acosta C, Wen B, Wu Z, Montano C, Onyango P, et al. The human colon cancer methylome shows similar hypo- and hypermethylation at conserved tissue-specific CpG island shores. Nat Genet. 2009 Jan 18;41(2):178–

86.

301. Doi A, Park I-H, Wen B, Murakami P, Aryee MJ, Irizarry R, et al. Differential methylation of tissue- and cancer-specific CpG island shores distinguishes human induced pluripotent stem cells, embryonic stem cells and fibroblasts. Nat Gen. 2009 Dec;41(12):1350–3.

302. Rao X, Evans J, Chae H, Pilrose J, Kim S, Yan P, et al. CpG island shore methylation regulates caveolin-1 expression in breast cancer. Oncogene. 2013 Sep 19;32(38):4519–28.

303. Sproul D, Meehan RR. Genomic insights into cancer-associated aberrant CpG island hypermethylation. Brief Funct Genomics. 2013 May;12(3):174–90.

304. Ahuja N, Mohan AL, Li Q, Stolker JM, Herman JG, Hamilton SR, et al. Association between CpG Island Methylation and Microsatellite Instability in Colorectal Cancer. Cancer Research. 1997 Aug 15;57(16):3370–4.

305. Yamashita K, Dai T, Dai Y, Yamamoto F, Perucho M. Genetics supersedes epigenetics in colon cancer phenotype. Cancer Cell. 2003 Aug;4(2):121–31.

306. Anacleto C, Leopoldino AM, Rossi B, Soares FA. Colorectal cancer "methylator phenotype": fact or artifact? Neoplasia. 2005;72(1):179.

307. Issa J-P. CpG island methylator phenotype in cancer. Nat Rev Cancer. 2004 Dec;4(12):988–93.

308. Ogino S, Kawasaki T, Brahmandam M, Cantor M, Kirkner GJ, Spiegelman D, et al. Precision and Performance Characteristics of Bisulfite Conversion and Real-Time PCR (MethyLight) for Quantitative DNA Methylation Analysis. The Journal of Molecular Diagnostics. 2006 May 1;8(2):209–17.

309. Samowitz WS, Albertsen H, Herrick J, Levin TR, Sweeney C, Murtaugh MA, et al. Evaluation of a Large, Population-Based Sample Supports a CpG Island Methylator Phenotype in Colon Cancer. Gastroenterology. 2005 Sep;129(3):837–45.

310. Ogino S, Cantor M, Kawasaki T, Brahmandam M, Kirkner GJ, Weisenberger DJ, et al. CpG island methylator phenotype (CIMP) of colorectal cancer is best characterised by quantitative DNA methylation analysis and prospective cohort studies. Gut. 2006 Jul;55(7):1000–6.

311. Weisenberger DJ, Siegmund KD, Campan M, Young J, Long TI, Faasse MA, et al. CpG island methylator phenotype underlies sporadic microsatellite instability and is tightly associated with BRAF mutation in colorectal cancer. Nat Genet. 2006 Jul;38(7):787–93.

312. Ogino S, Kawasaki T, Kirkner GJ, Loda M, Fuchs CS. CpG island methylator phenotype-low (CIMP-low) in colorectal cancer: possible associations with male sex and KRAS mutations. The Journal of Molecular Diagnostics. 2006 Nov;8(5):582–8.

313. Hinoue T, Weisenberger DJ, Lange CPE, Shen H, Byun H-M, Van Den Berg D, et al. Genome-scale analysis of aberrant DNA methylation in colorectal cancer. Genome Research. 2012 Feb;22(2):271–82.

314. Cancer Genome Atlas Network. Comprehensive molecular characterization of human colon and rectal cancer. Nature. 2012 Jul 19;487(7407):330–7.

315. Yagi K, Akagi K, Hayashi H, Nagae G, Tsuji S, Isagawa T, et al. Three DNA Methylation Epigenotypes in Human Colorectal Cancer. Clin Cancer Res. 2010 Jan 1;16(1):21–33.

316. Yagi K, Takahashi H, Akagi K, Matsusaka K, Seto Y, Aburatani H, et al. Intermediate methylation epigenotype and its correlation to KRAS mutation in conventional colorectal adenoma. Am J Pathol. 2012 Feb;180(2):616–25.

317. Hawkins N, Norrie M, Cheong K, Mokany E, Ku SL, Meagher A, et al. CpG island methylation in sporadic colorectal cancers and its relationship to microsatellite instability. Gastroenterology. 2002 May 1;122(5):1376–87.

318. Ogino S. CpG island methylator phenotype (CIMP) of colorectal cancer is best characterised by quantitative DNA methylation analysis and prospective cohort studies. Gut. 2006 Feb 16;55(7):1000–6.

319. Ogino S, Kawasaki T, Kirkner GJ, Kraft P, Loda M, Fuchs CS. Evaluation of markers for CpG island methylator phenotype (CIMP) in colorectal cancer by a large population-based sample. The Journal of Molecular Diagnostics. 2007 Jul;9(3):305–14.

320. Xu Y, Hu B, Choi A-J, Gopalan B, Lee BH, Kalady MF, et al. Unique DNA methylome profiles in CpG island methylator phenotype colon cancers. Genome Research. 2012 Feb 1;22(2):283–91.

321. Hur K, Cejas P, Feliu J, Moreno-Rubio J, Burgos E, Boland CR, et al. Hypomethylation of long interspersed nuclear element-1 (LINE-1) leads to activation of proto-oncogenes in human colorectal cancer metastasis. Gut. 2014 Apr;63(4):635–46.

322. Ogino S, Nosho K, Kirkner GJ. A cohort study of tumoral LINE-1 hypomethylation and prognosis in colon cancer. Journal of the National Cancer Institute. 2008;100(23):1734–8.

323. Ogino S, Kawasaki T, Nosho K, Ohnishi M, Suemoto Y, Kirkner GJ, et al. LINE-1 hypomethylation is inversely associated with microsatellite instability and CpG island methylator phenotype in colorectal cancer. Int J Cancer. 2008 Jun 15;122(12):2767–73.

324. Nosho K, Irahara N, Shima K, Kure S, Kirkner GJ, Schernhammer ES, et al. Comprehensive biostatistical analysis of CpG island methylator phenotype in colorectal cancer using a large population-based sample. PLoS ONE. 2008;3(11):e3698.

325. Tahara T, Yamamoto E, Madireddi P, Suzuki H, Maruyama R, Chung W, et al. Colorectal carcinomas with CpG island methylator phenotype 1 frequently contain mutations in chromatin regulators. Gastroenterology. 2014 Feb;146(2):530–5.

326. Nosho K, Shima K, Irahara N, Kure S, Firestein R, Baba Y, et al. SIRT1 histone deacetylase expression is associated with microsatellite instability and CpG island methylator phenotype in colorectal cancer. Mod Pathol. 2009 Jul;22(7):922–32.

327. Vertino PM, Yen RW, Gao J, Baylin SB. De novo methylation of CpG island sequences in human fibroblasts overexpressing DNA (cytosine-5-)-methyltransferase. Mol Cell Biol. 1996;16(8):4555–65.

328. Rhee I, Jair KW, Yen RW, Lengauer C, Herman JG, Kinzler KW, et al. CpG methylation is maintained in human cancer cells lacking DNMT1. Nature. 2000 Apr 27;404(6781):1003–7.

329. Rhee I, Bachman KE, Park BH, Jair K-W, Yen R-WC, Schuebel KE, et al. DNMT1 and DNMT3b cooperate to silence genes in human cancer cells. Nature. 2002 Apr 4;416(6880):552–6.

330. Robert M-F, Morin S, Beaulieu N, Gauthier F, Chute IC, Barsalou A, et al. DNMT1 is required to maintain CpG methylation and aberrant gene silencing in human cancer cells. Nat Genet. 2003 Jan;33(1):61–5.

331. Ting AH, Jair K-W, Suzuki H, Yen R-WC, Baylin SB, Schuebel KE. CpG island hypermethylation is maintained in human colorectal cancer cells after RNAi-mediated depletion of DNMT1. Nat Genet. 2004 Jun;36(6):582–4.

332. Jair K-W, Bachman KE, Suzuki H, Ting AH, Rhee I, Yen R-WC, et al. De novo CpG Island Methylation in Human Cancer Cells. Cancer Research. 2006 Jan 15;66(2):682–92.

333. Eads CA, Nickel AE, Laird PW. Complete Genetic Suppression of Polyp Formation and Reduction of CpG-Island Hypermethylation in ApcMin/+ Dnmt1-Hypomorphic Mice. Cancer Research. 2002 Mar 1;62(5):1296–9.

334. Hagemann S, Kuck D, Stresemann C, Prinz F, Brueckner B, Mund C, et al. Antiproliferative effects of DNA methyltransferase 3B depletion are not associated with DNA demethylation. PLoS ONE. 2012;7(5):e36125.

335. Steine EJ, Ehrich M, Bell GW, Raj A, Reddy S, van Oudenaarden A, et al. Genes methylated by DNA methyltransferase 3b are similar in mouse intestine and human colon cancer. J Clin Invest. 2011 May;121(5):1748–52.

336. Widschwendter M, Fiegl H, Egle D, Mueller-Holzner E. Epigenetic stem cell signature in cancer. Nature. 2007;39(2):157–8.

337. Eads CA, Danenberg KD, Kawakami K, Saltz LB, Danenberg PV, Laird PW. CpG island hypermethylation in human colorectal tumors is not associated with DNA methyltransferase overexpression. Cancer Research. 1999 May 15;59(10):2302–6.

338. Nosho K, Shima K, Irahara N, Kure S, Baba Y, Kirkner GJ, et al. DNMT3B expression might contribute to CpG island methylator phenotype in colorectal cancer. Clin Cancer Res. 2009 Jun 1;15(11):3663–71.

339. Ibrahim AEK, Arends MJ, Silva AL, Wyllie AH, Greger L, Ito Y, et al. Sequential DNA methylation changes are associated with DNMT3B overexpression in colorectal neoplastic progression. Gut. 2011 Mar 4;60(4):499–508.

340. Roll JD, Rivenbark AG, Jones WD, Coleman WB. DNMT3b overexpression contributes to a hypermethylator phenotype in human breast cancer cell lines. Mol Cancer. 2008 Jan 25;7(1):15.

341. Turcan S, Rohle D, Goenka A, Walsh LA, Fang F, Yilmaz E, et al. IDH1 mutation is sufficient to establish the glioma hypermethylator phenotype. Nature. 2012 Mar 22;483(7390):479–83.

342. Mardis ER, Ding L, Dooling DJ. Recurring mutations found by sequencing an acute myeloid leukemia genome. NEJM. 2009;361(11):1058–66.

343. Amary MF, Bacsi K, Maggiani F, Damato S, Halai D, Berisha F, et al. IDH1 and IDH2 mutations are frequent events in central chondrosarcoma and central and periosteal chondromas but not in other mesenchymal tumours. J Pathol. 2011 Jul 1;224(3):334–43.

344. Murugan AK, Bojdani E, Xing M. Identification and functional characterization of isocitrate dehydrogenase 1 (IDH1) mutations in thyroid cancer. Biochemical and Biophysical Research Communications. 2010 Mar 12;393(3):555–9.

345. Dang L, White DW, Gross S, Bennett BD, Bittinger MA, Driggers EM, et al. Cancer-associated IDH1 mutations produce 2-hydroxyglutarate. Nature. 2009 Dec 10;462(7274):739–44.

346. Figueroa ME, Abdel-Wahab O, Lu C, Ward PS, Patel J, Shih A, et al. Leukemic IDH1 and IDH2 Mutations Result in a Hypermethylation Phenotype, Disrupt TET2 Function, and Impair Hematopoietic Differentiation. Cancer Cell. 2010 Dec 14;18(6):553–67.

347. Borger DR, Tanabe KK, Fan KC, Lopez HU, Fantin VR, Straley KS, et al. Frequent mutation of isocitrate dehydrogenase (IDH)1 and IDH2 in cholangiocarcinoma identified through broad-based tumor genotyping. Oncologist. 2012;17(1):72–9.

348. Hartman DJ, Binion D, Regueiro M, Schraut W, Bahary N, Sun W, et al. Isocitrate dehydrogenase-1 is mutated in inflammatory bowel disease-associated intestinal adenocarcinoma with low-grade tubuloglandular histology but not in sporadic intestinal adenocarcinoma. Am J Surg Pathol. 2014 Aug;38(8):1147–56.

349. Tougeron D, Guilloteau K, Karayan-Tapon L. Absence of IDH mutation in colorectal cancers with microsatellite instability. Dig Liver Dis. 2016 Jun;48(6):681–3.

350. Ichimura N, Shinjo K, An B, Shimizu Y, Yamao K, Ohka F, et al. Aberrant TET1 Methylation Closely Associated with CpG Island Methylator Phenotype in Colorectal Cancer. Cancer Prev Res (Phila). 2015 Aug;8(8):702–11.

351. Rawłuszko-Wieczorek AA, Siera A, Horbacka K, Horst N, Krokowicz P, Jagodziński PP. Clinical significance of DNA methylation mRNA levels of TET family members in colorectal cancer. J Cancer Res Clin Oncol. 2015 Aug;141(8):1379–92.

352. Neri F, Incarnato D, Krepelova A, Rapelli S, Anselmi F. Single-base resolution analysis of 5-formyl and 5-carboxyl cytosine reveals promoter DNA methylation dynamics. Cell Reports. 2015;34(32):4168–76.

353. Kawasaki T, Nosho K, Ohnishi M, Suemoto Y. Correlation of β-catenin localization with cyclooxygenase-2 expression and CpG island methylator phenotype (CIMP) in colorectal cancer. Neoplasia. 2007;9(7):569–77.

354. Uribe-Lewis S, Stark R, Carroll T, Dunning MJ, Bachman M, Ito Y, et al. 5-hydroxymethylcytosine marks promoters in colon that resist DNA hypermethylation in cancer. Genome Biol. 2015;16(1):69.

355. Ogino S, Nosho K, Kirkner GJ, Kawasaki T, Meyerhardt JA, Loda M, et al. CpG island methylator phenotype, microsatellite instability, BRAF mutation and clinical outcome in colon cancer. Gut. 2009 Jan;58(1):90–6.

356. Cancer Genome Atlas Network. Comprehensive molecular characterization of human colon and rectal cancer. Nature. 2012 Jul 19;487(7407):330–7.

357. Nagasaka T, Sasamoto H, Notohara K, Cullings HM, Takeda M, Kimura K, et al. Colorectal cancer with mutation in BRAF, KRAS, and wild-type with respect to both oncogenes showing different patterns of DNA methylation. J Clin Oncol. 2004 Nov 15;22(22):4584–94.

358. Nagasaka T, Koi M, Kloor M, Gebert J, Vilkin A. Mutations in both KRAS and BRAF may contribute to the methylator phenotype in colon cancer. Gastroenterology. 2008;134(7):1950–1.

359. O'Brien MJ, Yang S, Mack C, Xu H, Huang CS, Mulcahy E, et al. Comparison of microsatellite instability, CpG island methylation phenotype, BRAF and KRAS status in serrated polyps and traditional adenomas indicates separate pathways to distinct colorectal carcinoma end points. Am J Surg Pathol. 2006 Dec;30(12):1491–501.

360. Sawada T, Yamamoto E, Yamano H-O, Nojima M, Harada T, Maruyama R, et al. Assessment of epigenetic alterations in early colorectal lesions containing BRAF mutations. Oncotarget. 2016 Jun 7;7(23):35106–18.

361. Minoo P, Moyer MP, Jass JR. Role of BRAF-V600E in the serrated pathway of colorectal tumourigenesis. J Pathol. 2007 Jun;212(2):124–33.

362. Hinoue T, Weisenberger DJ, Pan F, Campan M, Kim M, Young J, et al. Analysis of the association between CIMP and BRAF in colorectal cancer by DNA methylation profiling. PLoS ONE. 2009;4(12):e8357.

363. Hou P, Liu D, Dong J, Xing M. The BRAF(V600E) causes widespread alterations in gene methylation in the genome of melanoma cells. Cell Cycle. 2012 Jan 15;11(2):286–95.

364. Fang M, Ou J, Hutchinson L, Green MR. The BRAF Oncoprotein Functions through the Transcriptional Repressor MAFG to Mediate the CpG Island Methylator Phenotype. Molecular Cell. 2014 Sep;55(6):904–15.

365. Fang M, Hutchinson L, Deng A, Green MR. Common BRAF(V600E)-directed pathway mediates widespread epigenetic silencing in colorectal cancer and melanoma. Proc Natl Acad Sci USA. 2016 Feb 2;113(5):1250–5.

366. Ordway JM, Williams K, Curran T. Transcription repression in oncogenic transformation: common targets of epigenetic repression in cells transformed by Fos, Ras or Dnmt1. Oncogene. 2004 May 6;23(21):3737–48.

367. Toyota M, Ohe-Toyota M, Ahuja N, Issa JP. Distinct genetic profiles in colorectal tumors with or without the CpG island methylator phenotype. Proceedings of the

National Academy of Sciences. 2000 Jan 18;97(2):710–5.

368. Samowitz WS, Albertsen H, Herrick J, Levin TR, Sweeney C, Murtaugh MA, et al. Evaluation of a Large, Population-Based Sample Supports a CpG Island Methylator Phenotype in Colon Cancer. Gastroenterology. 2005 Sep;129(3):837–45.

369. Serra RW, Fang M, Park SM, Hutchinson L, Green MR. A KRAS-directed transcriptional silencing pathway that mediates the CpG island methylator phenotype. eLife. 2014 Mar 12;3:1171–22.

370. Bestor TH. Unanswered questions about the role of promoter methylation in carcinogenesis. Ann N Y Acad Sci. 2003 Mar;983:22–7.

371. Deaton AM, Bird A. CpG islands and the regulation of transcription. Genes & Development. 2011 May 15;25(10):1010–22.

372. Sproul D, Nestor C, Culley J, Dickson JH, Dixon JM, Harrison DJ, et al. Transcriptionally repressed genes become aberrantly methylated and distinguish tumors of different lineages in breast cancer. Proc Natl Acad Sci USA. 2011 Mar 15;108(11):4364–9.

373. Keshet I, Schlesinger Y, Farkash S, Rand E, Hecht M, Segal E, et al. Evidence for an instructive mechanism of de novo methylation in cancer cells. Nat Genet. 2006 Feb;38(2):149–53.

374. Sproul D, Kitchen RR, Nestor CE, Dixon JM, Sims AH, Harrison DJ, et al. Tissue of origin determines cancer-associated CpG island promoter hypermethylation patterns. Genome Biol. 2012;13(10):R84.

375. Elinav E, Nowarski R, Thaiss CA, Hu B, Jin C, Flavell RA. Inflammation-induced cancer: crosstalk between tumours, immune cells and microorganisms. Nat Rev Cancer. 2013 Nov;13(11):759–71.

376. Federico A, Morgillo F, Tuccillo C, Ciardiello F, Loguercio C. Chronic inflammation and oxidative stress in human carcinogenesis. Int J Cancer. 2007 Dec 1;121(11):2381–6.

377. O'Hagan HM, Wang W, Sen S, Destefano Shields C, Lee SS, Zhang YW, et al. Oxidative damage targets complexes containing DNA methyltransferases, SIRT1, and polycomb members to promoter CpG Islands. Cancer Cell. 2011 Nov 15;20(5):606–19.

378. Foran E, Garrity-Park MM, Mureau C, Newell J, Smyrk TC, Limburg PJ, et al. Upregulation of DNA Methyltransferase-Mediated Gene Silencing, Anchorage-Independent Growth, and Migration of Colon Cancer Cells by Interleukin-6. Molecular Cancer Research. 2010 Apr 14;8(4):471–81.

379. Kominsky DJ, Keely S, MacManus CF, Glover LE, Scully M, Collins CB, et al. An endogenously anti-inflammatory role for methylation in mucosal inflammation identified through metabolite profiling. J Immunol. 2011 Jun 1;186(11):6505–14.

380. Hahn MA, Hahn T, Lee D-H, Esworthy RS, Kim B-W, Riggs AD, et al. Methylation of polycomb target genes in intestinal cancer is mediated by inflammation. Cancer Research. 2008 Dec 15;68(24):10280–9.

381. Hsieh CJ, Klump B, Holzmann K, Borchard F, Gregor M, Porschen R. Hypermethylation of the p16INK4a promoter in colectomy specimens of patients with long-standing and extensive ulcerative colitis. Cancer Research. 1998 Sep 1;58(17):3942–5.

382. Issa JP, Ahuja N, Toyota M, Bronner MP, Brentnall TA. Accelerated age-related CpG island methylation in ulcerative colitis. Cancer Research. 2001 May 1;61(9):3573–7.

383. Konishi K, Shen L, Wang S, Meltzer SJ, Harpaz N, Issa J-PJ. Rare CpG island methylator phenotype in ulcerative colitis-associated neoplasias. Gastroenterology. 2007 Apr;132(4):1254–60.

384. Olaru AV, Cheng Y, Agarwal R, Yang J, David S, Abraham JM, et al. Unique patterns of CpG island methylation in inflammatory bowel disease-associated colorectal cancers. Inflamm Bowel Dis. 2012 Apr;18(4):641–8.

385. Ricciardiello L, Laghi L, Ramamirtham P, Chang CL, Chang DK, Randolph AE, et al. JC virus DNA sequences are frequently present in the human upper and lower gastrointestinal tract. Gastroenterology. 2000 Nov;119(5):1228–35.

386. Laghi L, Randolph AE, Chauhan DP, Marra G, Major EO, Neel JV, et al. JC virus DNA is present in the mucosa of the human colon and in colorectal cancers. Proceedings of the National Academy of Sciences. 1999 Jun 22;96(13):7484–9.

387. Goel A, Li M-S, Nagasaka T, Shin SK, Fuerst F, Ricciardiello L, et al. Association of JC virus T-antigen expression with the methylator phenotype in sporadic colorectal cancers. Gastroenterology. 2006 Jun;130(7):1950–61.

388. Nosho K, Yamamoto H, Takahashi T, Mikami M, Hizaki K, Maehata T, et al. Correlation of laterally spreading type and JC virus with methylator phenotype status in colorectal adenoma. Hum Pathol. 2008 May;39(5):767–75.

389. Nosho K, Shima K, Kure S, Irahara N, Baba Y, Chen L, et al. JC virus T-antigen in colorectal cancer is associated with p53 expression and chromosomal instability, independent of CpG island methylator phenotype. Neoplasia. 2009 Jan;11(1):87–95.

390. Karpinski P, Myszka A, Ramsey D, Kielan W, Sasiadek MM. Detection of viral DNA sequences in sporadic colorectal cancers in relation to CpG island methylation and methylator phenotype. Tumour Biol. 2011 Aug;32(4):653–9.

391. Castellarin M, Warren RL, Freeman JD, Dreolini L, Krzywinski M, Strauss J, et al. Fusobacterium nucleatum infection is prevalent in human colorectal carcinoma. Genome Research. 2012 Feb;22(2):299–306.

392. Kostic AD, Gevers D, Pedamallu CS, Michaud M, Duke F, Earl AM, et al. Genomic analysis identifies association of Fusobacterium with colorectal carcinoma. Genome Research. 2012 Feb;22(2):292–8.

393. Swidsinski A, Dörffel Y, Loening-Baucke V, Theissig F, Rückert JC, Ismail M, et al. Acute appendicitis is characterised by local invasion with Fusobacterium nucleatum/necrophorum. Gut. 2011 Jan;60(1):34–40.

394. Ohkusa T, Sato N, Ogihara T, Morita K, Ogawa M, Okayasu I. Fusobacterium

varium localized in the colonic mucosa of patients with ulcerative colitis stimulates species-specific antibody. Journal of Gastroenterology and Hepatology. 2002 Aug;17(8):849–53.

395. Tahara T, Yamamoto E, Suzuki H, Maruyama R, Chung W, Garriga J, et al. Fusobacterium in colonic flora and molecular features of colorectal carcinoma. Cancer Research. 2014 Mar 1;74(5):1311–8.

396. Ito M, Kanno S, Nosho K, Sukawa Y, Mitsuhashi K, Kurihara H, et al. Association of Fusobacterium nucleatum with clinical and molecular features in colorectal serrated pathway. Int J Cancer. 2015 Sep 15;137(6):1258–68.

397. Mima K, Nishihara R, Qian ZR, Cao Y, Sukawa Y, Nowak JA, et al. Fusobacterium nucleatum in colorectal carcinoma tissue and patient prognosis. Gut. 2015 Aug 26.

398. Cheng Y, Zhang C, Zhao J, Wang C, Xu Y, Han Z, et al. Correlation of CpG island methylator phenotype with poor prognosis in hepatocellular carcinoma. Exp Mol Pathol. 2010 Feb;88(1):112–7.

399. An C, Choi I-S, Yao JC, Worah S, Xie K, Mansfield PF, et al. Prognostic significance of CpG island methylator phenotype and microsatellite instability in gastric carcinoma. Clinical Cancer Research. 2005 Jan 15;11(2 Pt 1):656–63.

400. Toyota M, Ahuja N, Suzuki H, Itoh F, Ohe-Toyota M, Imai K, et al. Aberrant methylation in gastric cancer associated with the CpG island methylator phenotype. Cancer Research. 1999 Nov 1;59(21):5438–42.

401. Noushmehr H, Weisenberger DJ, Diefes K, Phillips HS, Pujara K, Berman BP, et al. Identification of a CpG island methylator phenotype that defines a distinct subgroup of glioma. Cancer Cell. 2010 May 18;17(5):510–22.

402. Barreau O, Assié G, Wilmot-Roussel H, Ragazzon B, Baudry C, Perlemoine K, et al. Identification of a CpG island methylator phenotype in adrenocortical carcinomas. J Clin Endocrinol Metab. 2013 Jan;98(1):E174–84.

403. Tanemura A, Terando AM, Sim M-S, van Hoesel AQ, de Maat MFG, Morton DL, et al. CpG island methylator phenotype predicts progression of malignant melanoma. Clinical Cancer Research. 2009 Mar 1;15(5):1801–7.

404. Arai E, Chiku S, Mori T, Gotoh M, Nakagawa T, Fujimoto H, et al. Single-CpG-resolution methylome analysis identifies clinicopathologically aggressive CpG island methylator phenotype clear cell renal cell carcinomas. Carcinogenesis. 2012 Aug;33(8):1487–93.

405. Ueki T, Toyota M, Sohn T, Yeo CJ, Issa JP, Hruban RH, et al. Hypermethylation of multiple genes in pancreatic adenocarcinoma. Cancer Research. 2000 Apr 1;60(7):1835–9.

406. Ciriello G, Miller ML, Aksoy BA, Senbabaoglu Y, Schultz N, Sander C. Emerging landscape of oncogenic signatures across human cancers. Nat Gen. 2013 Oct;45(10):1127–33.

407. Kim JH, Karnovsky A, Mahavisno V, Weymouth T, Pande M, Dolinoy DC, et al. LRpath analysis reveals common pathways dysregulated via DNA methylation

across cancer types. BMC Genomics. 2012 Oct 4;13(1):526.

408. Sánchez-Vega F, Gotea V, Margolin G, Elnitski L. Pan-cancer stratification of solid human epithelial tumors and cancer cell lines reveals commonalities and tissue-specific features of the CpG island methylator phenotype. Epigenetics Chromatin. 2015;8(1):14.

409. Moarii M, Reyal F, Vert J-P. Integrative DNA methylation and gene expression analysis to assess the universality of the CpG island methylator phenotype. Human Genomics. 2015 Oct 13;9(1):26.

410. Krueger F, Andrews SR. Bismark: a flexible aligner and methylation caller for Bisulfite-Seq applications. Bioinformatics. 2011 Jun 1;27(11):1571–2.

411. Hansen KD, Langmead B, Irizarry RA. BSmooth: from whole genome bisulfite sequencing reads to differentially methylated regions. Genome Biol. 2012 Oct 3;13(10):R83.

412. Kim D, Pertea G, Trapnell C, Pimentel H, Kelley R, Salzberg SL. TopHat2: accurate alignment of transcriptomes in the presence of insertions, deletions and gene fusions. Genome Biol. 2013 Apr 25;14(4):R36.

413. Trapnell C, Hendrickson DG, Sauvageau M, Goff L, Rinn JL, Pachter L. Differential analysis of gene regulation at transcript resolution with RNA-seq. Nature Biotechnology. 2013 Jan;31(1):46–53.

414. Ibrahim AEK, Arends MJ, Silva A-L, Wyllie AH, Greger L, Ito Y, et al. Sequential DNA methylation changes are associated with DNMT3B overexpression in colorectal neoplastic progression. Gut. 2011 Apr;60(4):499–508.

415. Nosho K, Shima K, Irahara N, Kure S, Baba Y, Kirkner GJ, et al. DNMT3B expression might contribute to CpG island methylator phenotype in colorectal cancer. Clin Cancer Res. 2009 Jun 1;15(11):3663–71.

416. Chen Z-X, Mann JR, Hsieh C-L, Riggs AD, Chédin F. Physical and functional interactions between the human DNMT3L protein and members of the de novo methyltransferase family. J Cell Biochem. 2005 Aug 1;95(5):902–17.

417. Beard C, Hochedlinger K, Plath K, Wutz A, Jaenisch R. Efficient method to generate single-copy transgenic mice by site-specific integration in embryonic stem cells. Genesis. 2006 Jan 6;44(1):23–8.

418. Cong L, Ran FA, Cox D, Lin S, Barretto R, Habib N, et al. Multiplex genome engineering using CRISPR/Cas systems. Science. 2013 Feb 15;339(6121):819–23.

419. Mali P, Yang L, Esvelt KM, Aach J, Guell M, DiCarlo JE, et al. RNA-guided human genome engineering via Cas9. Science. 2013 Feb 15;339(6121):823–6.

420. Sanjana NE, Shalem O, Zhang F. Improved vectors and genome-wide libraries for CRISPR screening. Nat Methods. 2014 Aug;11(8):783–4.

421. Mali P, Yang L, Esvelt KM, Aach J, Guell M, DiCarlo JE, et al. RNA-guided human genome engineering via Cas9. Science. 2013 Feb 15;339(6121):823–6.

422. Rhee I, Bachman KE, Ben Ho Park, Jair K-W, Yen R-WC, Schuebel KE, et al.

DNMT1 and DNMT3b cooperate to silence genes in human cancer cells. Nature.; 2002 Apr 4;416(6880):552–6.

423. Ibrahim AEK, Arends MJ, Silva AL, Wyllie AH, Greger L, Ito Y, et al. Sequential DNA methylation changes are associated with DNMT3B overexpression in colorectal neoplastic progression. Gut. 2011 Mar 4;60(4):499–508.

424. Nosho K, Shima K, Irahara N, Kure S, Baba Y, Kirkner GJ, et al. DNMT3B Expression Might Contribute to CpG Island Methylator Phenotype in Colorectal Cancer. Clinical Cancer Research. 2009 Jun 1;15(11):3663–71.

425. Nagasaka T, Koi M, Kloor M, Gebert J, Vilkin A, Nishida N, et al. Mutations in Both KRAS and BRAF May Contribute to the Methylator Phenotype in Colon Cancer. Gastroenterology. 2008 Jun;134(7):1950–1.

426. Minoo P, Moyer MP, Jass JR. Role of BRAF-V600E in the serrated pathway of colorectal tumourigenesis. J Pathol. 2007 Jun;212(2):124–33.

427. Nosho K, Shima K, Irahara N, Kure S, Baba Y, Kirkner GJ, et al. DNMT3B Expression Might Contribute to CpG Island Methylator Phenotype in Colorectal Cancer. Clinical Cancer Research. 2009 Jun 1;15(11):3663–71.

428. Ibrahim AEK, Arends MJ, Silva A-L, Wyllie AH, Greger L, Ito Y, et al. Sequential DNA methylation changes are associated with DNMT3B overexpression in colorectal neoplastic progression. Gut. 2011 Apr;60(4):499–508.

429. Pawlikowski JS, McBryan T, van Tuyn J, Drotar ME, Hewitt RN, Maier AB, et al. Wnt signaling potentiates nevogenesis. Proc Natl Acad Sci USA. 2013 Oct 1;110(40):16009–14.

430. Rad R, Cadiñanos J, Rad L, Varela I, Strong A, Kriegl L, et al. A genetic progression model of Braf(V600E)-induced intestinal tumorigenesis reveals targets for therapeutic intervention. Cancer Cell. 2013 Jul 8;24(1):15–29.

431. Jass JR. Classification of colorectal cancer based on correlation of clinical, morphological and molecular features. Histopathology. 2007 Jan;50(1):113–30.

432. Robertson KD, Keyomarsi K, Gonzales FA, Velicescu M, Jones PA. Differential mRNA expression of the human DNA methyltransferases (DNMTs) 1, 3a and 3b during the G(0)/G(1) to S phase transition in normal and tumor cells. Nucleic Acids Research. 2000 May 15;28(10):2108–13.

433. Lin H, Yamada Y, Nguyen S, Linhart H, Jackson-Grusby L, Meissner A, et al. Suppression of Intestinal Neoplasia by Deletion of Dnmt3b. Molecular and Cellular Biology. 2006 Mar 30;26(8):2976–83.

434. Steine EJ, Ehrich M, Bell GW, Raj A, Reddy S, van Oudenaarden A, et al. Genes methylated by DNA methyltransferase 3b are similar in mouse intestine and human colon cancer. J Clin Invest. 2011 May 2;121(5):1748–52.

435. Wang J, Bhutani M, Pathak AK, Lang W, Ren H, Jelinek J, et al. Delta DNMT3B variants regulate DNA methylation in a promoter-specific manner. Cancer Research. 2007 Nov 15;67(22):10647–52.

436. Schroeder A, Mueller O, Stocker S, Salowsky R, Leiber M, Gassmann M, et al.

The RIN: an RNA integrity number for assigning integrity values to RNA measurements. BMC Mol Biol. 2006 Jan 31;7(1):3.

437. Mootha VK, Lindgren CM, Eriksson K-F, Subramanian A, Sihag S, Lehar J, et al. PGC-1alpha-responsive genes involved in oxidative phosphorylation are coordinately downregulated in human diabetes. Nat Genet. 2003 Jul;34(3):267–73.

438. Subramanian A, Tamayo P, Mootha VK, Mukherjee S, Ebert BL, Gillette MA, et al. Gene set enrichment analysis: a knowledge-based approach for interpreting genome-wide expression profiles. Proceedings of the National Academy of Sciences. 2005 Oct 25;102(43):15545–50.

439. Ogino S, Kawasaki T, Kirkner GJ, Ogawa A, Dorfman I, Loda M, et al. Down-regulation of p21 (CDKN1A/CIP1) is inversely associated with microsatellite instability and CpG island methylator phenotype (CIMP) in colorectal cancer. J Pathol. 2006 Oct;210(2):147–54.

440. Acosta JC, Banito A, Wuestefeld T, Georgilis A, Janich P, Morton JP, et al. A complex secretory program orchestrated by the inflammasome controls paracrine senescence. Nat Cell Biol. 2013 Aug 1;15(8):978–90.

441. Correia-Melo C, Marques FDM, Anderson R, Hewitt G, Hewitt R, Cole J, et al. Mitochondria are required for pro-ageing features of the senescent phenotype. EMBO J. 2016 Apr 1;35(7):724–42.

442. Juan J, Muraguchi T, Iezza G, Sears RC, McMahon M. Diminished WNT -> β-catenin -> c-MYC signaling is a barrier for malignant progression of BRAFV600E-induced lung tumors. Genes & Development. 2014 Mar 15;28(6):561–75.

443. Coppé J-P, Desprez P-Y, Krtolica A, Campisi J. The senescence-associated secretory phenotype: the dark side of tumor suppression. Annu Rev Pathol. 2010;5(1):99–118.

444. Ahmed D, Eide PW, Eilertsen IA, Danielsen SA, Eknæs M, Hektoen M, et al. Epigenetic and genetic features of 24 colon cancer cell lines. Oncogenesis. 2013 Sep 16;2(9):e71.

445. Hagemann S, Kuck D, Stresemann C, Prinz F, Brueckner B, Mund C, et al. Antiproliferative Effects of DNA Methyltransferase 3B Depletion Are Not Associated with DNA Demethylation. PLoS ONE. 2012 May 1;7(5):e36125–10.

446. Kuilman T, Michaloglou C, Vredeveld LCW, Douma S, van Doorn R, Desmet CJ, et al. Oncogene-induced senescence relayed by an interleukin-dependent inflammatory network. Cell. 2008 Jun 13;133(6):1019–31.

447. Ye X, Zerlanko B, Kennedy A, Banumathy G, Zhang R, Adams PD. Downregulation of Wnt Signaling Is a Trigger for Formation of Facultative Heterochromatin and Onset of Cell Senescence in Primary Human Cells. Molecular Cell. 2007 Jul;27(2):183–96.

448. Wu Z-Q, Brabletz T, Fearon E, Willis AL, Hu CY, Li X-Y, et al. Canonical Wnt suppressor, Axin2, promotes colon carcinoma oncogenic activity. Proc Natl Acad Sci USA. 2012 Jul 10;109(28):11312–7.

449. Niida A, Hiroko T, Kasai M, Furukawa Y, Nakamura Y, Suzuki Y, et al. DKK1, a negative regulator of Wnt signaling, is a target of the beta-catenin/TCF pathway. Oncogene. 2004 Nov 4;23(52):8520–6.

450. Finch PW, He X, Kelley MJ, Uren A, Schaudies RP, Popescu NC, et al. Purification and molecular cloning of a secreted, Frizzled-related antagonist of Wnt action. Proceedings of the National Academy of Sciences. 1997 Jun 24;94(13):6770–5.

451. Caldwell GM, Jones C, Gensberg K, Jan S, Hardy RG, Byrd P, et al. The Wnt antagonist sFRP1 in colorectal tumorigenesis. Cancer Research. 2004 Feb 1;64(3):883–8.

452. Elzi DJ, Song M, Hakala K, Weintraub ST, Shiio Y. Wnt antagonist SFRP1 functions as a secreted mediator of senescence. Mol Cell Biol. 2012 Nov;32(21):4388–99.

453. Ibrahim AEK, Arends MJ, Silva AL, Wyllie AH, Greger L, Ito Y, et al. Sequential DNA methylation changes are associated with DNMT3B overexpression in colorectal neoplastic progression. Gut. 2011 Mar 4;60(4):499–508.

454. Mercer K, Giblett S, Green S, Lloyd D, DaRocha Dias S, Plumb M, et al. Expression of endogenous oncogenic V600EB-raf induces proliferation and developmental defects in mice and transformation of primary fibroblasts. Cancer Research. 2005 Dec 15;65(24):11493–500.

455. Pritchard C, Carragher L, Aldridge V, Giblett S, Jin H, Foster C, et al. Mouse models for BRAF-induced cancers. Biochem Soc Trans. 2007 Nov;35(Pt 5):1329–33.

456. Ireland H, Kemp R, Houghton C, Howard L, Clarke AR, Sansom OJ, et al. Inducible cre-mediated control of gene expression in the murine gastrointestinal tract: effect of loss of β-catenin. Gastroenterology. 2004 May;126(5):1236–46.

457. Kemp R. Elimination of background recombination: somatic induction of Cre by combined transcriptional regulation and hormone binding affinity. Nucleic Acids Research. 2004 Jun 21;32(11):e92–2.

458. Marjou el F, Janssen K-P, Chang BH-J, Li M, Hindie V, Chan L, et al. Tissue-specific and inducible Cre-mediated recombination in the gut epithelium. Genesis. 2004 Jul;39(3):186–93.

459. Madison BB, Dunbar L, Qiao XT, Braunstein K, Braunstein E, Gumucio DL. Cis elements of the villin gene control expression in restricted domains of the vertical (crypt) and horizontal (duodenum, cecum) axes of the intestine. Journal of Biological Chemistry. 2002 Sep 6;277(36):33275–83.

460. Shibata H, Toyama K, Shioya H, Ito M, Hirota M, Hasegawa S, et al. Rapid Colorectal Adenoma Formation Initiated by Conditional Targeting of the Apc Gene. Science. 1997 Oct 3;278(5335):120–3.

461. Sansom OJ, Reed KR, van de Wetering M, Muncan V, Winton DJ, Clevers H, et al. Cyclin D1 is not an immediate target of beta-catenin following Apc loss in the intestine. Journal of Biological Chemistry. 2005 Aug 5;280(31):28463–7.

462. Sato T, Clevers H. Growing self-organizing mini-guts from a single intestinal stem cell: mechanism and applications. Science. 2013 Jun 7;340(6137):1190–4.

463. Gao J, Aksoy BA, Dogrusoz U, Dresdner G, Gross B, Sumer SO, et al. Integrative analysis of complex cancer genomics and clinical profiles using the cBioPortal. Sci Signal. 2013 Apr 2;6(269):pl1–pl1.

464. Cerami E, Gao J, Dogrusoz U, Gross BE, Sumer SO, Aksoy BA, et al. The cBio cancer genomics portal: an open platform for exploring multidimensional cancer genomics data. Cancer Discov. 2012 May;2(5):401–4.

465. Xie Z-H, Huang Y-N, Chen Z-X, Riggs AD, Ding J-P, Gowher H, et al. Mutations in DNA methyltransferase DNMT3B in ICF syndrome affect its regulation by DNMT3L. Human Molecular Genetics. 2006 May 1;15(9):1375–85.

466. Pongor L, Kormos M, Hatzis C, Pusztai L, Szabó A, Győrffy B. A genome-wide approach to link genotype to clinical outcome by utilizing next generation sequencing and gene chip data of 6,697 breast cancer patients. Genome Med. 2015 Oct 16;7(1):104.

467. Li M, Wang Y, Song Y, Bu R, Yin B, Fei X, et al. Expression profiling and clinicopathological significance of DNA methyltransferase 1, 3A and 3B in sporadic human renal cell carcinoma. Int J Clin Exp Pathol. 2014;7(11):7597–609.

468. Chen M-F, Lu M-S, Lin P-Y, Chen P-T, Chen W-C, Lee K-D. The role of DNA methyltransferase 3b in esophageal squamous cell carcinoma. Cancer. 2012 Aug 15;118(16):4074–89.

469. Arai E, Nakagawa T, Wakai Ushijima S, Fujimoto H, Kanai Y. DNA methyltransferase 3B expression is associated with poor outcome of stage I testicular seminoma. Histopathology. 2012 May 1;60(6B):E12–8.

470. Oh B-K, Kim H, Park H-J, Shim Y-H, Choi J, Park C, et al. DNA methyltransferase expression and DNA methylation in human hepatocellular carcinoma and their clinicopathological correlation. Int J Mol Med. 2007 Jul;20(1):65–73.

471. Bae JM, Kim JH, Kwak Y, Lee D-W, Cha Y, Wen X, et al. Distinct clinical outcomes of two CIMP-positive colorectal cancer subtypes based on a revised CIMP classification system. Br J Cancer. 2017 Mar 9;58:5248.

472. Bae JM, Kim JH, Cho N-Y, Kim T-Y, Kang GH. Prognostic implication of the CpG island methylator phenotype in colorectal cancers depends on tumour location. Br J Cancer. 2013 Aug 20;109(4):1004–12.

473. Shen L, Catalano PJ, Benson AB, O'Dwyer P, Hamilton SR, Issa J-PJ. Association between DNA methylation and shortened survival in patients with advanced colorectal cancer treated with 5-fluorouracil based chemotherapy. Clinical Cancer Research. 2007 Oct 15;13(20):6093–8.

474. Juo YY, Johnston FM, Zhang DY, Juo HH, Wang H, Pappou EP, et al. Prognostic value of CpG island methylator phenotype among colorectal cancer patients: a systematic review and meta-analysis. Annals of Oncology. 2014 Nov 20;25(12):2314–27.

475. Samowitz WS, Sweeney C, Herrick J, Albertsen H, Levin TR, Murtaugh MA, et al. Poor survival associated with the BRAF V600E mutation in microsatellite-stable colon cancers. Cancer Research. 2005 Jul 15;65(14):6063–9.

476. Seligmann JF, Fisher D, Smith CG, Richman SD, Elliott F, Brown S, et al. Investigating the poor outcomes of BRAF-mutant advanced colorectal cancer: Analysis from 2530 patients in randomised clinical trials. Ann Oncol. 2017 Mar 1;28(3):562-568.

477. Sanz-Garcia E, Argiles G, Elez E, Tabernero J. BRAF mutant colorectal cancer: prognosis, treatment, and new perspectives. Ann Oncol. 2017 Nov 1;28(11):2648–57.

478. Dankort D, Filenova E, Collado M, Serrano M, Jones K, McMahon M. A new mouse model to explore the initiation, progression, and therapy of BRAFV600E-induced lung tumors. Genes & Development. 2007 Feb 15;21(4):379–84.

479. Hinoue T, Weisenberger DJ, Pan F, Campan M, Kim M, Young J, et al. Analysis of the association between CIMP and BRAF in colorectal cancer by DNA methylation profiling. Wong CM, editor. PLoS ONE. 2009;4(12):e8357.

480. Cao W, Ribeiro R de O, Liu D, Saintigny P, Xia R, Xue Y, et al. EZH2 promotes malignant behaviors via cell cycle dysregulation and its mRNA level associates with prognosis of patient with non-small cell lung cancer. PLoS ONE. 2012;7(12):e52984.

481. Li Y, Wei J, Xu C, Zhao Z, You T. Prognostic significance of cyclin D1 expression in colorectal cancer: a meta-analysis of observational studies. PLoS ONE. Public Library of Science; 2014;9(4):e94508.

482. He TC, Sparks AB, Rago C, Hermeking H, Zawel L, da Costa LT, et al. Identification of c-MYC as a target of the APC pathway. Science. 1998 Sep 4;281(5382):1509–12.

483. Tetsu O, McCormick F. beta-Catenin regulates expression of cyclin D1 in colon carcinoma cells. Nature. 1999 Apr 1;398(6726):422–6.

484. Miwa N, Furuse M, Tsukita S, Niikawa N, Nakamura Y, Furukawa Y. Involvement of Claudin-1 in the β-Catenin/Tcf Signaling Pathway and its Frequent Upregulation in Human Colorectal Cancers. Oncol Res. 2001 Nov 1;12(11):469–76.

485. Blache P, van de Wetering M, Duluc I, Domon C, Berta P, Freund J-N, et al. SOX9 is an intestine crypt transcription factor, is regulated by the Wnt pathway, and represses the CDX2 and MUC2 genes. J Cell Biol. 2004 Jul 5;166(1):37–47.

486. Barolo S. Transgenic Wnt/TCF pathway reporters: all you need is Lef? Oncogene. 2006 Dec 4;25(57):7505–11.

487. Scholer-Dahirel A, Schlabach MR, Loo A, Bagdasarian L, Meyer R, Guo R, et al. Maintenance of adenomatous polyposis coli (APC)-mutant colorectal cancer is dependent on Wnt/beta-catenin signaling. Proc Natl Acad Sci USA. 2011 Oct 11;108(41):17135–40.